# STUDY OF THE FRACTURE AND FATIGUE PROPERTIES OF SOME SINTERED STEELS

A thesis submitted for the degree of
Doctor of Philosophy

by

Glenn Andrews

May, 1976

CONTENTS


SUMMARY ..... 1

AIMS OF RESEARCH PROJECT ..... 2

1. INTRODUCTION ..... 3
   1.1 GENERAL AND ECONOMIC OUTLINE OF POWDER METALLURGY ..... 3
   1.2 IRON POWDER METALLURGY ..... 7
   1.3 LIMITATIONS OF THE P/M APPROACH FOR PRODUCTION OF ENGINEERING COMPONENTS ..... 9

2. LITERATURE REVIEW ..... 13
   2.1 IRON POWDER CHARACTERISTICS AND PROPERTIES ..... 13
   2.2 FRACTURE MECHANICS ..... 18
      2.2.1 THEORY ..... 18
      2.2.2 MECHANICAL PROPERTIES OF SINTERED MATERIALS AND APPLICATION OF FRACTURE TOUGHNESS TESTING... 29
      2.2.3 FRACTURE MECHANISMS ..... 37
   2.3 FATIGUE ..... 38
      2.3.1 HISTORICAL ..... 38
      2.3.2 EMPIRICAL FATIGUE LAWS ..... 41
      2.3.3 THE MECHANISMS OF FATIGUE FAILURE ..... 45
      2.3.4 FATIGUE CRACK INITIATION AND GROWTH ..... 47
      2.3.4.1 INITIATION LAWS ..... 48
      2.3.4.2 PROPAGATION LAWS ..... 58
      2.3.5 FATIGUE PROPERTIES OF SINTERED MATERIALS ..... 64

3. RAW MATERIALS AND EXPERIMENTAL TECHNIQUES ..... 69
   3.1 POWDERS ..... 69
      3.1.1 UNALLOYED IRON ..... 69
      3.1.2 LOW ALLOY STEEL (ANCOLOY SA) ..... 69
   3.2 PRODUCTION OF COMPACTS ..... 70
      3.2.1 COMPACTION ..... 70
      3.2.2 SINTERING ..... 72
      3.2.3 CARBON CONTROL AND HEAT TREATMENT ..... 74
   3.3 MECHANICAL TESTING ..... 75
      3.3.1 TENSILE TESTING ..... 75
      3.3.2 FATIGUE TESTING ..... 76
      3.3.3 FRACTURE TOUGHNESS TESTING ..... 85
   3.4 METALLOGRAPHY ..... 87
   3.5 FRACTOGRAPHY ..... 89

4. RESULTS ..... 90
   4.1 IRON POWDERS ..... 90
      4.1.1 MECHANICAL PROPERTIES ..... 90
      4.1.2 FRACTOGRAPHY ..... 92
   4.2 ANCOLOY SA ..... 92
      4.2.1 MECHANICAL PROPERTIES ..... 92
      4.2.2 FATIGUE CRACK INITIATION AND PROPAGATION ..... 94
      4.2.3 FRACTOGRAPHY ..... 98
      4.2.4 OPTICAL VERSUS ELECTRIC POTENTIAL METHOD FOR MONITORING CRACK GROWTH ..... 99

5. DISCUSSION .....101
   5.1 IRON POWDERS .....101
   5.2 LOW ALLOY STEEL POWDER (ANCOLOY SA) .....110

6. RECOMMENDATIONS FOR FURTHER WORK .....129

7. CONCLUSIONS ..... 132
8. ACKNOWLEDGEMENTS ..... 132
9. TABLES AND FIGURES ..... 133
APPENDIX I ..... 206
APPENDIX II ..... 207
10. REFERENCES ..... 208

## SUMMARY

Fracture toughness data for four types of iron powder and one low alloy steel powder is evaluated. The possibility of measuring toughness on notched specimens is assessed and some theoretical treatment of toughness data presented with a view to correlating toughness and tensile strength.

The fatigue crack initiation and propagation behaviour of the low alloy steel is investigated. Correlations of initiation data with both $K_t \Delta S$ and $\Delta K/\rho^{\frac{1}{2}}$ is presented and the applicability of each analysis discussed. Fatigue crack growth rates, da/dN are plotted against $\Delta K$ and the exponent in the Paris equation[130] - $da/dN = C\Delta K^m$ - is correlated with material density, composition and treatment. Curves of crack length, a against number of load cycles, N are proposed as a means of determining relative material behaviour.

The electric potential method is employed in generating initiation and propagation data and this method is also compared with the optical method of crack monitoring.

## AIMS OF RESEARCH PROJECT

There is a general lack of knowledge concerning the measurement and meaning of the fracture toughness of sintered material. This is a major limitation to the promotion of sintered materials for structural purposes. Further, paucity of fatigue data seriously inhibits more widespread use of sintered components.

This project attempts to clarify some of the difficulties concerning the applicability of fracture toughness, and provide information concerning the effect of various parameters. Included in these latter are density, powder type, composition and treatment.

An attempt is made to establish which are the major factors influencing fatigue crack initiation and propagation in a low alloy steel in various conditions. A fracture mechanics approach is proposed to enable the derivation of quantitative relationships.

# 1. INTRODUCTION

## 1.1 GENERAL AND ECONOMIC OUTLINE OF POWDER METALLURGY

Powder metallurgy, (P/M), has made considerable advances over the last decade and is finding increasingly more applications. It is misleading to view the P/M industry as a single integrated entity as it is made up of a number of sectors of industry linked by a common technology. The components produced by P/M techniques can be conveniently separated into two groups as described below.

Firstly, P/M processes can provide components with specific properties often unobtainable by other means. This group includes the hard metal industry where P/M techniques provide a method of obtaining mechanical alloys between hard metals and hard metal carbides for producing tools, e.g. tungsten, tungsten carbide and cobalt or niobium, niobium carbide and cobalt. In addition the process enables the production of alloys of incompatible materials as in friction materials avoiding the necessity to cast - a considerable advantage where high melting point materials are involved. A further important application is in the use of high porosity parts for filters and bearings where lubricants are run into the open pore system imparting self-lubricating properties. Recent advances in aerospace and nuclear technology demand unique alloys and this demand is often satisfied by means of P/M. The use of P/M parts of this type is seldom inhibited by the lower cost of alternative wrought materials as the properties developed are so advantageous. For instance, the higher cost of cemented carbide tools relative to alloy tool

steels is more than compensated by the higher machining rates permissible and the longer life of carbide tools.

Secondly, P/M provides an alternative fabrication method to conventional production engineering techniques such as casting, extrusion, forging and machining. In this case economic viability is afforded to P/M parts production by virtue of the repetitive nature and large numerical outputs where cost per unit is low. Considerable difficulty is encountered in this sector of the industry with respect to specifications and acceptance levels. In many cases properties of P/M parts are markedly inferior to those of equivalent wrought materials, in particular ductility, although adequate, is often near minimum acceptance levels. However, the low cost per unit of P/M compared to wrought parts is the decisive factor as engineers begin to recognise and accept that the P/M component has a valuable contribution to make if applied intelligently.

It becomes apparent from the above broad outlines of the two classes of P/M product that a comparison may be made on the basis of cost. For engineering components low cost is the prime factor but where the objective is a specific property, cost assumes a secondary role and therefore the corresponding manufacturing philosophies for each class of product are different.

This assessment of the importance of economic factors governing the P/M process is confirmed by MOWBRAY[1] who extended it to an examination of the technological and commercial aspects. The P/M process can be divided into four major sections as far as cost contributions are concerned. These are raw materials, design, compaction and sintering. The absence of finishing costs

in this list is significant as the aim is to eliminate or at least minimise these.

A wide variety of powders are available to the P/M parts producer either in the pure state or pre-alloyed. The cost reflects the abundance, ease of production and the demand for a particular powder.

Design is the most significant factor involved because it is possible to invoke design principles to reduce costs at all stages of the P/M process. Design is primarily concerned with the properties of the finished product and attaining minimum acceptance levels. In many cases over-design has proved restrictive where a P/M product could not meet a specific property requirement which may or may not have had any bearing on its ultimate performance. It is in this area that considerable cost savings may be realised where problems associated with over-design can be overcome. Property improvement often requires higher density parts with resultant disproportionate increases in tooling costs. A powder of increased compressibility may be required which necessitates higher purity and once again increases costs. Alternatively, higher compacting pressures will require better tooling or more frequent replacement due to higher wear rates. The need to meet closer tolerances may involve a repressing or coining operation with the necessary extra tooling.

Presses and tooling, as indicated above, generally constitute a high proportion of the total cost of parts. TAYLOR[2] gives a detailed account of the effect of press tool design on the economics of sintered components. Sintering is an area where considerable economic savings may be realised and a brief guide

to sintering furnace design is provided by JONES[3]. In practice the mesh belt type of furnace is very satisfactory below 1150°C but at higher temperatures the wear problems are severe and more costly equipment is often required. As a consequence, considerable research effort is being directed towards reducing sintering temperatures.

Finally, to complete this general review of the P/M industry it is necessary to examine the producer/customer relationship. This may be suitably defined by two terms - in common use in the U.S.A. - "in plant" and "custom". The former is where producer and customer are closely linked within an organisation and the latter where the two are related on a trading basis only.

The "in plant" organisation is considerably advantageous in that producer and customer are working towards common objectives and conditions are more favourable to satisfactory compromises. In addition, the ability to monitor components closely during use is an added advantage which can lead to useful data for future design. The one disadvantage of this type of arrangement is that quantities may be uneconomic where a limited number of a wide variety of parts may be required.

The "custom" organisation suffers from competition not only in the form of alternative processes but also from rival firms. This is not necessarily disadvantageous where economic margins become critical and survival depends on the ability to maintain these. For this organisation the minimum order, less than which cannot be economically produced, may become inhibitive. Prospective customers tend to avoid committing themselves to very large quantities which may be 10,000 or more[1]. Some companies are able

to operate on a small scale and in such cases may show promising growth rates.

## 1.2 IRON POWDER METALLURGY

Iron powders are the most important in terms of output and constitute a large proportion of the total powder consumption in both the U.K. and the U.S.A. despite recent increases in aluminium powder usage in aerospace and defence applications.

In 1972 the iron powder consumed in the U.K. amounted to 15,000 tons[4] and in the U.S.A. 180,000 tons[5]. Of the total U.K. consumption, 10,000 tons went into the production of engineering components[6] and 160,000 tons in the U.S.A. However, it should be noted that about 25 million tons of steel were produced in the U.K. in 1972 and 120 million tons in the U.S.A.[7] which serves to put powder production in perspective.

The majority of powders used for iron and alloyed iron structural parts feed the automotive industry where the repetitive nature of products allied with vast turnover lends itself very well to the economics of the P/M process. This interdependence however, means that recessions in the automotive industry invariably lead to recessions in the P/M trade.

The extensive use of iron powders may be ascribed to their abundance, cheapness and the high strength levels obtained with small alloy additions. They may be produced by a variety of methods and a number of types and grades are commercially available[8]. This multiplicity of process routes is fortunate in one sense as a wide range of properties are available and unfortunate in that the development of powder property standards is difficult. There are seven basic processes in common commercial use; atomisation;

Carbonyl decomposition; electrolytic deposition; gaseous reduction; grinding; oxide reduction (i) by carbon and (ii) by gases. An account of these processes, their relative costs, properties, advantages, disadvantages and applications is given by BACKENSTO[9].

The morphology of iron powders is dependent to a large extent on the production method and, of even more significance, the properties are dependent on the powder morphology. A brief description of five common powders is given below together with scanning electron micrographs.

(1) Hoganas - irregularly shaped particles with many protruding asperities on individual particles. Produced by solid state reduction of very pure iron concentrates with carbon in continuous tunnel kilns. Often referred to as 'sponge iron', Fig. 1

(2) Atomised - (i) by the action of water jets and (ii) gas jets, (nitrogen or argon) on molten streams of low carbon iron. Irregularly shaped particles which tend to form hollow spheres with some protruberances, Fig. 2

(3) Domtar - (U.K. equivalent ROSPOL) - similar in appearance to Hoganas powder but asperities are removed by subsequent attrition. Produced by water atomisation of molten high carbon iron followed by removal of carbon with millscale at 1100°C and subsequent break up of loose 'cake', Fig. 3

(4) Carbonyl - very small solid spheres produced by precipitation from gaseous iron carbonyl, Fig. 4

(5) Electrolytic - Produced by deposition from acid iron bearing electrolytes. Particles have a tendency to be long, flat and dendritic in nature, Fig. 5

## 1.3 LIMITATIONS OF THE P/M APPROACH FOR PRODUCTION OF ENGINEERING COMPONENTS.

The author believes that the greatest single obstacle to P/M expansion is the lack of basic design data. Typically, the P/M components are regarded as low cost replacements for conventional materials in lowly stressed applications. Very often they are evaluated on a 'go/nogo' basis which can be particularly damaging to the reputation of the P/M part. A new philosophy seems desirable where the P/M component evaluation is based on its suitability for a specific purpose or application. With suitable design information the use of P/M parts could be extended to relatively highly stressed applications and this should be the aim.

It is the responsibility of both user and producer to adopt and nurture this new philosophy because, until this occurs, the expansion of P/M components into markets involving their use in relatively highly stressed situations will be severely restricted. There appears to be a basic lack of information pertaining to sintered parts in general and such data that is available seems to be based on practical experience.

The recently developed concept of fracture mechanics may be one such method of obtaining pertinent design data for P/M parts, if only on a materials selection basis. It is necessary that the engineer be able to assess the merit of a sintered

component in relation to the equivalent cast or wrought counterpart. The use of fracture toughness parameters derives from the continuum mechanics analysis of linear elastic fracture which has proved particularly useful for bodies containing crack-like defects. This technique enables not only the assessment of critical defect sizes but also can be extended to sub-critical crack growth in fatigue situations where growth rate is related to applied loads.

It may prove possible to apply these concepts of design theory to sintered products and indeed, there seem no major obstacles to this approach. It is necessary then, to develop such techniques to fit the situation for sintered parts and attempt to ascertain the important parameters which control their toughness. In addition it is more important to attempt to correlate fracture toughness with other more easily measurable properties, as toughness testing is generally relatively expensive. Finally, it is necessary to examine the possibility of applying these design concepts to P/M parts in a similar manner to the case for conventional parts. In this latter respect examination of fatigue crack initiation and propagation would seem most applicable. It is in this situation that fracture mechanics concepts are of considerable use.

Fig. 1: Höganäs NC 100 (x 1000)

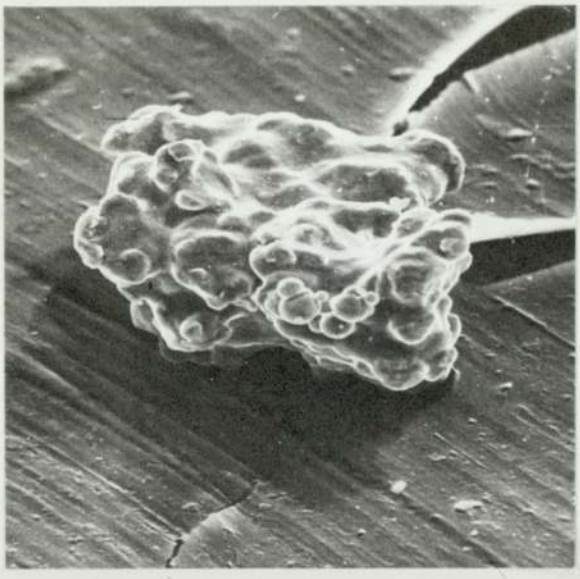

Fig. 2: Höganäs ASC 100 (x 1000)

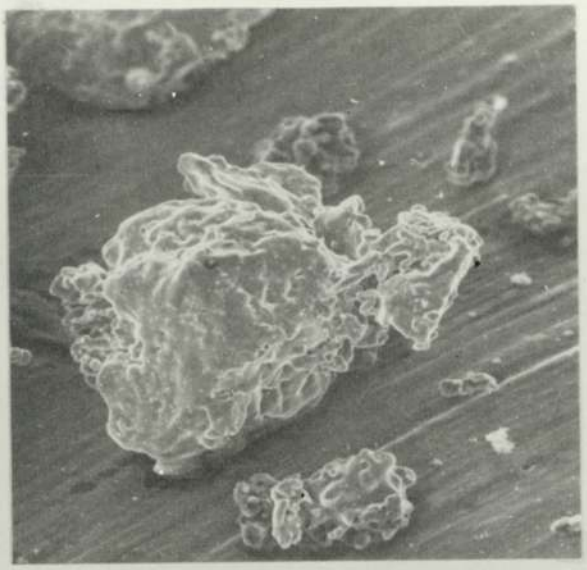

Fig. 3: Rospol MP 32
(x 1000)

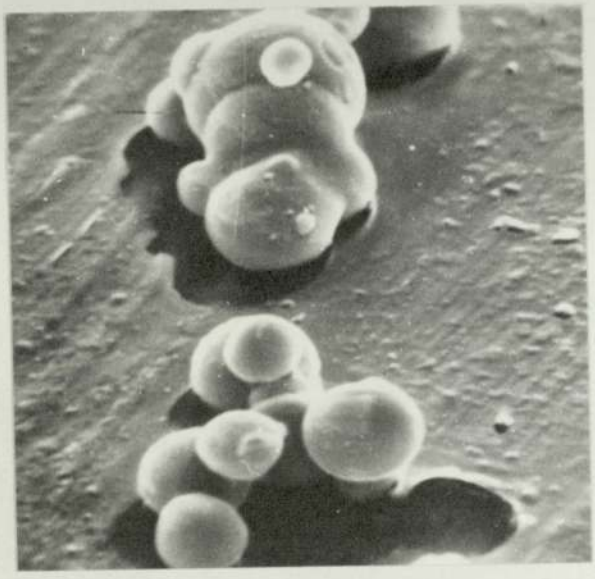

Fig. 4: Carbonyl
(x 1000)

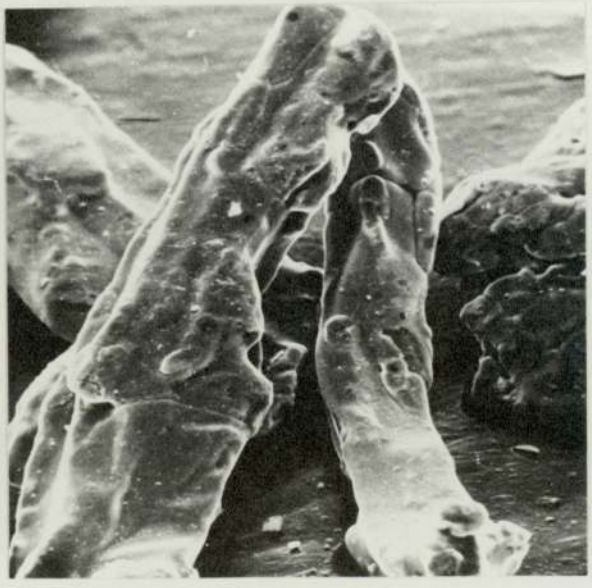

Fig. 5: Electrolytic
(x 1000)

# 2. LITERATURE REVIEW

## 2.1 IRON POWDER CHARACTERISTICS AND PROPERTIES

The term "characteristics of a powder" is complex and incorporates many factors some of which are intrinsically connected and difficult to examine in isolation. In the majority of cases the properties of the sintered compact are greatly dependent on the properties of the initial powder and only in very few cases is there little or no correlation. Evidence of a relationship between powder manufacturing process and the properties of subsequent sintered compacts is provided by POSTER[10] and LEADBEATER et al[11], who conducted detailed surveys. It is apparent from their work that there are two dominant features of the powders which determine sintered properties.

The first concerns the properties which determine pressing quality. These include the size, shape, density, purity, plasticity and surface conditions of the powder particles. The second is closely allied with the first in that it concerns the particle size distribution of a powder, where a certain proportion of fine particles is beneficial to the finished properties.

Further work by KRISHNAMOORTHY[12] analysed the effects of differing powder manufacturing processes on finished properties and indicated that the effects are more pronounced at lower density levels. This latter effect most probably arises out of the lower pressing pressures used in obtaining low green density levels, where the effect of the initial morphology is still prevalent. The particle deformation involved in obtaining higher densities is sufficient to eradicate much of the effect of initial particle morphology.

The most important property is final density and it was found that mechanical properties such as tensile, impact strength and elongation increased as densities were raised[13]. The decreases in ductility and impact strength accompanying increases in tensile strength in wrought and cast materials is well known and the reverse behaviour observed in sintered materials might be thought anomalous. It must, however, be realised that it is the reduction in porosity which accounts for this effect in sintered materials and at 0% porosity the behaviour of sintered materials should be no different from conventional materials.

Numerous attempts have been made to formulate equations relating density or porosity to specific properties. The work of McADAM[14] showed that modulus of elasticity was dependent on porosity but not particle size. The following equation was fitted to the experimental results obtained:

$$E = 29\ (1 - \nu)^{3.4} \times 10^6 \text{ p.s.i.} \qquad \ldots\ldots (1)$$

A high degree of correlation was observed and extrapolating to zero porosity the value of the modulus of elasticity was found to be in good agreement with that of low carbon steels. EUDIER[15] also carried out similar experiments and produced a theoretical relationship comparing the strengths of porous with fully dense materials. The equation relating the relative ultimate strength is:

$$\frac{R}{Ro} = 1 - KE^{\frac{2}{3}} \qquad \ldots\ldots\ldots\ldots\ldots (2)$$

Where E = porosity

This equation was based upon calculations of the reduction in load bearing section due to the pores and for low levels of

porosity, (< 10%) was in good agreement with the experimental results. The deviation of the experimental results from those predicted by theory at high levels of porosity would seem to suggest that the major factor is not simply reduction of load bearing section. It is feasible to suggest that stress concentration effects may be responsible for this deviation as these are not accounted for in the equation. At low levels of porosity, pore spacing can be expected to be relatively large, such that stress concentrations, due to the widely spaced pores, were ineffective explaining the good agreement with the theory observed at low levels of porosity.

The work of MORGAN[16] showed a relationship between the modulus of elasticity in compression and porosity, where the expected rise in modulus occurred with decreasing porosity. An interesting point arises out of the modulus values found at low strains which leads to the suggestion that the metal matrix itself is being examined as the stress is not high enough to exceed interparticle weld strength.

The effects of density on many properties are well documented and there is general agreement that as density increases there is a rise in properties.[10, 11, 13, 17-19]

Particle size has been well investigated, the general consensus of opinion being that strength rises accompany reduction in particle size.[10, 11, 17, 18] From these, particle shape is perhaps a more important parameter than particle size with respect to properties. Bulk properties such as compressibility, green strength and apparent density are dependent upon particle shape[9]. Sintered density is also a function of particle shape since it depends on the behaviour of particles under compression[14]. In

addition to this effect on sintered density particle shape influences the modulus of elasticity which exhibits a decrease as particles become increasingly irregular. Particle shape is responsible for the resultant pore shape which is irregular with irregular shaped particles. Tensile strength increases as particles become spherical[20, 21] and this is due to the more spherical pores produced as a result of sintering compacts of spherical particles. The suggested explanation for the effect of pore shape is that irregular pores have a notch effect[22]. Further evidence substantiating this suggestion is that microcracks have been found to initiate at pores of irregular shape[23]. An explanation of microcrack formation is that the pores cause stress concentrations and local plastic deformation is inhibited by the surrounding matrix with consequent build up of stress, eventually exceeding the cohesive strength of the matrix and giving rise to microcrack formation.

At this point it is thought useful to discuss the comparisons which have been made between P/M parts and cast irons[13, 17]. The justification for this arises from previous work on the internal deformation of cast iron where graphite is likened to voids in a steel matrix[24-30]. In order to develop an understanding of the internal deformation of sintered compacts it is perhaps beneficial to closely examine any possible similarities with cast irons.

In their original work SCHWARTZ and JUNGE[24] investigated the density/modulus of elasticity relationship for cast irons concluding that this was linear. They concluded that the graphite acted as voids within the matrix and the modulus was in fact

proportional to the volume of metallic phase present when the matrix was interrupted only by graphite as approximately spherical voids. Further to this was the fact that graphite in the flake form caused a greater decrease in modulus than an equivalent amount of graphite nodules. This latter effect was because stress concentrations associated with flakes were greater than those associated with nodules. This is analagous to the increased notch effect of irregular pores over spherical pores.

MEYERSBERG[25], carried out extensive work on the internal deformation of cast iron, extending the fundamental researches of THUM and UDE[26-28]. It was concluded that a graphite flake transmitted no tensile stresses and was in fact equivalent to a void. This confirmed the earlier work[27] where notched steel plates were used to simulate cast iron with a good degree of success. It was concluded that the role of graphite could be defined by two factors. These were, the distribution of graphite with respect to the resultant reduction in cross-sectional area and the notch effect defined by the form of development of the graphite.

Research in this field was continued by GILBERT[29, 30] who carried the development a stage further. Although it has been demonstrated earlier that for a cast iron containing 2.5% graphite this would occupy a cube of side 44% of the cast iron cube, the possible resultant reductions in cross-sectional area which it was shown were variable, could not account for the average 50% reduction in modulus as compared with steel. From an examination of the manner in which lines of stress were forced to deviate around the graphite flakes, it was possible to show that this had

an equivalent reduction in cross-sectional area and as such accounted for the corresponding additional reduction in modulus. It was further demonstrated that graphite had a notch effect which caused deviations from linearity of the stress/strain curve, even at low values of stress.

It was demonstrated also that the notch effect of a graphite flake is greater than that of a graphite nodule.

It is interesting in view of the obvious similarities that cast irons suffered the same problems of acceptance as structural materials as is experienced by sintered materials. Abraham Darby, however, seems to have found a way to overcome these problems and his structure at Ironbridge proudly stands today, a tribute to his ingenuity. This merely serves to reinforce the view that many problems can be overcome if materials are chosen which fit the purpose.

## 2.2. FRACTURE MECHANICS

### 2.2.1 THEORY

Fracture mechanics is the continuum mechanics analysis of fracture which has proved extremely useful for assessing the behaviour of elastic bodies containing crack-like defects. A critical appraisal of fracture mechanics concepts and their applicability to general engineering design has been published by WEI and YUKAWA[31]. A paper by BARNBY[32] reviews the theory and shows how the original fracture concept developed by GRIFFITH[33] was modified by IRWIN[34]. The Griffith analysis refers to an elliptical through crack of length 2c in an infinite plate in tension. It is an energy approach in which the surface energy required for the production of new surfaces is equated with

release of stored elastic strain energy when the crack extends. The relevant material property in this case is the specific free surface energy and the resultant simple formula is :-

$$\sigma_F = \sqrt{\frac{2E\gamma}{\pi c}} \qquad \text{.....(3)}$$

where $\sigma_F$ is the fracture stress, E, the modulus of elasticity, $\gamma$ the surface energy and C, the half crack length. IRWIN[34] first modified this approach by using a material property, $G_c$, in place of the surface energy term, $2\gamma$, in the Griffith theory. $G_c$ was defined as the total energy absorbed during cracking per unit increase in crack length, per unit thickness. Where extensive plastic deformation occurs at the crack tip in addition to the production of new surfaces $G_c$ includes this, an advance on the Griffith theory which neglected the stress problems.

Irwin went on to review the theories of crack tip stress in elastic bodies and applying the equations of SNEDDON[35] and WESTERGAARD[36] noted that the local stress distribution was always of the same form, described by:-

$$\sigma_L = \frac{K}{\sqrt{2\pi x}} \qquad \text{.....(4)}$$

where $\sigma_L$ is the local tensile stress, x the distance ahead of the crack tip and K, a constant determining the level of the stress distribution, Fig. 6. As the distribution of the local tensile stress is always of the same form in the region ahead of the crack tip, the criterion for failure can be taken as the attainment of a sufficiently high level of stress distribution. The constant K, can thus be defined as the stress intensity factor having a critical value at the onset of fracture.

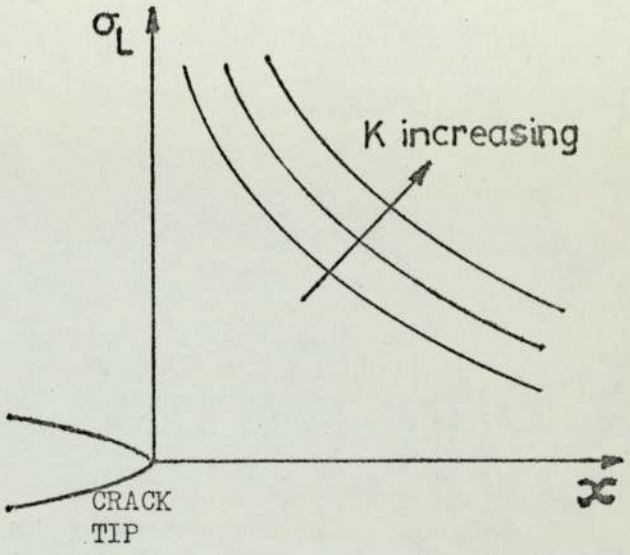


Fig. 6 - Local tensile stress distribution at crack tip

Invoking the principle of virtual work Irwin proved that the attainment of a critical stress intensity factor, $K_c$ was exactly equivalent to the Griffith approach which required the attainment of a stored elastic strain energy, $G_c$. It was further proved that $K_c$ and $G_c$ were related:

$$K_c^2 = E^1 G_c \quad \ldots\ldots\ldots\ldots\ldots\ldots (5)$$

where $E^1$ is the relevant extensional modulus, being equal to Youngs Modulus, E for plane stress and $E/1 - \nu^2$ for plane strain ( $\nu$ = Poisson's Ratio). The simple Griffith formula could then be rewritten:

$$\sigma_F = \sqrt{\frac{E^1 G_c}{\pi c}} = \frac{K_c}{\sqrt{\pi c}} \quad \ldots\ldots\ldots\ldots (6)$$

$G_c$ and $K_c$ are thus material properties representing the resistance to fracture at $\sigma_F$ and at stresses lower than $\sigma_F$, G is the non-critical crack driving force and K, the non-critical stress intensity factor.

The above advances are the basis of the sophisticated theory of fracture mechanics as it is known today and are major contributions

to engineering theory. The more general use of $K_c$ instead of $G_c$ to represent the fracture toughness of a material arises from the need to use the relevant values of $E^1$ as scaling factors. When comparing the fracture resistance of two materials the use of $K_c$ circumvents the latter necessity.

It is evident that plastic deformation at the crack tip gives rise to the formation of a plastic zone within which mico-structural damage is initiated preparing the way for fracture. If the plastic zone size is small in comparison to the dimensions of the body, the macroscopic behaviour can be approximately elastic except within this small region at the crack tip. Adopting this latter as the basic premise the theory of linear elastic fracture mechanics, (LEFM) can be applied to design problems.

The process of initiating microstructural damage within the plastic zone consumes most of the energy of fracture and therefore the size of the plastic zone is an important feature. The load carried by a purely elastic stress distribution must be borne by the material within the plastic zone at a constant stress level $\sigma_{Y.S.}$, the uniaxial yield stress. The size of plastic zone generated is very dependent on the state of stress at the crack tip. In thin sheets in tension containing through cracks, conditions are those of plane stress where crack tip stresses lie in the plane of the sheet and stress in the thickness direction is virtually zero. The tensile stress in the plastic zone is the uniaxial yield stress and fracture occurs on $45^{\circ}$ shear planes through the plastic zone. As sheet thickness increases, however, tensile constraint stresses arise in the thickness and width

Fig. 7: Triaxial stresses in the centre of thick plate specimen

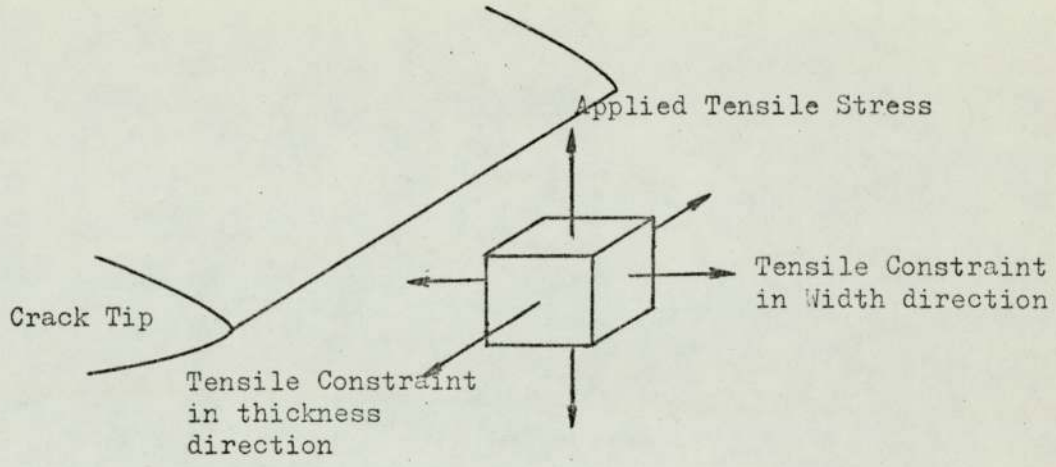


directions, Fig. 7. This arises out of the large plastic stretch occurring within the plastic zone, the surrounding material being required to undergo a large Poisson contraction. Material remote from the crack tip resists this contraction setting up tensile constraint stresses in the width and thickness directions. This results in a hydrostatic state of stress at the crack tip and the resolved shear components of the local stress are reduced such that yielding cannot occur until the local stress reaches a value of about three times the uniaxial yield stress. The actual degree by which the yield stress is raised depends on whether the Tresca or Von Mises yield criterion is applied. This results in a reduced plastic zone size as shown in Fig. 8. (see over)

The radius of the plastic zone is given by

$$r_p = \frac{1}{A}\left(\frac{K_c}{\sigma_{Y.S.}}\right)^2 \qquad \ldots\ldots\ldots\ldots\ldots (7)$$

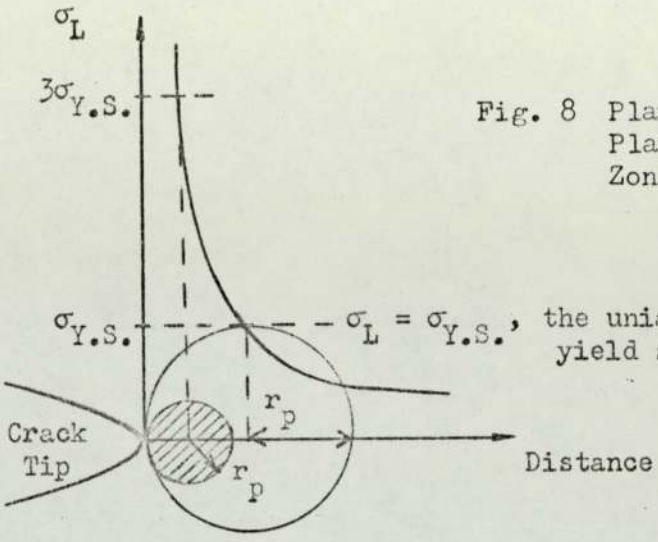


Fig. 8 Plane Stress and Plane Strain Plastic Zones

where A is a constant equal to $2\pi$ for plane stress and equal to $4\sqrt{2}\,\pi$ for plane strain. The reduced plastic zone under plain strain conditions gives rise to a flat fracture whose crack faces are normal to the applied stress.

At free surfaces no constraint stresses in the thickness direction may exist and therefore conditions approach those of plane stress. The net result is a mixed plastic zone whose size at free surfaces is that for plane stress conditions, decreasing in size along $45^{\circ}$ shear lines into the thickness until it attains a size corresponding to plane strain conditions, Fig.9.

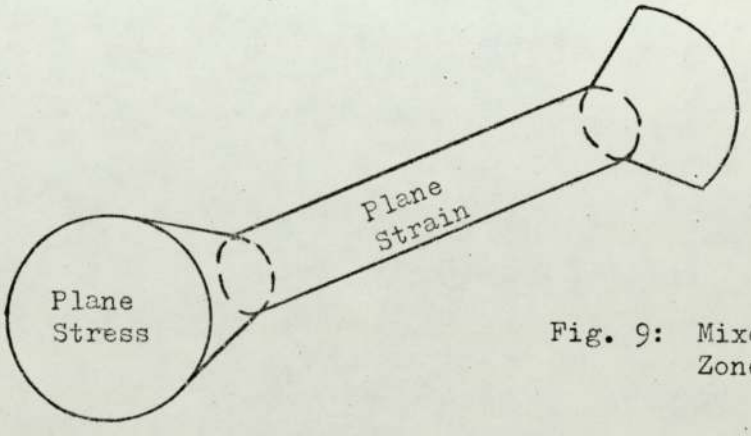


Fig. 9: Mixed Plastic Zone Size

It is found that as thickness is increased or decreased the size of plane stress regions remains constant.[37] In thin sheets the extent of the plane stress plastic zone is limited by the sheet dimensions and gives rise to $45^{\circ}$ shear failure in such material. At greater thicknesses the regions of plane stress plastic zone become a negligible proportion of the total, this being so when the plane strain zone occupies 90% of the total thickness. This gives rise to the formation of shear lips at the edges of the specimen. As the plane strain zone consumes less energy than the plane stress zone, the value of $G_c$ or $K_c$, decreases as sheet thickness increases, and once the plane stress regions become negligible the value of $G_c$ or $K_c$ reaches a minimum level which is termed $G_{IC}$ or $K_{IC}$, the plane strain fracture toughness.

A further pure size effect enters into the analysis relating crack length to specimen width where a factor may be used to relate this ratio to the geometry of specimen or loading. Equation (6) can be rewritten to incorporate this factor.

$$K_c = \sigma_F . Y' \qquad \ldots\ldots\ldots\ldots (8)$$

Y is thus a geometrical factor, equal to $\sqrt{\pi}$ in the Griffith analysis (equation 6) and $Y^1$ incorporates in addition a. K-calibration curves for a given class of geometry may be constructed by plotting Y against the ratio of crack length to gross specimen width, $^a/_W$, as shown in Fig. 10.

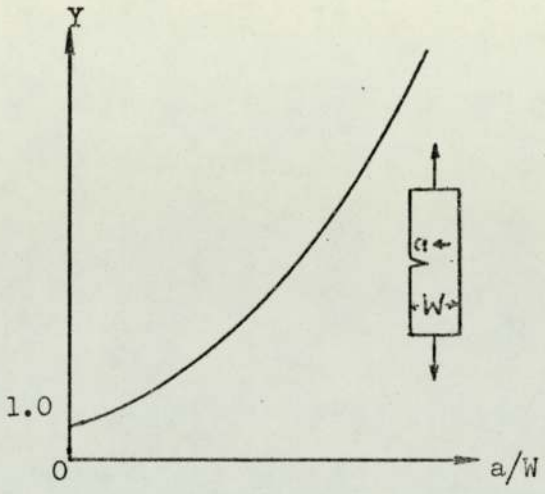


Fig.10: K-calibration Curve for a single edge notched specimen in tension.

For this particular class of geometry use of the appropriate Y-value accounts for changes in the ratio, $a/W$. Different classes of geometry will naturally require different K-calibrations, and where the cracking mode is varied, K-calibration curves are equally applicable. The possible modes of cracking are described in Fig. 11 and a K-calibration can be applied to each mode.

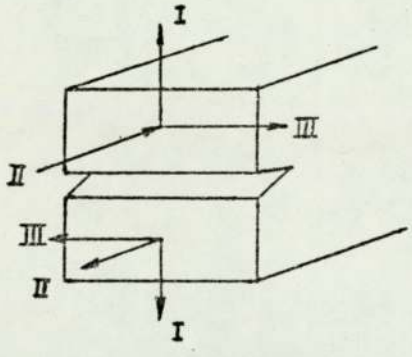


Fig.11: Cracking Modes.
Mode I - Tensile
Mode II - In-Plane Shear
Mode III - Anti-Plane Strain

Considerable effort has been directed towards establishing K-calibration curves for the above cracking modes and are to be published in the form of tables of Y-values by ROOKE and CARTWRIGHT, (in ref. 32).

Details of testing procedure to obtain plain strain fracture toughness values is laid down in B.S.I. Draft for Development No.3 and a brief description is given below.

Single edge notched 3-pt. bend specimens with a 4:1 span to width ratio are used in this work and consequently the relevant

test procedure for this type of specimen only will be given. Specimens are pre-cracked in fatigue under controlled conditions in order to give a sharp crack. In fatigue the maximum and minimum stresses are characterised by maximum and minimum stress intensities, $K_{max}$ and $K_{min}$. The difference between these, $K_{max}$ and $K_{min}$ is termed $\Delta K$, the fatigue stress intensity, calculated as below:

$$\Delta K = \frac{\Delta P Y}{B W^{\frac{1}{2}}} \qquad \ldots\ldots\ldots\ldots\ldots (9)$$

where $\Delta P$ is the applied load range, Y the relevant factor for this class of geometry and loading, B specimen thickness and W the gross specimen width. The maximum value of $\Delta K$ should not exceed $0.67K_c$ in order to ensure a sharp crack and the absence of blunting of the crack tip. As an added precaution, it is recommended that the last 0.125 mm of crack growth should occur in not less than 50,000 cycles. The total crack length, (machined notch plus fatigue crack) must result in a crack length to width ratio, $a/W$, between 0.45 and 0.55 for the test to be valid. Included in the specifications are details concerning the straightness of the fatigue crack front which must not deviate by more than 2.5%W at positions corresponding to 25%, 50% and 75% of the thickness and at the surfaces by not more than 5% of the width.

In toughness measurement, linear elastic conditions are satisfied if a plot of applied load versus the opening displacement at the notch mouth is linear up to fracture. Deviations from linearity can arise from two sources, either development of an excessive plastic zone or because cracking has commenced, Fig.12.

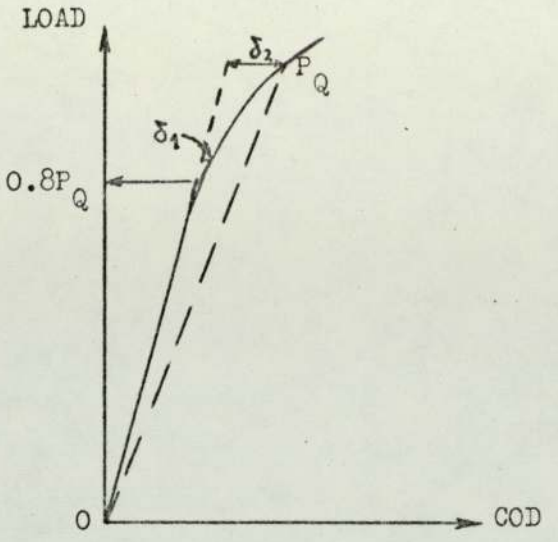


Fig. 12: Load vs. Crack Opening Displacement

If all the deviation, $\delta_2$ is due to cracking, unloading will proceed down the slope $OP_Q$ to zero due to an effective drop in modulus. $P_Q$ is taken as the load corresponding to the gross stress at fracture and the line $OP_Q$ is a secant having 5% less slope than the elastic slope of the initial trace. Load versus some measure of opening displacement is monitored by means of a clip gauge and an X-Y recorder. It is shown by experience that if the deviation from linearity, $\delta_1$ at $0.8P_Q$ is less than one quarter of the deviation at $P_Q$, $\delta_2$ then $\delta_2$ is almost entirely due to cracking and corresponds to an extension of the crack of about 2% of its initial length.

The test corresponds to linear elastic conditions if the above conditions are fulfilled. The corresponding toughness value may be evaluated from:

$$K_Q = \frac{P_Q Y}{BW^{\frac{1}{2}}} \qquad \ldots\ldots\ldots\ldots\ldots\ldots (10)$$

In order to assess whether $K_Q$ corresponds to the minimum value, $K_{IC}$, the following equality should be applied:

$$B > 2.5 \left(\frac{K_Q}{\sigma_{Y.S.}}\right)^2 \qquad \ldots\ldots\ldots\ldots\ldots\ldots (11)$$

The value of 2.5 is arbitrary but ensures that plane strain conditions are fulfilled for most materials and the $K_Q$ value is then the $K_{IC}$ value.

A crack opening displacement method (COD) for measuring toughness is applicable to ductile materials of low yield strength where the requisite thickness to attain LEFM conditions is prohibitively large due to the generation of large plastic zones. This method was developed by WELLS[38] and is based on the attainment of a critical opening displacement at the crack tip to produce fracture.

With reference to Fig. 8, the crack can be thought of as having a 'notional tip' a distance $r_y$ ahead of the real tip and a plastic region extending a distance $r_y$ beyond this. At the original crack tip there is a displacement of the crack faces almost parallel to their original position, Fig. 13

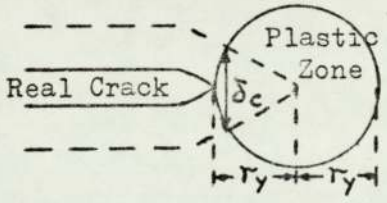


Fig. 13 Opening Displacement at Crack Tip

The opening displacement at the real tip when cracking commences is that which obtains when a critical level of stress intensity is attained, i.e. $K_c$. It has been further demonstrated[39] than an adequate measure of toughness is afforded by $\delta_c$ even beyond the range of LEFM conditions. Furthermore, the crack opening displacement can be related to LEFM parameters throughout the range of LEFM conditions and almost up to general yield,

(about $\sigma/\sigma_{Y.S.} = 0.8$):

$$G_c = n \sigma_{Y.S.} \delta_c \qquad \text{.....(12)}$$

where n is a factor arising out of yield stress elevation within the plastic zone, being equal to 1 for plane stress and 2 for plane strain. Even beyond general yield $\delta_c$ is a good measure of toughness but cannot be precisely linked with LEFM parameters. Equation (12) still holds beyond general yield if plane stress conditions prevail. Under plane strain conditions beyond general yield the unknown triaxial stresses within the plastic zone give rise to difficulties.

### 2.2.2 MECHANICAL PROPERTIES OF SINTERED MATERIALS AND APPLICATION OF FRACTURE TOUGHNESS TESTING.

P/M components have found their main use in relatively lowly stressed applications. This may be due, in part, to the lack of fundamental understanding on the part of both producers and designers alike. The main problem is the design of suitable testing techniques with respect to fitness for purpose of sintered materials. It is so often the case that a sintered material meets specified strength levels but is rejected on the grounds of low ductility and indeed this is a big drawback to the acceptance and use of sintered components. Add to the above problem the difficulty of determining the precise nature of service loads and how these can be related to the basic properties of sintered materials. These and allied problems appear to be the major limitations to the expansion of the P/M market into the field of relatively highly stressed structural components.

Porosity is a major controlling factor as far as strength properties are concerned and as this decreases strength rises, at first slowly and then rapidly. Since porosity is such an important parameter it is pertinent to discuss its effect on various mechanical properties. A decrease in porosity is accompanied by rises in strength[13,18] and an increased work hardening exponent, approaching the value for annealed very low carbon steels at 0% porosity[40]. In addition, Poisson's ratio for plastic deformation is observed to be less than 0.5, approaching 0.5 at 0% porosity[40]. Porosity therefore, has a pronounced effect on the deformation characteristics of sintered materials.

A more important observation as far as design considerations are concerned is the fact that as porosity is reduced not only does strength increase but increases in elongation and impact resistance are also observed, a reversal of the effect observed in wrought or cast materials.[13] The fracture toughness of sintered materials has been shown to increase as the percentage porosity is reduced.[41,42] Since it has been established that porosity plays a major role in determining mechanical properties it still remains to evaluate the nature of this role and examine porosity in greater detail.

Incorporated in the general term porosity are other factors of importance such as its geometry, size and distribution. These factors have been shown to exert considerable influence on mechanical properties, where pore shape appears to be of particular importance.[20,21] Increasing irregularity has a detrimental effect on strength, a fact whichis attributed to the greater 'notch' effect of irregular pores compared to spherical or rounded pores.[19,22]

It has been suggested that the decrease in elastic modulus exhibited by porous bodies should be related not only to the total volume of pores but also to their dimensions[43] and indeed, this is an important consideration. A pore will act as a concentrator of stress and strain depending on its relative size and shape,[44] small rounded pores being less effective than angular pores. The tendency for neighbouring pores of radius, r and spacing, x to join by internal necking increases as the ratio of x to r becomes smaller and as r increases internal necking type fracture becomes prevalent.[44] Fracture paths connect pores by the shortest possible route and the fracture surface thus depends on the 3-D pore distribution.[19] The development of plastic zones around pores which extend and overlap gives rise to a 'weakening' of the load bearing cross-section. The mean pore spacing, dependent on pore size and distribution can therefore be recognised as an important factor.

A considerable amount of work has been carried out on the development of models of microvoid coalescence[45-48] and the mathematical problems connected with the analysis of three-dimensional distributions are extremely complex. The majority of this work was done in connection with the development of microvoids around inclusions but nevertheless it can be applied on a general basis to porous bodies where the 'microvoids' exist initially. Pores commonly found in sintered materials are of irregular geometries and have wide size ranges. The situation is far from the ideal, i.e. regular arrays of voids of equal size, assumed in the development of the above models, not only for solid materials but also for porous materials. These models therefore, can be

used to explain some of the features of sintered materials.

In one model[46], where specimens containing through thickness holes of cylindrical geometry were tested, it was demonstrated that if the hole diameters were large or the spacing small low strain fracture resulted due to coalescence. Consequently, large volume fractions of voids can be said to promote low strain fracture. Extending this to sintered materials it can be readily understood that increasing porosity leads to lower ductility. A further model[47] showed that when void spacing was large it is easier to deform the body 'en masse' then to produce internal necking between voids. This latter observation serves as an explanation of the increased ductility of sintered materials at low levels of porosity. Volume fraction of voids is thus expected to be the main single factor controlling ductility where the work hardening exponent decreases with increasing volume fraction of voids[49], a characteristic observed in sintered materials as stated previously.[41]

A very limited amount of work has been carried out on the deformation of sintered materials and the information that is available is mainly qualitative. It would, however, seem necessary to understand fundamental behaviour under applied loads with a view to future applications as structual parts not only as replacements for more costly conventional materials but also in their own right. Before the engineer can incorporate the requisite safety margins in design it is important to understand the basic material behaviour. Analysis of the behaviour of sintered materials is likely to be complex due to the three-dimensional distribution

of porosity. The situation could perhaps be simplified by estimation of upper and lower bounds using existing theories for 100% dense materials. An example of this might be the equating of pore shape to simple spheres or ellipsoids and applying upper and lower bounds to this type of analysis. Ideally, simple design rules are required and until this situation arises the 'status quo' will be maintained and the use of sintered materials will be restricted to relatively lowly stressed applications. Some examples of designing with sinterered materials are provided in the literature[50] but a basic lack of knowledge of the stress-strain behaviour of these materials would seem prohibitive.

The plane strain fracture toughness of a material, $K_{IC}$ which is proving a useful design parameter for conventional materials may be a means of overcoming some of the basic design problems. Fracture toughness testing, although expensive could perhaps be modified for use in connection with sintered materials. This modification would entail a simplifying of the test and allow one to dispense with the large amount of expensive ancillary equipment required. An example of this, would be the substitution of the standard fatigue pre-cracked specimen by a simple notched specimen of small root radius avoiding the need for fatigue machines. The plastic zone at the tip of a fatigue crack is less extensive than that that at the root of a machined notch[51] and LEFM applies strictly to sharp cracks but this procedure has been shown to yield an adequate measure of toughness.[41] TETELMAN[52] has already demonstrated that below a certain root radius (0.254 mm) no decrease in toughness $K_{IC}$ occurs as root radius is reduced. The need for ancillary

equipment such as clip gauges and X-Y recorders can be overcome if, as suggested by BARNBY[41], some accurate measure of bend angle can be made and crosshead movement of the testing machine is monitored.

A very limited amount of work has been published to date on the fracture toughness of sintered materials but some work is being carried out in industry.[53,54] A paper on iron powders[41] describes the effect of density and copper and copper/carbon additions on toughness. The most significant point to arise from this report is the increase in toughness observed with increase in yield strength, a reversal of the situation observed for wrought and cast materials. In order to understand this apparent paradox the reasons for the raised yield strength must be sought. It is clear that the yield strength can be raised by reducing porosity on the one hand and by strengthening the matrix by conventional metallurgical means on the other. It can be expected that this observed relationship tends towards a limit, sensibly at 100% density where material behaviour should parallel that observed for conventional materials. Obviously, the levels of porosity obtained near 100% density are of little interest to the powder metallurgist except in the case of sinter forging or powder rolling. The area of particular interest is the area where this relationship is observed, i.e. 6.2-7.0 $Mgm.m^{-3}$ for iron compacts and a combination of reducing porosity and metallurgical effects may prove fruitful. This would possibly lead to wider acceptance of sintered materials for use as stressed structural parts.

An additional limitation to the use of sintered parts is their relatively small sizes. This pure size effect was highlighted by BARNBY et al[41] by use of the simple formula for critical defect size:

$$a_c = \left(\frac{K_{IC}}{\sigma_w}\right)^2 \cdot \left(\frac{1}{Y}\right)^2 \qquad \ldots\ldots\ldots\ldots (13)$$

where $\sigma_w$ is the working stress and Y is a geometrical factor taking account of loading and specimen geometry. The important factor is Y which appears in the denominator as a square term. The Y-value increases as the ratio of defect size to gross specimen dimensions increases such that the smaller the component the smaller the tolerable defect size. This indicates that the 'brittleness' is not simply an inherent material property but is exaggerated by the limited size of sintered components. Unfortunately, the size of components is limited by compacting parameters, themselves severely constrained by economic factors and it is difficult to envisage the elevation of limiting size by future development of present techniques. The small scale of components is thus an inherent problem of sintered materials and it is thus necessary to increase toughness by attention to other relevant parameters.

Once it is established where the main area for development lies the task of increasing the toughness of sintered materials can be initiated. There is a limit to reducing porosity by the normal compacting process which is mainly due to economic factors. As compacting pressure increases the die-wear problems become severe and it is more difficult to maintain tolerances due to elastic deformation of the tools. Porosity may be reduced by thermo-mechanical treatments such as sinter forging or powder rolling and here residual porosity and oxide inclusions become extremely important. In this respect fracture toughness data is very useful for calculating critical defect sizes and safe working stresses.

It has been observed[42] that whilst the amount of porosity affects toughness the grain size and pore geometry exert little if any effect. This is an important finding as the current process employs powders of different size distribution and morphology with resultant differing pore geometries. If toughness is not sensitive to variations in pore geometry then toughness values measured at the same density for different types of powder should not be variable. This fact has been established on the basis of limited data for one material, namely 316L stainless steel[42]. It remains for this observation to be confirmed for other powders especially where alloying elements may alter pore geometry significantly.

Relationships such as that proposed by KRAFFT[55] attempting to relate toughness to basic tensile properties might seem applicable to sintered materials. This was an attempt to relate the modulus, E, strain hardening exponent, n, and the spacing of defects, $d_T$, to the plane strain fracture toughness, $K_{IC}$.

$$K_{IC} = En\sqrt{2\pi d_T} \qquad \ldots\ldots\ldots\ldots\ldots (14)$$

It is difficult to assess the defect spacing for porous bodies but as a first approximation it might be considered to be the interpore spacing. Unfortunately the situation is far from simple as any number of small defects may be present between pores. These can be expected to be very small pores, especially at grain boundaries resulting from interparticle welds which act as vacancy sinks during sintering, and oxide inclusions within interparticle bonds as a result of break up of oxide films during

compaction. The distribution of these defects is by no means regular and it is this fact which renders the application of the Krafft relationship to sintered materials doubtful.

The most fruitful direction in which to progress would seem to be an attempt to correlate a simple property such as tensile strength with fracture toughness. It may be possible to show that the two tests are not dissimilar in the case of sintered materials and that the tensile test is merely a small scale toughness test.

In conclusion there would appear many areas which warrant extensive investigation and fracture toughness would seem to be an important material property directly applicable to design problems.

### 2.2.3 FRACTURE MECHANISMS

Fractographic studies of sintered materials is difficult due to the 'in and out of plane' nature of the fractures produced. The use of the scanning electron microscope (S.E.M.) can considerably aid the interpretation of fracture surfaces due to the large depth of focus afforded by this instrument. It is important to establish the micromechanisms of failure in sintered materials in order to gain an understanding of the effect of porosity on bulk properties. In the model for microvoid coalescence developed by THOMASON[47] a state of triaxial stress is said to exist between voids and if triaxial stresses exist between the pores in a sintered material this will markedly affect the fracture mode. It has been further demonstrated[48] that even small increases in triaxiality within a specimen increase the rate of void coalescence. The importance of the latter cannot be too highly stressed particularly

where some notch like feature of component geometry such as grooves, fillets and keyways can generate hydrostatic stress states.

Observed fracture paths are from pore to pore and on tensile testing stringering or drawing out of porosity has been reported[56]. The macromechanism of fracture is necking down of the ligaments between voids and the micromechanism is one of ductile dimple formation within these ligaments[41].

## 2,3 FATIGUE

### 2.3.1 HISTORICAL

The failure of metallic materials under alternating loads has been a problem to engineers and metallurgists for many years. The fact that this is an insidious failure mechanism with no permanent deformation to warn of impending catastrophic fracture renders it all the more dangerous. The problem was recognised as early as 1823 when ALBERT[57] carried out crude fatigue tests on mine-hoist chains. Later in 1843 it was RANKINE[58] who, whilst examining failure of railway axles, recognised the importance of avoiding sharp angles and abrupt section changes in fatigue situations. Much early research was carried out by WOHLER[59] who constructed the first testing machine. The main outcome of this work was the realisation that fracture could occur at stresses not merely below the tensile strength but below the elastic limit and that there existed a fatigue limit, below which an infinite number of cycles could be endured. These were two fundamental 'laws' of fatigue and were a useful contribution to the then limited knowledge of the fatigue process.

As time progressed engineers turned their attention to the process of fatigue but it was not until 1900 that any attempt was

made to attack the problem from a microstructural aspect. EWING, ROSENHAIN and HUMFREY[60,61] observed the formation of slip bands and fatigue cracks in iron crystals which was later confirmed by GOUGH and HANSON[62]. About this time the theory that fatigue cracks resulted from localised stresses exceeding the rupture strength of the metal was advanced by GILCHRIST[63].

In experiments to determine the cause of fatigue failure, LAUTE and SACKSE[64] were able to show by testing and intermediate annealing that internal strain hardening and damage to the metallic crystals were the main contributory factors. More recent work has confirmed this[65-67] where slip has been inhibited in single crystals by means of testing at suitable temperatures, e.g. Germanium at room temperature and Zinc at -196°C at which complete resistance to fatigue is exhibited.

Considerable effort was expended in studying the behaviour of metallic materials when subjected to cyclic loads but no general fatigue law could be advanced at this stage. In 1939 OROWAN[68] developed a model for the fatigue process. About this time GOUGH and WOOD[69] were able to show by means of X-ray techniques that the processes involved in fatigue fracture were identical to those occurring in static fracture. The essential difference was that in fatigue the process was localised. Orowan had realised that high localised stresses were important and was able to incorporate this feature of the fatigue process in a model. The model consisted of a stiff spring, representing the overall elastic behaviour of the body, in parallel with a weaker spring itself in series with a plastic element. The weaker spring and the plastic element represent localised plastic behaviour responsible for the energy consumption during cycling but the overall stiffness is very nearly that of

the stiff spring. Orowan envisaged that the plastic element was physically located at the crack tip and ahead of this plastic strains were relaxed in a region of steeply varying stress. There was thus a local strain distribution ahead of a crack tip and, up to some distance beyond, the strain exceeded the fracture strain of the material. During cycling progressive rupture occurred at a rate determined by the stress amplitude.

This model contributed considerably to our understanding of the fatigue mechanism, being consistent with many of the phenomena associated with the process but it did not incorporate the important features of plastic behaviour[70]. On reversing the stress, effective yield stresses are lower than those in the forward direction, an effect observed by BAUSCHINGER[71] and subsequently taking his name. The tensile and compressive half cycles were not symmetrical due to crack closure which occurred in compression. The differences in effective forward and reverse yield stresses has been observed to be very great in two phase materials[72] particularly with high strength second phases. The effect was observed to disappear after a very low number of cycles[73] showing that symmetry was soon established with respect to forward and reverse yielding. It is important to realise that during the compressive half-cycle stresses were not concentrated at the crack tip due to crack closure. This resulted in a plastic zone of only one quarter the size of the original produced during the tensile half of the cycle. The original plastic zone spread from the crack tip during the tensile half-cycle reaching a maximum size determined by the magnitude of the maximum applied tensile stress. With unloading to zero the plastic deformation was reversed by the spread of a reverse

plastic zone from the crack tip. At zero load the plastic deformation in the forward direction was just reversed, although the extent of the plastic zone was only about one quarter the size of the forward plastic zone. During the compressive half-cycle nothing further happened as the stress was not concentrated due to crack closure.

Many empirical laws have been advanced since that time and have been shown to fit the data obtained in tests on various materials. More recently the continuum mechanics analysis of fracture has been applied to fatigue with a limited degree of success. The existing fatigue laws and the more recent developments are reviewed in subsequent sections.

### 2.3.2 EMPIRICAL FATIGUE LAWS

A considerable amount of experimental fatigue data has been accumulated over the years and has resulted directly in the postulation of many empirical laws of fatigue. These laws are utilised in design against fatigue failure but it is important to note that these laws are not general and can only be applied to materials which are known to obey them closely.

One of the most common methods of representing fatigue data is in the form of an S-N curve, where stress amplitude, S is plotted against the logarithm of the number of cycles to failure, $N_f$ referred to as the fatigue life. There are two common forms of S-N curve, both showing an initial increase in fatigue life with decreasing stress amplitude. Some materials exhibit a 'knee' in the S-N curve, the fatigue limit which generally represents some stress amplitude below which failure never occurs, generally at $10^5$ - $10^7$ cycles. This effect has been attributed to strain ageing[74] and occurs notably

in mild steel and low carbon, low alloy steels. Other materials such as aluminium do not exhibit fatigue limits, although they have been observed in some aluminium alloys[75] which is said to be a zone ageing effect[76]. From S-N curve data attempts have been made to formulate fatigue laws.

One of the first attempts was made by BASQUIN[77] as early as 1910 from tests at stress amplitudes above the fatigue limit and such that the overall specimen behaviour was elastic. The Basquin relation was:

$$S^a N_f = \text{CONSTANT} \qquad \ldots\ldots\ldots\ldots (15)$$

where the exponent, a, was between 8 and 20 indicating that fatigue life was extremely sensitive to stress amplitude.

One important point had been omitted from the analysis of S-N curves because the system was not completely defined. A mean stress effect was observed and has been discussed at length by POPE[78]. A popular form of expressing this mean stress effect is by means of the Goodman diagram[79]. On a plot of mean stress against stress amplitude for failure in $N_f$ cycles, a line can be drawn joining the stress amplitude for zero mean stress and the maximum mean stress which is sensibly the u.t.s., Fig. 14

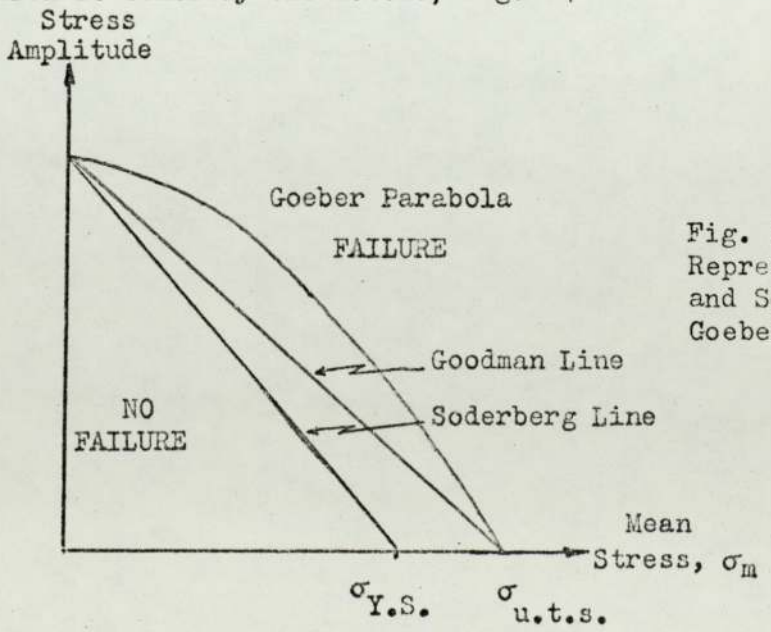


Fig. 14: Mean Stress Effects Represented by the Goodman and Soderberg Lines and the Goeber Parabola.

This line delineates regions of failure in less than $N_f$ cycles to the right and no failure in $N_f$ cycles to the left. This is a useful design guide and a modification by GERBER[80] has been suggested to make it less conservative at low mean stresses. This substitutes a parabola for the Goodman line as shown in Fig. 14. A further modification which is more acceptable from a design viewpoint was suggested by SODERBERG[81]. This approach substitutes the yield stress for the u.t.s. in the Goodman diagram thus producing a similar but more conservative approach, Fig. 14.

The main limitation associated with the above guides to design against fatigue is that they are valid only for uniaxial loading. Components are commonly subjected to more complex stress systems particularly where component shape results in effective notches. Methods are available for analysis of fatigue in more complex states of stress and have been reviewed by POPE[82]. Briefly, these are the maximum shear stress and maximum shear strain energy criterion applicable to ductile metals and the maximum principle stress criterion applicable to brittle metals. These basic criteria arise from elasticity theory and are based on the attainment of a critical value of maximum shear stress, maximum shear strain energy or maximum principle stress respectively. These criteria seem applicable to fatigue but it should be noted that they are no more than empirical guides but once this is accepted they can be successfully applied. Other methods involve the generation of individual S-N curves for various types of loading and invoking the ellipse quadrant law to obtain an S-N curve for various combinations of loading. The above approach is found to be applicable to ductile metals but for brittle metals or notched specimens an ellipse arc law is applicable.

A cumulative damage law which incorporates a fractional life concept was proposed by MINER[83]. This law states that if a material

has fatigue lives of $N_{f1}$, $N_{f2}$, $N_{f3}$..... at stress amplitudes $S_1$, $S_2$, $S_3$..... then for spectrum loading the number of cycles, n spent at each stress amplitude divided by the appropriate value of $N_f$ can be thought of as a fraction of the total life such that:

$$\frac{n_1}{N_{f1}} + \frac{n_2}{N_{f2}} + \frac{n_3}{N_{f3}} + \ldots\ldots = 1 \quad \ldots\ldots(16)$$

Objections to this approach are based on arguments concerning the cumulative nature of the damage[84] and fatigue lives can be seriously over-estimated by this method. The loading sequence is found to influence the process considerably[85] as would be expected since the extent of work hardening in the process zone which must effect the damage process, is dependent on the magnitude of applied loads. The characteristic scatter in fatigue results prevents the verification of this law and raises serious doubts as to its reliability as a design law.

Finally, where strain amplitude is the major controlling factor as is the case in thermal fatigue, the law proposed by COFFIN[86] and MANSON[87] is applicable when plastic strains are considerable. The law can be represented by the following equation:

$$\Delta\varepsilon_p \cdot N_f^{\frac{1}{2}} = \text{CONSTANT} \quad \ldots\ldots\ldots (17)$$

where $\Delta\varepsilon_p$ is the total strain amplitude and $N_f$, the number of cycles to failure.

Knowledge of fatigue has been growing for over 150 years but even now it is not possible to formulate a general design law which can be applied to all materials. This is perhaps not surprising

since much of the experimental data is based on the final fracture being the criterion of failure. The mechanism of fatigue crack growth differs for different materials and thus prevents the accurate prediction of fatigue behaviour by simple laws. The empirical laws described above can, however, be extensively used for design purposes provided that the designer is aware of their drawbacks and limitations. If these laws are applied intelligently and their limitations accounted for in the design analysis they can be useful guides.

### 2.3.3. THE MECHANISMS OF FATIGUE FAILURE

The development of slip bands due to localised plasticity has long been recognised as a feature of the fatigue process[60-62]. FORSYTH observed that slip bands caused steps on the surface of a fatigue specimen leading to extrusions[88] and intrusions[89], the latter being considered to constitute the first stages of microcrack formation. In some cases, microcracks originated at voids[90] but in all cases slip bands were observed. The resultant microcrack propagated in a direction at 45° to the applied tensile stress, mainly on crystallographic directions. This was termed Stage I crack propagation[91] and the crack progressed slowly for one or two grains in this manner. Stage II growth then superceded Stage I and the crack began to propagate on planes at 90° to applied stress due to the increased tensile component introduced by the crack. This stage of crack growth was characterised by conchoidal 'ripple markings' or striations and for single phase materials it was postulated[90] that each striation corresponded to one cycle. In some cases the mechanism of Stage II propagation

was more complex and the formation of microvoids in the damage zone which linked back onto the crack tip have been reported[91]. CRUSSARD et al[92] measured striation spacings in mild steel and correlated these with macroscopic crack growth rates, but could not decide that each successive cycle produced one striation, concluding that: "the passage of the rupture front from one striation to the next requires one cycle or at most a few cycles of stress". There was thus the possibility of redundant cycles during crack growth.

Several mechanisms of striation formation have been advanced[90,93-96]. Briefly, these were (i) fracture and void formation ahead of the crack tip with subsequent linking with the crack tip;[90] (ii) successive sharpening and plastic blunting in compressive and tensile half cycles respectively leading to advance of the crack tip[93]; (iii) a dislocation model for plastic blunting where, when a critical value of dislocation density is reached, sub-grain formation occurs which limits growth in one cycle;[94] (iv) a shear decohesion model where 'sliding off' occurs on planes of maximum stress[95] and (v) crack extension by shear on alternative planes which may or may not be crystallographic.[96] It is thought that the models incorporating plastic blunting and shear decohesion seem the most widely applicable as they are the least rigorous and independent of structure. It is highly likely that each of the proposed mechanisms is valid for a specific case as a great variety of striation profiles have been observed.[93]

The position is far from clear as to the exact mechanism of Stage II propagation but the overiding factor would seem to be microstructure. The type of loading may also be important since this determines the form of deformation occurring at the crack tip.

## 2.3.4 FATIGUE CRACK INITIATION AND GROWTH

Numerous attempts have been made to characterise fatigue crack initiation and growth in terms of applied loads and dimensional features. The formulation of general laws which adequately predict the initiation and growth behaviour of all materials is necessarily difficult due to the large variation in the microstructures of materials. The determination of theoretical laws which incorporate the various microstructural features on which the initiation and growth processes are dependent is fraught with difficulties.

It is generally accepted that the fatigue process can be divided into two parts, initiation and growth. Originally the emphasis was on initiation because it was considered that the two processes, initiation and growth, were fundamentally similar, an idea modified by recent work.[97] It had been observed that a large proportion of the fatigue life was spent initiating cracks[98] in high cycle fatigue. In low cycle fatigue however, initiation may occupy such a small proportion of the total lifetime that it is negligible and only growth need be considered.

Two philosophies necessarily emerge when considering design against fatigue failure and arise out of the magnitude of the applied loads and component geometries. If applied loads are high the crack propagation rates can be expected to be high and lead to growth of cracks to a critical length such that catastrophic failure eventually occurs. In such cases it is necessary to design against initiation of fatigue cracks choosing materials of high resistance to fatigue crack initiation. If applied loads are low and where naturally occurring defects can be likened to

cracks a reasonable engineering approach is to apply suitable non-destructive testing techniques and monitor fatigue cracks in service, withdrawing components when necessary. The recent advances in continuum mechanics are particularly applicable to this situation where the use of growth rate data enables calculation of the number of reversals of stress required for the crack to grow to a critical length. Application of suitable safety factors allows withdrawal and replacement to be made before ultimate failure occurs.

2.3.4.1 INITIATION LAWS

The majority of components have notch like features in the form of section changes, oil holes, keyways and splines. The examination of notched fatigue properties is therefore a necessity as these correspond to the real life situation and many attempts to resolve this problem have been made.

There are two cases of general interest: (i) the elastic case, where both the nominal stress range, $\Delta S$ and strain range, $\Delta e$ and local stress and strain ranges, $\Delta\sigma$ and $\Delta\xi$ are elastic; (ii) the elastic-plastic case, where nominal stress and strain ranges are elastic but local stress and strain ranges are plastic. It is this element of plasticity which leads to the complexity of the analysis in the second case.

In the elastic case nominal and local stresses can be related through the elastic stress concentration factor, $K_t$ by

$$K_t \Delta S = \Delta\sigma \qquad \ldots\ldots\ldots\ldots\ldots (18)$$

This has been found to be accurate for blunt notches (low $K_t$)

but for notches of increasing sharpness (high $K_t$) this formula becomes increasingly conservative. This is a well-known size effect and is overcome by replacing $K_t$ by $K_f$, the fatigue stress concentration factor (the ratio of stress to cause failure in a given number of cycles for a smooth specimen, normally $10^6$ - $10^8$ cycles, to the nominal stress to cause failure in the same number of cycles for a notched specimen.)

Plasticity at the notch root affects initiation in the elastic-plastic case and here $K_f$ accounts for plasticity in addition to size effect replacing $K_t$ in equation (18). A major drawback to the $K_f$ approach is the need to generate the complete fatigue curves for each possible notch root radius in order to obtain the requisite values for $K_f$. This approach has, however, been successfully applied, and good agreement between theory and experiment noted.[98]

Plasticity at the notch root has been examined by TOPPER et al[100] using Neuber's Rule [99]. This rule states that the elastic stress concentration factor, $K_t$ is equal to the geometric mean of the stress and strain concentration factors, $K_\sigma$ and $K_\xi$ and is expressed by:

$$K_t = (K_\sigma . K_\xi)^{\frac{1}{2}} \quad \ldots\ldots\ldots\ldots\ldots (19)$$

Although this rule was derived for shear strained prismatical bodies, its applicability to axially loaded notches has been demonstrated.[101] It was envisaged[100] that this rule provided indexes of equal damage for notched and smooth specimens. Here again, $K_t$ requires correction for size effects for increasing notch acuity and can be replaced by $K_f$. This method is valid

only for completely reversed loading but it has been suggested that it can be extended to other types of loading cycle[102].

If equation (19) is considered in terms of nominal stress and strain range, $\Delta S$ and $\Delta e$ and local stress and strain range, $\Delta\sigma$ and $\Delta\xi$, then:

$$K_t = \left\{\frac{\Delta\sigma}{\Delta S} \cdot \frac{\Delta\xi}{\Delta e}\right\}^{\frac{1}{2}} \qquad \ldots\ldots\ldots\ldots\ldots (20)$$

Rearranging and multiplying by the square root of the elastic modulus, $E^{\frac{1}{2}}$:

$$K_t(\Delta S.\Delta e.E)^{\frac{1}{2}} = (\Delta\sigma.\Delta\xi.E)^{\frac{1}{2}} \qquad \ldots\ldots\ldots\ldots\ldots (21)$$

When nominal stresses and strains are elastic

$$\Delta e.E = \Delta S$$

and therefore:

$$K_t\,\Delta S = (\Delta\sigma.\Delta\xi.E)^{\frac{1}{2}} \qquad \ldots\ldots\ldots\ldots\ldots (22)$$

The important parameter is therefore, $K_t \Delta S$ (or $K_f \Delta S$ for sharp notches) and from a conversion of smooth specimen data a plot of $(\Delta\sigma.\Delta\xi.E)^{\frac{1}{2}}$ against $K_t \Delta S$ can be obtained and used to predict the lives of notched specimens in a given material.

A more recent approach is based on the continuum mechanics analysis which has been developed over the last decade and applied to the fatigue process. During cyclic loading the maximum and minimum stresses, $\sigma_{max}$ and $\sigma_{min}$ can be characterised by maximum and minimum stress intensity factors, $K_{max}$ and $K_{min}$, related through:

$$K_{max} = \sigma_{max} Y a^{\frac{1}{2}} \quad \ldots\ldots\ldots\ldots\ldots (22)$$

$$K_{min} = \sigma_{min} Y a^{\frac{1}{2}} \quad \ldots\ldots\ldots\ldots\ldots (23)$$

The algebraic difference between $K_{max}$ and $K_{min}$ is then termed the fatigue stress intensity factor, $\Delta K$:

$$\Delta K = K_{max} - K_{min} \quad \ldots\ldots\ldots\ldots (24)$$

This approach concentrates on the deformation at the tip of stress concentrators whereby it is sought to describe this deformation in terms of applied loads and specimen geometries. Developments of elastic and elastic-plastic modelling of crack tip deformation are discussed at length by RICE[103]. The elastic treatment of stress concentrations is well documented[104-107] but work on elastic-plastic stress analysis seems far from complete.

Recognising the importance of deformation at the tip of a stress concentrator, BILBY, COTTRELL and SWINDEN[108] developed a model of plastic relaxation within the plastic zone which was subsequently used to relate the number of cycles to initiate a crack, $N_i$, to the fatigue stress intensity factor, $\Delta K$[109,110]. Accordingly it was reasoned that the plastic displacement per cycle due to plastic relaxation could be summated to obtain a critical value of displacement sufficient to constitute crack initiation. Experimental results yield an inverse square relationship between $N_i$ and $\Delta K$[110] :

$$N_i \propto 1/(\Delta K)^2 \quad \ldots\ldots\ldots\ldots\ldots (25)$$

JACK and PRICE[111] conducted experiments on mild steel plates and obtained an inverse relationship between $N_i$ and $\Delta K$ but the

exponent in this case was 4:

$$N_i \propto 1/(\Delta K)^4 \quad \ldots\ldots\ldots\ldots\ldots\ldots \quad (26)$$

They justify this relationship, which conflicts with that predicted by the plastic relaxation model,[108] by asserting that the summation of plastic displacements, assumed linear for the model, is in fact proportional to the square of plastic displacements. This they based on the statistical analyses described by MAY[112,113] and GITTUS[114] as theoretical justification for the Coffin-Manson Law.

Since the continuum mechanics analysis strictly applies to sharp cracks it is clear that some modification of the theory is required to account for finite notch root radii before this analysis can be meaningfully applied to notched fatigue. A method has been devised to make this finite root radius correction[115] which indicates that the analysis which is valid for sharp cracks[110] is equally valid for notches.

A marked variation in $N_i$ with notch root radius has been demonstrated[116] and on a log-log plot of $K_t \Delta S$ against $N_i$ a linear relationship is observed. FORMAN[117] attempted to correct for finite root radius postulating that crack initiation was a function of the relative stress intensity range $\Delta K/K_c$. Here, $K_c$ is the fracture toughness or apparent fracture toughness, $K_a$ which was shown to be dependent on notch root radius. $K_a$ is related to $K_c$ by multiplying the latter by the ratio of plastic zone sizes for a notch and a sharp crack of the same length:

$$K_a = \left(\frac{r}{W}\right).K_c \quad \ldots\ldots\ldots\ldots\ldots \quad (27)$$

Values of r/w were obtained from the data published by CREAGER and PARIS.[51] Forman showed that this law fitted the data for sheet specimens of an aluminium alloy and also fitted other published data.[118]

An additional attempt to correct for notch root radius, $\rho$ suggests that $N_i$ can be correlated with $\Delta K/\rho^{\frac{1}{2}}$.[111] Noting a half power relationship between $N_i$ and $\rho$ this method was applied to notched mild steel specimens and shown to be a good fit for the experimental data. Furthermore, it was noted that below a certain value of root radius, 0.25 mm, initiation was independent of root radius for mild steel and this was ascribed to the fact that a minimum volume or critical element is required over which a particular mechanism can act.

There is considerable discussion about the applicability of either the method based on Neuber's Rule employing the parameter $K_t \Delta S$ or the method based on modified continuum mechanics analysis employing $\Delta K/\rho^{\frac{1}{2}}$. Examination of experimental results indicates that each approach can give good agreement with specific sets of data. It is noted that the data reported exhibits a 'banding' effect where results for various notch root radii lie within approximately parallel bands.[118] This is true for whichever method is utilised to represent the results. It is therefore necessary to examine the cause of banding particularly where the modified fracture mechanics parameters are expected to eliminate banding of results.

The important factor is the criterion of initiation which has been variously described in the literature. Examples of this are: growth of a crack to 0.1 mm in surface length[116], growth

of a crack to engineering size, (0.05 - 0.25 mm)[117] and the growth of a crack to 0.25 mm[119]. This admits an element of growth into the measured $N_i$ values and it is clear that due to the limitations of detection techniques all such values will contain an element of growth such that:

$$N_i \text{ (measured)} = N_i \text{ (true)} + N_g \text{ (growth)} \quad \ldots\ldots (28)$$

The time required to grow to the minimum detectable length is therefore important and thus $N_i$ is very sensitive to the criterion of initiation employed which essentially controls the magnitude of the growth contribution, $N_g$.

Consideration of the stress gradients which prevail at notches reveals that at equal values of maximum stress at the notch root the gradient at a sharp notch is steeper than at a blunt notch[120]. This is well established and is often referred to as a 'size effect'. Once initiation has occurred at a sharp notch growth must occur through a region of steeply falling stress whereas for a blunt notch the stress falls off less steeply. Growth rates are different in each case as they are dependent on the stress distribution ahead of the crack tip and will be higher at the blunter notch. The number of cycles required to grow to the minimum detectable size, $N_g$ must therefore, be less for the blunter notch. Therein lies the reason for the banding effects exhibited by the experimental data. The factor $\rho^{\frac{1}{2}}$ in the fracture mechanics parameter, although in theory can account for the finite root radius of a notch, cannot account for stress gradient effects upon which the measured values of $N_i$ so critically depend. Neither can the elastic stress concentration factor, $K_t$ account for stress gradients and this leads to the necessary

replacement of $K_t$ by $K_f$, the fatigue stress concentration factor. Both the methods suffer from this inherent difficulty associated with measurement of $N_i$ values by experiment.

Neither of the two methods is wholly satisfactory but in the absence of a better method it remains for the engineer to decide which approach is most suitable to a particular situation. As both the parameters in question, $K_t \Delta S$ and $\Delta K / \rho^{\frac{1}{2}}$ have units of stress it is relevent to examine the relationship between them. The formula for the determination of stress intensity factors for tensile opening, mode I, is stated to be[107] :

$$K_I = \lim_{\rho \to 0} \frac{\pi^{\frac{1}{2}}}{2} \cdot \sigma_{max} \rho^{\frac{1}{2}} \qquad \ldots\ldots\ldots\ldots\ldots\ldots (29)$$

Applying this to fatigue and substituting for the maximum stress, $\sigma_{max}$:

$$\Delta K = \frac{\pi^{\frac{1}{2}}}{2} \cdot K_t \Delta S \cdot \rho^{\frac{1}{2}} \qquad \ldots\ldots\ldots\ldots\ldots\ldots (30)$$

$\Delta S$ is the applied gross stress range and $K_t$ the elastic stress concentration factor. Rearranging the equation:

$$\left(\frac{2}{\pi^{\frac{1}{2}}}\right) \frac{\Delta K}{\rho^{\frac{1}{2}}} = K_t \Delta S \qquad \ldots\ldots\ldots\ldots\ldots\ldots (31)$$

Plotting the left-hand side of the equation against the right hand side results in a straight line of slope equal to 1. This line passes through the origin but it is clear that $K_t$ can never be less than 1, the value for a notch of infinite root radius, i.e. a smooth specimen. At some point, on this straight line, as low $K_t$ values are approached, $K_t \Delta S$ becomes increasingly greater than $\Delta K / \rho^{\frac{1}{2}}$, Fig. 15. At low values of $K_t$ therefore, the two approaches become separated, and in this range the $K_t \Delta S$

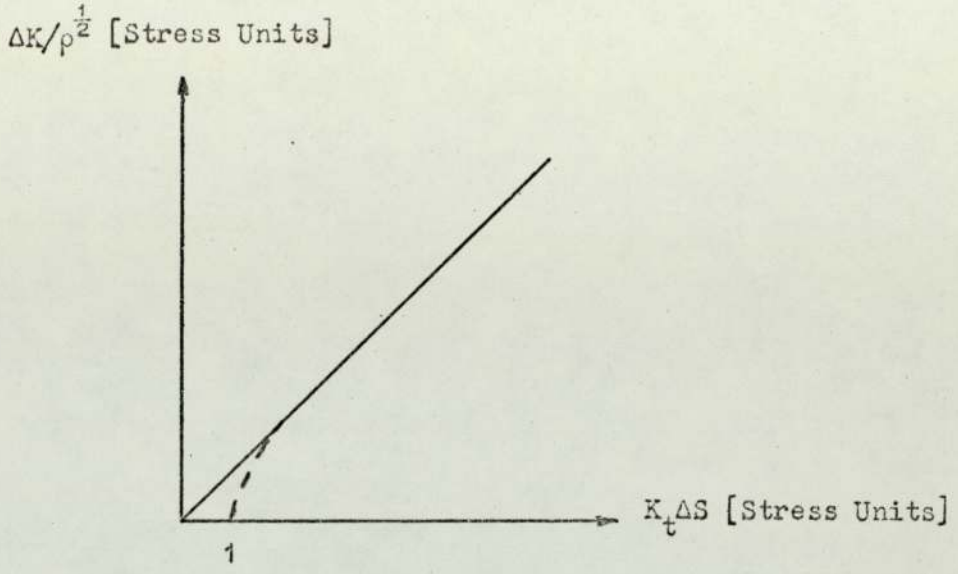


Fig.15. Theoretical relationship between $K_t \Delta S$ and $\Delta K/\rho^{\frac{1}{2}}$

approach seems more suitable. Where the range over which the two approaches are equivalent, i.e. for high $K_t$ values it would seem more useful to use the $\Delta K/\rho^{\frac{1}{2}}$ parameter. This arises out of the need to obtain the whole range of specimen data in order to replace $K_t$ by $K_f$ and also the availability of K-calibration curves for various component geometries. Although the indications are that $K_t$ is in some way proportional to $K_f$ and the need to obtain $K_f$ values can be overcome as long as the range of applicability of the $\Delta K/\rho^{\frac{1}{2}}$ approach is known this approach would appear advantageous. Extrapolation of data beyond the applicable range is of course extremely hazardous and much care is required in the interpretation of experimental data. It is unfortunate perhaps that the range of general interest to the engineer is one where low $K_t$ values prevail. Naturally, the practice is to design against severe stress concentrators and thus in most components root radii are likely to be very large and $K_t$ values correspondingly low. In such cases the $K_t \Delta S$ approach seems more viable but it is clearly advantageous to develop the alternative approach further in order to extend its range.

A more recent approach[121] is based on the interaction of notch stress-strain field, the crack tip stress-strain field and the bulk stress-strain field. Recognising the inherent difficulties discussed above it was sought to account for the interaction and relate this to the growth rate of the crack within the notch stress-strain field. This region was thought to be of major importance since the majority of the fatigue life was spent in this region. The method was based on an equivalent notch length which was stated to have an increasing contribution to crack length, ranging from zero prior to initiation to its full length when the crack has just reached the end of the zone of influence of the notch. The contribution of the notch e, to the crack length l, is calculated from theoretical solutions and the total equivalent length can be expressed by:

$$L = e + l \qquad \ldots\ldots\ldots\ldots\ldots\ldots (32)$$

Calculation of the notch contribution and applying the appropriate value of growth rate, obtained from growth data for an unnotched specimen enables life prediction:

$$N = \int_{l_0}^{l_N} \left(\frac{1}{R}\right).dl \qquad \ldots\ldots\ldots\ldots\ldots\ldots (33)$$

Here, R is the appropriate growth rate, $l_N$ the final crack length and $l_o$, the original crack length. This represents a simple law which can be applied to design problems since the effect of the notch is equated to a parameter (length) that is of major concern in fatigue studies. Comparison of theory with the experimental results yielded very good agreement and this

approach would seem more desirable than either of the two methods discussed earlier which were based on detection of fatigue cracks which can only be approximate. The drawback to this method is that it is necessary to determine the exact notch contribution function for all notch profiles encountered. The further work required is thus extensive and the method seems a useful base from which to progress.

2.3.4.2 PROPAGATION LAWS

Many theories of fatigue crack growth have been evolved in order to generate growth laws applicable to design and a comprehensive review was presented by PLUMBRIDGE[122]. Fatigue crack propagation from notches can be expected to be of the Stage II type, notches eliminating Stage I growth due to the triaxiality introduced by the notch at its root. McCLINTOCK[123] described two approaches to the prediction of growth rates. The first approach involved the computation of damage accummulating in the small region ahead of the crack tip and equating this to some critical value, dependent on the criterion of failure. The growth rate predicated by this approach was proportional to the square of the crack tip plastic zone size. The second approach, applicable to ductile metals, estimated the extent of non-cyclic deformation of the crack tip predicting a linear dependence of growth rate on plastic zone size.

Growth laws have attempted to relate growth rates, applied stress levels, crack length and material properties. The cyclic stress amplitude was found to be the dominant parameter and attempts were made to incorporate this in a law leading to a squared and

a cubic relationship[125]:

$$\frac{da}{dN} = C_1 \left(\frac{\Delta\sigma^2 a}{\sigma_{Y.S.} - \Delta\sigma}\right) \quad \text{.....(34)}$$

$$\frac{da}{dN} = C_2 \, \Delta\sigma^3 a \quad \text{.....(35)}$$

where $\Delta\sigma$ is the applied stress range, a the crack length and $\sigma_{Y.S.}$ is the appropriate yield stress. An alternative approach incorporating the elastic stress concentration factor predicts a half-power relationship between growth rate and crack length:[126]

$$\frac{da}{dN} = f\left\{\Delta\sigma[1 + 2\,(a/\rho)^{\frac{1}{2}}]\right\} \quad \text{.....(36)}$$

where $\rho$ is the crack tip radius. The above together with various other laws,[127,128] predicting relationships between the various parameters most certainly apply to some regime of the fatigue crack propagation period for the materials tested. This emphasises the necessity of testing over a wide load range in order to determine the complete range of growth behaviour of a material and it is clear that the above laws are inadequate and not generally applicable.

The most recent growth law to be advanced has arisen from the application of fracture mechanics concepts to fatigue crack propagation.[129-131] The general form of the law is now widely accepted:

$$\frac{da}{dN} = C(\Delta K)^m \quad \text{.....(37)}$$

According to the damage approach described by McClintock[123], growth rate is proportional to the square of the plastic zone size, given by 132:

$$r_p = \frac{1}{A}\left(\frac{K}{\sigma_{Y.S.}}\right)^2 \qquad \ldots\ldots\ldots\ldots\ldots (38)$$

where A is a constant equal to $2\pi$ for plane stress and $6\pi$ for plane strain. The value of m in equation (37) should thus be 4 and for the second approach, where there is a linear proportionality between growth rate and plastic zone size, m is equal to 2. The value of m has been shown experimentally to lie between these two values but 4 seems to be the most common and much experimental data was provided in a review by PARIS and ERODGAN[130]. The validity of this approach, where the fatigue stress intensity factor is the controlling parameter, has been demonstrated in load shedding experiments.[133] These experiments employ a technique whereby $\Delta K$ remains constant as crack length increases and a constant growth rate was observed.

One objection to this approach was that it should only be applied where conditions of linear elastic fracture mechanics prevail and for ductile materials this was not strictly applicable. In addition, the stress intensity approach did not include material properties and microstructural effects on growth. It is clear however, that such effects will be reflected in the value of the exponent, m determined experimentally. The general applicability seems justified by the high degree of correlation observed between theory and experimental results[130,131,134-136] and also in the absence of a better approach.

The general form of the growth law is, then acceptable and it remains only to establish for a particular material the limits over which it applies together with the appropriate value

of the constant, C and the exponent, m. It should be noted that there is a specific range over which this law is valid and it has been demonstrated that the overall growth curve consists of three portions[137], Fig. 16

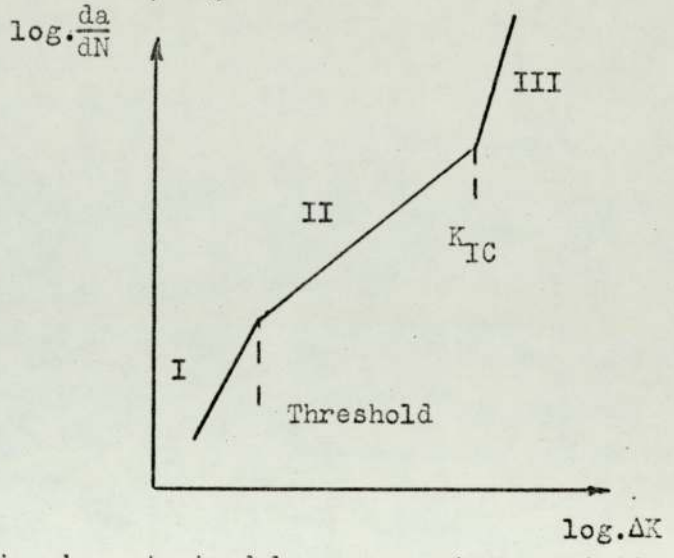


Range I is characterised by a very steep variation in da/dN with $\Delta$ K up to some 'threshold' value, the estimation of which is the subject of a current investigation.[138] Beyond this threshold Range II up to the fracture toughness of the material, the growth law, equation (37) is applicable. Range III is a region of very steep slope corresponding to $\Delta$ K values above the static fracture toughness, where in fatigue, fast monotonic failure is thought to be prevented due to the dynamic nature of loading.

In the light of the preceding discussion it is of paramount importance that the engineer knows the precise nature of the whole growth curve before attempting to apply growth laws to design where care must be exercised when extrapolation of experimental data is involved.

The effect of mean stress, $\sigma_m$, is not reflected by the parameters in the growth law (equation 37). Fatigue generally involves cycling about a non-zero stationary stress in practical

situations and thus design must incorporate modifications to account for mean stress effects. Experimental data indicates that increased mean stress results in higher growth rates,[126,134,139,140] although in some cases no measurable effect is reported[125,141,142] and this is attributed to relaxation of stress at the crack tip by plastic deformation[139]. It is now more usual to represent mean stress in the form of a stress ratio, $R(= \sigma \text{ min}/ \sigma \text{ max})$. At constant $\Delta K$ the growth rate increases as R increases greater than zero, showing that compressive mean stresses have little influence on propagation. Some attempts have been made to incorporate mean stress in growth laws[139,140,143] but as yet a completely adequate description is lacking. The formulae advanced are connected with relating mean stress or R-value to growth rate via the fracture toughness of the material. For thin specimens FORMAN et al[143] propose:

$$\frac{da}{dN} = \frac{C(\Delta K)^m}{(1-R)K_c - \Delta K} \quad \ldots\ldots\ldots\ldots (39)$$

but specimens of increased thickness require that the plane strain fracture toughness, $K_{IC}$ be utilised in place of $K_C$ and the formula proposed by PEARSON[140] is more applicable in this case:

$$\frac{da}{dN} = \frac{C(\Delta K)^m}{[(1-R)K_{IC} - \Delta K]^{\frac{1}{2}}} \quad \ldots\ldots\ldots\ldots (40)$$

It is important that the data at the engineer's disposal includes all the relevant variables and although the modified growth laws (equations 39 and 40) indicate good agreement between theory and experiment they are insufficient even as

general guides. This indicates that extensive testing will be required before safe designs can be produced. A reasonable approach would be to test over the appropriate range of mean stress likely to be encountered in service and use the maximum growth rate values to ensure safety. The range might be up to the yield stress and although this approach will be perhaps too conservative, in the absence of better methods, it is necessary to over-design in this way.

It has been proposed that where mechanisms of fracture are dependent on a hydrostatic component of stress at the crack tip, such as void coalescence, these mechanisms could be promoted by an increase in mean stress.[144] This increase in mean stress manifests itself as an increase in $K_{max}$, the maximum stress intensity during cycling and can give rise to accelerated growth rates. Such accelerated growth is said to be due to 'bursts' of monotonic fracture[143] which add to the cyclic growth and are most significant in materials exhibiting low static fracture toughness[144-148]. The growth rate exponent, m has been shown to be abnormally high for such materials and is known empirically to be inversely related to fracture toughness[149]. Microstructure is said to be of prime importance as this dictates the form and extent of 'static' modes of failure.[150] At high growth rates where values of $K_{max}$ are correspondingly high the contribution of 'static' modes is reported to be considerable whereas at lower growth rates the effect is minimal. The extent of the above ranges will be naturally dependent on the microstructural effects responsible for 'static' modes of failure and the corresponding fracture stress required to produce this for a

particular microstructural feature, e.g. fracture of grain boundary inclusions or carbides giving rise to cleavage across a grain. In low growth rate ranges $\Delta K$ is the controlling parameter and any small contributions due to $K_{max}$ effect are reflected by C and m in equation (37). In this range where $\Delta K$ controls crack growth processes no serious objections can be raised pertaining to the validity of the general growth law proposed earlier, (equation 37).

KRAFFT[151] has attempted to include $K_{max}$ in a fatigue crack growth law for 'brittle' materials, proposing that:

$$\frac{da}{dN} = \frac{C(\Delta K)^2 (Kmax)^2}{K_{IC}^2} \quad \ldots\ldots\ldots\ldots\ldots\ldots \text{'41)}$$

A fourth power dependence of growth on $\Delta K$ is assumed which does not necessarily fit for all materials. The law is based on plane strain instability at the crack tip being attained and growth being envisaged as extension of the crack by a distance dependent on microstructural features. Damage processes at the crack tip are said to be included by means of empirical correction factors. In general this approach to fatigue crack growth is unsatisfactory due to the continuous nature of crack extension and the widely differing failure processes involved.

### 2.3.5 FATIGUE PROPERTIES OF SINTERED MATERIALS

Limited information concerning the response of sintered materials to cyclic loading is available. The information presented in the literature is of the conventional type being concerned with fatigue strength as determined from the standard S-N curves[152-154]. An excellent summary is provided by HAYNES[153]

where most of the available data is reviewed and compared with wrought and cast materials. Useful information has been provided for the engineer and indicates that the behaviour of sintered materials in fatigue situations is not unlike that of conventional materials. In this respect the available data suggests that sintered materials would prove no more hazardous in fatigue situations than wrought or cast material and that they can be applied to such situations with similar confidence.

A characteristic of some materials is the existence of an 'endurance limit' and where this is true for wrought and cast metals and alloys it is also true for their sintered counterparts[153]. The main difference appears to be that the endurance limits of sintered materials tend to be at longer lives ($10^6$ - $10^8$ cycles), than those of wrought or cast materials, ($10^5$ - $10^7$ cycles).[153,155,156] This indicates that the porosity does not simply reduce fatigue strength but has a deleterious effect on the resistance of the structure to fatigue failure. Fatigue ratios for smooth specimens tend to be in the region of 0.4 and exhibit the same decrease with increasing tensile strength observed for conventional materials[152-155].

The most important factor is the porosity[155,157-161] which is the parameter controlling most mechanical properties as discussed earlier (Section 2.1). Fatigue limits may be raised by reduction in percentage porosity although fatigue ratios appear independent of porosity content[152]. The rate of fall of fatigue strength with increasing porosity has been observed to be constant. Sintered materials are also relatively notch insensitive and in this respect show a marked similarity with cast irons as observed previously (Section 2.1). The notch sensitivity of sintered low

alloy nickel steels is increased by heat treatment[155] and thus sintered materials can be considered to be structure sensitive and the properties in fatigue are not merely a consequence of the porosity. It is clear that there is a certain degreee of interaction between porosity and microstructure a feature again observed in cast irons.[157] The normal effects of microstructure on fatigue properties are in some way modified by the presence of the pore distribution. The nature of this modification is difficult to predict and a certain amount of caution must be exercised in this respect. There is obvious need for extensive investigation into the nature of fatigue processes in sintered material as present information is sparse.

The distribution of porosity can be expected to enhance some mechanisms of failure and inhibit others and the extent to which this occurs governs the failure mechanism during cyclic loading. It is generally accepted that fatigue failure occurs most readily at a free surface and although this seems likely for sintered materials conclusive proof is not available. Experiments based on the removal of surface layers after half the predicted lifetimes of specimens had elapsed, whilst showing the expected trend - a tendency towards increased fatigue life - were inconclusive.[152] The possibility of crack nucleation at pores seems probable but the stress concentrating effect of a surface pore is greater than an internal pore. Microcrack nucleation has been observed at pores[156] and occurs at sharp corners but further growth of these microcracks may be inhibited by the structure. If stress is concentrated at a sharp pore the stress gradient will be very steep and the stress consequently falls off rapidly. The stress may thus be insufficient to allow propagation of the microcrack, i.e. the

stress rapidly falls to below the fracture stress. Barriers to propagation are likely to be grain boundaries and if the local stress at the tip of the microcrack does not exceed the fracture stress for a distance extending beyond this barrier propagation cannot proceed. Microcracks may well form internally but do not appear to cause fatigue failure although they may enhance subsequent growth of the fatigue crack.

In tests involving rotating bending of sintered iron detailed metallographic studies have been conducted and show distinct similarities with conventional materials.[153] Below the fatigue limit no microcrack formation is evident and a faint cellular structure is observed together with fine slip in a limited number of grains. Above the fatigue limit fine slip is observed throughout the structure and in a few grains adjacent to the fracture surface coarse slip was evident. In addition, cellular regions are formed and said to be the means of microcrack propagation, linking being enhanced by regions of coarse slip. The overall crack growth is of mixed character, exhibiting both trans-and intergranular modes. This is due to the distribution of porosity and oxide inclusions within the grains and at the thick grain boundaries which occur at the original interparticle bonds. The overall fracture surface shows a marked absence of the conchoidal markings[163] which often accompany fatigue failure. This can be attributed to the porosity where fatigue crack growth is liable to be discontinuous and not continuous as in cases where these markings are observed. The failure mechanism, although far from clear at this time, would seem from the above evidence to be gradual link-up of microcracked pores by a damage process across the specimen until the fracture

strength of the remaining ligament is reached. A specimen may thus contain many microcracks long before complete failure which is potentially dangerous where static overloads may cause sudden linking of these microcracks and subsequent rapid growth leading ultimately to catastrophic failure.

It is essential to know the precise nature of failure in porous bodies before attempting to apply them in relatively highly stressed situations involving dynamic loading. Little attempt has been made by the P/M industry to solve this problem and in view of this the reticence of engineers in the use of sintered materials is hardly surprising. There is an obvious need for extensive research in this area and this must encompass not only the broad field of fatigue properties but also an attempt to formulate a clearer understanding of the complex interactions between porosity, microstructure and properties.

# 3. RAW MATERIALS AND EXPERIMENTAL TECHNIQUES

## 3.1 POWDERS

### 3.1.1. UNALLOYED IRON

Four types of iron powder were utilised, each produced via a different process route and of consequently differing morphology. These powders were Hoganas NC100 and ASC100, ROSPOL MP32 and Sintrex Electrolytic. A description of the processes and morphologies together with micrographs was presented earlier in Section 1. Sieve analyses were carried out on these powders the results of which are given in Table 1.

Initial compaction pressure/green density curves were obtained for each powder using a nominal 100gm. sample compacted in a die of 'dogbone' configuration. Compaction was based on the floating die technique which simulated a double acting press by allowing movement of the die relative to a fixed bottom punch whilst moving the top punch. Density was calculated on a mass per unit volume basis by simple weighing of compacts, the volume being obtained from compact dimensions. The dogbone specimens had an area of 645 $mm^2$ ($1in^2$) and thickness was determined by means of a micrometer, taking the average of five measurements. This was found to be sufficiently accurate and far simpler than the method based on the "Archimedes Principle" involving impregnating with light oil under vacuum and several weighings both in water and in air.

### 3.1.2 LOW ALLOY STEEL (ANCOLOY SA)

This is a pre-alloyed sponge iron powder containing 1.5% Cu, 1.75% Ni and 0.5% Mo to which carbon may be added in the form of graphite. The alloying elements as micron size powders are diffusion

bonded to the iron powder particles. This process aids diffusion during sintering improving homogenization. The copper and nickel are balanced in order to prevent dimensional changes during sintering and the molybdenum in conjunction with nickel and carbon imparts considerable hardenability. This material offers a wide range of properties in both the as-sintered and quenched and tempered conditions, dependent on sintered density and carbon content.

Carbon additions were made to the powder in the form of natural graphite powder. Additions of 0.65 wt-% zinc stearate were made prior to mixing to reduce die-wall friction and facilitate compact ejection. Blending of powder, graphite and zinc stearate in 5 kgm batches was carried out in a jar rigidly fixed in one end of a double-cone rotary blender. As agglomeration of powders was considered undesirable samples were taken from the batch at five minute intervals and apparent density determined. Since agglomeration was shown by a reduction in apparent density, the optimum mixing time was taken to be the time to give maximum apparent density. This was found to be twenty-five minutes and subsequent batches of powder were mixed for this period. Compaction pressure/green density curves were produced for this material as for the iron powders described in 3.1.1.

## 3.2 PRODUCTION OF COMPACTS

### 3.2.1 COMPACTION

Compaction was carried out on a 3MN capacity Denison compression machine which had a high and a low load range. The low range for loads up to 0.5 MN had an accuracy of $\pm$ 1.25 x $10^{-3}$ MN and the high

range for loads up to 3 MN, an accuracy of $\pm$ 5 x $10^{-3}$ MN. Compaction of iron powders involved lubrication of the die walls with a saturated solution of stearic acid in ether, but this procedure was found unnecessary in the case of Ancoloy due to the admixed lubricant. Segregation during powder fill was avoided by varying the cavity depth using blocks to allow compression of the springs supporting the die block. Powder was gradually added as the cavity depth was progressively increased until all the powder had been added and could be 'strickled' to the level of the upper surface of the die block. The blocks were then removed, the top punch inserted and pressure applied. The machine was taken slowly up to the required pressure, held for about two seconds then slowly released. The fine strain control was utilised for purposes of load control. Ejection was achieved by use of blocks to allow compression of the supporting springs, the bottom punch forcing out the compact from the cavity. No difficulty was encountered in ejecting compacts either for iron powders using alubricated die or for Ancoloy using admixed lubricant.

A die was designed to enable the production of standard three-point bend SEN fracture toughness specimens of 4 : 1 span to width ratio. The design was based on the floating die technique. The cavity of this die was 110 x 25 mm in section and provision was made for variation of the compact thickness by incorporation of adjustable retaining collars. Initially, whilst this die was being commissioned, compacts for fracture toughness specimens were produced by B.S.A. Sintered Products Limited in the form of 150 x 25 x 100 mm blocks. Toughness specimens were then obtained by slitting these blocks to give the required specimen thickness and maintaining the

4 : 1 span to width ratio. Specimens of iron powders only were made industrially and on obtaining the die, duplicate specimens were produced to enable comparison of the two manufacturing routes. All fracture toughness specimens of Ancoloy were produced in the tool set designed specifically for this purpose. The relationship between pressing and notching directions for each type of specimen is illustrated in Fig. 17.

3.2.2 SINTERING

The sintering furnace utilised in this work consisted of a nichrome tube, externally heated by crucilite elements and encased in refractory bricks and asbestos plates, Fig. 18. The hot zone had a length of 140 mm for $\pm$ 5$^{o}$C at both 1100 and 1120$^{o}$C, Fig. 19. All sintering was carried out under a 90% nitrogen/10% hydrogen atmosphere dried prior to entry to the furnace. The drying train consisted of a 75 mm diameter glass tube of length, 1m with three sections separated by wire gauze. The first sector contained a hydrogen catalyst to remove oxygen, the second silica gel and the third magnesium perchlorate, the latter two substances being drying agents. An added precaution, to prevent sucking back of moisture into the furnace via the exit line, was a drying tower containing silica gel. This preceded a further tower containing water through which the spent gas was bubbled. Gas flow was controlled by means of a flow meter although no quantitative control was applied, the flow being maintained at the same arbitrary level for all sintering operations. The furnace was flushed out by means of a high flow rate for a minimum of 15 minutes prior to charging green compacts to the hot zone.

Initially, iron compacts pressed industrially were sintered

at the same works for $\frac{1}{2}$ - 1 hour at 1100°C in cracked ammonia (reports being rather vague). A mesh belt furnace was used for this operation. It was noted that the compact surfaces were oxidised but this was restricted to the surface layers and was probably due to premature removal from the furnace before they were sufficiently cool. Subsequent iron compacts were sintered in the laboratory furnace, described in Fig. 18, for one hour at 1100°C. The procedure was to load green compacts into a boat in a cold zone and to flush out the furnace. After the 15 minute purge the boat was drawn into the hot zone by means of an attached wire. The compacts were soaked for one hour at temperature and then drawn into a water-cooled zone of the furnace. The cooling period was 45 minutes as this enabled withdrawal of the sintered compacts without surface oxidation occurring, i.e. no oxide colour was observed on compact surfaces.

Ancoloy compacts contained admixed lubricant and therefore required a 'dewaxing' treatment prior to sintering. This was originally attempted in the same furnace as the sintering by holding the boat for a 15 minute period in a 400 - 500°C zone to enable volatilisation of the lubricant. The severity of the temperature gradient gave rise to incomplete 'burn-off' during the holding period and caused scabbing and blistering of compact surfaces. This effect was particularly severe in high density compacts, (6.90 and 7.00 $Mgm.m^{-3}$) and could be attributed to rapid expansion of residual lubricant on charging to the sintering zone. High densities prevented escape of volatilised lubricant and caused compacts to swell and in some cases the high pressures developed gave rise to removal of surface material. It was found necessary to carry out a separate

treatment to overcome this problem. This consisted of a separate 15 minute treatment at 450°C in the furnace followed by cooling to room temperature. The atmosphere for this treatment was again 90%$N_2$/10%$H_2$. This gave satisfactory results although increased the processing time substantially. Industrially, this would not be a problem since temperature gradients in mesh belt furnaces are not nearly so severe. Sintering was then carried out for one hour at 1120°C in 90%$N_2$/10%$H_2$ and the cooling procedure was as described previously for iron compacts. The sintering temperature was chosen on the basis of the recommendations of the powder manufacturers[1]. Beyond 1120°C, little improvement in mechanical properties was evident from their data whilst a pronounced shrinkage was apparent. At times shorter than one hour expansion of compacts was experienced and at longer times no significant benefits were evident. In addition, this treatment was shown to result in a high degree of homogeneity of the alloying elements. Times of one hour are also of the correct order for industrial processes, a point obviously noted in the development of this powder.

### 3.2.3 CARBON CONTROL AND HEAT TREATMENT

Carbon additions were made only to Ancoloy powder and this section is therefore only relevant to this powder. The problems associated with carbon control were considered to begin at the powder mixing stage and were not simply confined to sintering or heat treatment. It was found that 0.1% carbon was lost during mixing and this loss was observed irrespective of the addition made, within the range 0.5 - 0.85 wt.-% carbon addition. This

[1] Höganäs Corporation Technical Bulletin: PM70-1 "Ancoloy SA"

was thought to be due to 'dusting' of the relatively light graphite. Die-fill was a further stage where carbon could be lost from individual compacts and great care was exercised when carrying out this operation.

Since equipment was not available for carbon control during sintering an extra graphite addition was made initially to counteract the carbon loss incurred during this process. It was observed that for the sintering treatment employed - 1 hour at 1120°C in 90%$N_2$/10%$H_2$ - a constant 0.1% carbon was lost. The graphite addition was therefore increased by this amount plus a further amount to counteract mixing losses. In this simple manner, some measure of carbon control was effected and whilst this method is not wholly adequate gave reproducible results and was therefore considered satisfactory.

Heat treatment involved austenitising for 30 minutes at 850°C (0.4% carbon material) under an argon atmosphere to prevent further decarburisation, followed by a quench into an oil bath. Tempering consisted of a one hour treatment in an air circulating furnace at 200°C. Carbon analysis of heat treatment specimens initially proved difficult due to absorption of the quenching oil, not completely removed during tempering. Specimens for carbon analysis were subsequently placed in a vacuum chamber and heated to 300°C to remove any residual oil and this proved satisfactory.

## 3.3 MECHANICAL TESTING

### 3.3.1 TENSILE TESTING

Hounsfield No. 12 and dogbone specimens were tested on a Hounsfield Tensometer which had a variable load range and crosshead speed. Movement of the crosshead could be effected manually or by means of

a motorised belt-drive. All tensile tests carried out in this work employed the belt-drive at the slowest speed, maintaining a constant strain rate. The load during tests was monitored by means of a slide-arm maintained at the meniscus level of the mercury in a column. A pointer was attached to the slide-arm and enabled a graph to be punched on to paper fitted to a rotating drum synchronised with the movement of the crosshead. The magnification of crosshead displacement could be attained by pre-selection of the gearing between the crosshead and drum actuating mechanism.

Elongation and reduction in area were not measured for dogbone specimens but for Hounsfield No.12 specimens instruments specifically designed for this purpose enabled the determination of these values. These instruments were set with the initial specimen dimensions as the datum point and recorded the percentage elongation or reduction in area based on the final dimensions.

The yield stress was difficult to estimate since very often no clear yield point was exhibited. Yield stress was generally taken as the stress at the first deviation of the trace from elastic behaviour. Where yield stress is used for the purpose of calculations the method of derivation will be stated.

### 3.3.2 FATIGUE TESTING

Fatigue tests were only carried out on Ancoloy specimens but since pre-cracking of fracture toughness specimens of iron compacts involved the use of the same machine both test procedures will be described here for convenience.

The Amsler Vibrophore was employed with a three-point bend jig attachment using both the 0 - 4 and 0 - 20 kN load ranges. This

machine is based on a resonance principle, the number of cycles always coinciding with the natural frequency of the vibrating elements, i.e. jig and specimen. This condition is realised by a feedback control by means of an amplifier which excites the machine. The natural frequency depends on the size and elasticity of the specimen and on the weight of the oscillating masses. This latter can be varied by means of weights which can be added to the main mass.

The load acting on the specimen is measured by an optical dynamometer. A beam of light indicates directly on a scale the static as well as dynamic loads. The latter indication appears in the form of a band, the extremeties of which correspond to the upper and lower load limits. The load can be alternating ($\pm$) or fluctuating (0 to - or 0 - +) with any desired tensile or compressive pre-load. This load amplitude can be regulated exactly and maintained constant by means of a photo-electric regulating device controlled by a light beam of the dynamometer. A synchronous counter indicates the total number of load cycles applied to the specimen and in conjunction with a stop-clock incorporated in the control panel can be used to determine the operating frequency.

Fatigue pre-cracking of fracture toughness specimens of iron compacts was carried out on this machine. A frequency of approximately 140 Hz was recorded in these tests. The load required to initiate a fatigue crack was initially calculated from the following formula relating $\Delta K$, the fatigue stress intensity to Youngs Modulus E.

$$\Delta K = 0.00005\ E \qquad \ldots\ldots\ldots\ldots\ldots\ldots \quad (41)$$

where E was calculated from McAdams formula (equation 1). This

was found to under-estimate the loads required to cause initiation in a reasonable number of cycles (100,000), and in subsequent tests the loads were based on calculations of the notch tip stress. The maximum gross tensile stress in bending is given by :-

$$\sigma = \frac{6P}{BW} \quad \ldots\ldots\ldots\ldots\ldots\ldots \quad (42)$$

If the stress required is assumed to lie between the yield stress and the u.t.s., the application of the appropriate stress concentration factor allows estimation of the required load. This factor is given approximately by:

$$K_t = 1 + 2\,(t/\rho)^{\frac{1}{2}} \quad \ldots\ldots\ldots\ldots \quad (43)$$

where t is notch depth and $\rho$ notch root radius. Propagation loads for conventional materials are generally lower than initiation loads. In the case of sintered materials initiation and propagation loads were very similar. In order to meet the condition that the last 1.25 mm of crack growth occurs in not less than 50,000 cycles generally ensuring that $\Delta K$ does not exceed 0.67 $K_{IC}$, the load was gradually reduced during test. At no time throughout the test did $\Delta K$ exceed $0.75K_{IC}$. This ensured that pre-cracking conformed with the recommended practice stipulated in B.S.I.DD3[165]. Crack growth was monitored by optical microscope in conjunction with lines scribed at 1 mm intervals on the specimen surfaces. The crack length was taken to be the average of each surface measurement which was reasonably reliable since bowing of the crack front was not extensive and in some cases not observed. Final crack lengths were always in the range 0.45 - 0.55 a/W, a requirement for the subsequent fracture toughness test.

Fatigue testing of Ancoloy involved determination of the number of cycles to initiate a crack, $N_i$ for machined notches of various root radii, 0.127, 0.508 and 1.588 mm. Crack propagation data was also recorded. Notched specimens were loaded in three-point bending and cycled from zero to maximum load, the mean load being half the maximum load.

Since meaningful initiation data could only be obtained if a crack could be detected upon nucleation, an extremely sensitive technique was required. Cracks were expected to form in the central regions of the specimen at the notch root where plane strain conditions prevail. It is only possible to detect cracks optically once they have broken through to the specimen surface. A technique based on the electric potential drop enabled detection of cracks within the central regions of a specimen. Growth of a crack to a minimum detectable size was necessary but this method was still considered very sensitive. The minimum detectable size will naturally depend on the current, the material and potential points chosen and will vary for different materials.

The method was initially devised by GILBEY and PEARSON[166] for centrally cracked sheets. Because of the symmetry of the electric potential field about the crack centre-line it was suggested that the theory is equally applicable to edge notched sheet or single edge notched (S.E.N.) specimens. A constant current from a d.c. source was passed through the specimen and the electric potential drop across the notch and/or crack was monitored. The potential drop was measured at points $x \pm y$ at opposite sides of the notch centre line and near the origin, a condition shown to provide adequate sensitivity at all crack lengths. In order to avoid the use of the

small initial potential drop, Va in subsequent determination of crack lengths the potential gradient, Vo was measured independently. The ratio of the initial potential drop to potential gradient, standardised to account for specimen width could then be plotted as a function of crack length. The published curves of Va/VoW against a/W at various values of potential point separation x and y are reproduced in Fig. 20. It was suggested that initial values of Va/VoW be used to determine the separation of potential points, since measurement of these was difficult due to their close proximity. It was then possible to ascertain which of the family of curves was appropriate.

It was realised that the majority of tests carried out to determine fatigue crack initiation involved nucleation of cracks at notches or machined slots. This technique was consequently applied to notched specimens and found to be equally valid. It was concluded that notches merely caused an apparent increase in potential point separation and were equivalent to cracks of the same length as the notch depth[166].

Measurements of the following quantities were made during test: Vo, the potential gradient in the uncracked specimen; $Va_o$, the potential drop between points (x,y) and (x, -y) with a crack or notch of known length, $a_o$ and Va, the potential drop for the unknown crack lengths, $a_1$, $a_2$, $a_3$ etc....

The method was adapted for use in tests carried out on notched specimens in three-point bending assuming notches to be cracks of the same length. The electric circuit is shown schematically in Fig. 21a. In all cases specimens were insulated from the loading bars by inserting thin shims of cardboard sandwiched between mild

steel sheet. This was found to provide adequate electrical insulation for relatively low loads employed in these these tests, ($< 5kN$), but for higher loads the use of an insulated loading rig is recommended. The potential leads were iron wires, 0.30 mm diameter. Iron was selected to avoid thermal e.m.f.'s which could have been generated by temperature fluctuations. The leads were spot welded to the specimens as described in Fig. 21b, the value of y being 0.05W. Since the potential drop was a function of the area of crack and not merely its maximum length, this was considered the optimum arrangement as it encompasses the whole specimen thickness. This condition was thought likely to give a reasonable representation of the average crack length. The potential gradient was measured at a position intermediate between current leads and notch centre line. This was considered to be a region of uniform potential field. The separation of the probes was then measured after test with a travelling microscrope. Independent measurement of the potential gradient was not practical due to difficulties in accurate setting of the applied current from test to test. It was thus considered equally accurate to adopt the former procedure rather than measure the gradient on an unnotched specimen. The current in every test was nominally 15A which provided adequate sensitivity and did not result in heating up of the specimen.

The calibrations published by Gilbey and Pearson were found inadequate for this application and it was necessary to determine experimental calibration curves. Initially a fatigue crack was introduced into a specimen and allowed to propagate at different values of $\Delta K$. In this manner, alternate periods of growth at high and low values of $\Delta K$ gave rise to different fracture surface appear-

ance resulting in 'beach marks'. These differences in appearance arose from transitions in the fracture surface from rough to smooth at high and low $\Delta K$ values respectively. Simultaneous monitoring of crack growth with the potential drop enabled construction of a fatigue crack length vs potential curve. Crack lengths were measured using a travelling microscope after static fracture of the specimen. The extremely rough nature of the fracture surface of sintered material proved problematic in that accurate determination of the boundaries between different regions of fracture was difficult. In view of this fatigue cracks of various lengths were grown in a number of specimens, fractured under static load and finally the crack length measured. Crack length/potential curves were then built up over a range, 0.22 - 0.70 and 0.34 - 0.70 a/W. It was then possible to apply curve fitting techniques to the data so obtained and calibration curves for the above a/W ranges were produced. These curves are reproduced in Fig.22 for the various notch depths used in this work. Some tests were monitored both optically and by means of electrical potential such that surface crack length could be compared with the crack lengths predicted from the potential drop/crack length curves, Fig.23.

The test procedure was to set up the specimen in the bend rig, apply the pre-load, pass the current and allow a minimum of thirty minutes to obtain steady state conditions. After this initial thirty minute period the potentiometer was standardised and the microvoltmeter zeroed. Values of Vo and $Va_o$ were then measured in turn. The full scale deflection of the microvoltmeter could be varied but was used on the most sensitive scale, 50 $\mu$V and the excess voltage was balanced by means of the potentiometer. The

fatigue machine was then set in resonance and when maximum load was attained the chart recorder was set in motion. The number of load cycles was recorded from this point and monitored throughout the test. This was to prevent errors arising from variations in frequency which occur with Vibraphore resonnance machines, notably when the modulus of the specimen changes due to cracking.

The number of cycles to 'initiate' a crack was assumed to correspond to the first deviation of the potential trace from the initial value. Due to electrical noise inherent in the system the minimum detectable deviation was 0.25 $\mu$V. Once initiation had occurred the crack was propagated to a distance of 2 mm below the notch root, determined by surface crack length measurement. To ensure that overloading effects did not invalidate subsequent growth data this initial 2 mm of growth was conducted at ever decreasing loads. The final portion of growth was at a load below the propagation load. Propagation of the crack was then monitored by the potential as it grew at constant load. When the full scale deflection of the microvoltmeter had been almost exceeded the balance voltage was increased to bring the pen recorder back to 'zero'. Initially, the potential trace was a curve but eventually became a series of straight lines.

Successive increments in potential were used to calculate the appropriate crack length and the corresponding values of fatigue stress intensity. Recording the number of load cycles for each increment of crack length enabled calculation of growth rate, da/dN.

$$\frac{da}{dN} = \frac{a_2 - a_1}{N_2 - N_1} \qquad \text{.....(44)}$$

The fatigue stress intensity could then be calculated at each length, $a_1$ and $a_2$ and the average value over the crack length increment estimated. Growth curves were constructed from this data and log-log plots of da/dN against $\Delta K$ gave straight lines whose slope was equal to the growth exponent.

Initiation tests were carried out on notched specimens with notch root radii of 0.127, 0.508 and 1.588 mm and a depth of 5.5 mm. Material was tested over a range of densities, 5.95 - 7.00 $Mgm.m^{-3}$ a range of carbon contents, 0 - 0.65% at a density of 6.70 $Mgm.m^{-3}$ in the as-sintered condition. Heat treated material of 0.4% carbon content was also tested at densities of 5.95, 6.70 and 7.00 $Mgm.m^{-3}$. Tests were conducted over a range of loads (zero to maximum loading) in order to investigate the relationship between the number of cycles to initiation, $N_i$ and some function of stress. Two specimens were tested at each value of applied load. The stress function used was either that based on the elastic stress concentration factor, $K_t$ or the fracture mechanics parameter, $\Delta K/ \rho^{\frac{1}{2}}$. The two approaches were also compared graphically, Fig. 24.

Determination of the elastic stress concentration factor was based on Neuber's rule and his analysis of double notched bending[104]. A solution for three-point bending is not available and the analysis applies strictly to pure bending (four-point). The solution is outlined briefly in Appendix I. This method gave a reasonable approximation but the data reported would be of little use in design and applies only to the specimen configuration and loading geometry used in this work. Although this was an approximation it served to elucidate material behaviour and allowed rating of the various materials used in both the as-sintered and heat treated conditions.

The applicability of fracture mechanics parameters was also assessed.

Growth experiments were also carried out as previously described for the same material as in initiation tests. Growth rate data was the average of 3 - 8 specimens. In each case the load range was maintained constant to overcome problems associated with $K_{max}$ effects, important in low toughness materials.

### 3.3.3 FRACTURE TOUGHNESS TESTING

All toughness testing was carried out on a 50 kN Instron testing machine in three-point bending. The machine was calibrated prior to testing by means of weights and had an error of less than 1% on load measurements. The opening displacement of the crack tip was monitored by means of a clip gauge supported between knife-edges attached to the specimens. The load and displacement signals were fed into an X - Y plotter, the sensitivity of the displacement scale being adjustable to enable the correct slope of the trace ($45^{\circ}$ - $65^{\circ}$) to be obtained. The clip gauge was not calibrated and displacement was arbitrary but the gauge was set such that it could not drop out of the knife-edges during test. At the end of the test the fatigue crack length was measured on a travelling microscope at 0, 25, 50, 75 and 100% of specimen thickness. The average crack length was used in subsequent calculation of fracture toughness.

Iron powder specimens for toughness testing were initially pressed and sintered by B.S.A. Sintered Products Limited. Toughness specimens of thicknesses in the range 4 - 20 mm were obtained as previously described in 3.2.1. Four types of powder were tested each of a sintered density of 6.70 $Mgm.m^{-3}$. Notch depth was 8.5 mm, width 1.5 mm and root radius 0.127 mm. with an included angle of

$60^{\circ}$. Surface grinding was carried out after the notching operation. Three specimens were tested at each thickness and the average result recorded.

Additional specimens of these four powder types were prepared in the tool set described in 3.2.1 with dimensions of 110 x 25 x 12.5 mm at the same density as above. The machining operation was exactly as described for the industrially prepared specimens. A further experiment was carried out to compare the toughness of notched and pre-cracked specimens. Each of the four powder types were utilised at a sintered density of 6.70 $Mgm.m^{-3}$. A batch of 24 specimens six of each powder, was divided into two equal parts. Each part was notched as described previously, the first part to a depth of 8.5 mm and the remainder to a depth of 12.5 mm. Fatigue pre-cracking was carried out on the first portion under carefully controlled conditions such that the notch plus final crack length totalled 12.5 mm. Toughness tests were carried out on each of these two portions of the batch in the normal way.

Toughness tests on Ancoloy were carried out to investigate the relationship between toughness and sintered density in the range 5.95 - 7.00 $Mgm.m^{-3}$ at a carbon content of 0.4 wt-% in both as-sintered and heat treated conditions. At a density of 6.70 $Mgm.m^{-3}$ the effect of varying carbon content over the range 0 - 0.65 wt-% was examined in the as-sintered condition only. Additional specimens were used to compare the toughness values of notched and pre-cracked specimens as described previously for the four iron powders. The material in these latter tests was of 6.70 $Mgm.m^{-3}$ density and 0.65 wt-% carbon. Choice of material for this particular experiment was based on the requirements in BSI.DD3[165] for

valid toughness data which were shown to be met by this material. The force/crack opening displacement trace for this material was linear almost up to fracture.

Tensile specimens of the Hounsfield No.12 type were machined from the broken ends of toughness specimens. This was considered better practice than the use of dogbone specimens. Irrespective of the precautions taken to accurately reproduce the same conditions for dogbones as for toughness specimens this cannot be guaranteed. Hounsfield specimens were taken from the same piece of material and therefore, were considered to be preferable. Dogbones can provide a very useful means of obtaining data but this data should not be considered absolute. This can be attributed to the sharp corners of these specimens and for this reason care is to be exercised in use of data so generated.

Metallographic and fractographic samples were also taken from broken ends of toughness specimens. Fracture surfaces were maintained in their pristine condition by application of a protective lacquer applied immediately after fracture. This coating could be easily dissolved in acetone or a suitable solvent just prior to examination.

## 3.4. METALLOGRAPHY

The true pore structures present in these sintered materials were found difficult to examine due to flow of the metallic phase into the pores during polishing. This resulted in distortion of the pore structure and a method was devised to overcome this problem. Samples were first polished and deeply etched by normal metallographic techniques. Specimens were subsequently submerged in araldite and placed in a vacuum chamber which was then evacuated. The air was removed from the pores due to the prevailing vacuum

and on readmission of air araldite was forced into the pores. The araldite was allowed to harden, the process being accelerated by means of a low temperature curing treatment at 80°C in an oven. Repolishing the specimen in the normal manner gave satisfactory results which provided a truer representation of the actual pore structure. All metallographic work was carried out on araldite impregnated samples especially where quantitative work was involved.

Quantitative metallography was carried out on the Image Analysing Computer, Quantimet 'B'. This instrument can be set to detect either black or white phases. Adjustment of the threshold control can be used to determine the amount of any discriminated phase. Accuracy is very dependent on the ability of the operator to determine when the total area of the phase to be measured is being detected.

It was not possible to distinguish between porosity and inclusions and therefore the total measurement consisted of the area due to pores and inclusions. No attempt to correct for this was made and porosity measurements were consequently higher than values calculated from density measurements. Projection measurements were also recorded in order to calculate the mean linear intercept of pores and matrix. These measurements also contain a proportion of the total due to inclusions which could not be eliminated. In all quantitative work a minimum of 50 fields was taken using a x5 objective. The procedure was to set the threshold at a value judged to be correct. This was based on the position resulting in clearest delineation of the phase being measured. Once set, this position was not adjusted and on moving to a different field

the only adjustment made was to focus.

The measurement of both area and projection of a field allowed subsequent calculation of the mean pore intercept. The following formula was used for this purpose:

$$\text{Mean Linear Intercept} = L.A.P./M \quad \ldots\ldots\ldots \quad (45)$$

L is the length of field examined; A the fractional area of the phase; P the projection value and M, the magnification on the screen.

## 3.5. FRACTOGRAPHY

Fracture surfaces were examined by means of a scanning electron microscope, the depth of focus afforded by this instrument being considerably beneficial to this type of work. The main difficulty in fractographic studies of these materials was the extremely rough nature of the fracture surfaces. This was due to propagation of the crack from pore to pore by the easiest route involving considerable variation in the plane of the crack front. In some cases this deviation was so great that even with the depth of focus of the S.E.M. all parts of the image could not be focussed simultaneously. This did not severely limit the study of fracture surfaces and by adjustment of the beam angle adequate images could be obtained. Both fatigue and fast fractures were examined in order to assess the fracture mechanisms prevalent in each case. This was of particular advantage in fatigue where fracture appearance could be correlated with growth rates or more specifically growth exponents.

# 4. RESULTS

## 4.1 IRON POWDERS

### 4.1.1 MECHANICAL PROPERTIES

The four powder types used, Hoganas ASC 100, Electrolytic, Hoganas NC100 and ROSPOL MP32 were shown to have compressibilities at 400 MN. $m^{-2}$ of 6.83, 6.70, 6.62 and 6.42 Mgm.$m^{-3}$ respectively, Table 2 and Fig. 25.

Over the range of densities investigated the tensile strength measured on dogbone specimens was shown to exhibit an almost linear relationship with density for each powder, Fig. 26. The tensile and yield strengths at a density of 6.70 Mgm.$m^{-3}$ for each powder obtained from Hounsfield specimens (no.12) from toughness test pieces were consistently higher than dogbone data, Table 3.

The fracture toughness did not vary significantly with powder type at a density of 6.70 Mgm.$m^{-3}$ which was not in keeping with tensile strength data. Specimens made by the two routes described in 3.3.3 were shown to have different toughness values, laboratory produced specimens being tougher than industrially pressed specimens. The former laboratory values exhibited a trend of increased toughness with reduction in mean linear intercept of pores but the actual differences were not significant at the 5% level, Tables 4 & 5. The pore structures of each powder are shown in Fig. 27 which includes micrographs and S.E.M. photographs.

Toughness was shown to be constant over the range of specimen thicknesses tested, 4 - 20 mm for each powder type, Fig. 28. The results exhibited considerable scatter as indicated in the graphs. The fracture surfaces were flat over the whole range of thicknesses

with only slight evidence of shear lips, Fig. 29. In 4 mm thick specimens there was a tendency to fracture on other planes than that perpendicular to the applied stress, (see discussion). Evidence of plasticity on the surface of these specimens was also noted and can be distingusihed in the photographs.

The critical thickness supposed to ensure plane strain conditions, indicated on Fig. 28, was between 6 and 8 mm. This indicated that the range of thickness tested was adequate in each case. The force/displacement traces for these powders, shown in Fig. 30, indicated that extensive deviation from linearity occurred prior to final fracture and in all tests $P_{max}$ was greater than $1.1.P_Q$. $K_Q$ values were therefore invalid and could not be termed plane strain fracture toughness values, $K_{IC}$. For purposes of comparison a force/displacement trace for the low alloy steel (Ancoloy) is also shown in Fig. 30 and this latter trace resulted in a valid $K_{IC}$ value.

The toughness values of notched specimens were generally lower than those for pre-cracked specimens. There was, however, little difference between these results and they were statistically the same at the 5% significance level. Force/displacement traces comparing pre-cracked with notched specimens, Fig. 31, indicated that they were of the same form. Both traces showed substantial deviation from linearity prior to final fracture. Toughness values could not be termed $K_{IC}$ values in either case, $P_{max}$ being greater than $1.1.P_Q$. The maximum loads for notched specimens were higher than for pre-cracked specimens when the notch plus fatigue crack was equal to the machined notch depth.

### 4.1.2 FRACTOGRAPHY

Fatigue fracture surfaces indicated that propagation occurred by progressive failure of interparticle bonds between pores shown in S.E.M. photographs, Fig. 32. Two basic forms of bond failure were apparent. The most prevalent type of bond failure was ductile dimple formation but, in general, many of the features of the fracture surface were obscured, probably by friction of adjacent crack faces. The second type consisted of flat areas of bond failure with very few recognisable features. These latter areas did not occupy an extensive proportion of the total fracture surface in these powders. All four powders exhibited similar fatigue fracture surfaces and no differences were observed between individual powders.

The fast fractures exhibited basically the same type of fracture mechanism in as far as rupture occurred by interparticle bond failure in a pore to pore manner. The actual bond failures consisted of ductile dimple features and were essentially identical to the fractures observed in tensile specimens, Figs. 33 and 34. In some cases particles were observed in dimples.

## 4.2 ANCOLOY SA

### 4.2.1 MECHANICAL PROPERTIES

The compaction characteristics of this powder allowed production of compacts with a range of densities from 5.95 - 7.00 $Mgm.m^{-3}$ for compaction pressures in the range 200 - 600 $MN.m^{-2}$, Fig.35. The compressibility at 400 $MN.m^{-2}$ was 6.70 $Mgm.m^{-3}$, comparable with the electrolytic iron powder in 4.1.1 and higher than the sponge iron powder, Hoganas NC100, from which it was made.

The yield and tensile strengths of this material over the above density range increased with increasing density. This behaviour was observed in both the as-sintered and heat treated material, Fig. 36. The density/strength relationships for as-sintered and heat treated conditions were approximately parallel. Compacts with yield strengths ranging from 171 - 324 $MN.m^{-2}$ and tensile strengths of 191 - 388 $MN.m^{-2}$ were obtained in as-sintered material of 0.4 wt-% carbon and the same material heat treated gave 246 - 461 $MN.m^{-2}$ yield strength and 286 - 506 $MN.m^{-2}$ tensile strength. Variation in the carbon content enabled further extension of the property range. The relationship between carbon content and yield and tensile strength was approximately linear for as-sintered compacts of 6.70 $Mgm.m^{-3}$ density, Fig. 37. These results, which were obtained from Hounsfield No.12 specimens machined from the broken ends of fracture toughness test pieces, are recorded in Table 6a).

Fracture toughness was shown to vary from 11.5 - 25.8 $MN.m^{-3/2}$ over the density range 5.95 - 7.00 $Mgm.m^{-3}$ for as-sintered material of 0.4 wt-% carbon. At the same carbon content and over the same density range toughness in the heat treated condition varied from 18.0 - 33.9 $MN.m^{-3/2}$, Fig. 38. Increase in carbon content from 0 to 0.65 wt-% gave rise to an approximately linear increase in toughness from 14.9 - 26.4 $MN.m^{-3/2}$ for as-sintered material of 6.70 $Mgm.m^{-3}$ density, Fig. 39 and Table 6b).

A plot of toughness against compaction pressure, Fig. 40, showed that the toughness tends to a limiting value with compaction pressure in a similar manner to other strength properties.

A linear relationship between tensile strength and fracture

toughness was observed, Fig. 41 and all results could be represented by the same line irrespective of density, carbon content or condition (as-sintered or heat treated). A similar relationship was also observed between yield strength and toughness, Fig. 42, although yield strength was assumed to correspond to the stress where the force/extension curve deviated from linearity. Both relationships exhibited remarkably narrow scatter bands when the source of these results is considered.

A comparison of notched and pre-cracked toughness indicated that higher toughness was obtained for notched specimens, although the differences were only minimal, Table 6. Material used for these tests had densities of 6.70 and 7.00 $Mgm.m^{-3}$ and 0.65 wt.-% carbon in the as-sintered condition which gave a valid pre-cracked toughness of 26.4 and 29.1 $MN.m^{-3/2}$ respectively.

### 4.2.2 FATIGUE CRACK INITIATION AND PROPAGATION

Fatigue crack initiation results were interpreted in the form of log-log plots of $N_i$, the number of cycles to initiate a crack - represented by the first deviation of the potential trace - against a function of stress. Log $N_i$ was plotted against the parameter based on the elastic stress concentration factor, $K_t \Delta S$ and another on fracture mechanics $\Delta K / \rho^{\frac{1}{2}}$, Figs. 43 - 50. These results were obtained from specimens of density 5.95, 6.40, 6.70, and 7.00 $Mgm.m^{-3}$ in the as-sintered condition for notch root radii of 0.127, 0.508 and 1.588 mm. Irrespective of the parameter used the results exhibited a marked 'banding' effect where results for each root radius lay on approximately parallel bands. The smallest root radius gave rise to better resistance to initiation of fatigue cracks

in all cases. Two equations may be used to represent initiation behaviour:

$$N_i = A/(K_t \Delta S)^n \quad \ldots\ldots\ldots\ldots (46)$$

for the approach based on Neuber's Rule: and

$$N_i = A/(\Delta K/\rho^{\frac{1}{2}})^n \quad \ldots\ldots\ldots (47)$$

based on fracture mechanics. The corresponding values of A and n together with the initiation data are given in Tables 7 (a - d).

Similar treatment of the results from specimens in the heat treated condition were obtained and are shown in Figs. 51 and 52 and recorded in Table 7(e).

Comparisons between the initiation behaviour of specimens at each density were made and revealed a gradual increase in resistance to fatigue crack initiation with increasing density, becoming less pronounced at the higher densities. These results are given in Figs. 53 and 54. A notch root radius of 0.508 mm was chosen in order to compare as-sintered and heat treated material which was tested only at this particular root radius. The difference between as-sintered and heat treated material was noticeable at the lowest density but no significant differences were evident at higher densities, Fig. 55.

The exponents in equations 46 and 47, representing initiation behaviour and given by the slopes of log-log plots of $N_i$ versus $K_t \Delta S$ or $\Delta K/\rho^{\frac{1}{2}}$ were between 2.5 and 4.5. The exponents for heat treated material appeared generally higher than for as-sintered material at all density levels examined.

The fatigue crack propagation data was plotted in terms of da/dN versus $\Delta K$, fatigue stress intensity, on log-log scales giving

rise to straight lines. These data can be represented by the power law:

$$\frac{da}{dN} = C \Delta K^m \quad \ldots\ldots\ldots\ldots\ldots\ldots (48)$$

In log-log plots of the data the slope represents the growth exponent, m and the constant C, the intercept. The data for as-sintered material at various densities and 0.4 wt-% carbon were compared as shown in Figs. 56 - 60. Indicated on these graphs are the respective static fracture toughness values for each density which represent the upper limiting fatigue stress intensity for growth according to equation 48. No attempt was made to determine the lower limit or 'threshold' values of $\Delta K$ in this work. The general trend was a decrease in growth rate at a particular fatigue stress intensity with increasing density. The growth behaviour of heat treated and as-sintered material at a carbon content of 0.4 wt-% and densities of 5.95, 6.70 and 7.00 $Mgm.m^{-3}$ were also compared, Figs. 61 and 62. The effect of carbon content for as-sintered material of 6.70 $Mgm.m^{-3}$ density was also examined, Fig. 63.

The constants and growth exponents together with the corresponding growth rate and fatigue stress intensity data are given in Tables 8, 9 and 10. The as-sintered material exhibited a decrease in growth exponent as density was raised, the effect being more pronounced at lower density levels and showing little significant difference at the higher end of the density range. Heat treated material showed a similar trend and in addition, exponents were lower than those of the as-sintered counterparts. As-sintered material at a density of 6.70 $Mgm.m^{-3}$ indicated a decrease in exponent with increasing carbon content in the range 0 - 0.65 wt-%. For purposes

of discussion at a later stage these results were thought best represented in the form of a plot of fracture toughness against growth exponent, Fig. 64. This graph portrays the increase in exponent observed as fracture toughness values decrease.

A more convenient method of representing these data from a design point of view is in the form of life plots. Here crack length, a is plotted against the number of load cycles, N. The critical crack length for static fracture can be obtained from fracture toughness data and marks the limit of component life. This analysis is based on equation 48:

$$\frac{da}{dN} = C\ \Delta K^m$$

where

$$\Delta K = \frac{\Delta P\ Y}{BW^{\frac{1}{2}}} \qquad \ldots\ldots\ldots\ldots\ldots\ldots\ (49)$$

Substituting for $\Delta K$ and rearranging

$$dN = C^{-1} \left(\frac{\Delta P\ Y}{BW^{\frac{1}{2}}}\right)^{-m} .da$$

$$\int dN = C^{-1} \left(\frac{\Delta P}{BW^{\frac{1}{2}}}\right)^{-m} \int \frac{1}{Y^m} \cdot da$$

Since $Y = f(a)$

Applying limits to the integrals, $N_f$, $a_f$ and $N_o$, $a_o$ where $N_o$ and $a_o$ are the initial number of cycles and initial crack length respectively.

$$N_f - N_o = N = C^{-1} \left(\frac{\Delta P}{BW^{\frac{1}{2}}}\right)^{-m} \int_{a_o}^{a_f} \frac{1}{Y^m}. da \qquad \ldots\ldots\ (50)$$

and $N_f$ and $a_f$ are the values of N and a at failure.

Since Y is a polynomial function of a;

$$Y = 6\,[1.93(a/w)^{\frac{1}{2}} - 3.07(a/w)^{3/2} + 14.53(a/w)^{5/2} - 25.11(a/w)^{7/2} + 25.80(a/w)^{9/2}] \quad \ldots\ldots (51)$$

The value of the integral between the limits $a_o$ and $a_f$ can be estimated by means of Simpson's One Third Rule as described in Appendix II.

Any desired value of $a_o$ and load range $\Delta P$ may be chosen and this fixes $a_f$ when the fracture toughness is known. A life plot may thus be constructed for any particular material when the fatigue crack growth equation is known together with the appropriate fracture toughness data. Such plots were constructed for material of 6.70 $Mgm.m^{-3}$ density at various carbon levels and compared with the plot for 0.4 wt-% carbon material in the heat treated condition, Fig. 65. An initial crack length of 0.5 mm. was selected together with a load range which gave a fatigue stress intensity of 6 $MN.m^{-3/2}$ for three-point bend specimens. This load range gave a gross stress of approximately half the yield stress of 0.4 wt-% carbon, as-sintered material. The limiting crack lengths, $a_f$ were obtained from toughness data and are marked on the plots. In this way it was shown that it would be possible to obtain similar lives for 0.4 wt-% carbon heat treated material and 0.65 wt-% carbon material, as-sintered. Raising the carbon content of as-sintered material was in this case equivalent to heat treating lower carbon material.

### 4.2.3 FRACTOGRAPHY

Various materials were examined using the scanning electron microscope. Examples are shown in Fig. 67. These micrographs will be referred to in more detail in the discussion section.

### 4.2.4 OPTICAL VERSUS ELECTRIC POTENTIAL METHOD FOR MONITORING CRACK GROWTH

The optical method of monitoring crack growth was compared with the electric potential method for two specimens, one for growth from a 5.5 mm deep notch and the other for growth from an 8.5mm deep notch. Two different calibration curves were constructed for these two specimens, Fig. 22 and these results also serve as a means of assessing the accuracy of these curves. The results clearly showed that there was little difference between the two methods. The optical method, based on surface crack length, gave rise to under-estimation of crack lengths. The electric potential method, based on average crack length across the whole section of the specimen, is expected to more nearly represent the true crack length. The graph indicates that the crack length/potential relationships for each method were parallel. The results for optical measurement were off-set to lower crack lengths. The small differences observed indicated that only slight bowing of the crack front - the major source of error in optical measurements- occurred in these materials, although some bowing was evident when actual crack front positions were measured.

# 5. DISCUSSION

## 5.1 IRON POWDERS

The four types of iron powder used in this work exhibit different compacting properties, Fig.25, which can be attributed to the differences in particle morphology as illustrated in scanning electron micrographs, Figs. 1 - 5. At a particular density level tensile strength shows little variation indicating that similar strength levels may be attained with different powders by varying compaction pressures. Assessment of the relative advantages of a powder in terms of compressibility necessitates a cost balance. This entails evaluation of the cost savings realised from a reduction in die-wear when powders of improved pressing quality are used. This saving must be equated with the increased cost of powders of higher compressibility, Table 2. It is observed that a powder of increased compressibility, Hoganas ASC100 is about twice as expensive as a sponge iron powder of normal compressibility, Hoganas NC100. In the long production runs characteristic of the P/M industry where numerical outputs are large, savings in die-life can be considerable if compaction pressure can be reduced, even if only by a small amount. Lubricants are very useful in reducing die-wear but the savings realised by reducing compaction pressures may still be significant. Other properties must be considered, in particular, flow properties which control die-fill may be improved in conjunction with compressibility and must be taken into account. Die-fill is important since this to a large extent controls the number of compacts which may be produced in a given period. Labour costs are currently a large proportion of the final compact cost and it is therefore

advantageous if production rates can be increased.

Comparison of fracture toughness values of sintered compacts of these four iron powders reveals no significant differences between individual powders. The pore morphology and distribution is shown to vary for each powder, Figs. 27a) - 27h), the extent of this variation being indicated by the results of lineal analysis in Table 4. A more detailed examination of the pores utilising scanning electron microscopy reveals that there are always sharp corners present, Figs. 27i) - 27l). It is the presence of these sharp corners which appears to be of major importance with respect to toughness; more important than the overall morphology and distribution, within the range of material studied.

Advance of the fatigue crack in a fracture toughness specimen is dependent on the region immediately ahead of its tip and the microstructural features within this 'process zone'. The crack appears to propagate from pore to pore, being attracted by the stress concentrations around the pores. Deformation within the plastic zone associated with the crack tip can be concentrated at the sharp corners of pores leading to large plastic strains eventually exceeding the fracture strain of the matrix. This then results in the possible nucleation of microcracks at the sharp corners of pores. Extension of the crack is thus due to advance of its tip in conjunction with the linking back of microcracks formed at pores within the plastic zone. The distance between the crack tip and adjacent pores is therefore an important feature since toughness is controlled by processes occurring ahead of the crack tip. Pore spacing would therefore seem a major factor influencing the toughness of sintered materials.

The relatively small differences in pore distribution observed in the four powder types tested appear insignificant and the important feature of pores would seem to be their morphology. This is similar to the effect of graphite morphology in cast irons discussed in Section 2.

Two interesting points arise when comparing toughness values for industrially produced compacts (B.S.A.) and for those produced in the laboratory, Table 5. For convenience, these two groups of compacts are termed A and B respectively.

Firstly, the fracture toughness values of B compacts are slightly higher than A compacts. There is a difference in the processing of groups A and B which merits consideration. The sintering time for group A was $\frac{1}{2}$ - 1 hour, the producers being rather vague concerning this matter and the time for group B was 1 hour. This time difference is not expected to influence the strengths but the ductility of B compacts could have been increased by the longer sintering time. This latter fact would induce an increase in toughness but the uncertainty concerning sintering time for A compacts prevents further comment on this point. It seems more likely that an explanation of this effect will be found by examining the relationship between pressing and notching directions, Fig. 17. The notching direction in A compacts is in the pressing direction and density variation is also in this direction. The central regions of the specimen are of lower density relative to the surfaces. Notching is perpendicular to the pressing direction for B compacts and the density variation is in the direction of the compact thickness. In the latter case the material across the crack front varies in density but through the thickness the average density is experienced

and the toughness reflects the average density. The crack front in A compacts, however, is always in a region of lower density than the average compact density, since crack length in toughness specimens is always between 0.45 and 0.55 W. It is possible that this density effect accounts for the observed higher toughness of B compacts. It is notable also that the scatter in results is less pronounced for B compacts which lends further support to an argument based on density variation. The foregoing discussion indicates that directionality effects cannot be overlooked in sintered materials where density variations through different sections of a component are always present.

The second point is that B compacts exhibit a clear relationship between toughness and pore distribution. The highest toughness values correspond to the smallest mean pore intercept and spacing in Hoganas NC100. The lowest toughness corresponds to the largest mean pore intercept and spacing exhibited by Hoganas ASC100, Table 4. The important point is that the powders which have the lowest mean pore intercept and spacing tend to have rounder pores. The incidence of sharp corners is thus diminished in these powders and is responsible for the slightly higher toughness. This effect is undoubtedly masked by scatter in the results for A compacts. The actual differences observed in toughness are only small and statistically insignificant at the 5% level.

The results obtained indicated that if one proceeds via the normal processing route no significant differences in toughness are observed between the four powder types investigated. A wide range of powder types are used industrially and powder usage is far from standardised. Where toughness does not vary significantly from

powder to powder, provided the process route remains the same, there are obvious advantages.

The absence of variation in toughness with specimen thickness in the range 4 - 20 mm, Fig. 28, is indicative of the pronounced effect of porosity in sintered materials. The deformation of porous bodies is significantly influenced by the porosity distribution where bulk deformation is inhibited due to interruption of the matrix by pores. Localised deformation consequently occurs in the interpore regions leading to large local strains eventually exceeding the fracture strain of the matrix. The net result is low strain fracture which becomes less prevalent as porosity is reduced. In the toughness testing of pre-cracked specimens the constraint stresses generated at the tip of the crack in thick specimens are of extreme importance in conventional materials. The incidence of such triaxial stresses gives rise to flat plane strain fracture. This condition corresponds to low energy fracture and is characterised by a minimum value of fracture toughness, $K_{IC}$. In sintered materials relaxation of triaxial stresses may occur by extension of the pores which offer no constraint, the bond strength between pore and matrix being zero. Support for this postulate is the fact that triaxiality enhances coalescence of holes in the Thomason model for hole growth[47]. Advance of the crack is clearly dependent on the stress and strain distribution in the region immediately ahead of its tip. Since it is readily established that the crack propagates from pore to pore, the ligament of material between crack tip and adjacent pores is the critical element over which crack advance occurs. Within these microregions conditions can be considered to approach plane stress as a result of their limited size and the relaxation of tri-

axial stress by plastic deformation at the pore/matrix interfaces. A combination of these two facts is thought to be directly responsible for the constancy of toughness over the range of thickness tested because triaxial stresses can be relaxed irrespective of gross specimen thickness.

The critical thickness to ensure plane strain conditions, calculated from equation 38, is indicated on the graphs in Fig. 28 and lies between 6 and 8 mm for each powder. This indicates that the range of specimen thickness tested is adequate although it is questionable whether equation 38 is applicable to sintered materials. It is unlikely in this case that plane strain conditions exist and the applicability of equations derived for conventional materials seems doubtful because the porosity has such a pronounced effect on stress and strain distribution. In every case, however, the fracture surfaces were flat with slight evidence of shear lips, Figs. 29a) - 29e). Evidence of plasticity on specimen surfaces is clearly visible in these macrographs and appears more extensive than indicated by the calculated plane stress plastic zone size of about 0.5 mm.

In some 4 mm specimens low values of toughness were recorded and fracture surfaces indicated failure on planes other than those perpendicular to the applied stress, Fig. 29e). This is thought to be caused by elastic buckling of the specimen due to the small section size. Buckling induces mode III opening (described in 2.2.1.), and thus the toughness value is a combination of $K_I$ and $K_{III}$ values. As $K_{III}$ is lower than $K_I$ the toughness values can be expected to be reduced and this is reflected in the results. An example of a similar nature is reported in the literature where the introduction

of anti-buckling guides increased the toughness of aluminium sheet by a factor of two[167]. The effect is obviously not so pronounced in the case in question but the foregoing fact supports the theory.

Fatigue crack fronts were observed to be curved in B compacts and this is thought to be due to through thickness density variations. This was seldom observed in A compacts which exhibited flat crack fronts. The curvature of fatigue crack fronts arising from an increased resistance to propagation at specimen surfaces can be attributed to the higher density of these regions compared to the central zones. In conventional materials curved crack fronts generally arise from the plane strain/plane stress transition which occurs from centre to surface. The plane stress plastic zone, being larger than the plane strain plastic zone, consumes more energy and the propagation of the crack is thus slower at the specimen surfaces. The transition from plane stress to plane strain is not likely in sintered compacts for reasons explained previously and the original argument seems more applicable to this type of material.

The form of the force/crack opening displacement traces of these materials is interesting because relevant information concerning their fracture characteristics may be obtained. From Fig. 30 it is noted that considerable deviation from linearity occurs prior to attaining maximum load, $P_{max}$. Values of $P_Q$ obtained from the 5% off-set method are consequently considerably less than $P_{max}$ which was greater than $1.1P_Q$ in every test. In accordance with B.S.I. DD3[166], this invalidates the results and toughness values may therefore only be termed $K_Q$ and not $K_{IC}$. This does not exclude the use of these results for comparative purposes even though they cannot be regarded as absolute toughness values.

Deviation of the trace from linearity can arise from two sources, either excessive plasticity or crack extension. Plasticity in the small neck regions between pores and crack tip is liable to be extensive but on a macroscopic level this is restricted. The curve for the low alloy sintered steel indicates that raising the yield strength causes a reduction in this deviation. Plasticity can thus be related to the strain hardening capacity of the metallic matrix, being higher for the ferritic iron powders than for the ferrite/pearlite structure of the low alloy steel. The second possibility is crack extension, termed stable crack growth when occurring prior to attainment of maximum load and has been discussed by McCLINTOCK[168]. Briefly, the mechanism is as follows. Advance of the crack places its tip in a region of lower strain due to the strain gradient which prevails, Fig. 66. The increased length of the crack naturally results in elevation of the level of strain distribution ahead of its tip. Due to the steep slope of this distribution the strain is still, however, below the fracture strain by an amount $d\varepsilon$. The load must then be increased with resultant increase in strain before further crack extension may occur. In this manner stable crack growth progresses until instability is attained when extension of the crack occurs at ever decreasing load. At instability the elevation of strain distribution due to crack advance just compensates for the reduction in strain arising from the steepness of the slope of the strain distribution.

The form of the force/c.o.d. traces exhibited by iron powders probably arises from a combination of the two effects discussed above. It is not clear from this work which of the two effects is prevalent. Further work would be necessary before this could be

established and a suggested approach will be discussed in the further work section.

It is relevant at this stage to discuss the toughness values measured on notched specimens. In general, notched toughness values are lower than those for pre-cracked specimens although when a/W (notched) is equal to a/W (pre-cracked), the maximum loads are higher for notched specimens. Considering the force/c.o.d. traces shown in Fig. 31, it is observed that the deviation from linearity is greater for notched specimens. This can be attributed to the larger plastic zone associated with a notch compared to a fatigue crack. Values of $P_Q$ obtained via the 5% off-set procedure are thus lower for notched specimens since the elastic slopes are the same. The lower toughness of notched specimens is thus an apparent effect being due to the estimation technique employed. It is important to establish the validity of toughness measurement on notched specimens since the introduction of fatigue cracks is both costly and time-consuming. This is a very relevant consideration which would greatly facilitate the introduction of toughness determination in the industry as any means of reducing both costs and testing times is beneficial.

Scanning electron microscopy enables the assessment of the fracture mechanisms operating in sintered material under both fatigue and monotonic loading. The fatigue fracture surfaces indicate that cracks propagate from pore to pore by successive rupture of inter-pore material. Rupture appears to take two specific forms indicating that two failure modes occur. The most prevalent type consisted of ductile dimples but in some cases dimple free areas of fracture were observed, Fig.67. These latter areas are similar to some features

previously observed in cast iron specimens[169]. On these areas, 'ridge-like' features are visible and no evidence of void formation is observed. Some micropores are present on these features and are thought to be residual porosity.

Ductile dimples are thought to be associated with trans-particle fracture and ridged areas with interparticle fracture. This conclusion is reached after consideration of the conditions which prevail at interparticle bonds. Oxide films on particle surfaces are fragmented during the compaction process, leaving a 'plane of weakness' at interparticle boundaries. These are prime sites for this type of failure due to the presence of oxide inclusions. A similar mechanism is responsible for cleavage failure in mild steel. Fracture of a boundary carbide particle due to stress concentration resulting from a dislocation pile-up within a grain leads to cleavage. Ridge-like features are also observed in this type of fracture, normally referred to as river lines or tear marks. During fatigue such failure in sintered materials could possibly arise from a fast burst of rupture at maximum load during the cycle. This point will be expanded further later.

Static fractures appeared to be of the same nature as fatigue fractures, Fig. 67. Dimple size varied considerably and this can be attributed to the source of dimple formation. This can be due to either inclusions or to micropores of varying sizes.

## 5.2 LOW ALLOY STEEL POWDER (ANCOLOY SA)

The compressibility of this powder is comparable with electolytic iron powder and considerably higher than the sponge iron powder from which it is produced. This is possibly due to the fact that an

individual particle consists mainly of unaffected pure iron (ferrite) to which the finely divided alloying elements are diffusion bonded. The alloying elements themselves may allow better keying together of individual powders in addition to which the iron particles may be softer and more compressible than sponge iron.

The tensile and yield properties of this powder show the expected increase with reduction in porosity, the slope of the curves in Fig. 36 increasing on approaching higher compaction pressures. An interesting observation is the almost parallel behaviour of as-sintered and heat treated material indicating that strength is predominantly controlled by the percentage porosity. The improved strength properties obtained by heat treatment, whilst still controlled by the porosity, arise out of the increased resistance to deformation and fracture of the ligaments between pores. This fact is readily established when the mechanism of failure is considered. The tensile rupture of porous materials occurs by progressive linking of the pores across the specimen. This process occurs by concentration of stress at the tips of pores and their subsequent extension. The pores can be envisaged perhaps, as microcracks and thus the tensile strength is a function of the resistance of the matrix to the propagation of these 'microcracks'. Further discussion of this point will be deferred until the relationship between tensile strength and toughness is examined.

The low elongation values common in porous materials renders yield stress determination extremely difficult. Elongation in tensile tests on this low alloy steel rarely exceeding 2% and the elastic limit was utilised in place of the yield stress in calculations of plastic zone size and critical thickness to ensure plane

strain. In general, yield stress is difficult to measure on sintered materials and its use as a design parameter is questionable. This problem centres on the definition of the yield stress of sintered materials since on a microscale the relevant parameter is the yield stress of the metallic matrix. The value of yield stress is merely a reflection of the porosity content.

The variation of fracture toughness with sintered density in both as-sintered and heat treated conditions confirms earlier work[41]. The expected rise in toughness occurs as the density is increased, results for as-sintered and heat treated material lying on approximately parallel curves, Fig.38, as was the case for strength properties, Fig.36. This suggests that the factors which control strength properties also control fracture toughness.

When toughness is plotted against compaction pressure, Fig.40 a curve of ever decreasing slope is observed. This curve is of the same form as both density and tensile strength versus compaction pressure curves. This is an indication that there is a limit to property development by increase of compaction pressure. Further improvements in properties require other processes such as sinter-forging. If the conventional route for compact production is adopted other means must be sought in order to develop property levels beyond those attainable by increasing compaction pressure. Such means would be metallurgical and should be vigorously pursued by industry with a view to developing improved alloys.

The influence of carbon on fracture toughness is clearly beneficial, toughness increasing with carbon content by some 70% over the range 0 - 0.65 wt-%. This is an example of how manipulation of metallurgical factors can be utilised advanteously with respect

to toughness. A further example is connected with heat treatment. An oil quench followed by a 200°C tempering treatment carried out on a 0.4 wt-% carbon alloy at a density of 6.7 $Mgm.m^{-3}$ gives rise to a 30% increase in toughness, Table 6. Combinations of the above two factors can be employed successfully to develop toughness beyond present levels.

Tensile strength depends firstly, on the porosity content and secondly, on the resistance to deformation and fracture of the remaining metallic matrix. The resistance of the matrix to deformation and fracture is the same irrespective of porosity content, provided the condition of the material remains unchanged but the pores cause concentration of stress and strain.

Fracture toughness can be interpreted as a material's resistance to cracking and in a fracture toughness test piece extension of the fatigue crack depends on the resistance of the small region of material ahead of its tip. Because the crack propagates from pore to pore the distance between crack tip and the neighbouring pores is vitally important. This distance can be considered to represent the critical element over which fracture takes place, deformation being concentrated in this ligament of material.

The foregoing discussion clearly indicates that both tensile strength and fracture toughness tests are controlled by the same fundamental material parameters. Support for this hypothesis is provided by the linear relationship between these two properties illustrated in Fig. 41. This figure incorporates data from material in a wide range of conditions; various density levels, carbon contents and treatments. All the data can, however, be represented by one straight line. This suggests the possibility of correlating tensile

strength and fracture toughness. The relatively narrow scatter bands derived from the 95% confidence integral indicate a high degree of correlation. From a practical viewpoint this is an extremely useful finding because further development may allow the derivation of fracture toughness from the basic tensile test. This would render the application of toughness data more attractive to the P/M industry as it precludes the need to carry out expensive testing on costly equipment once the groundwork has been covered. It is important to note that development and application of toughness testing of sintered materials are in their early stages. Up to the present time little progress has been made either in measurement techniques or application of data. The use of fracture toughness data in general is shrouded in scepticism throughout all branches of industry. In the author's opinion, although there are many problems yet to be solved, the advent of toughness data for general engineering purposes is imminent. It is also felt that the P/M industry would benefit considerably by adopting a toughness approach to design. The aim should be to convince designers of the merits of fracture mechanics and to encourage their acceptance of sintered materials as structural parts. Toughness data allows the material to be placed in its correct position in order of merit compared to other materials. Confident design calculations based on such data are also possible. Current trends in the P/M industry are towards thermo-mechanical techniques of component production such as powder rolling and sinter-forging. It is in these types of material where oxide inclusions and residual porosity assume importance where maximum tolerable defect size must be established. These are the very problems which are suited to the application of modern fracture mechanics analyses.

It is pertinent at this stage to attempt to quantify the empirical relationship observed between tensile strength and fracture toughness. A number of K-calibrations can be applied to a tensile specimen with an array of defects[170]. No single solution ideally satisfies the conditions which pertain to a tensile specimen in uniaxial tension machined from sintered material containing porosity as defects. Taken to the extreme the total defect size in a central plane can be considered to be agglomerated to form a large central penny shaped crack, Fig. 68. The area of this 'defect' can be obtained as a proportion of the cross-sectional area by using the fractional porosity. Applying the relevant K-calibration for a penny shaped defect in a cylindrical bar axially loaded in tension, the value of $K_I$ at the maximum load in the tensile test can be calculated. This solution is based on the method of assymptotic approximation and was derived by BENTHEM and KOITER[171] with an accuracy better than 1%.

$$K_I = \sigma_{net} (\pi a)^{\frac{1}{2}} . f(a/r) \qquad \ldots\ldots\ldots\ldots (52)$$

where a is the defect radius and r the specimen radius. The net stress can be related to the tensile strength through the maximum load at fracture and subsequently to the value of $K_I$ at fracture which can be considered to be $K_{IC}$

$$\sigma_{net} = P_{max}/\pi(r^2 - a^2) \ldots\ldots\ldots\ldots (53)$$

$$P_{max} = \sigma_u \pi r^2 \qquad \ldots\ldots\ldots\ldots (54)$$

where $\sigma_u$ is the ultimate tensile strength. Thus,

$$\sigma_{net} = \sigma_u r^2/(r^2 - a^2)$$

Therefore:

$$K_{IC} = \frac{\sigma_u r^2}{(r^2 - a^2)} \cdot (\pi a)^{\frac{1}{2}} \cdot f(a/r) \quad \ldots\ldots\ldots \quad (55)$$

Values of f(a/r) are obtained from the graphs published in the original reference[171]. Assume a material of density 6.7 $Mgm.m^{-3}$ and 0.65 wt-%C for which the fractional porosity is 0.15. The radius of a defect is thus the radius which corresponds to an area 15% of that of a Hounsfield No.12 specimen of radius 1.602 mm. The defect radius is then 0.62 mm. The value of f(a/r) which corresponds to such a radius is equal to 0.56. The measured tensile strength for this material is 411 $MN.m^{-2}$. This gives a $K_{IC}$ value at fracture of 12 $MN.m^{-3/2}$. This value is only about 50% of the measured toughness value of 26 $MN.m^{-3/2}$. This is, of course, a gross approximation and not surprisingly the predicted toughness value is considerably less than the measured value. The separation of the defects is such that the ratio of the spacing to defect size is of the order of four although some porosity is interconnected and leads to interaction effects. The analysis is thus inadequate, the actual defects being far worse than the assumed defect.

An additional analysis can be applied to this situation, again an approximation and not entirely justifiable in terms of the real physical situation. The calibration is that for a circumferential crack in a cylindrical bar developed by BUECKNER[172], Fig. 69. This analysis is based on a singular integral equation and has an accuracy of better than 1%.

$$K_I = \sigma_{net} \ (\pi a)^{\frac{1}{2}} . f(a/r) \quad \ldots\ldots\ldots\ldots \quad (56)$$

where $\sigma_{net} = P/\pi b^2$

Using the same approach as in the last example.

At fracture,

$$\sigma_{net} = \sigma_u \frac{r^2}{b^2} \qquad \ldots\ldots\ldots\ldots\ldots (57)$$

$$K_{IC} = \sigma_u \left(\frac{r^2}{b^2}\right) . (\pi a)^{\frac{1}{2}} . f\,(a/r) \qquad \ldots\ldots\ldots\ldots\ldots (58)$$

where $f(a/r) = 0.46$

Inserting the relevant values in equation 58 yields a toughness value of about 28 $MN.m^{-3/2}$ which is slightly in excess of the measured value of 26 $MN.m^{-3/2}$. This method gives better numerical fit to the data but it is still necessary to justify its application in terms of the physical situation. This model seems more appropriate since surface defects are more effective stress concentrators than internal defects and thus more likely to lead to fracture at lower loads.

Theoretical analyses of the effect on stress intensity of rows of coplanar defects have shown that reduction in spacing leads at the most to a doubling of the stress intensity[173,174]. An additional effect of the interaction between parallel rows of defects is the reduction of the stress intensity[174]. This is said to be a stress relieving effect and results in a reduction in the K-value of about one third. These results are indicative of the complex nature of the interaction effects which occur between pores. A combination of the above effects undoubtedly leads to the inability of the above analyses to adequately represent the experimental results. It is important to investigate models incorporating the co-operative effects of pores in sintered materials. This could promote the development of tougher components manufactured from sintered materials with a view to application in stressed structures. An alternative

approach to the problem of model development would be to use an equivalence approach. An equivalent defect size could be advanced for any particular material. In this respect the circumferential type of defect seems most applicable. Since the effect of surface defects is more severe than the effect of internal defects, models based on this type of analysis seem most applicable.

Further examination of the observed tensile strength/fracture toughness relationship, Fig. 41, reveals the potential of this type of empirical relationship. Material of sintered density 6.7 $Mgm.m^{-3}$ is considered, being within the density range commonly used for industrial applications. Tensile strength or fracture toughness versus carbon content can be adequately represented by linear relationships of the form $y = mx + c$, Figs. 37 and 39 and Table 6. Regression lines obtained from this data result in the following equations:

$$\text{Tensile Strength } (T) = 260\ (\%C) + 240 \quad \ldots\ldots\ldots (59)$$

$$\text{Fracture Toughness } (F) = 18\ (\%C) + 15 \quad \ldots\ldots\ldots (60)$$

Considering the above material with a carbon content of 0.4 wt-%

$$T = 348\ MN.\ m^{-2}$$

and

$$F = 22.2\ MN.m^{-3/2}$$

The tensile strength/fracture toughness relationship can also be represented by a linear equation of the above form obtained from regression analysis of the data plotted in Fig. 41.

$$T = 14(F) + 36 \quad \ldots\ldots\ldots\ldots (61)$$

For a tensile strength of 348 $MN.M^{-2}$

$$F = 22.3\ MN.m^{-3/2}$$

The two values of toughness obtained in the above manner agree very closely. Comparison with the measured toughness value of 21.9 $MN.m^{-3/2}$ indicates that the correlation is extremely good. This is naturally a very simplified approach based on the limited amount of data available. Further investigation is warranted but the above example indicates that this is a viable method. Predictions based on empirical relationships such as the preceding equations could have a useful role in the development of fracture mechanics techniques applied to P/M components.

Fatigue crack initiation results for both as-sintered and heat treated material indicate that there is little advantage to be gained by using either $K_t \Delta S$ or $\Delta K/\rho^{\frac{1}{2}}$. For the specimen type used (SEN 3-point bend) the $\Delta K/\rho^{\frac{1}{2}}$ approach is more applicable since $K_t \Delta S$ applies strictly to pure (4-point) bending. In addition the fracture mechanics approach is the more versatile and open to future development which could bring about its more widespread application. Although this parameter is at present inadequate and not wholly satisfactory, it has more significance than $K_t \Delta S$ which has little meaning, save for the assessment of relative material behaviour. In future discussion reference will be made solely to $\Delta K/\rho^{\frac{1}{2}}$ data.

As-sintered material at various levels of density shows the expected increases in initiation life with increasing density, Fig.54. Initiation of a fatigue crack at a notch will occur at some defect at the root of the notch, arising from the machining process in conventional materials. Since pores can be considered to be defects, the amount of porosity is an important feature. It is clear that

reduction of porosity decreases the number of defects at the notch root with subsequent improvement in the resistance to fatigue crack initiation. Material with a density of 7.00 $Mgm.m^{-3}$ appears to have a lower resistance to initiation than material of 6.70 $Mgm.m^{-3}$ density. No physical explanation would seem immediately apparent to account for this effect. The most feasible explanation would seem to be that this is an effect of the scatter in the results which is considerable although not so apparent on log-log scales. Statistically there is no significant difference between the two sets of results at the 5% level.

The comparison of as-sintered and heat treated material is somewhat difficult to explain. Low density material shows a distinct improvement in the heat treated condition but medium and high density material appear the same in each condition, Fig. 55. These results are perhaps a manifestation of the machining process which constituted the final operation prior to testing in each case. The machining of notches with milling cutters may induce residual stresses in the material below the notch and these stresses are generally compressive[175]. Residual stresses of this nature would tend to cause improved initiation life, acting in an opposing direction to the notch root stress generated during cycling. It is possible that as-sintered material being of lower matrix yield strength can deform locally during machining resulting in compressive residual stresses at the notch root. Heat treated material having a higher matrix yield strength may not undergo such deformation and as a consequence no residual stresses remain. This, in part, may explain the apparent absence of differences between as-sintered and heat treated material at medium and high densities. It does not explain, however, the

improved properties of heat treated, low density material. The high residual porosity of the latter material - 10% greater than medium density material - may overshadow machining effects. That is to say, there are so many sites for initiation in addition to the relatively small amount of material between pores that other effects are insignificant. Consistent with this argument is the fact that the lines for as-sintered and heat treated material appear to merge at high values of $\Delta K/\rho^{\frac{1}{2}}$. A more detailed study would be necessary before any definite conclusions could be drawn concerning these data. It is clear that machining effects can exert considerable influence on initiation and this has, indeed, been illustrated in a previous study[176].

The effect of notch acuity on initiation life is clearly demonstrated in Figs. 44 - 50, sharply notched specimens exhibited greater resistance to initiation than bluntly notched specimens. It is apparent that the use of the factor $1/\rho^{\frac{1}{2}}$ to account for notch acuity is inadequate since banding of results occurs even when this correction is applied to $\Delta K$. The improved initiation lives of specimens containing sharp notches is believed to be a stress gradient effect. The electric potential technique, having limited sensitivity, can only detect cracks of a certain minimum length - about 0.05 mm. Inevitably, therefore, the measured initiation life, $N_{i(m)}$ must contain an element of growth $N_{i(g)}$ such that:

$$N_i(m) = N_i\,(\text{true}) + N_i\,(g) \quad \ldots\ldots\ldots\ldots \quad (62)$$

The initiation life is thus a function of the sensitivity of the measurement technique. The proportion of crack length due to growth requires a finite number of cycles which in turn depends on

the stress field at the notch root, or more precisely the stress gradient. The steeper this gradient the slower is the growth because the crack tip is continually growing into a region of steeply falling stress until it emerges from the notch tip stress field. Sharply notched specimens with steep stress gradients thus appear to have longer initiation lives than bluntly notched specimens where the gradients are less severe. In view of these factors it is not difficult to see that the derivation of an absolute relationship between initiation life, $N_i$ and some function of notch tip stress is arduous. The data obtained in this work is merely a reflection of the sensitivity of the measuring technique. It may be that a correction factor of the form $1/\rho^{\frac{1}{2}}$ is adequate but the inability to detect the true initiation event does not allow confirmation of this fact.

The initiation exponent, n in the equation

$$N_i = A/(\Delta K/\rho^{\frac{1}{2}})^n \qquad \ldots\ldots\ldots\ldots (46)$$

is in general about three for this material. In accordance with the Bilby-Cottrell-Swinden model for initiation, exponents of two are predicted[108]. Initiation in sintered material may be governed by this mechanism and two feasible theories may be advanced in order to explain the observed values of exponent. It is accepted that some growth of the crack occurs prior to its detection and this might be expected to be governed by the equation:

$$\frac{da}{dN} = C\,\Delta K^m \qquad \ldots\ldots\ldots\ldots\ldots (47)$$

The exponent for this equation is generally recognised to be four[130]. The measured initiation life is thus comprised of two components,

one due to true initiation and the other due to growth. An exponent between two and four would then seem reasonable on the basis of this argument. It is not certain, however, that the growth corresponds to equation 47. The notch stress field exerts considerable influence on growth rate, initially causing a reduction as was demonstrated in earlier work[121]. There is thus some doubt associated with the above argument as it is not certain that it adequately depicts the real physical situation.

An alternative explanation is that a unique model may be required to describe initiation in porous material, taking into account such factors as pore size, geometry and spacing. Pores represent defects in the structure and as such are sites for the nucleation of fatigue cracks, being expected to enhance initiation. The pore geometry and spacing determine subsequent growth of the crack since these factors affect the stress distribution and the critical element over which crack advance occurs during cycling. The above factors alone could account for the high values of exponent observed. This latter argument appears more viable than the previous since it attempts to accommodate factors pertaining to the real physical situation at the notch tip. It would require a more detailed research programme to isolate the relevant factors and incorporate them in a coherent theory of fatigue crack initiation in sintered material. Data at present is too sparse to permit such an attempt but it is worthy of further attention.

Before examining growth data it is necessary to give account of the accuracy of the measuring technique adopted. A comparison of optical and potential drop methods of crack monitoring is presented in Fig.23 and shows that there is little difference between the two methods. The electric potential method is considered more accurate

since it corresponds to the total area of the crack whereas the optical method only indicates average surface crack lengths. Fatigue crack fronts were observed to be slightly curved, tunnelling forward in central regions of the specimen. This is not thought to be due to a plane stress/plane strain transition from surface to centre of specimens for reasons discussed earlier with reference to toughness data. The curvature of the crack front is thought to result from the slightly higher densities at specimen surfaces compared to the central regions. Material at the surface thus has a slightly higher resistance to crack propagation which could account for bowing of the crack fronts.

The difference between the two measuring techniques is slight and the two curves are approximately parallel. The optical method indicates a shorter crack length than that predicted by the potential drop. The results are as expected and in good agreement to within 5%. This not only indicates that the optical method is adequate for this material but also that predictions of crack length by the electric potential technique are accurate. This latter point serves as additional confirmation of the accuracy of the calibration curves of Fig. 22.

The growth data is somewhat easier to explain than the initiation data. The comparatively large amount of experimental data ensures that spurious effects due to scatter are minimised, facilitating interpretation. An increased density produces a decreased growth rate at a particular fatigue stress intensity. Growth is shown to occur in a pore to pore manner, linking pores adjacent to the crack tip. Crack branching is commonly observed where the crack grows out of the plane of maximum stress between crack tip and lower

loading point. Once out of this plane growth ceases after some distance as the stress tails off, becoming insufficient to promote growth. In view of the large number of pores distributed throughout the structure bifurcation of the growing crack tip can easily occur.

The growth mechanism can be assessed by reference to scanning electron micrographs, Figs. 67a) - 67i) which show two types of fracture surface in each case. These were in the main of a ductile dimple nature in addition to some fracture areas of a flat and apparently featureless type. The latter type probably result from interparticle bond failure whereas ductile dimple type rupture is probably associated with transparticle failure. Interparticle rupture may occur as 'fast burst' monotonic failure at the maximum load during the fatigue cycle which corresponds to $K_{max}$, the maximum fatigue stress intensity. Monotonic failure is common in low toughness material, particularly at high $K_{max}$ values, approaching the static toughness value[177]. Although no quantitative measurement of the relative amounts of each type of fracture were made, interparticle fracture appeared more frequently in low density material. The sites for this type of fracture are probably large oxide inclusions or boundary carbides. The former arise from break-up of oxide films on powder particles during compaction and the resultant oxide inclusions provide paths of weakness through the material when suitably oriented. Consideration of the growth data and in particular the ratios of the maximum fatigue stress intensity, $K_{max}$ to the fracture toughness, $K_{IC}$ reveals that these are lower for low density material. The material under test is of low toughness and thus the available testing range is necessarily restricted, more so for low than high density material. It is recognised that the overall fatigue

curve is sigmoidal and this curve is approximated to three straight line regions on a log-log plot of da/dN versus $\Delta K$, Fig.16. The first region is generally of steep slope rising to some threshold value followed by a region of slope four and corresponding to the Paris equation[130]; $da/dN = C \Delta K^m$. The final region arises for values of $\Delta K$ in excess of $K_{IC}$ and is again of very steep slope. The second region corresponding to the Paris equation is of interest in this discussion. The incidence of 'fast burst' failure in low toughness materials is expected to occur as the fatigue stress intensity approaches the static fracture toughness. At such high $\Delta K$ values favourably oriented 'weak' ligaments of material rupture in a purely monotonic manner on attaining the maximum load during the cycle.

Where the test range is close to the transition between growth regions two and three higher growth exponents are expected. This is due to the contribution to growth rate of monotonic bursts of rupture. This may in part contribute to the reduction of growth exponent as density is increased since at low densities the testing range is closer to the toughness value. Additional factors may be involved in reducing growth exponents by increasing material density. The reduction in porosity itself may be a contributory factor where the amount of material through which fatigue cracks must propagate is increased. Interaction between neighbouring pores may also be important.

Toughness has been increased by several methods and the corresponding reduction in growth rate appears independent of the method employed. Raising the carbon content or density and heat treatment promote increased toughness and each method results in

reduced growth exponent and rate as indicated in Figs. 60, 62 and 63 and Tables, 8, 9 and 10. A plot of toughness against growth exponent confirms the relationship between these two factors, Fig.64. This is evidence of the link between increased toughness and improved resistance to crack propagation.

Increased carbon content improves the resistance of the matrix to propagation by virtue of the increased amount of pearlite and improved mechanical properties. Heat treatment produces a different structure and one which possesses improved mechanical properties compared to as-sintered material and hence is more resistant to crack propagation. In this latter case, heat treatment appears beneficial at each level of density tested 5.95, 6.70 and 7.00 $Mgm.m^{-3}$. The dominant feature is the porosity content of the material but other variables may be manipulated to obtain optimum properties. The most economic route must then be assessed in order to take best advantage of the beneficial effects of the above variables on fatigue crack propagation.

The range of material tested is somewhat limited but the general trend is one of increasing resistance to propagation with improved toughness.

A useful means of assessing the fatigue life of a material was outlined earlier in 4.2.2. This analysis applied to the experimental data illustrated in the 'a' versus 'N' plots of Fig. 65. It is apparent from these data that an increase in carbon content can be just as beneficial as heat treating. In terms of the economics of the process it would seem less costly to increase carbon additions than to carry out heat treatment. Where fatigue properties are considered important, an analysis such as this is advantageous.

A preliminary assessment gives a reasonable indication of relative material behaviour. Considerable cost savings may be realised where components are to be subjected to fatigue loading in service.

It is apparent from all the above work that a wide variety of properties are possible from this low alloy steel powder. Whilst only a limited range of data has been obtained it serves as a useful guide for assessing which variables are important and whether their influence is major or minor. Ancoloy is a material open to further investigation. The fracture mechanics concepts applied to this work provide a viable means of analysis. Such concepts allow assessment of material performance under both static and cyclic loading conditions. The direct application of such data for design purposes would still seem remote. Future development may well see the advent of design techniques based on fracture mechanics applied to sintered materials. It may then be possible to promote the use of such material for structural components by means of these powerful techniques. Progress in the P/M industry would seem very dependent on expansion of the sintered material market into the field of structural components. Fracture mechanics can assist this expansion considerably.

## 6. RECOMMENDATIONS FOR FURTHER WORK

There is considerable scope for further investigation to be carried out on the fracture toughness of sintered iron compacts. This would necessarily incorporate evaluation of the effects of process variables such as sintering temperatures and times in addition to alloying additions particularly where pore morphology is affected. The pore morphology is shown to be of the utmost importance in that the sharp corners control the toughness properties. An increase in the root radius of these sharp corners (pore rounding) tends to increase toughness values although the effect in this work is only minor. It would be of considerable interest to explore the effect of significant changes in pore morphology. The possibility of achieving such changes by means of activated sintering processes would seem attractive. It would be important to assess the significance of the increases in toughness which might be realised by such treatment. This naturally becomes a problem of economics in that it is necessary to assess the cost of increased toughness by this proposed route compared with a more conventional method such as alloying.

The absence of a specimen thickness effect on toughness was only noted at one density level, 6.70 $Mgm.m^{-3}$. It is important to confirm whether this effect persists as density levels are raised. It is possible that as density increases some effect of specimen thickness will manifest itself. As the amount of porosity is reduced the ability of the material to allow relaxation of constraint stresses is diminished. If the material is able to develop constraint stresses, a reduction in toughness, consistent with the associated transition from plane stress to plane strain is expected. This may have con-

siderable bearing on the ultimate application of toughness data.

The mechanism of crack advance during a fracture toughness test is not clear. Two possible explanations for the deviation from linearity of force/c.o.d. traces were discussed earlier. It is necessary to establish how this deviation arises, whether from excessive plasticity at the crack tip or from stable crack growth prior to instability. A means of establishing which of these two mechanisms is operative would be to monitor crack length during test. A convenient method would entail the use of the electric potential system. In this relatively simple manner the contribution of stable crack growth to opening displacement may be assessed. This is in fact an accepted technique applied to toughness testing of low and medium strength materials described in B.S.I DD19[178] where the onset of crack extension must be determined.

The correlation between fracture toughness and tensile data requires further investigation both for Ancoloy and other sintered materials. In order to provide a better understanding of this phenomenon it seems necessary to develop models which adequately describe the deformation of porous materials. The relationship suggested is empirical and some theoretical justification is required.

Initiation data is inconclusive and much further experimentation is necessary. It is not clear that correlation of initiation life, $N_i$ with $\Delta K/\rho^{\frac{1}{2}}$ provides an adequate means of expressing initiation data. A modification of this parameter is required and this should incorporate other factors such as the interaction effects of notch stress field, crack tip stress field and bulk stress field. Initiation studies are generally difficult and considerable effort should be directed towards outlining the major contributory factors relevant to sintered materials.

Growth data for Ancoloy indicates that many factors are important. A useful means of applying these data is in the form of life plots. This approach could be expanded and perhaps refined to incorporate initiation data. Further development is required, in particular, this approach, should be applied to real components and its validity assessed.

It is clear that many areas require clarification as very little research has been carried out on this aspect of the properties of sintered materials. Outlined above are just a few areas requiring further investigation and arising directly from current research.

## 7. CONCLUSIONS

Numerous minor conclusions connected with material type, composition and treatment may be inferred from this work. Three major conclusions are immediately apparent and of some relevance to the future development of mechanical properties of sintered materials.

(1) Pore morphology is the most important single variable controlling the fracture toughness properties of the iron powders tested.

(2) Experimental data for the low alloy steel powder indicate a clear relationship between fracture toughness and tensile strength which, although empirical, may be exploited as a cheap means of assessing toughness in this material.

(3) A fracture mechanics approach to fatigue crack propagation provides an adequate means of assessing material behaviour. In particular, life plots ( a versus N ) are shown to provide a very useful method of comparing data for material of differing composition and subjected to differing treatments.

## 8. ACKNOWLEDGEMENTS

The author wishes to thank Professor W.O. Alexander for provision of laboratory facilities and the University of Aston for provision of a maintainance grant. Thanks are also due to Dr J.C. Billington and Dr J.T. Barnby for guidance and helpful discussions.

## 2. TABLES AND FIGURES

| Mesh<br>Micron<br>Powder | +85<br>180<br>% | -85+100<br>149<br>% | -100+150<br>104<br>% | -150+200<br>74<br>% | -200+300<br>53<br>% | -300<br>-53<br>% | Average Particle size (um) |
|---|---|---|---|---|---|---|---|
| Höganäs NC 100 | 0.001 | 9.145 | 26.30 | 28.41 | 21.82 | 13.91 | 79 |
| Höganäs ASC 100 | 1.462 | 12.50 | 19.96 | 24.73 | 23.02 | 18.33 | 76 |
| ROSPOL MP 32 | 0.2228 | 3.029 | 21.61 | 32.48 | 25.71 | 16.97 | 73 |
| Electro-lytic | 0.01 | 0.1 | 0.2230 | 11.87 | 44.52 | 43.28 | 60 |
| Carbonyl | 1.118 | 3.575 | 3.058 | 9.672 | 5.940 | 76.67 | 57 |

Table 1: Sieve analysis of various iron powders (to MPIF Standard 5-62)

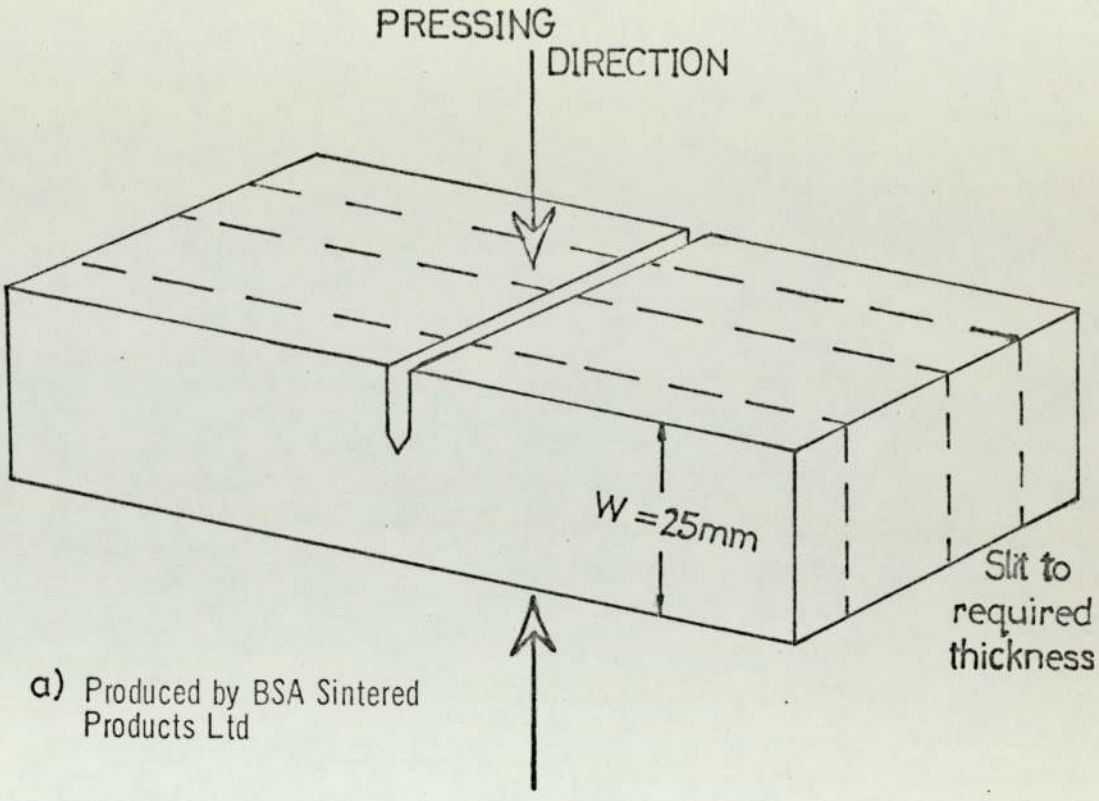


a) Produced by BSA Sintered Products Ltd

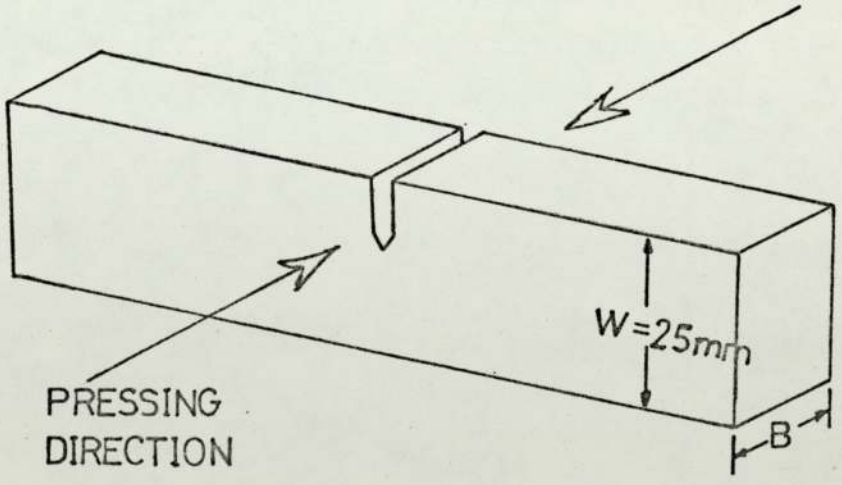


b) Produced in the Laboratory

Fig.17 - Relationship between pressing and notching directions in fracture toughness specimens

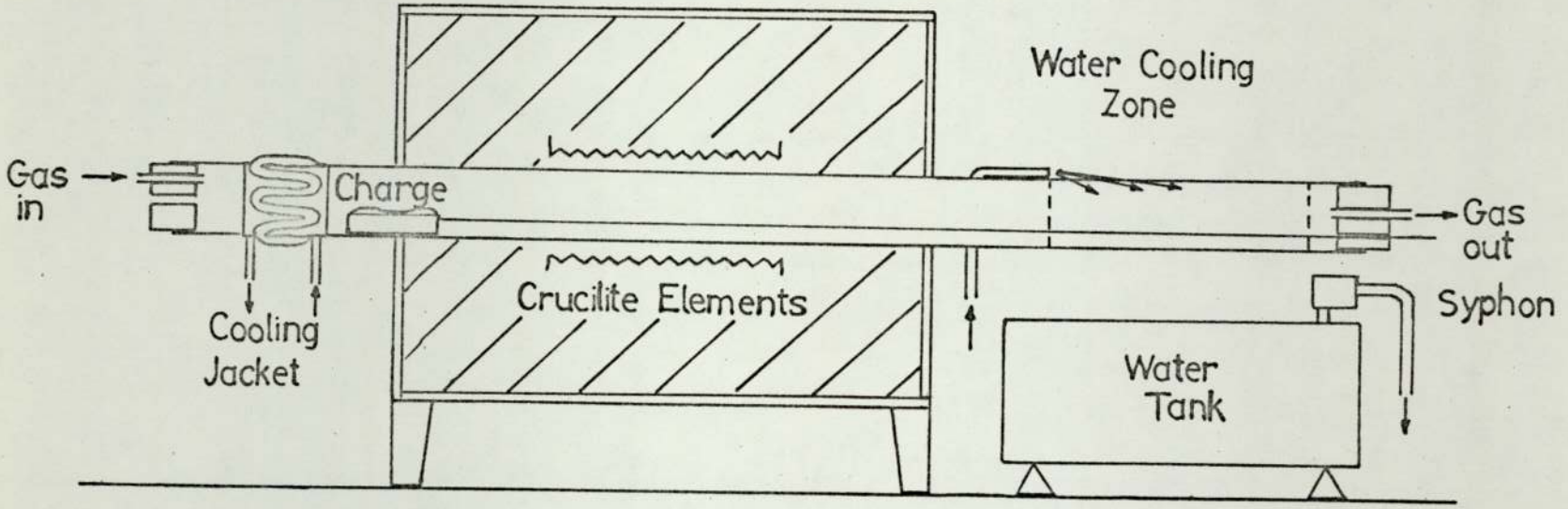


Fig.18 - Sintering furnace

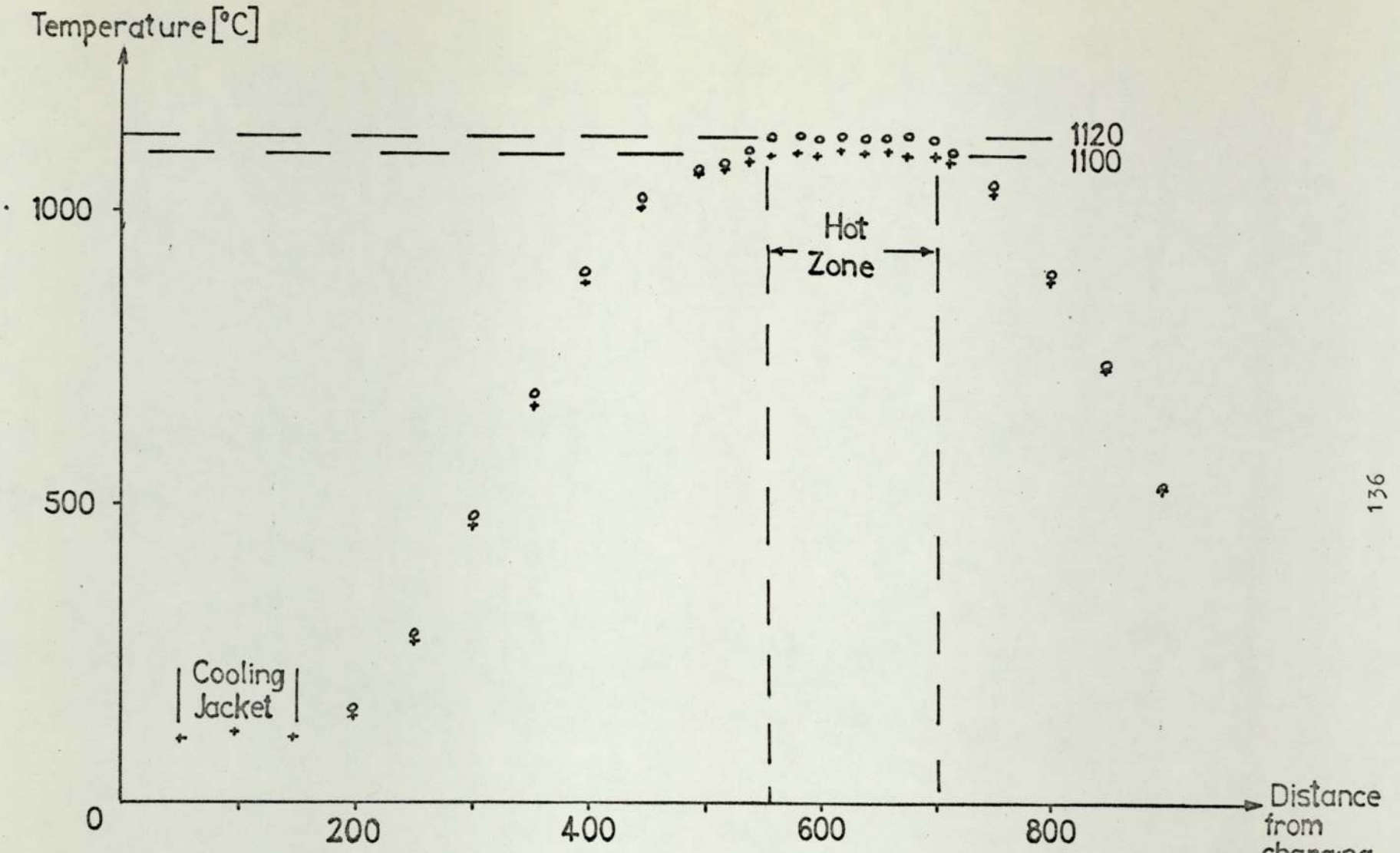


Fig.19 - Temperature gradient in sintering furnace

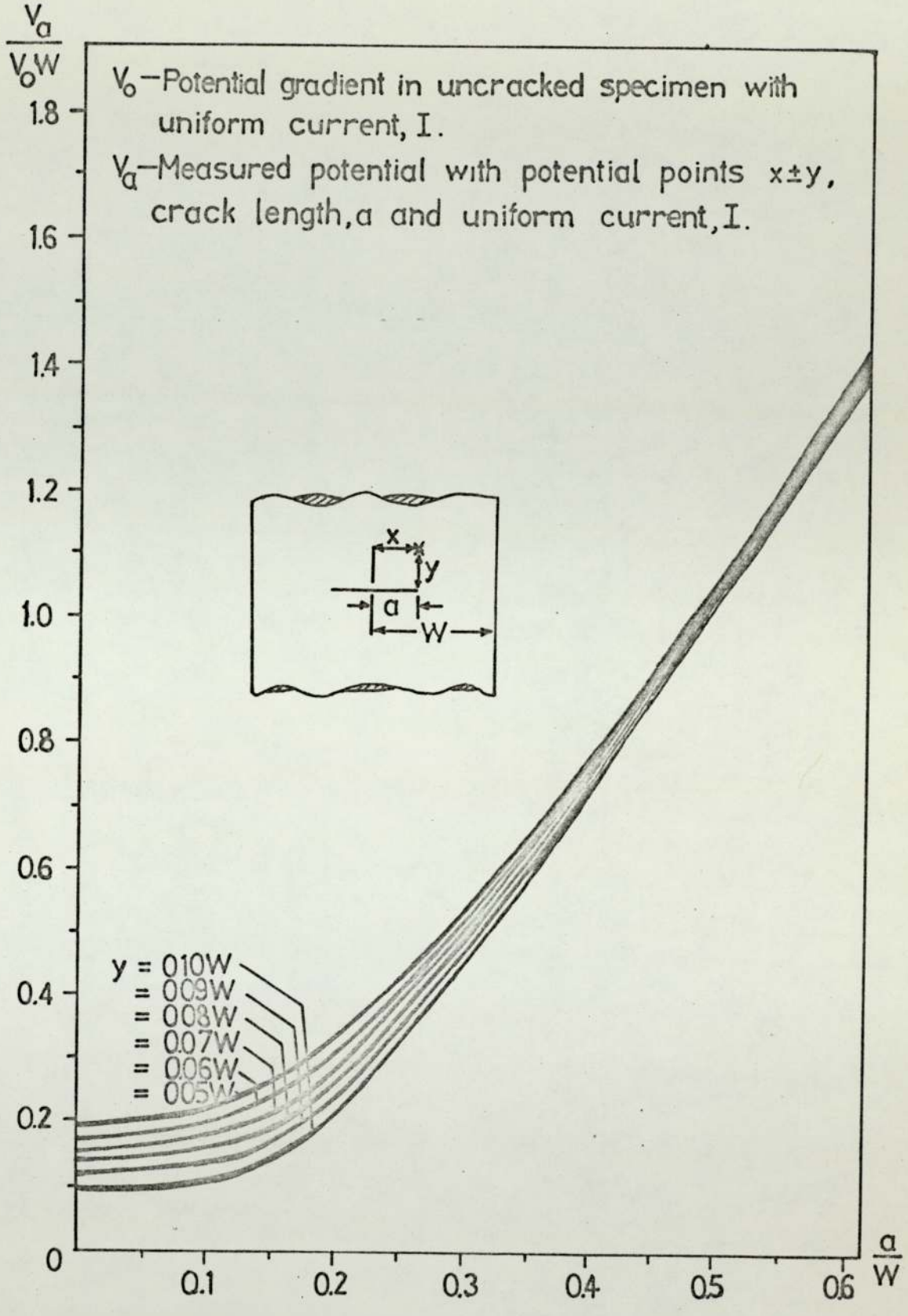


Fig.20 - Electric potential vs crack length

(after Gilbey and Pearson [166])

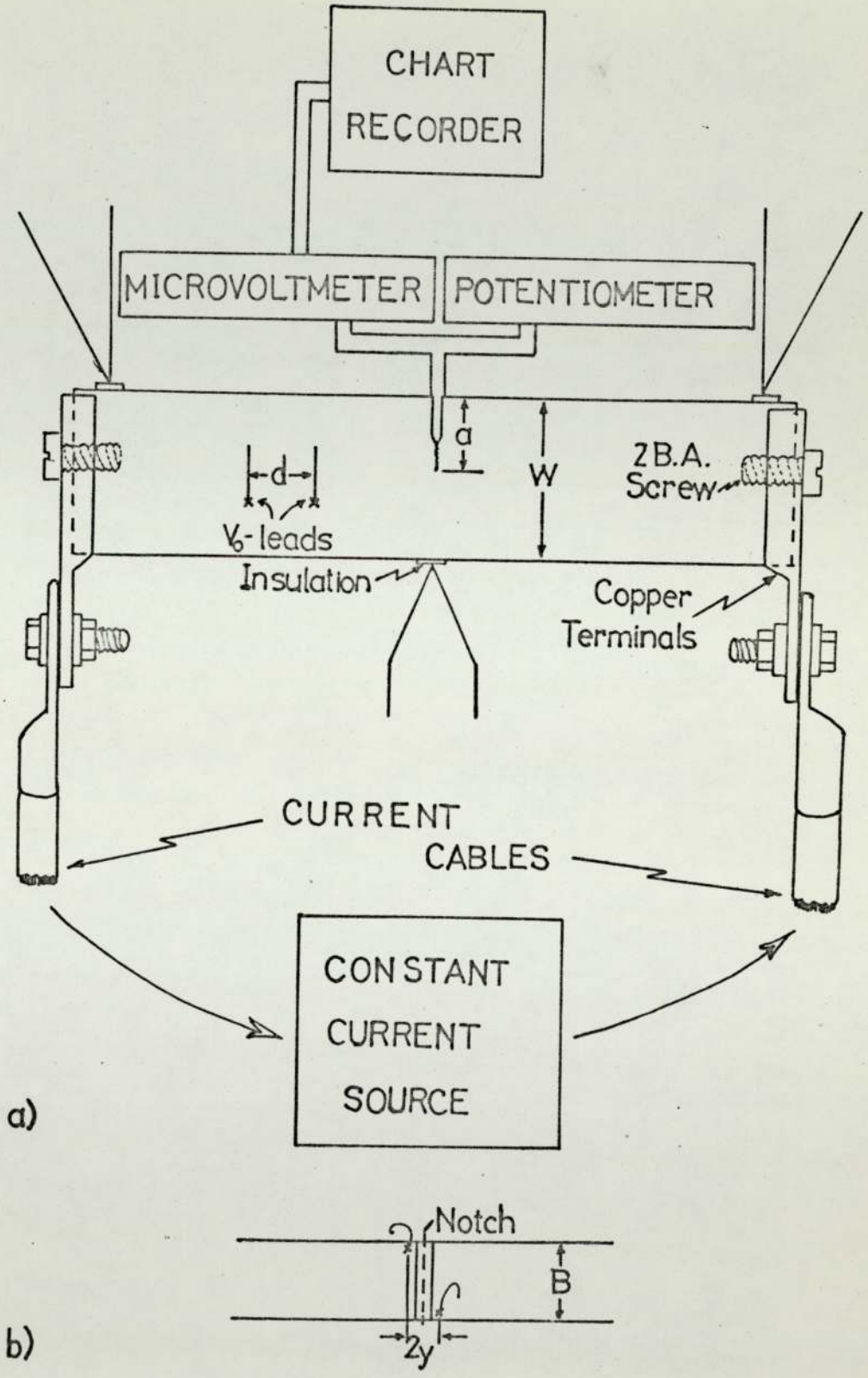


Fig.21 - a) Schematic representation of potential drop measurement
b) Positioning of potential probes

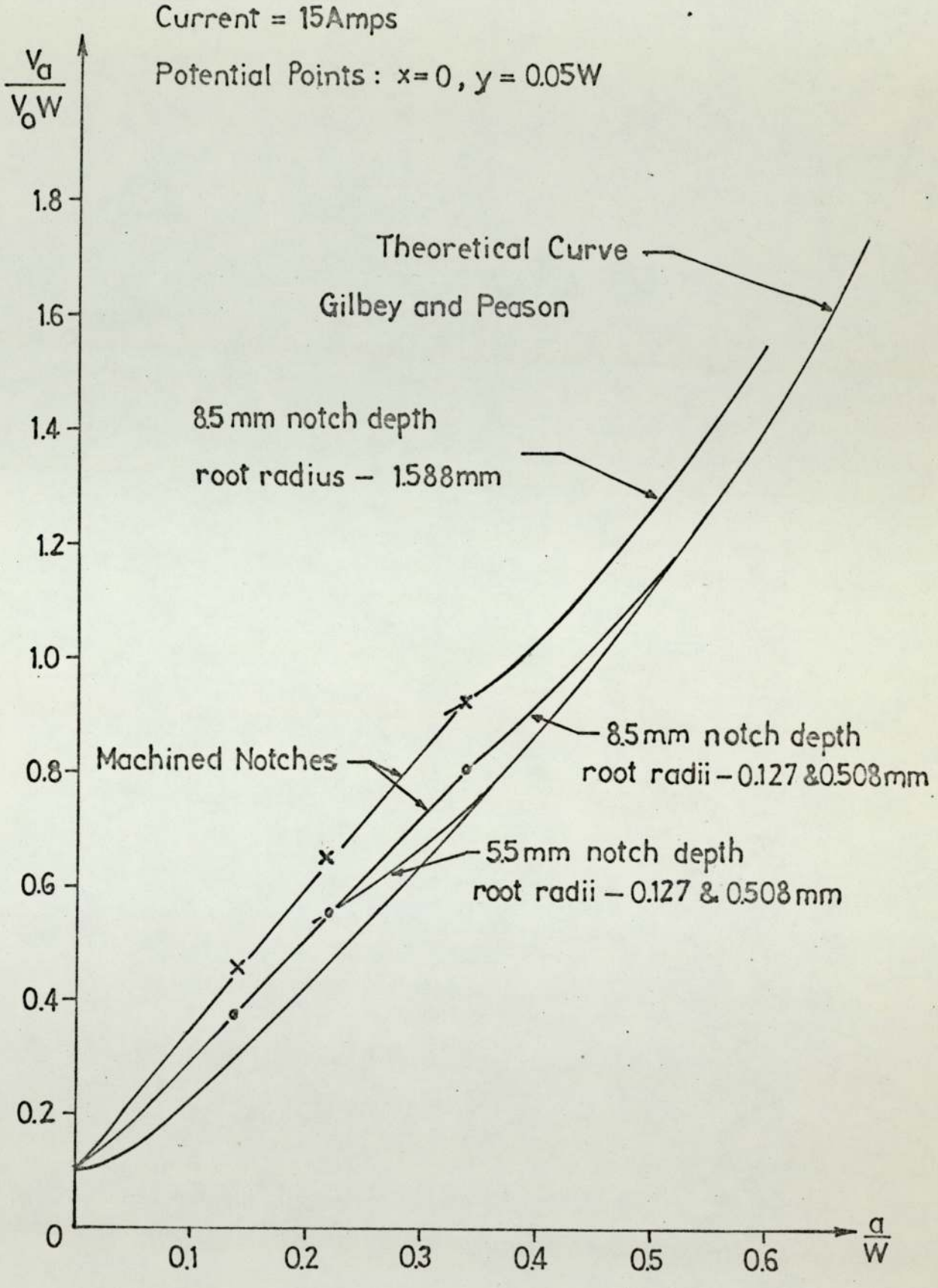


Fig.22 - Experimental calibration curves of potential drop vs crack length for SEN 3-point bend specimens

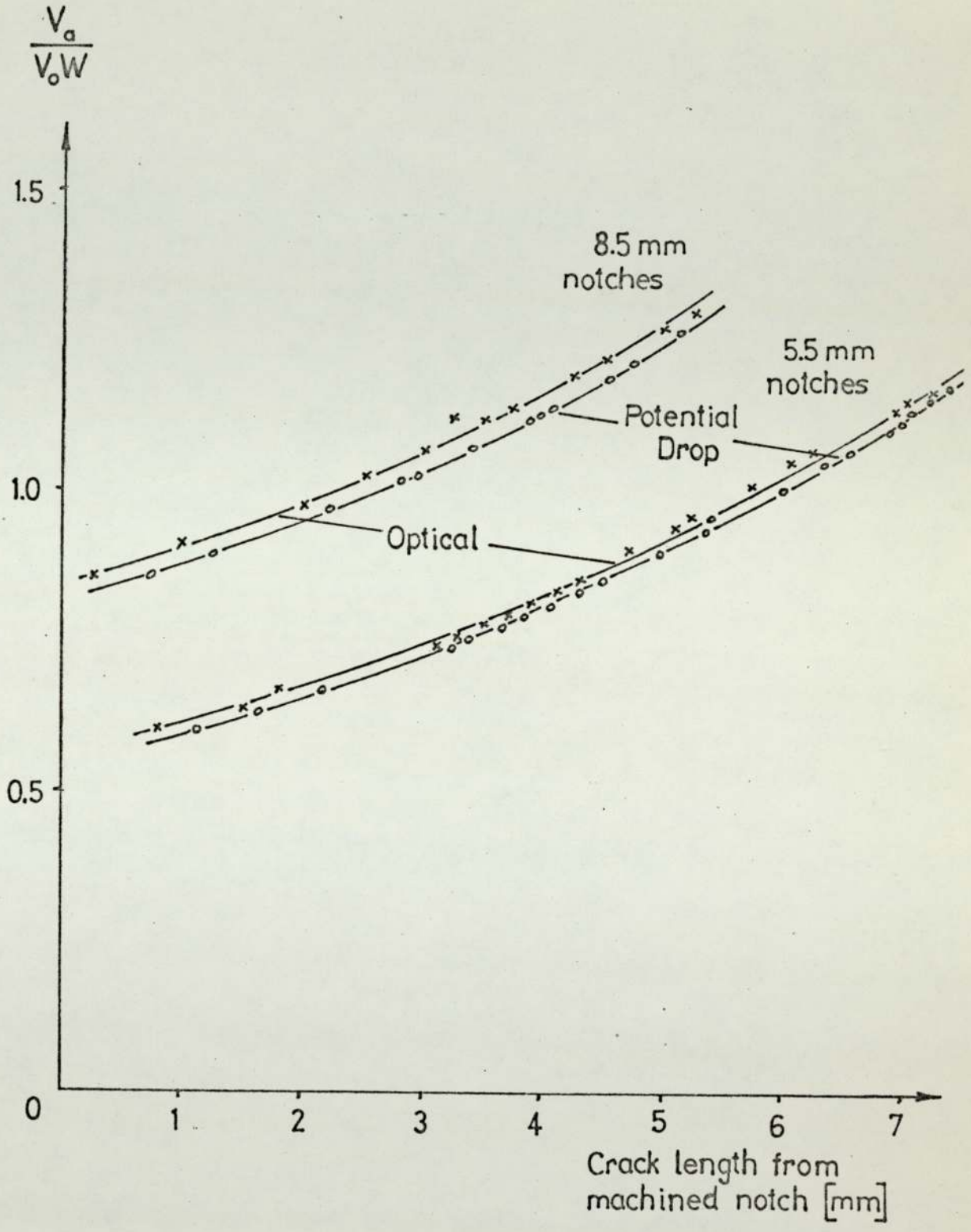


Fig.23 - Comparison of optical and potential methods of crack monitoring

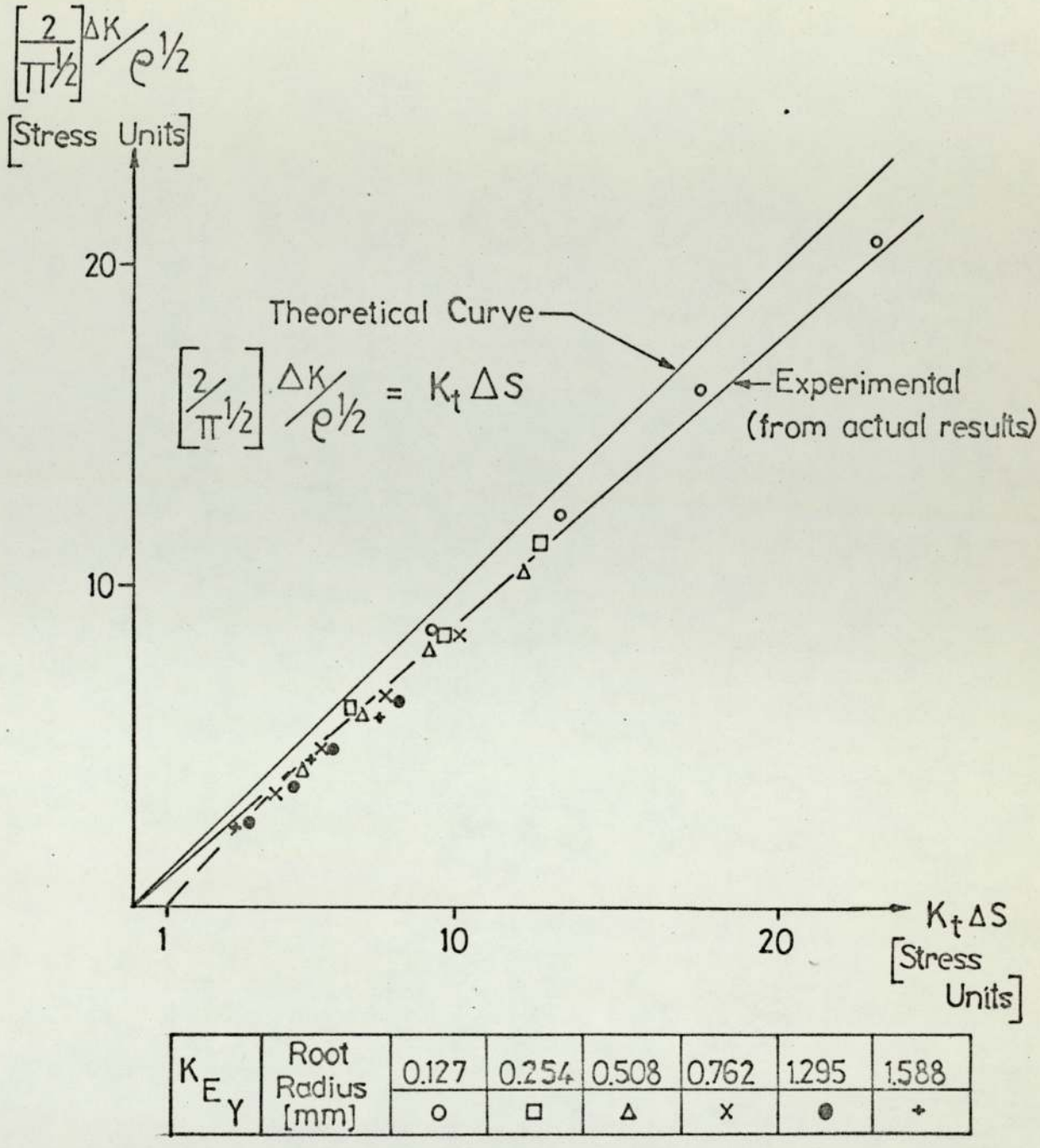


| $K_{E_Y}$ | Root Radius [mm] | 0.127 | 0.254 | 0.508 | 0.762 | 1.295 | 1.588 |
|---|---|---|---|---|---|---|---|
| | | o | □ | Δ | x | ● | + |

Fig.24 - Relationship between $\Delta K/\rho^{1/2}$ and $K_t \Delta s$ parameters for SEN 3-point bend specimens

| Powder Type | Cost £/tonne | Compressibility $Mgm.m^{-3}$ @ 400 $MN.m^{-2}$ |
|---|---|---|
| Höganäs ASC100 | 425 | 6.83 |
| Electrolytic | 500 | 6.70 |
| ROSPOL MP32 | 178 | 6.62 |
| Höganäs NC100 | 185 | 6.42 |

Table 2: Cost and compressibility of various iron powders

| Powder Type | Tensile Strength $MN.m^{-2}$ | |
|---|---|---|
| | Dogbones | Hounsfields |
| Höganäs ASC100 | 178 | 256 |
| Electrolytic | 188 | 257 |
| ROSPOL MP32 | 197 | 260 |
| Höganäs NC100 | 182 | 278 |

Table 3: Tensile strength for various iron powders measured on Dogbone and Hounsfield No.12 specimens

| KEY | | | | |
|---|---|---|---|---|
| Carbonyl | Höganäs NC 100 | Rospol MP 32 | Electrolytic -200 # | Höganäs ASC 100 |
| × | △ | ◇ | □ · | ○ |

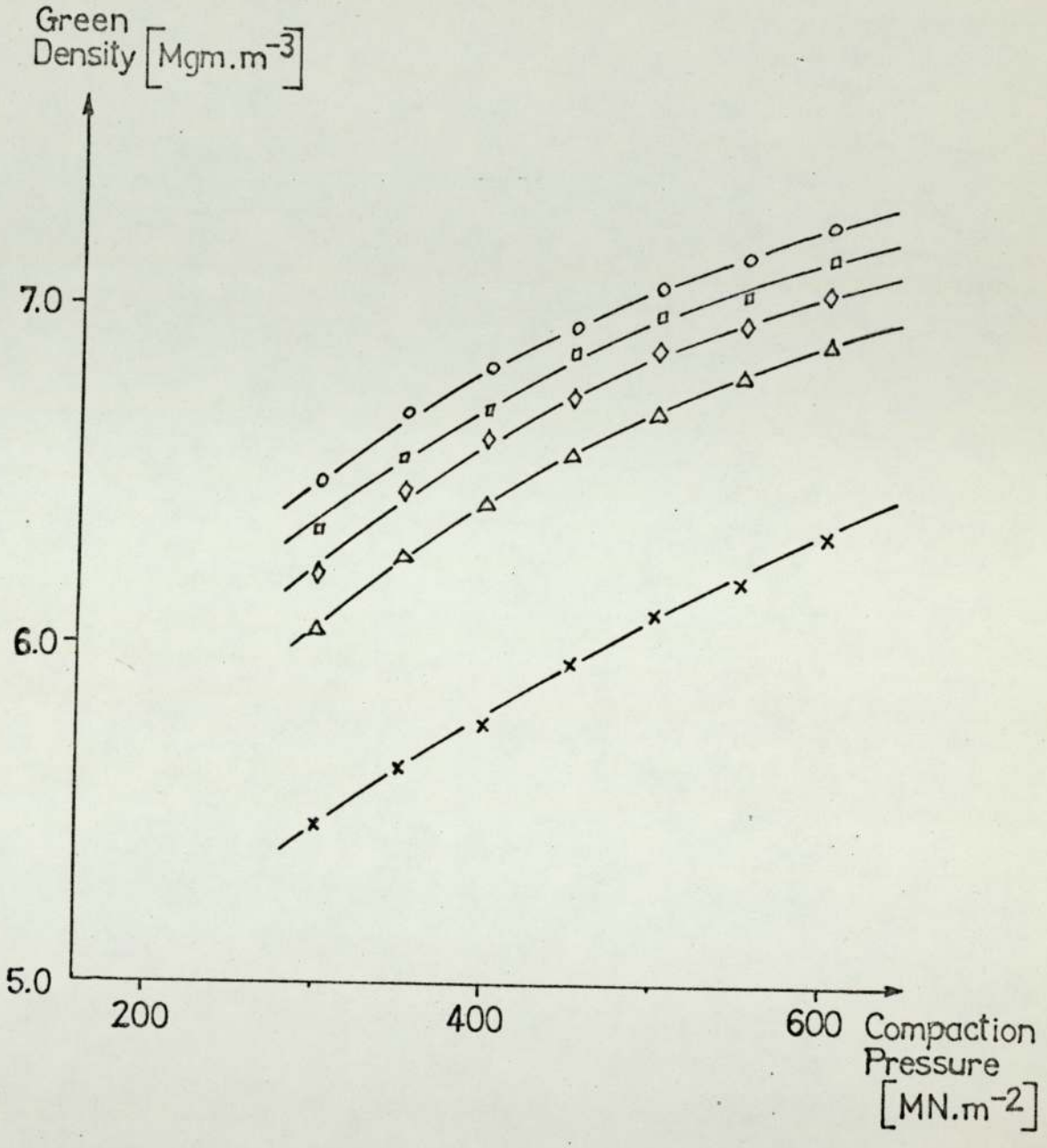


Fig.25 - Green density vs compaction pressure for various iron powders

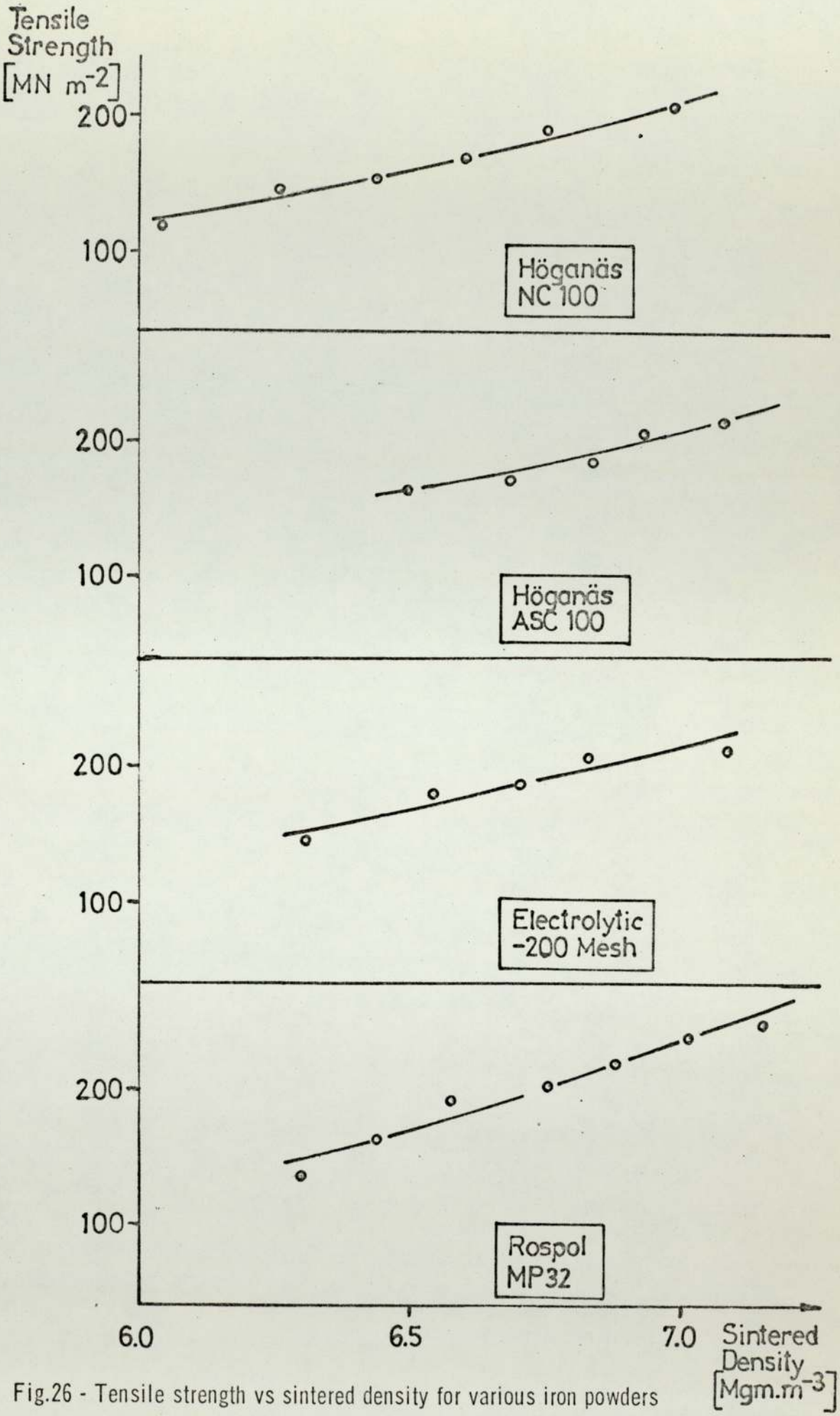


Fig.26 - Tensile strength vs sintered density for various iron powders

| Powder Type | Mean Linear Intercept (μm) | | Strength ($MN.m^{-2}$) | |
|---|---|---|---|---|
| | Pores | Matrix | Yield | Tensile |
| Höganäs ASC100 | 6.1 ± 2.3 | 5 98 ± 22.3 | 191 | 256 |
| Electrolytic | 5.5 ± 1.7 | 50.0 ± 17.7 | 197 | 257 |
| ROSPOL MP32 | 4.8 ± 1.3 | 39.6 ± 14.8 | 200 | 260 |
| Höganäs NC100 | 4.2 ± 1.2 | 39.2 ± 11.7 | 220 | 278 |

Table 4: Mean linear intercept of pores and matrix against yield and tensile strengths for iron powders

| Powder Type | Pre-cracked toughness | | Notched toughness |
|---|---|---|---|
| | Industrially produced | Laboratory produced | |
| | $MN.m^{-3}/2$ | | |
| Höganäs ASC100 | 10.68 | 11.03 | 9.71 |
| Electrolytic | 11.02 | 12.11 | 9.91 |
| ROSPOL MP32 | 11.07 | 12.55 | 12.25 |
| Höganäs NC100 | 10.87 | 13.11 | 12.90 |

Table 5: Comparison of the fracture toughness of industrially produced and laboratory produced sintered compacts of iron powders

Fig. 27: Pore morphologies of various sintered irons at a density of 6.70 Mgm. $m^{-3}$

a) Electrolytic (x 150)

b) Electrolytic (x 500)

c) Höganäs ASC 100 (x 150)

d) Höganäs ASC 100 (x 500)

e) Höganäs NC 100 (x 150)

f) Höganäs NC 100 (x 500)

g) Rospol MP 32 (x 150)

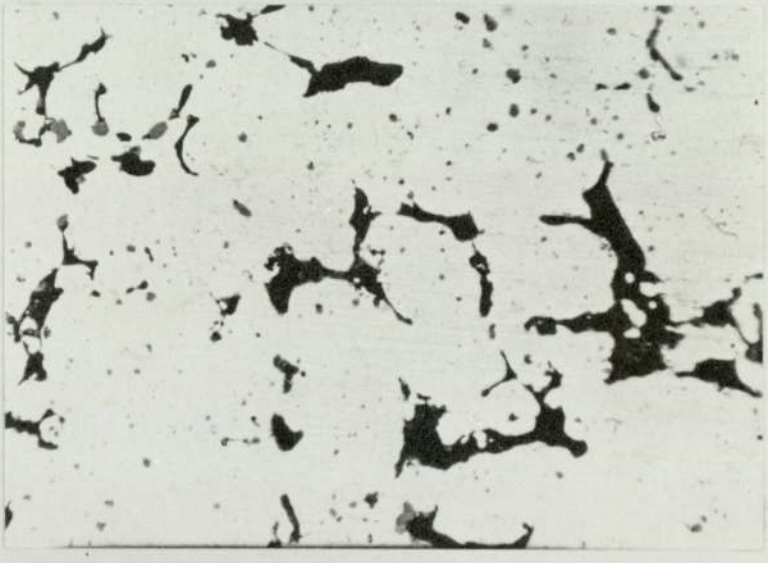

h) Rospol MP 32 (x 500)

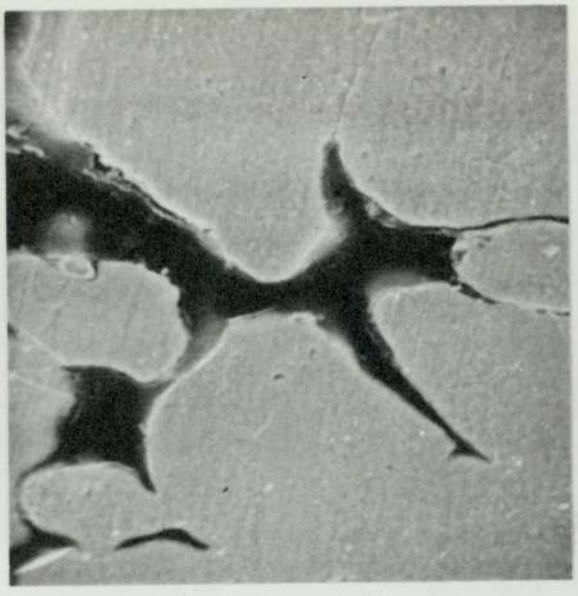

i) Electrolytic (S. E.M. x 2. 6 K)

j) Höganäs ASC 100 (S. E. M. x 2. 6 K)

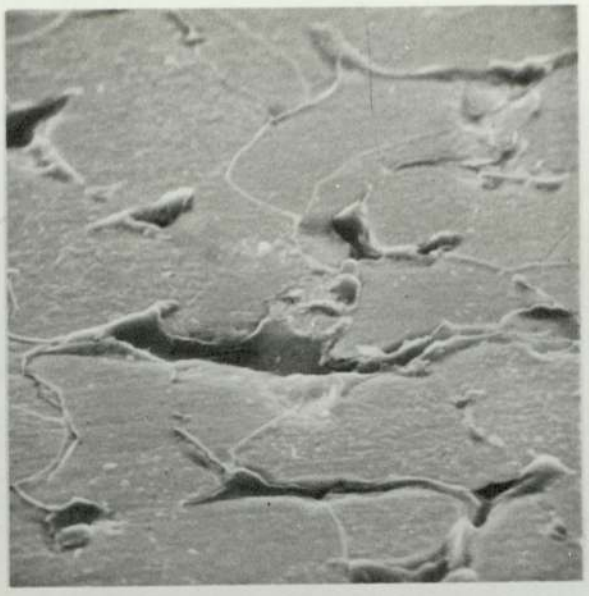

k) Höganäs NC 100 (S.E.M. x 2.6 K)

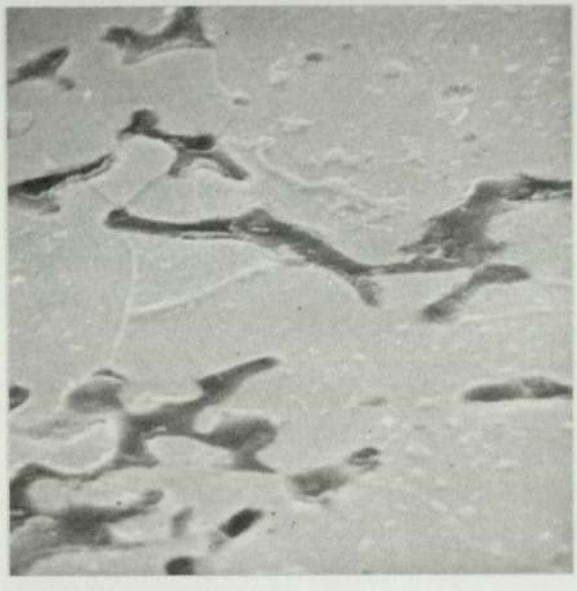

l) Rospol MP 32 (S.E.M. x 2.6 K)

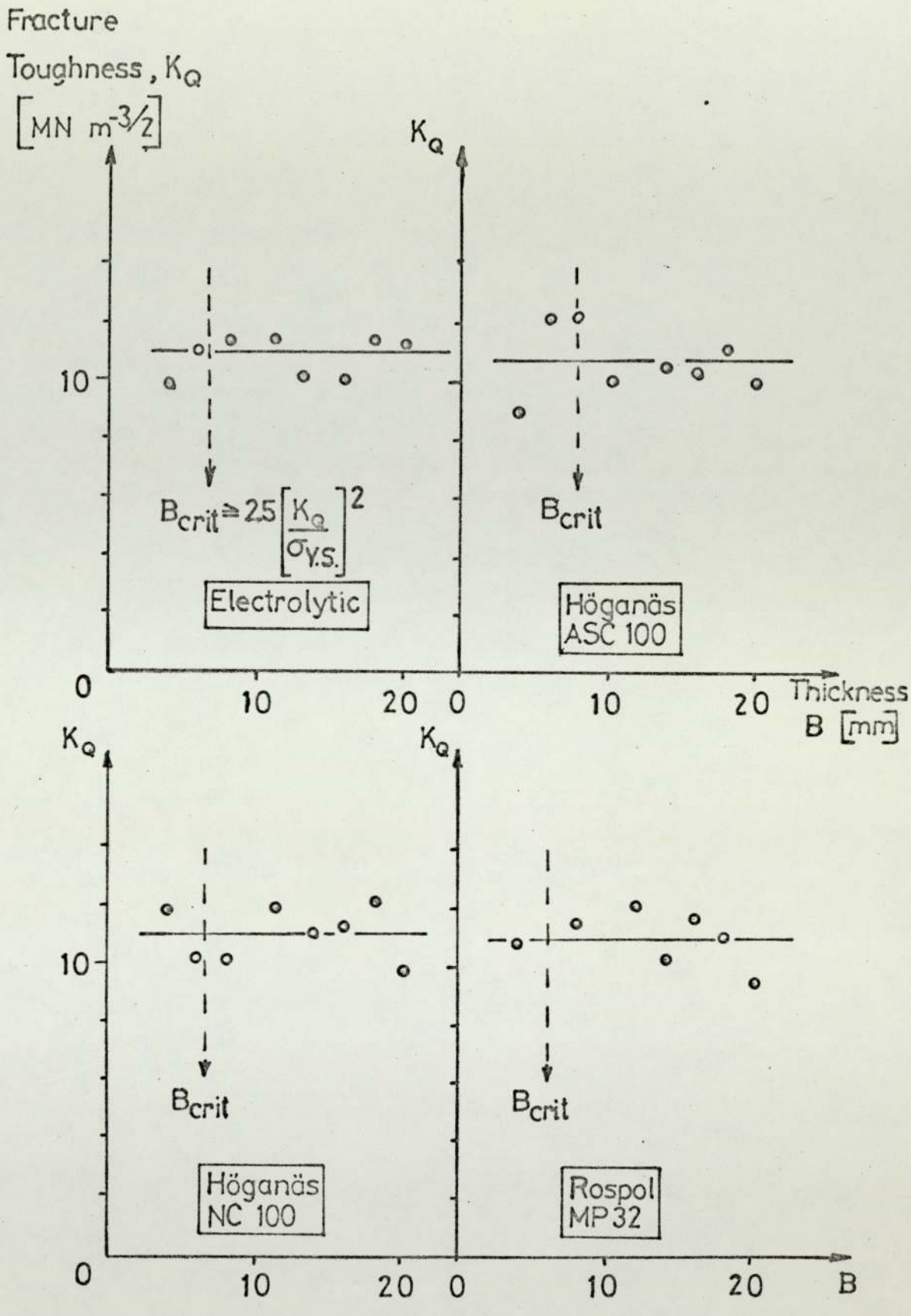


Fig.28 - Fracture toughness vs specimen thickness for various iron powders

Fig. 29: Fracture surfaces of sintered iron toughness specimens of various thicknesses, [B], (x $1\frac{1}{2}$)

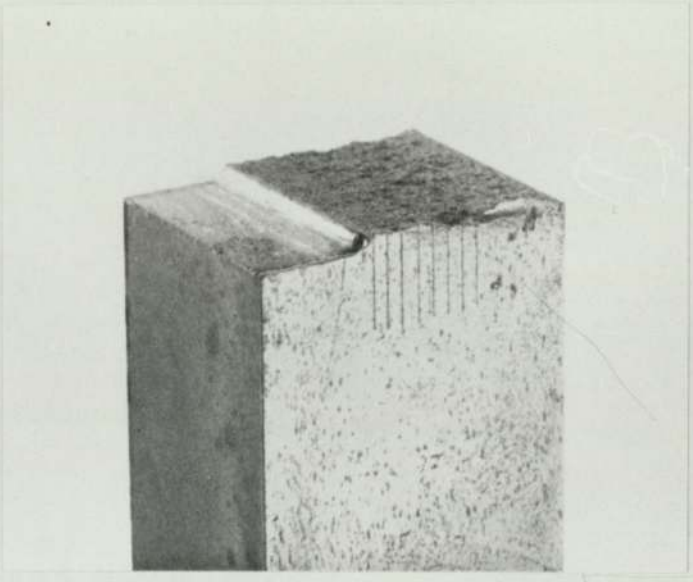

a) B = 20 mm

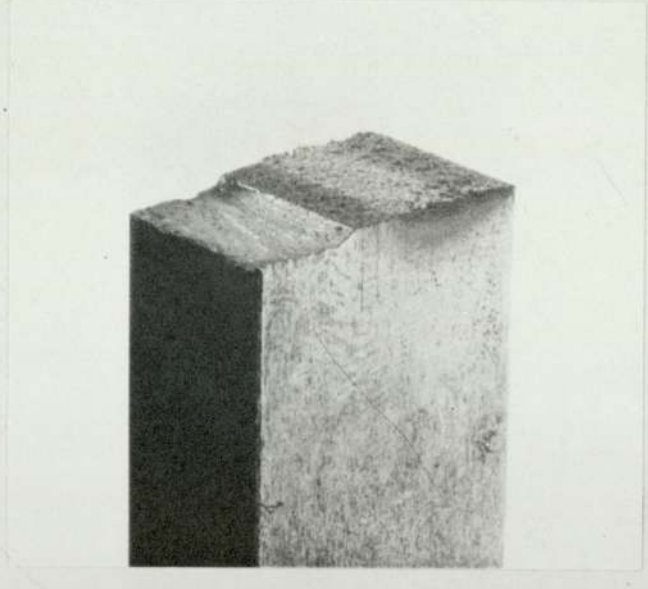

b) B = 16 mm

c) B = 12 mm

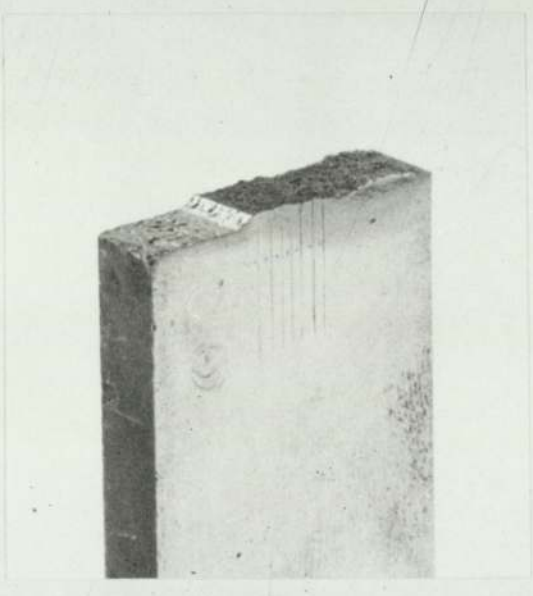

d) B = 6 mm

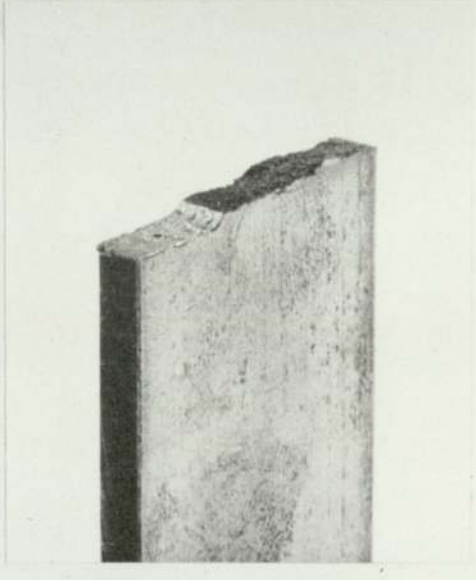

e) B = 4 mm

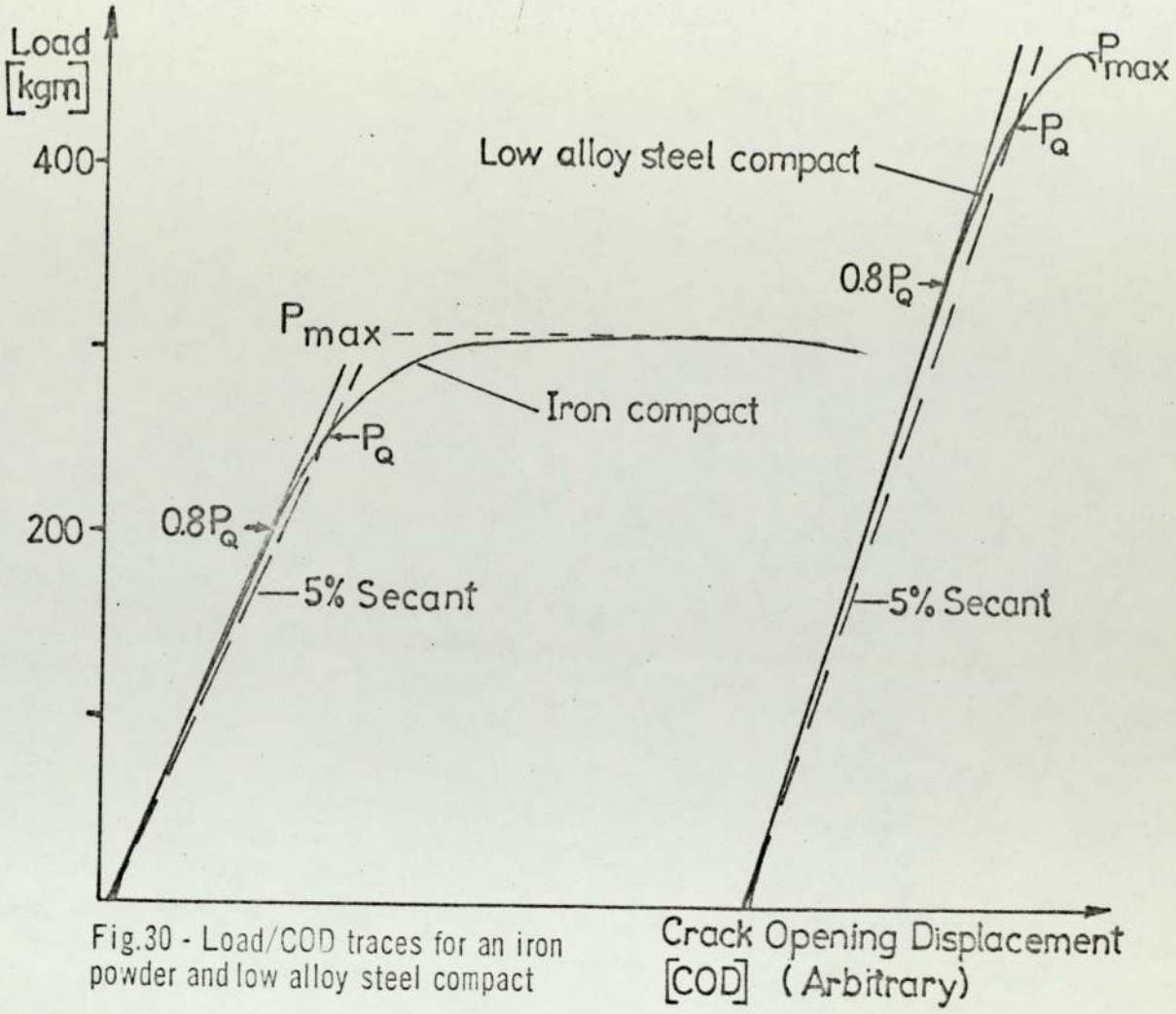


Fig.30 - Load/COD traces for an iron powder and low alloy steel compact

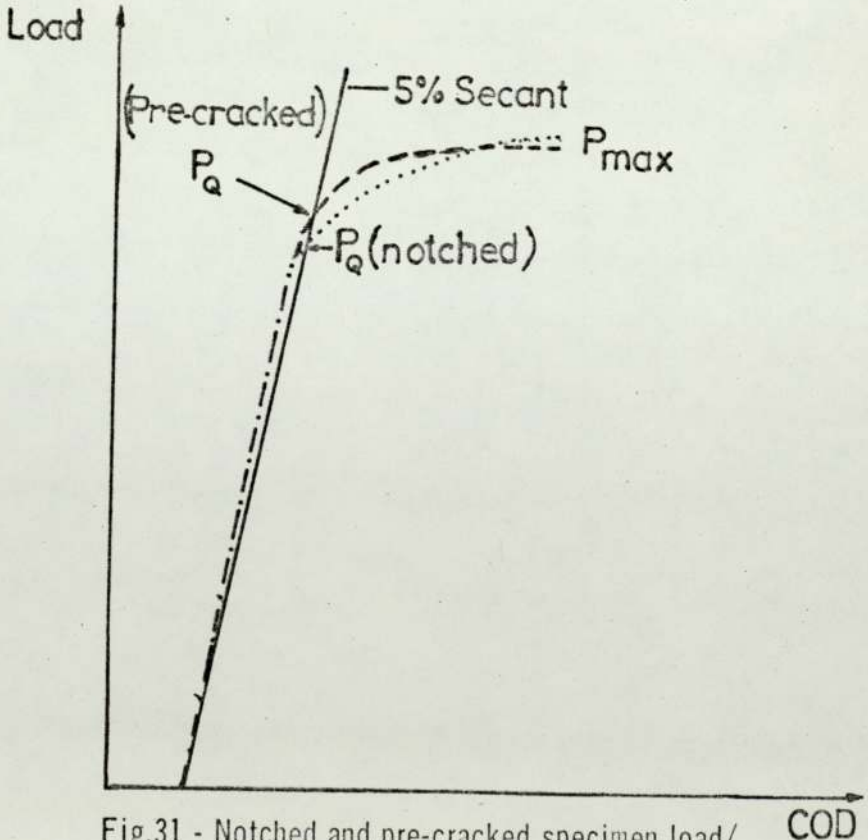


Fig.31 - Notched and pre-cracked specimen load/ COD traces for an iron powder

Fig. 32: Fatigue fracture surface of a sintered iron compact, (Höganäs ASC 100), $\Delta K = 5$ MN. $m^{-3/2}$

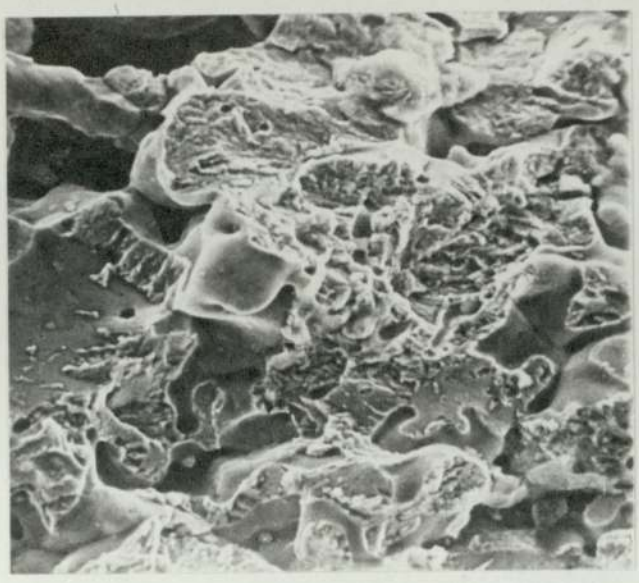

a) x 500 (S. E. M.)

b) x 1000 (S. E. M.)

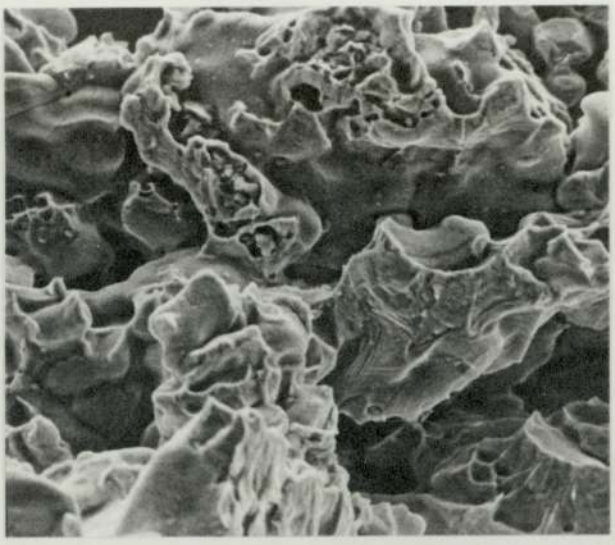

Fig. 33: Fast fracture (toughness test) of Höganäs ASC 100 showing ductile dimple rupture, (x 1000)

Fig. 34: Tensile fracture (Hounsfield No. 12) of Höganäs ASC 100 showing ductile dimple rupture, (x 500)

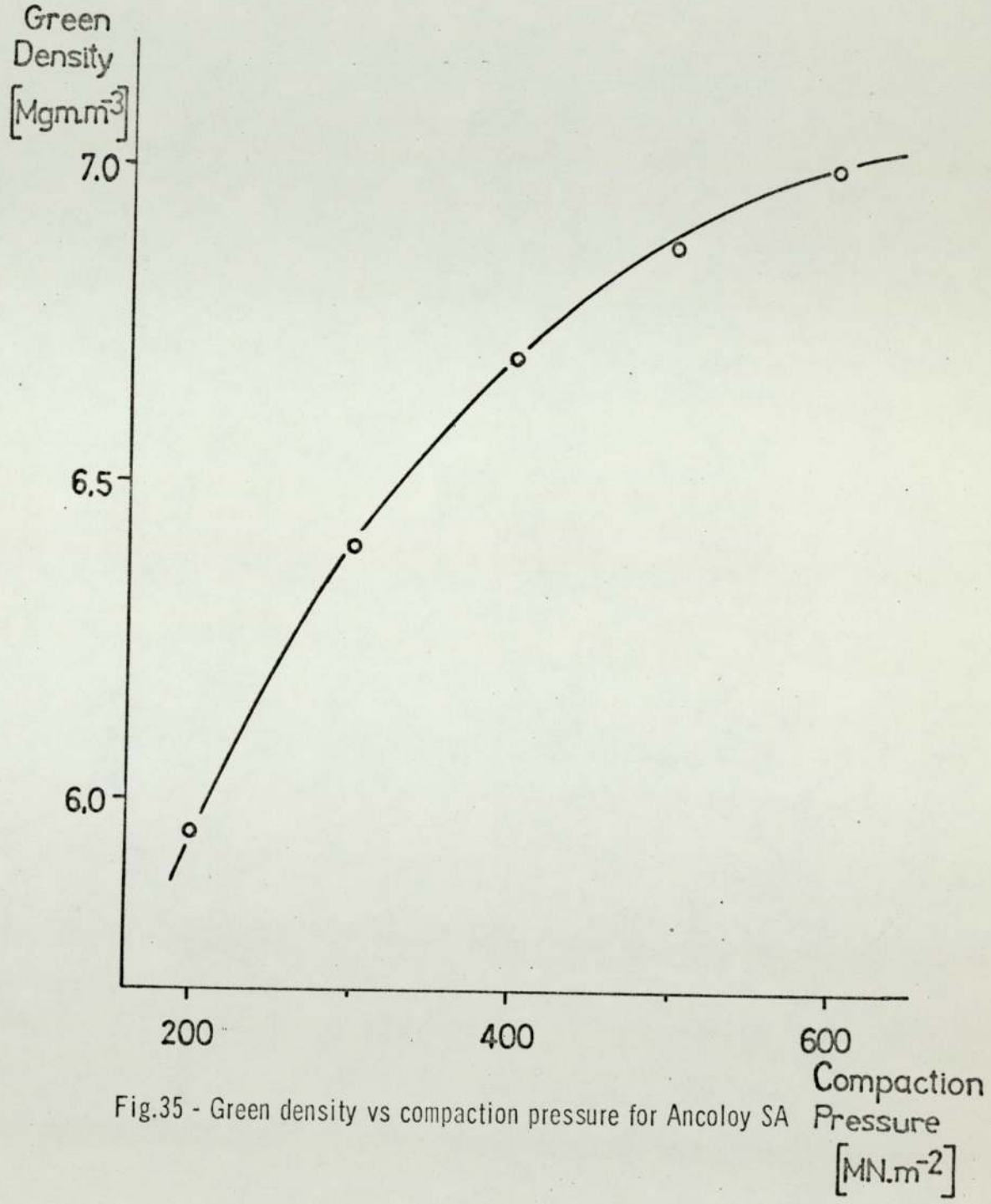


Fig.35 - Green density vs compaction pressure for Ancoloy SA

| Density [Mgm.m$^{-3}$] | Carbon Content [%] | Strength Yield [MN.m$^{-2}$] | Strength Tensile [MN.m$^{-2}$] |
|---|---|---|---|
| 5.95 | 0.40 | 171 | 191 |
| 5.95* | 0.40 | 246 | 286 |
| 6.40 | 0.40 | 195 | 232 |
| 6.70 | 0.00 | 195 | 245 |
| 6.70 | 0.30 | 254 | 316 |
| 6.70 | 0.40 | 260 | 340 |
| 6.70* | 0.40 | 394 | 427 |
| 6.70 | 0.65 | 318 | 411 |
| 6.90 | 0.40 | 308 | 366 |
| 7.00 | 0.40 | 324 | 388 |
| 7.00* | 0.40 | 461 | 501 |
| 7.00 | 0.65 | 401 | 469 |

*Heat treated

Table 6a): Density and carbon content versus yield and tensile strength for Ancoloy (SA).

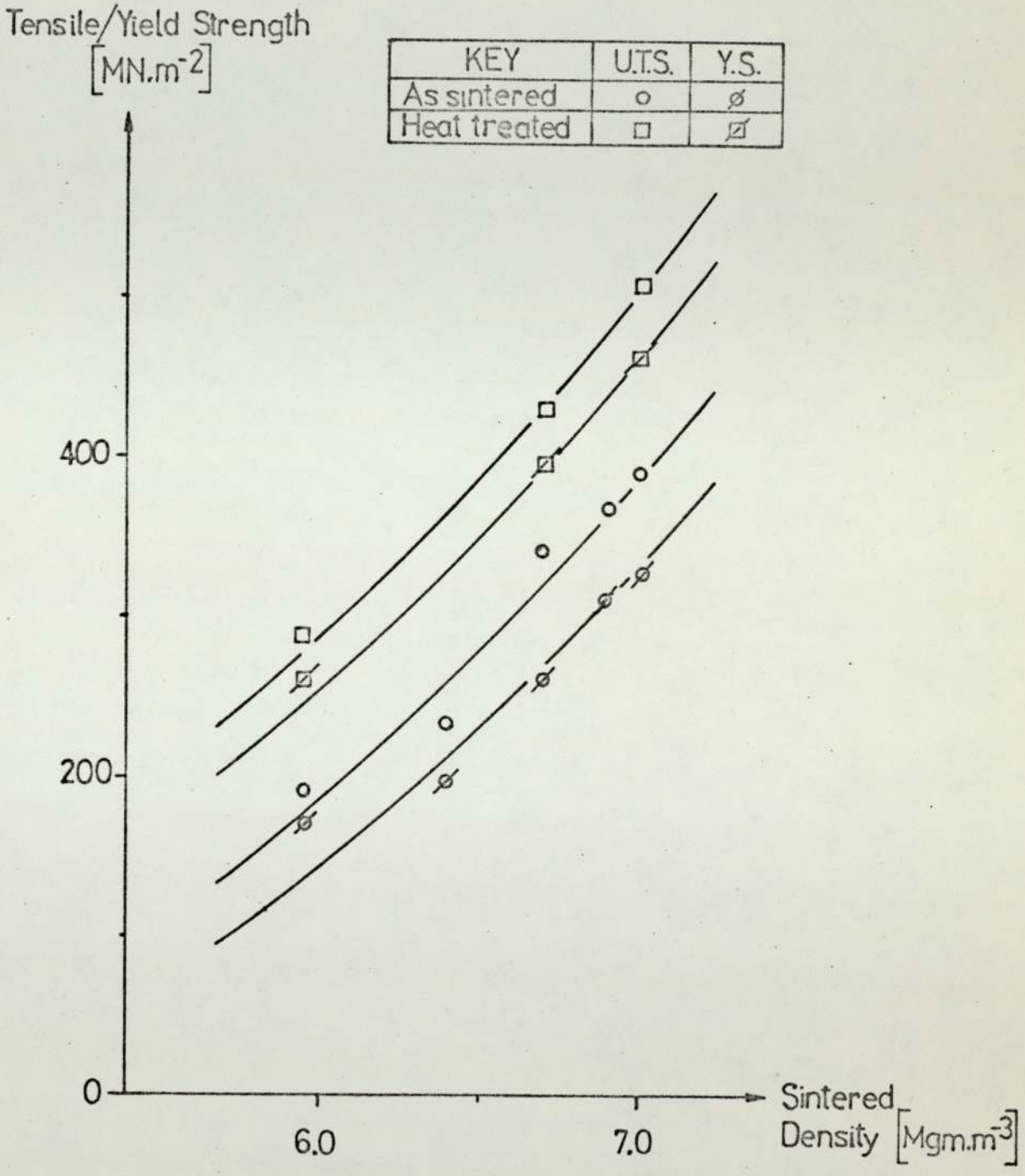


Fig.36 - Tensile and yield strength vs sintered density for Ancoloy SA

| Sintered density [Mgm.m$^{-3}$] | Carbon content [wt-%] | Fracture toughness [MN.m$^{-3/2}$] | Critical thickness [mm] $B_c \geq 2.5(K/\sigma YS)^2$ | Plastic zone size [mm] $r_p = \frac{1}{6\pi}(K/\sigma YS)^2$ |
|---|---|---|---|---|
| 5.95 | 0.40 | 11.48 | 9.00 | 0.24 |
| 5.95* | 0.40 | 18.03 | 13.50 | 0.29 |
| 6.40 | 0.40 | 13.46 | 12.25 | 0.25 |
| 6.70 | 0.00 | 14.86 | 12.25 | 0.31 |
| 6.70 | 0.30 | 20.18 | 16.00 | 0.33 |
| 6.70 | 0.40 | 21.94 | 13.25 | 0.38 |
| 6.70* | 0.40 | 29.18 | 13.75 | 0.29 |
| 6.70 | 0.65 | 26.39 | 17.25 | 0.36 |
| 6.70/ | 0.65 | 28.16 | 19.57 | 0.41 |
| 6.85 | 0.40 | 23.39 | 14.05 | 0.31 |
| 7.00 | 0.40 | 25.78 | 13.25 | 0.34 |
| 7.00* | 0.40 | 33.89 | 13.75 | 0.29 |
| 7.00 | 0.65 | 29.14 | 13.25 | 0.28 |
| 7.00/ | 0.65 | 31.56 | 15.45 | 0.33 |

*Heat treated; / Notched specimens

Table 6b): Fracture toughness, critical thickness for plane strain conditions and plane strain plastic zone size for Ancoloy at various densities and carbon contents in as-sintered and heat treated conditions

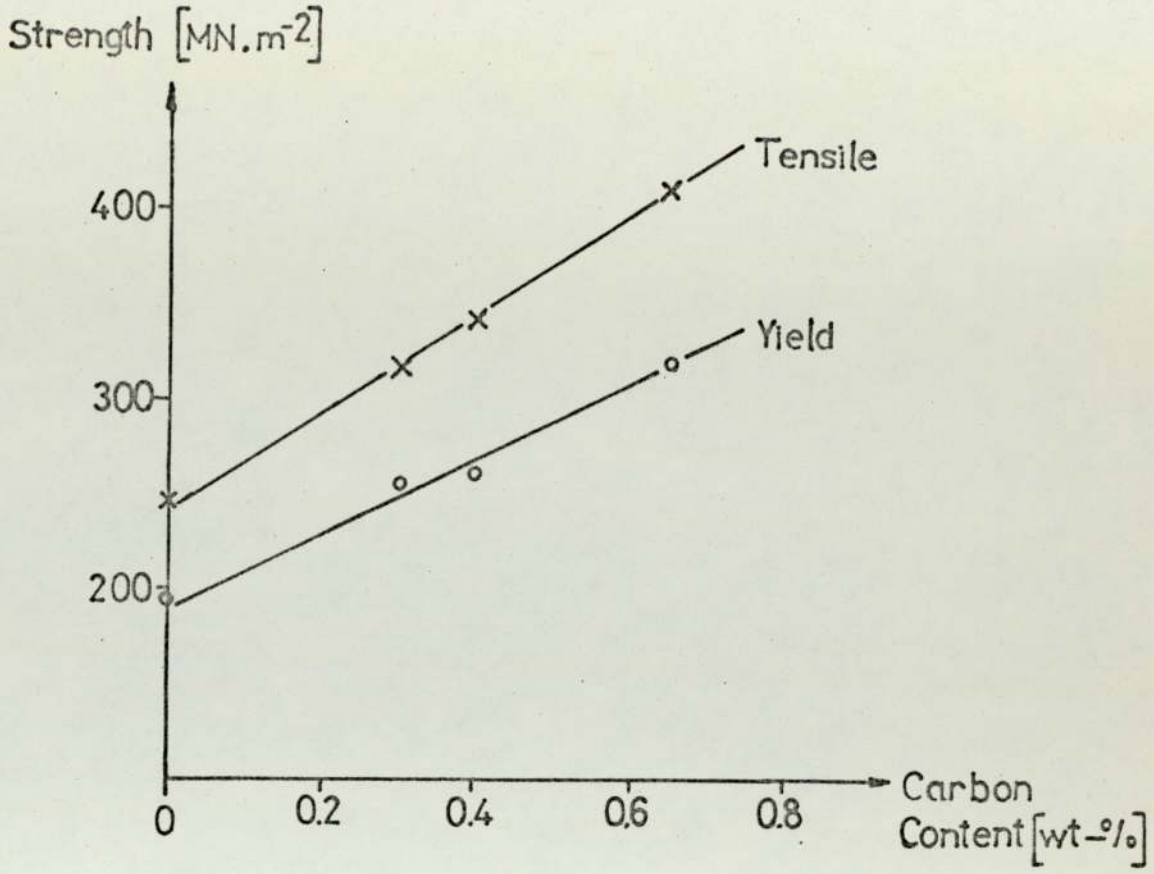


Fig.37 - Tensile and yield strength vs carbon content for Ancoloy SA, (as sintered)

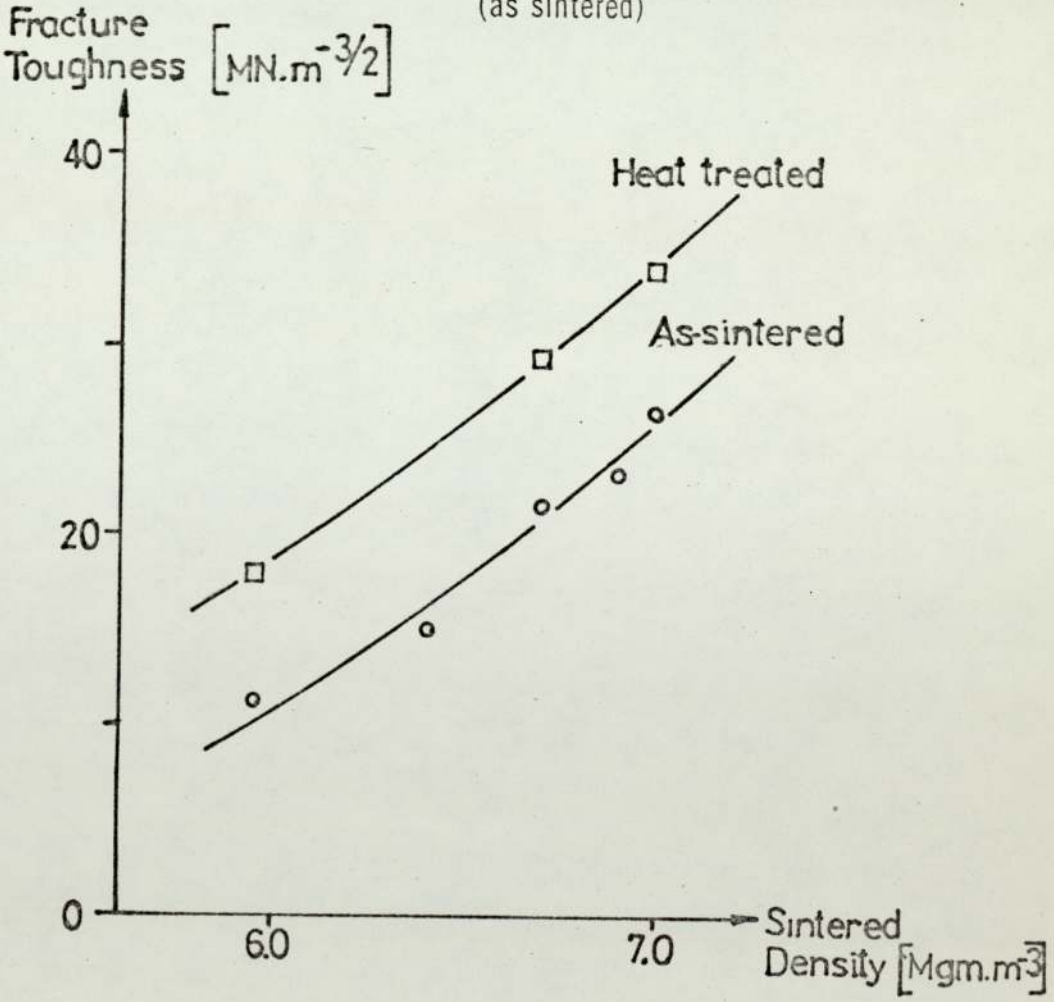


Fig.38 - Fracture toughness vs sintered density for Ancoloy SA

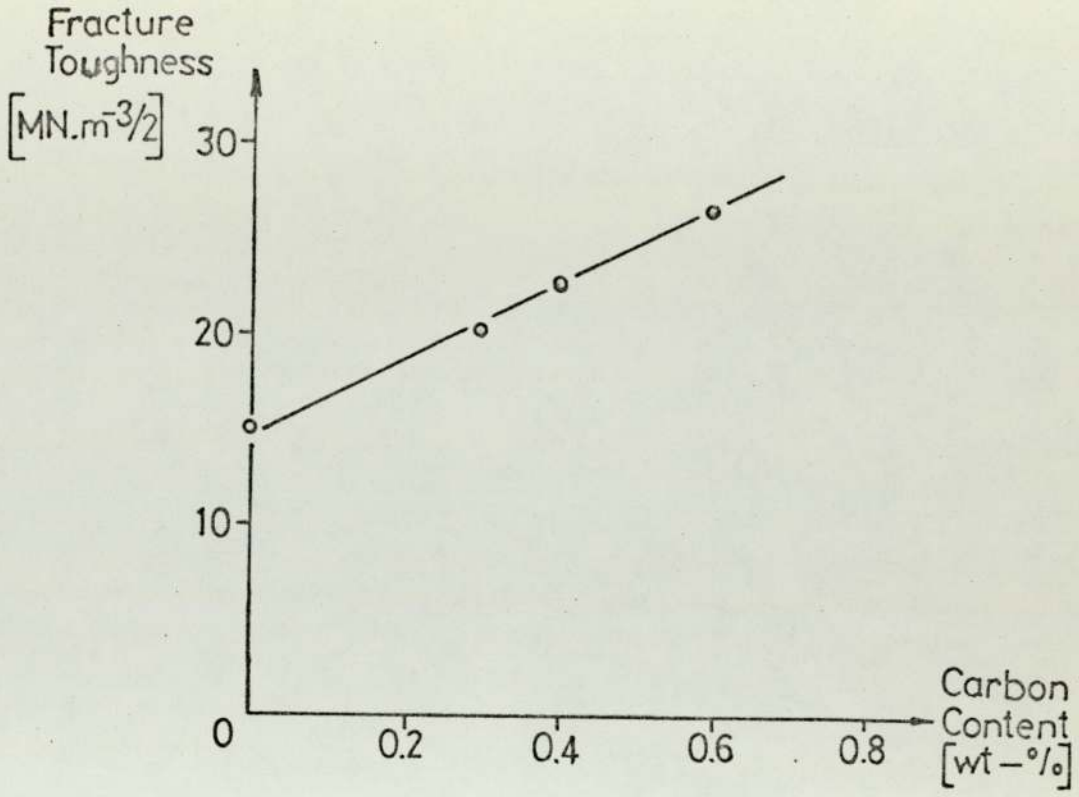


Fig.39 - Fracture toughness vs carbon content for Ancoloy SA, (as-sintered), density 6.70 Mgm.m-3

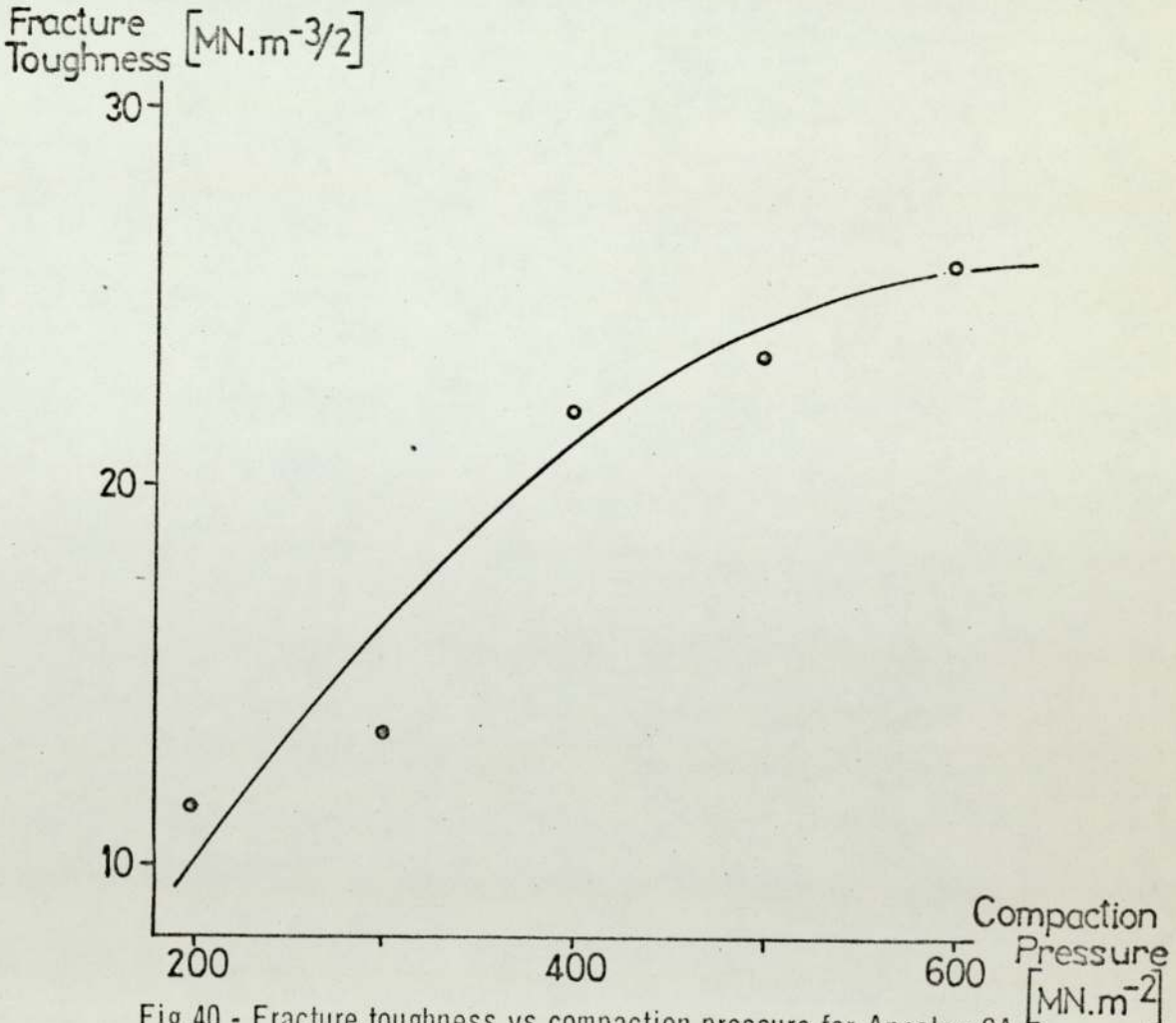


Fig.40 - Fracture toughness vs compaction pressure for Ancoloy SA.

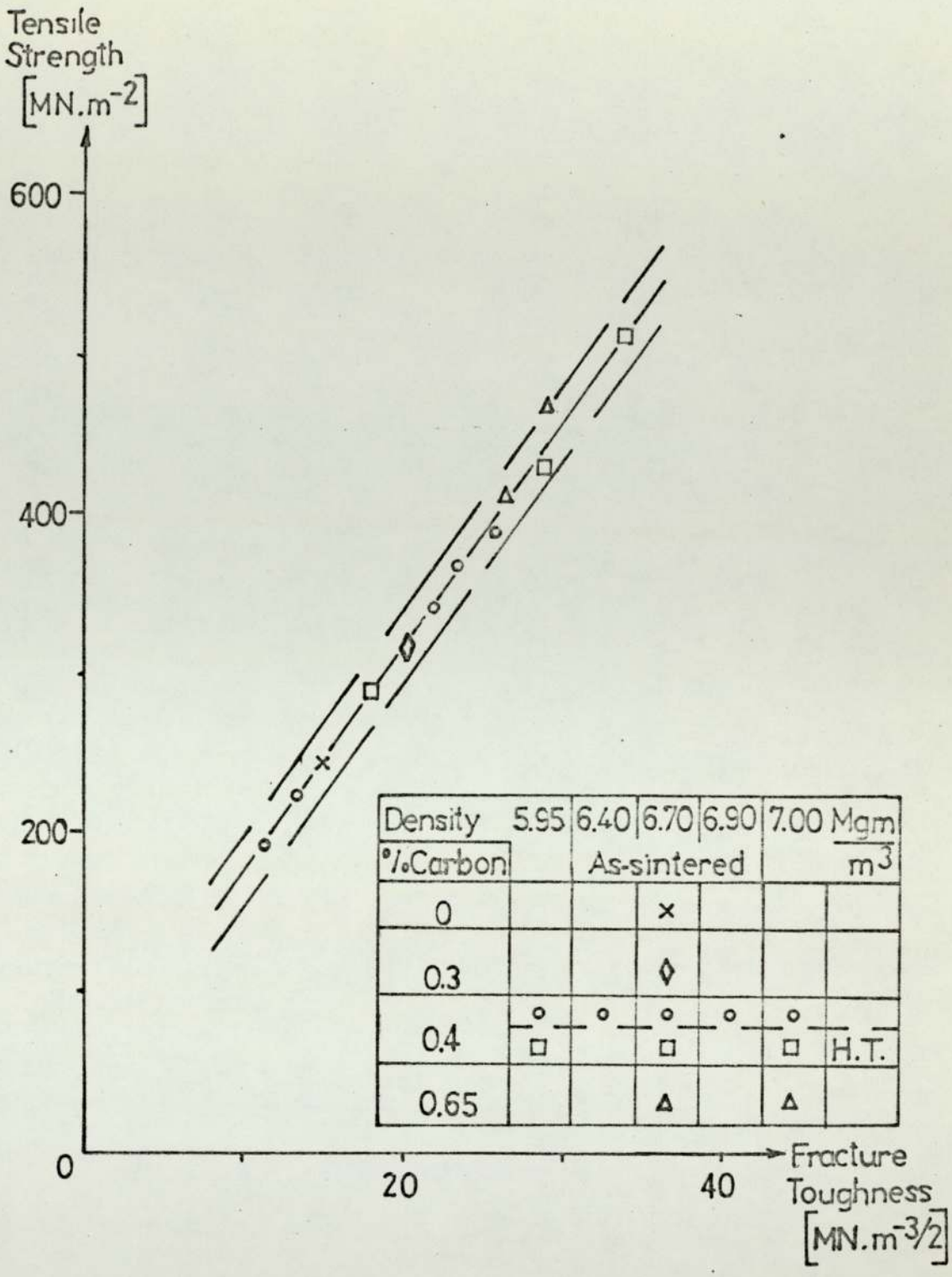


Fig.41 - Tensile strength vs fracture toughness for Ancoloy SA

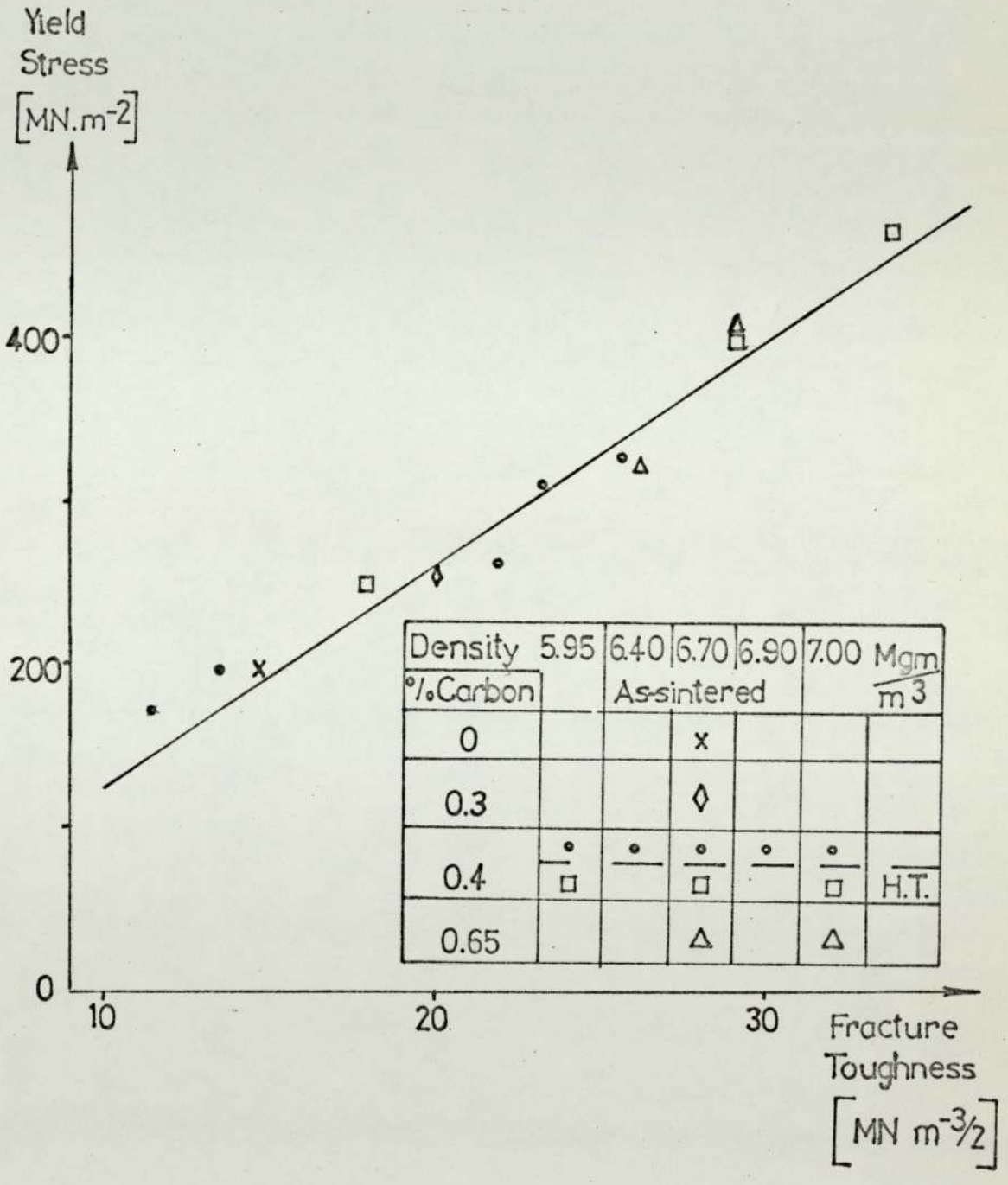


Fig.42 - Yield stress vs fracture toughness for Ancoloy SA

a)

| Density [Mgm.m$^{-3}$] | $K_t \Delta S$ [MN.m$^{-2}$] | $\Delta K/\rho^{\frac{1}{2}}$ [MN.m$^{-2}$] | Ni [cycles] |
|---|---|---|---|
| 5.95 | 216 | 178 | 24961 |
| | 324 | 266 | 3228 |
| $\rho$ = 0.127 mm | 548 | 355 | 1417 |
| | 658 | 532 | 547 |
| | Constant (A) | $10^{-11.6}$ | $10^{-12.0}$ |
| | Slope (n) | -3.12 | -3.45 |
| | 117 | 89 | 28581 |
| | 173 | 133 | 3644 |
| | 231 | 178 | 4608 |
| $\rho$ = 0.508 mm | 406 | 311 | 984 |
| | 464 | 355 | 602 |
| | A | $10^{-9.5}$ | $10^{-9.2}$ |
| | n | -2.51 | -2.51 |
| | 74 | 50 | 46053 |
| | 180 | 125 | 11035 |
| | 216 | 151 | 3881 |
| | 251 | 176 | 2799 |
| $\rho$ = 1.588 mm | 287 | 201 | 547 |
| | A | $10^{-10.1}$ | $10^{-9.5}$ |
| | n | -2.82 | -2.74 |

Table 7: Fatigue crack initiation data for notched 3 pt. bend specimens of Ancoloy

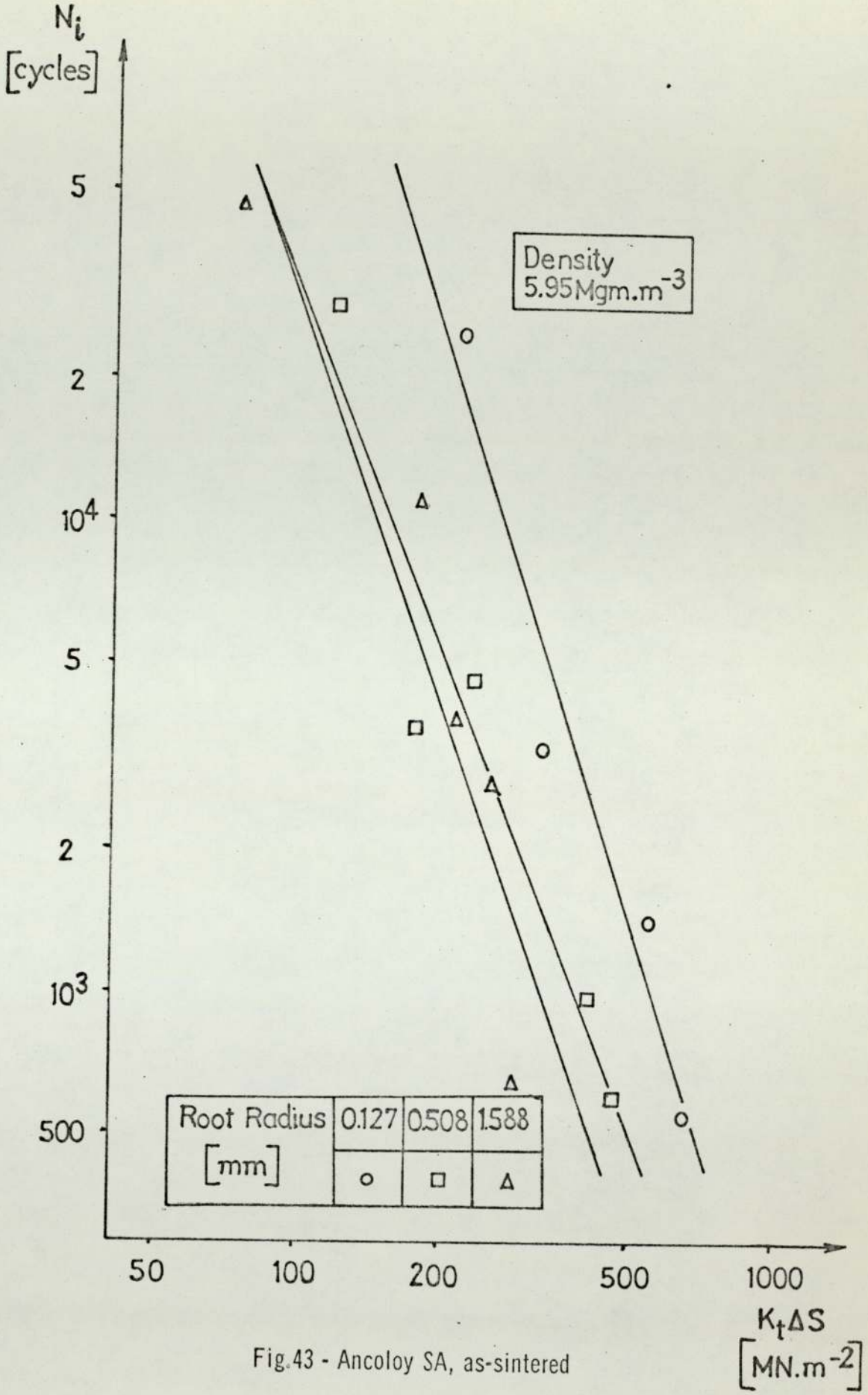


Fig.43 - Ancoloy SA, as-sintered

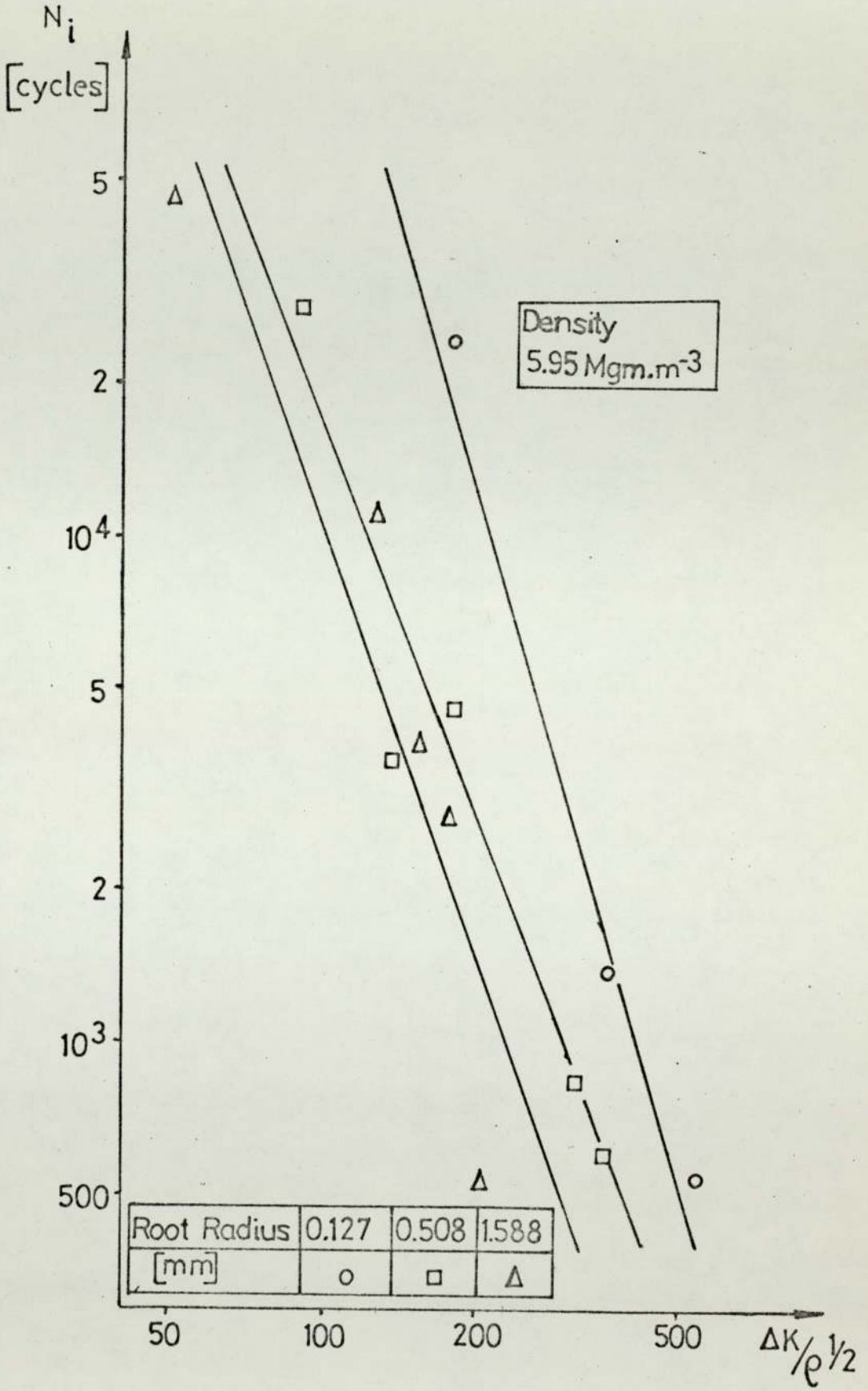


Fig.44 - Ancoloy SA, as-sintered

b)

| Density [Mgm.m$^{-3}$] | $K_t \Delta S$ [MN.m$^{-2}$] | $\Delta K/\rho^{\frac{1}{2}}$ [MN.m$^{-2}$] | Ni. [cycles] |
|---|---|---|---|
| | 216 | 178 | 58201 |
| 6.40 | 324 | 266 | 15915 |
| | 432 | 355 | 9972 |
| $\rho$ = 0.127 mm | 658 | 532 | 4492 |
| | 767 | 621 | 773 |
| | A | $10^{-11.7}$ | $10^{-11.5}$ |
| | n | -2.95 | -3.00 |
| | 117 | 89 | 21057 |
| | 175 | 133 | 9991 |
| | 231 | 178 | 6708 |
| | 288 | 222 | 2250 |
| $\rho$= 0.508 mm | 348 | 266 | 1094 |
| | 406 | 311 | 417 |
| | A | $10^{-10.9}$ | $10^{-10.4}$ |
| | n | -3.08 | -3.05 |
| | 111 | 75 | 29497 |
| | 149 | 100 | 8314 |
| | 180 | 125 | 5564 |
| $\rho$= 1.588 mm | 251 | 176 | 2194 |
| | 287 | 201 | 1353 |
| | A | $10^{-10.8}$ | $10^{-9.9}$ |
| | n | -3.10 | -2.96 |

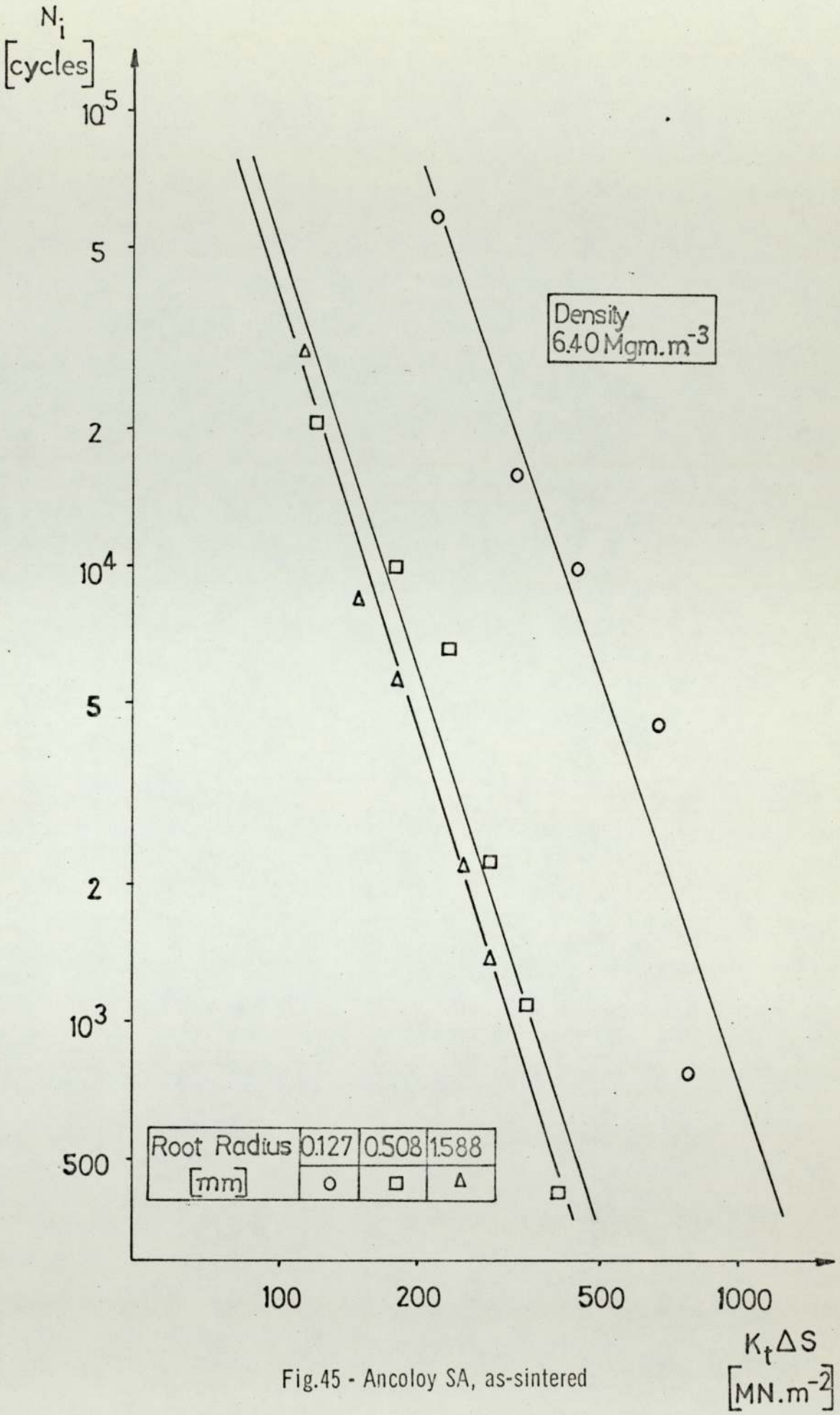


Fig.45 - Ancoloy SA, as-sintered

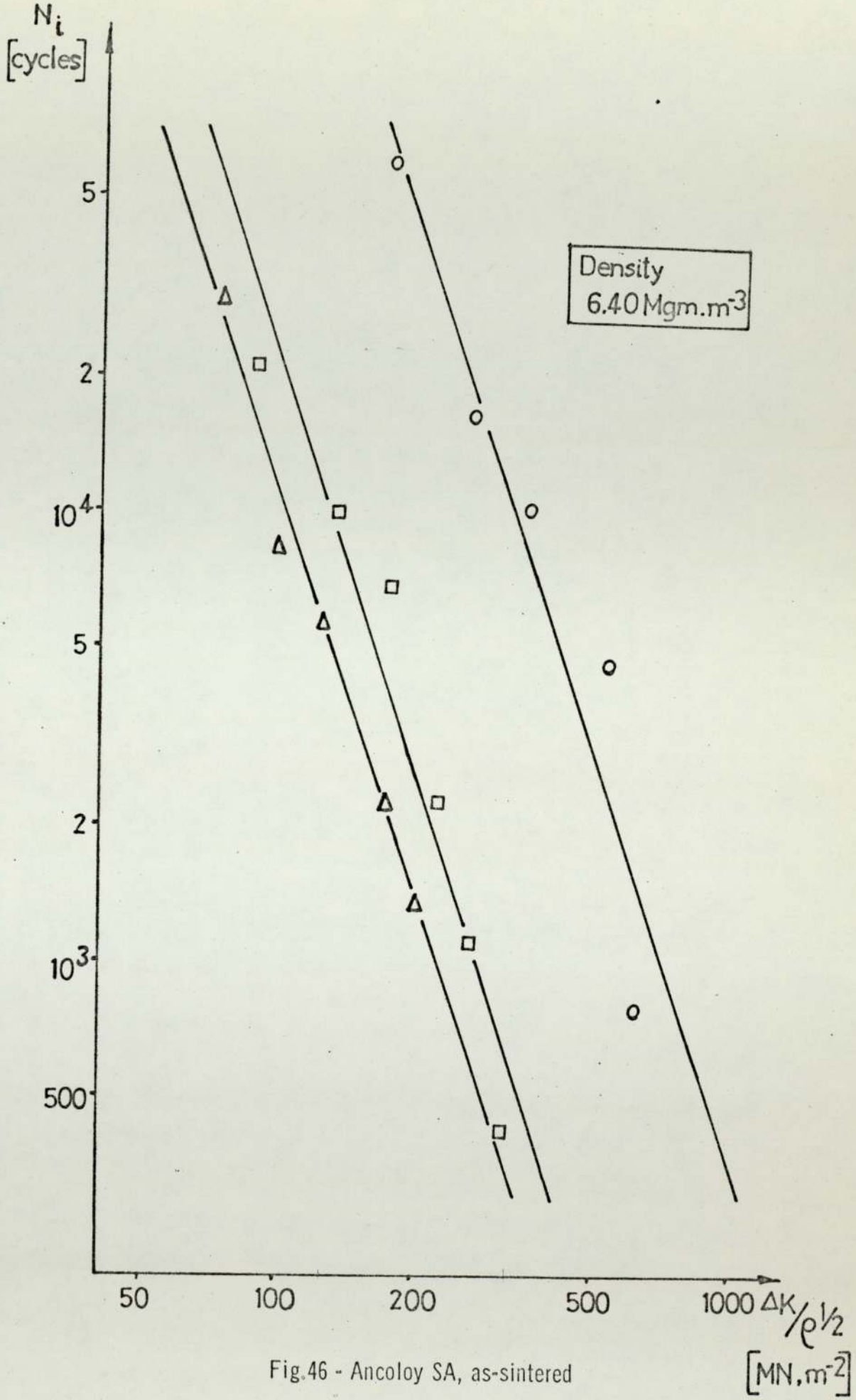


Fig.46 - Ancoloy SA, as-sintered

c)

| Density [Mgm.m$^{-3}$] | $K_t \Delta S$ [MN.m$^{-2}$] | $\Delta K/\rho^{\frac{1}{2}}$ [MN.m$^{-2}$] | Ni [cycles] |
|---|---|---|---|
| 6.70 | 972 | 799 | 18085 |
| | 1079 | 887 | 15476 |
| | 1188 | 976 | 10188 |
| | 1315 | 1065 | 7043 |
| | 1403 | 1154 | 5098 |
| | A | $10^{-14.9}$ | $10^{-14.7}$ |
| | n | -3.53 | -3.59 |
| $\rho$ = 0.508 mm | 464 | 355 | 15112 |
| | 584 | 444 | 9610 |
| | 700 | 488 | 2053 |
| | 750 | 577 | 2307 |
| | 1315 | 1007 | 417 |
| | A | $10^{-13.6}$ | $10^{-12.8}$ |
| | n | -3.56 | -3.43 |
| $\rho$ = 1.588 mm | 251 | 176 | 12432 |
| | 287 | 201 | 7692 |
| | 372 | 251 | 2996 |
| | 397 | 276 | 2247 |
| | 440 | 301 | 1859 |
| | 467 | 326 | 1424 |
| | A | $10^{-12.4}$ | $10^{-12.1}$ |
| | n | -3.48 | -3.56 |

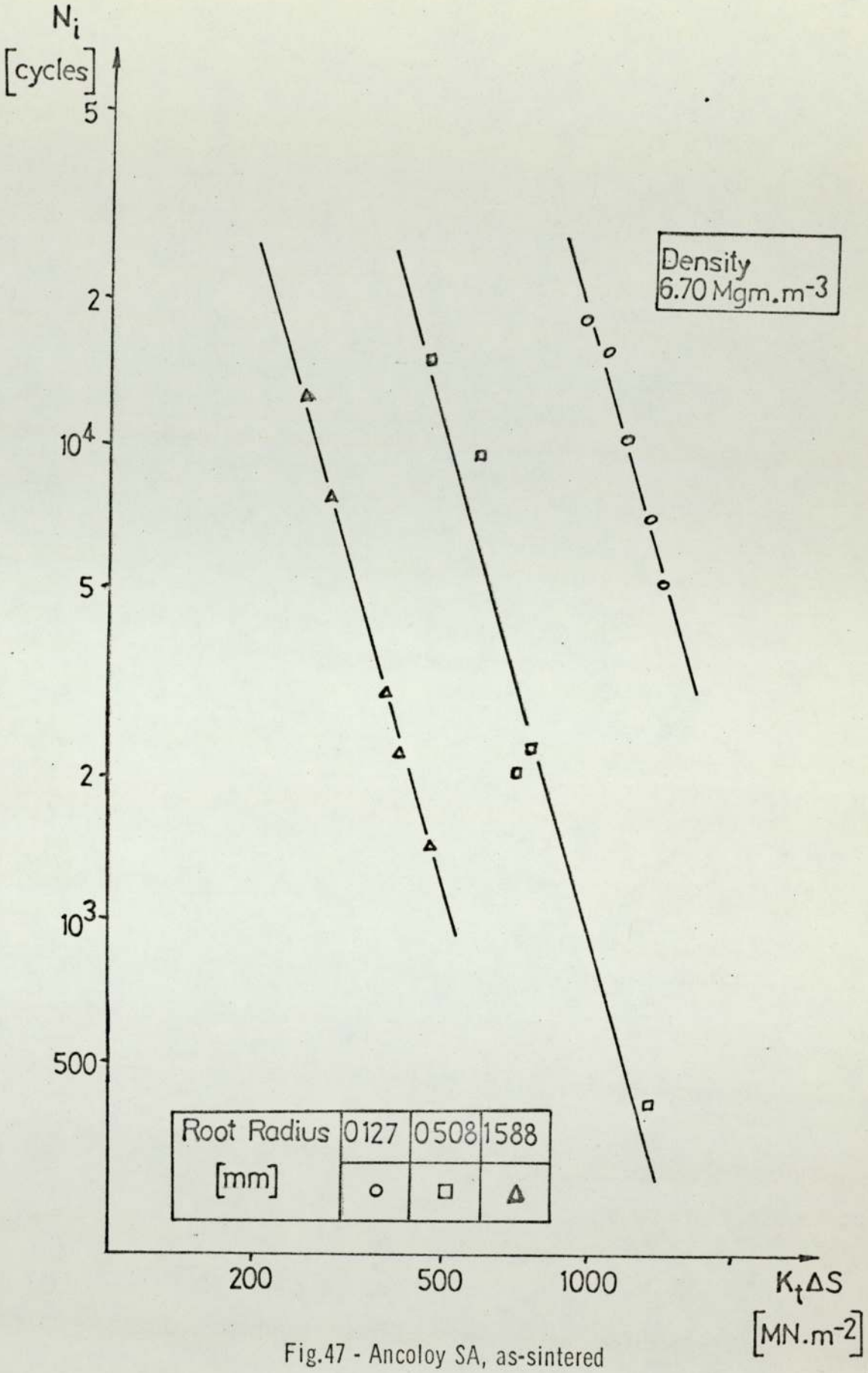


Fig.47 - Ancoloy SA, as-sintered

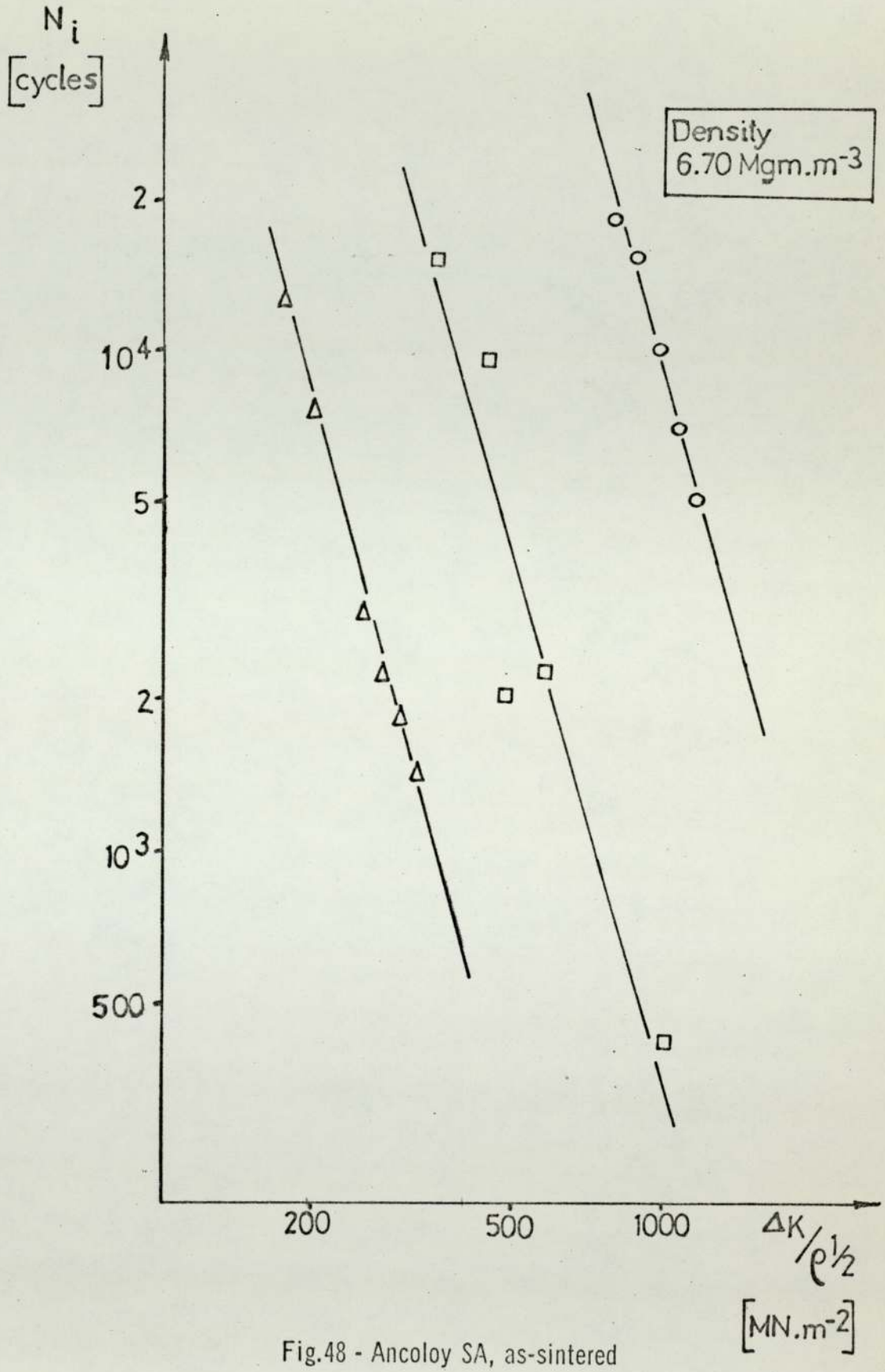


Fig.48 - Ancoloy SA, as-sintered

d)

| Density [Mgm.m$^{-3}$] | $K_t \Delta S$ [MN.m$^{-2}$] | $\Delta K/\rho^{\frac{1}{2}}$ [MN.m$^{-2}$] | $\dot{Ni}$ [cycles] |
|---|---|---|---|
| 7.00 | 972 | 799 | 11096 |
| | 1079 | 887 | 8245 |
| | 1188 | 976 | 4914 |
| | 1344 | 1065 | 4286 |
| $\rho$ = 0.127 mm | 1403 | 1154 | 2989 |
| | A | $10^{-14.1}$ | $10^{-14.4}$ |
| | n | -3.37 | -3.57 |
| | 464 | 355 | 13111 |
| | 584 | 444 | 12230 |
| | 635 | 488 | 7808 |
| | 710 | 532 | 4709 |
| $\rho$ = 0.508 mm | 750 | 577 | 1855 |
| | A | $10^{-14.0}$ | $10^{-13.7}$ |
| | n | -3.64 | -3.72 |
| | 287 | 201 | 15562 |
| | 372 | 251 | 10247 |
| | 397 | 276 | 4295 |
| | 440 | 301 | 3239 |
| $\rho$ = 1.588 mm | 483 | 326 | 2935 |
| | A | $10^{-12.9}$ | $10^{-13.0}$ |
| | n | -3.51 | -3.80 |

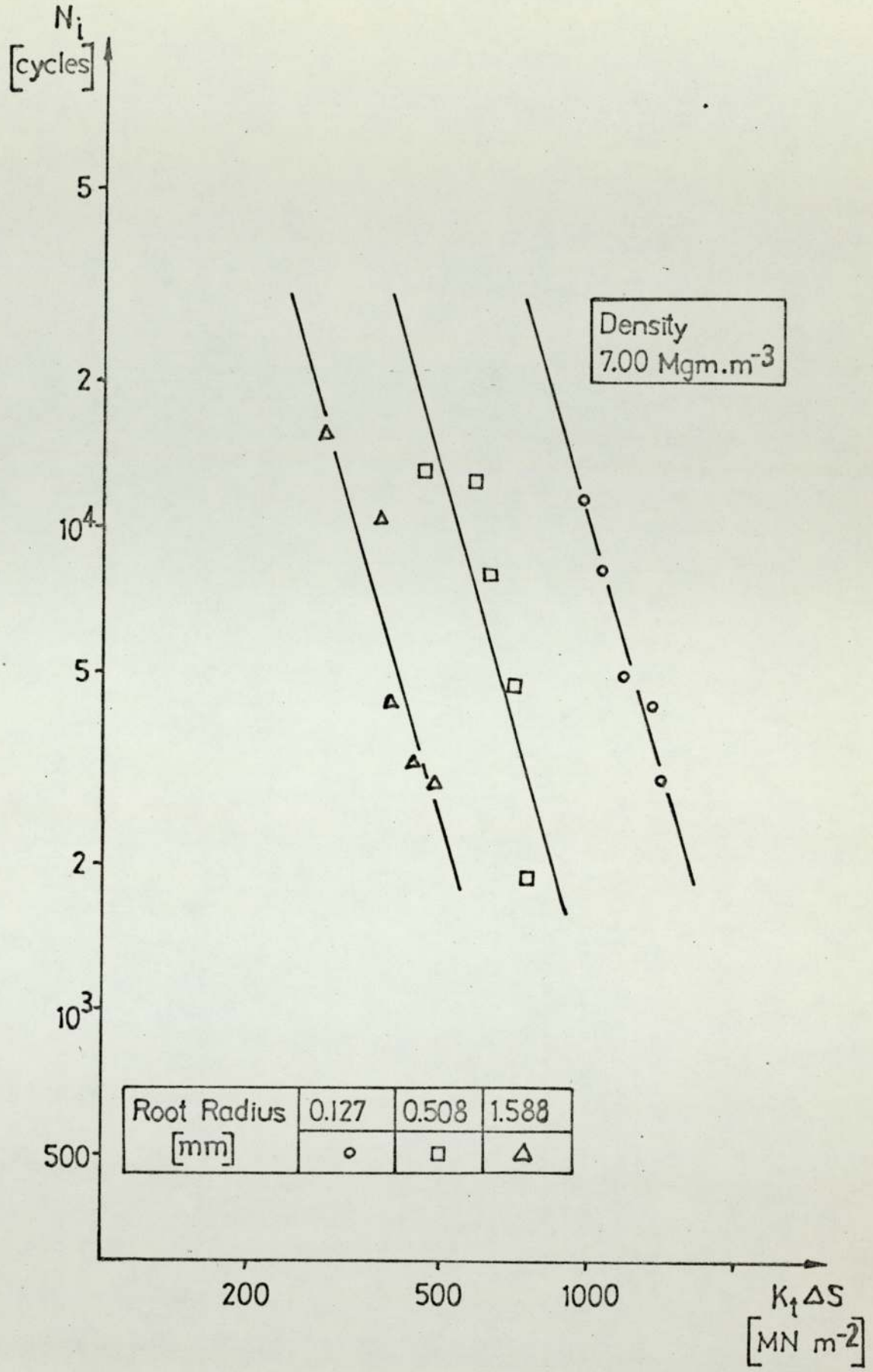


Fig.49 - Ancoloy SA, as-sintered

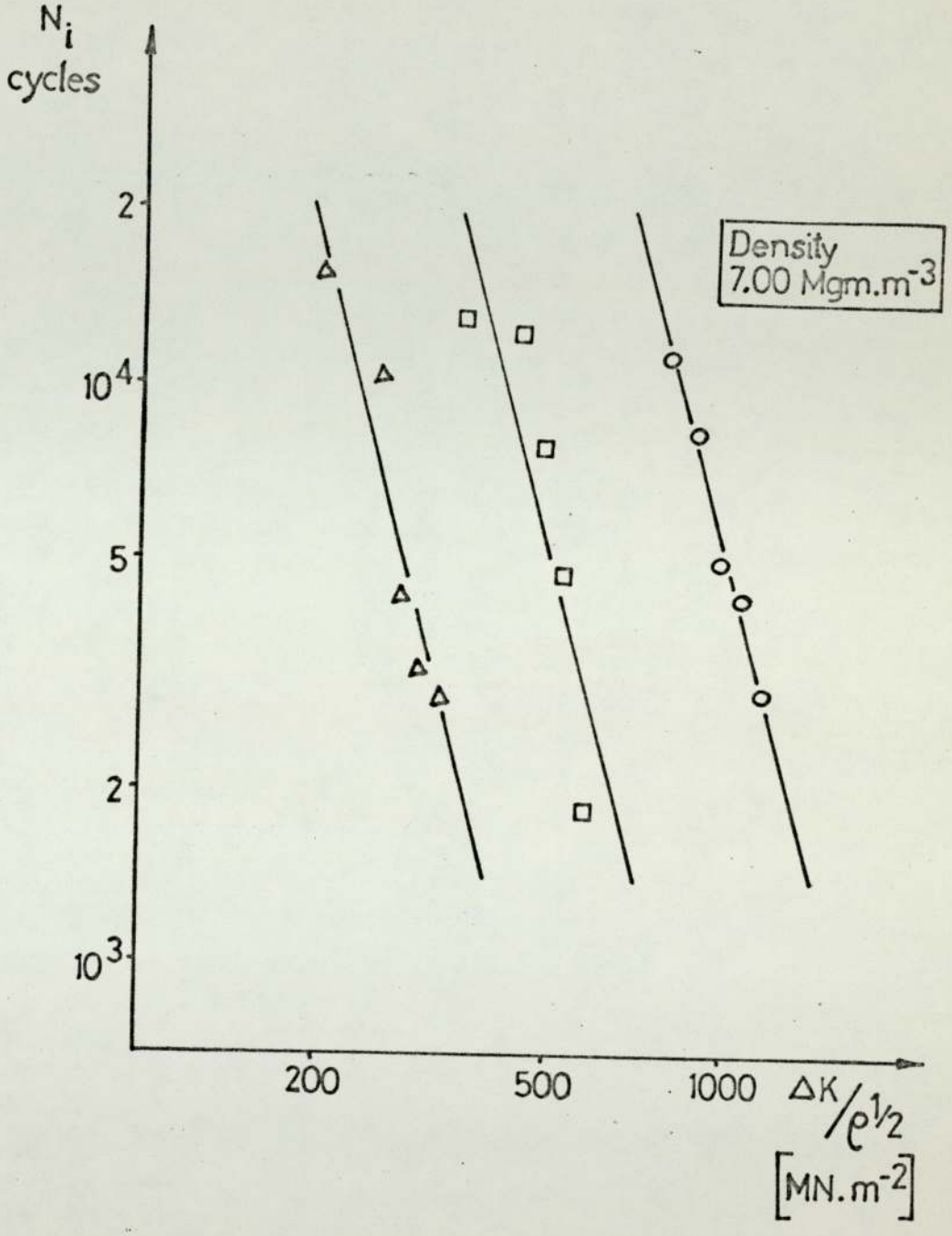


Fig.50 - Ancoloy SA, as-sintered

| Density [Mgm.m$^{-3}$] | $\Delta K_t S$ [MN.m$^{-2}$] | $\Delta K/\rho^{\frac{1}{2}}$ [MN.m$^{-2}$] | Ni · [cycles] |
|---|---|---|---|
| 5.95 | 173 | 133 | 20213 |
| | 231 | 178 | 12053 |
| | 288 | 222 | 9625 |
| | 346 | 266 | 2380 |
| | 404 | 311 | 864 |
| | 462 | 355 | 560 |
| | A | $10^{-13.2}$ | $10^{-12.7}$ |
| | n | -3.88 | -3.88 |
| 6.70 | 404 | 311 | 19000 |
| | 462 | 355 | 16160 |
| | 520 | 399 | 11360 |
| | 577 | 444 | 6240 |
| | 635 | 488 | 3280 |
| | 700 | 532 | 2400 |
| | A | $10^{-15.0}$ | $10^{-14.7}$ |
| | n | -4.07 | -4.13 |
| 7.00 | 404 | 311 | 27000 |
| | 462 | 355 | 24000 |
| | 520 | 399 | 11937 |
| | 577 | 444 | 7418 |
| | 635 | 488 | 3781 |
| | 700 | 532 | 3502 |
| | A | $10^{-15.5}$ | $10^{-15.2}$ |
| | n | -4.23 | -4.30 |

e) Heat treated : $\rho$ = 0.508 mm

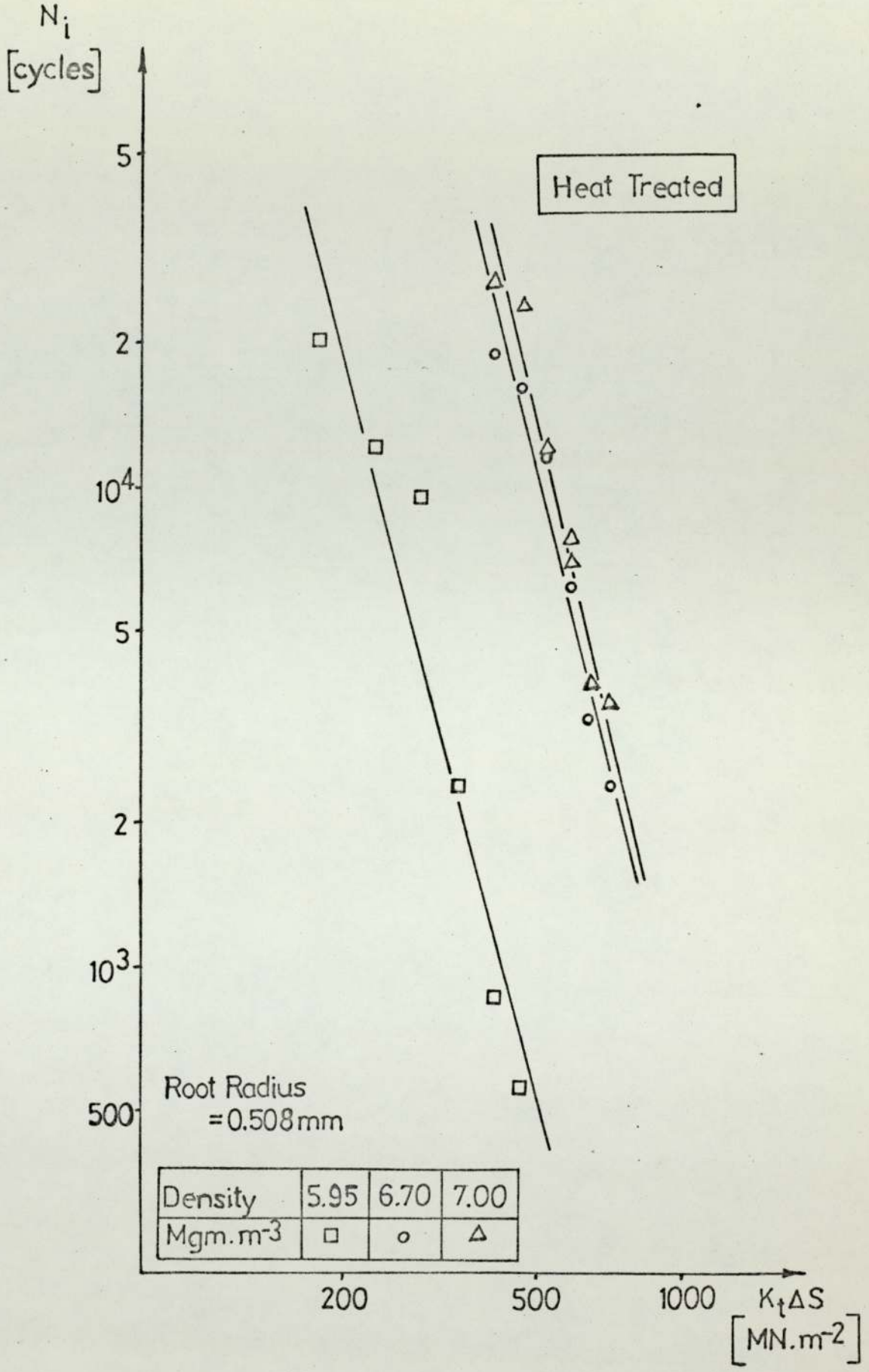


Fig.51 - Ancoloy SA, heat treated

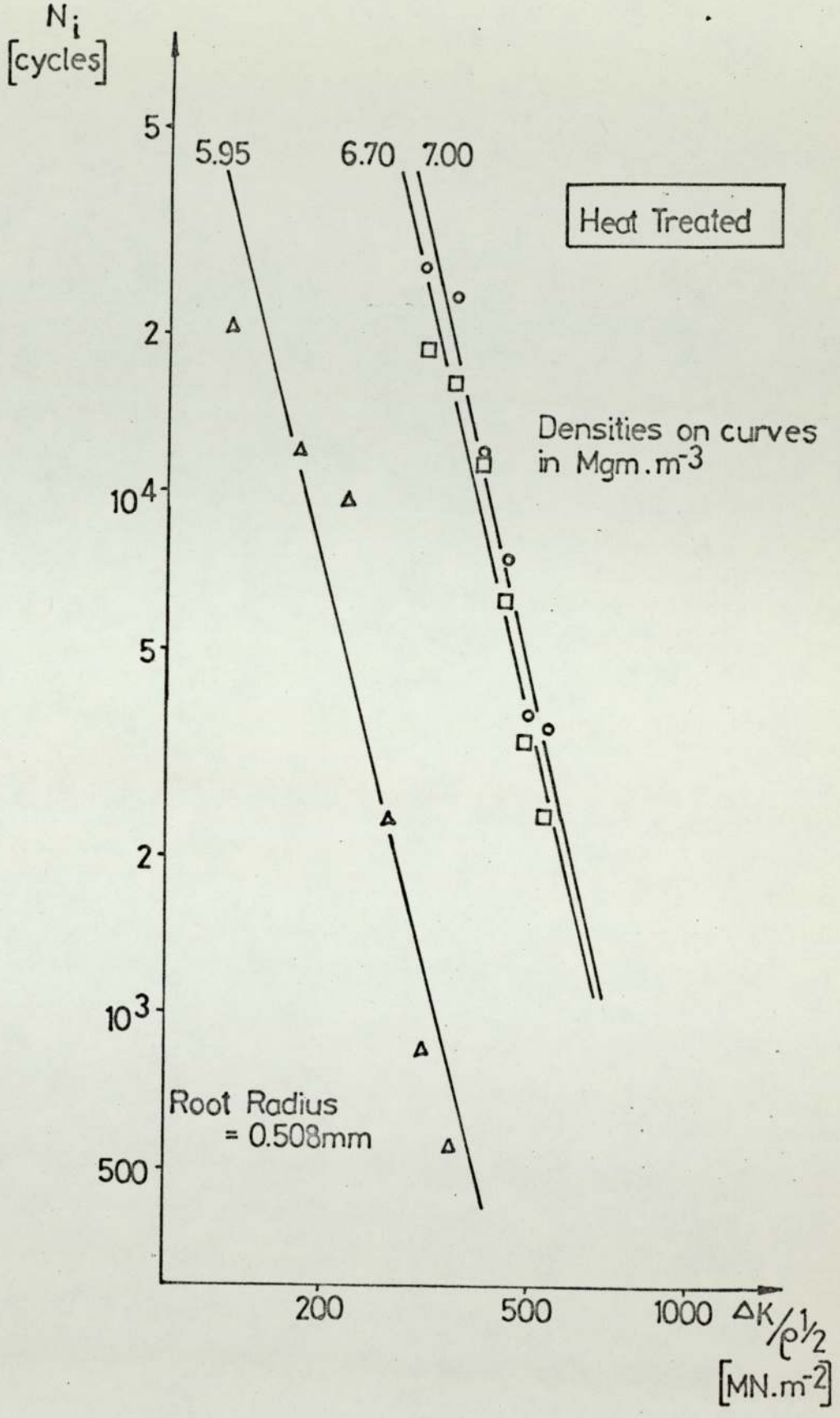


Fig.52 - Ancoloy SA, heat treated

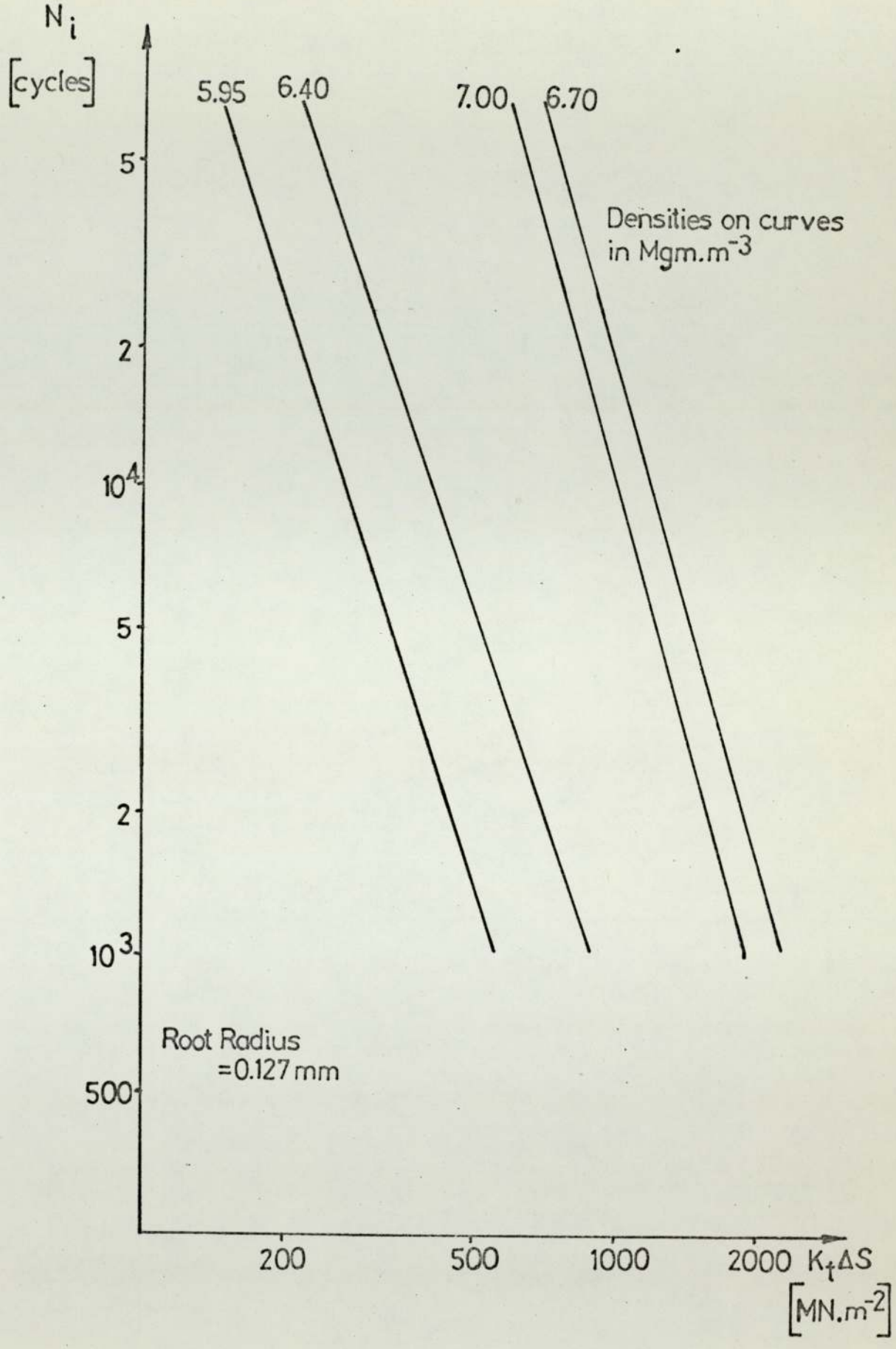


Fig.53 - Comparison of $N_i$ vs $K_t \Delta S$ curves for Ancoloy SA, as-sintered

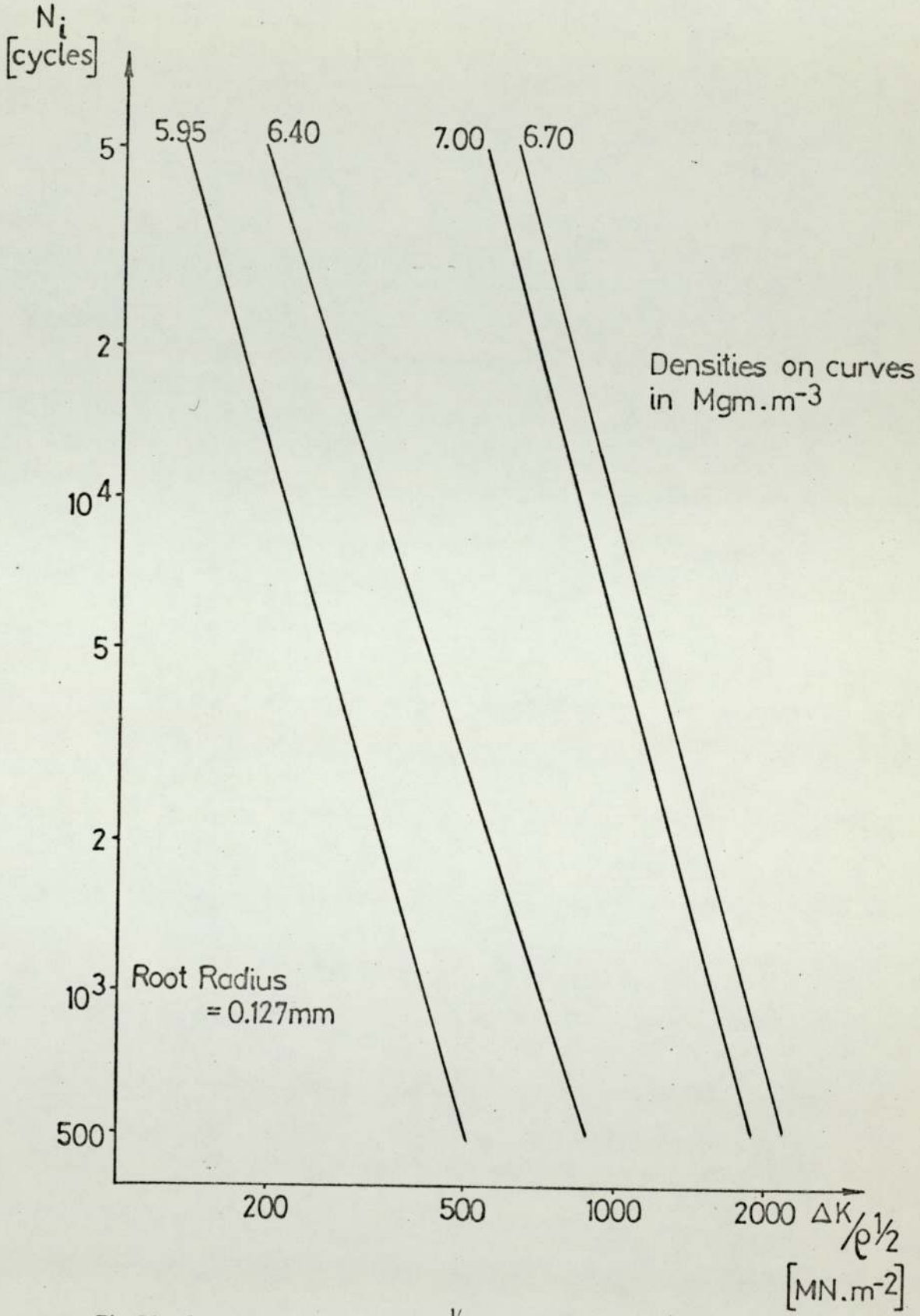


Fig.54 - Comparison of $N_i$ vs $\Delta K/\rho^{1/2}$ curves for Ancoloy SA, as-sintered

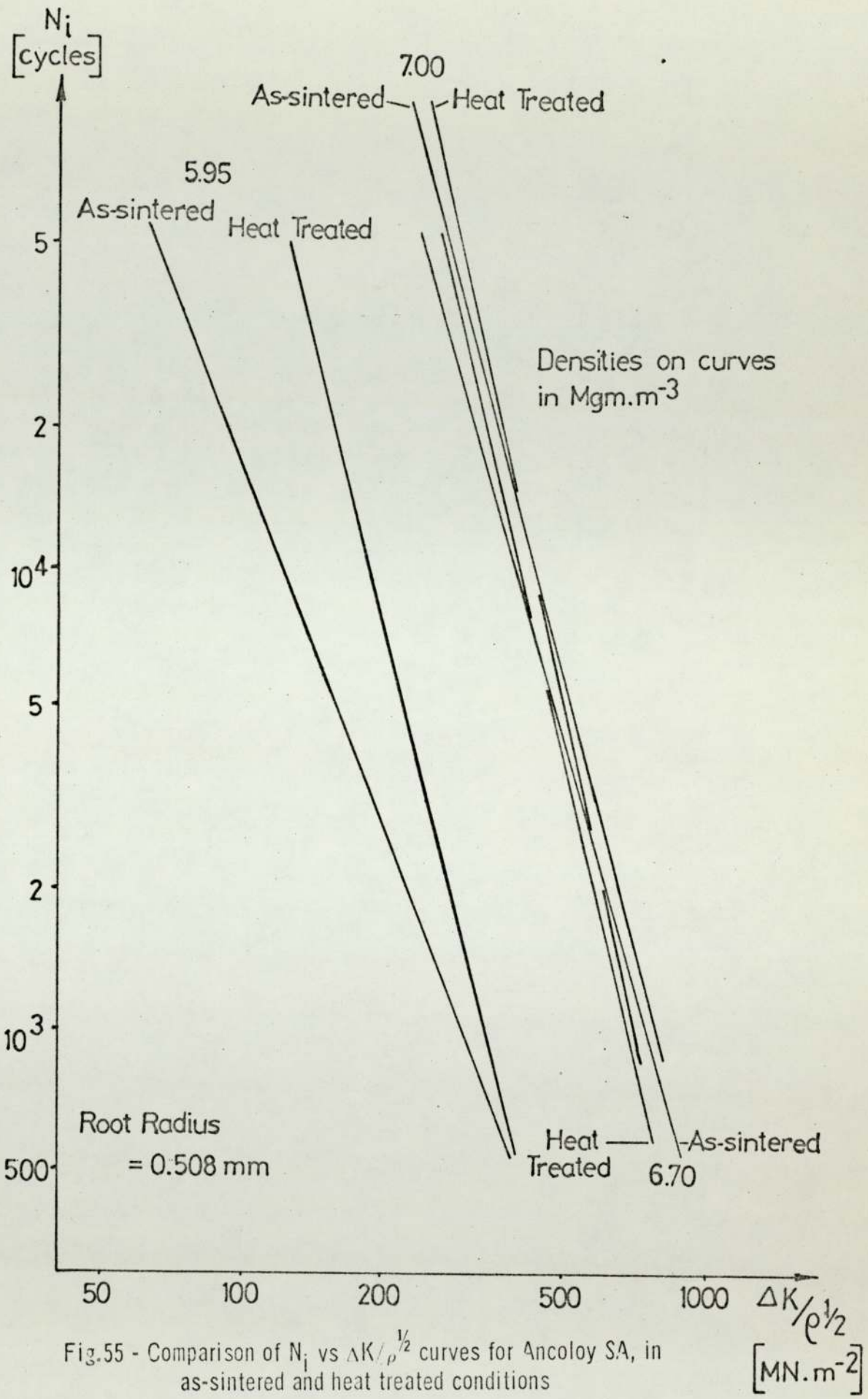


Fig.55 - Comparison of $N_i$ vs $\Delta K/\rho^{1/2}$ curves for Ancoloy SA, in as-sintered and heat treated conditions

| Density [Mgm.m$^{-3}$] | da/dNx10$^{6}$ [mm cycle$^{-1}$] | Δ K [MN.m$^{-3/2}$] | Density [Mgm.m$^{-3}$] | da/dNx10$^{6}$ [mm cycle$^{-1}$] | ΔK [MN.m$^{-3/2}$] |
|---|---|---|---|---|---|
| | 1.69 | 5.81 | 6.40 (cont) | 8.44 | 8.35 |
| | 2.58 | 6.63 | | 8.68 | 7.99 |
| | 3.30 | 6.39 | | 8.94 | 9.74 |
| | 4.09 | 7.21 | | 9.52 | 8.24 |
| | 4.73 | 6.79 | | 9.62 | 9.02 |
| | 5.10 | 8.03 | | 10.10 | 8.46 |
| | 5.57 | 8.26 | | 10.24 | 8.15 |
| | 6.86 | 8.43 | | 10.45 | 9.01 |
| | 10.05 | 8.59 | | 10.71 | 8.64 |
| | 11.63 | 8.16 | | 10.86 | 8.74 |
| | 12.94 | 8.02 | | 11.34 | 10.04 |
| | 13.86 | 10.29 | | 11.88 | 9.56 |
| | 16.28 | 8.30 | | 13.41 | 9.11 |
| | 16.69 | 9.18 | | 14.29 | 9.02 |
| 5.95 | 17.14 | 9.04 | | 14.76 | 8.90 |
| | 17.44 | 8.56 | | 15.14 | 8.39 |
| | 18.60 | 8.84 | | 15.22 | 10.39 |
| | 21.91 | 8.27 | | 15.68 | 9.45 |
| | 25.58 | 9.31 | | 16.86 | 9.24 |
| | 26.34 | 9.02 | | 16.89 | 9.84 |
| | 38.15 | 9.73 | | 17.70 | 10.10 |
| | 38.89 | 10.93 | | 17.71 | 8.68 |
| | 47.57 | 10.30 | | 17.86 | 9.39 |
| | 54.07 | 11.20 | | 17.86 | 9.83 |
| | 86.16 | 10.51 | | 19.23 | 10.61 |
| | 95.20 | 10.29 | | 19.96 | 10.75 |
| | 97.90 | 11.44 | | 20.52 | 10.33 |
| | 118.70 | 11.77 | | 27.19 | 11.30 |
| | Constant (C) | $10^{-10.4}$ | | 33.71 | 9.90 |
| | Slope (m) | 5.90 | | 36.49 | 11.68 |
| | | | | 46.29 | 10.39 |
| | | | | 52.20 | 12.37 |
| | | | | 72.20 | 13.08 |
| | 2.60 | 7.40 | | 76.59 | 10.94 |
| | 2.91 | 7.59 | | 109.0 | 11.49 |
| | 3.88 | 7.73 | | 164.0 | 12.38 |
| | 5.34 | 7.85 | | | |
| | 5.44 | 7.25 | | C | $10^{-10.0}$ |
| | 5.61 | 7.89 | | | |
| | 5.61 | 8.04 | | m | 5.33 |
| 6.40 | 6.41 | 8.55 | | | |
| | 6.55 | 7.69 | | | |
| | 7.72 | 8.10 | | | |
| | 7.75 | 9.35 | | | |
| | 7.84 | 7.66 | | | |
| | 8.41 | 8.83 | | | |

Table 8 : Fatigue crack propagation data: As-sintered 0.4% carbon

Table 8 continued:

| Density [Mgm.m$^{-3}$] | da/dNx10$^{6}$ [mm cycle$^{-1}$] | Δ K [MN.m$^{-3/2}$] | Density [Mgm.m$^{-3}$] | da/dNx10$^{6}$ [mm cycle$^{-1}$] | Δ K [MN.m$^{-3/2}$] |
|---|---|---|---|---|---|
| 7.00 | 3.74 | 11.00 | 7.00 (cont.) | 15.08 | 11.66 |
| | 3.78 | 10.01 | | 15.41 | 13.07 |
| | 3.91 | 10.38 | | 15.76 | 13.38 |
| | 4.40 | 10.17 | | 15.76 | 12.63 |
| | 4.75 | 11.18 | | 16.00 | 13.66 |
| | 5.03 | 10.57 | | 20.11 | 13.05 |
| | 5.87 | 10.75 | | 20.69 | 13.53 |
| | 5.87 | 10.96 | | 20.69 | 14.03 |
| | 6.01 | 11.45 | | 20.75 | 13.33 |
| | 6.13 | 10.36 | | 23.00 | 13.92 |
| | 6.82 | 11.77 | | 25.80 | 14.64 |
| | 7.87 | 10.53 | | 28.00 | 14.13 |
| | 8.38 | 11.22 | | 34.44 | 14.92 |
| | 8.60 | 12.08 | | 39.29 | 15.54 |
| | 9.17 | 10.75 | | 39.29 | 15.98 |
| | 9.40 | 11.10 | | 39.31 | 15.92 |
| | 9.61 | 12.11 | | 46.43 | 17.09 |
| | 11.43 | 12.60 | | 60.57 | 16.95 |
| | 11.73 | 12.05 | | 66.42 | 17.93 |
| | 11.73 | 12.32 | | 93.67 | 20.15 |
| | 12.92 | 12.60 | | 98.40 | 19.11 |
| | 14.98 | 12.58 | | 162.0 | 21.02 |
| | | | | C | $10^{-10.2}$ |
| | | | | m | 4.80 |

| Carbon content (%) | da/dNx10$^6$ [mm cycle$^{-1}$] | Δ K [MN.m$^{-3/2}$] | Carbon content (%) | da/dNx10$^6$ [mm cycle$^{-1}$] | Δ K [MN.m$^{-3/2}$] |
|---|---|---|---|---|---|
| 0% | 5.92 | 9.47 | 0.3% (cont.) | 94.90 | 18.51 |
| | 8.29 | 10.13 | | 95.40 | 16.79 |
| | 8.59 | 9.83 | | 99.57 | 15.85 |
| | 14.02 | 10.67 | | 112.6 | 10.41 |
| | 17.77 | 11.28 | | 115.9 | 16.42 |
| | 17.95 | 10.25 | | 157.4 | 18.19 |
| | 19.53 | 9.75 | | 168.3 | 17.09 |
| | 24.82 | 10.81 | | 172.6 | 10.79 |
| | 27.16 | 11.98 | | 179.5 | 18.73 |
| | 36.36 | 10.30 | | 223.7 | 16.06 |
| | 37.07 | 12.61 | | 255.8 | 19.19 |
| | 39.44 | 11.56 | | C | $10^{-9.8}$ |
| | 53.27 | 12.41 | | m | 4.79 |
| | 59.64 | 11.02 | | | |
| | 78.55 | 13.19 | | | |
| | 98.38 | 11.94 | | | |
| | 138.0 | 12.80 | | | |
| 0.3% | 0.67 | 8.68 | 0.4% | 4.86 | 11.55 |
| | 0.70 | 8.87 | | 5.76 | 11.65 |
| | 1.38 | 9.61 | | 5.76 | 11.80 |
| | 4.83 | 10.34 | | 5.79 | 11.81 |
| | 5.88 | 10.72 | | 6.46 | 15.15 |
| | 6.05 | 11.05 | | 7.21 | 9.91 |
| | 7.49 | 12.26 | | 7.68 | 12.04 |
| | 8.58 | 9.02 | | 8.22 | 15.27 |
| | 8.82 | 9.15 | | 8.26 | 12.00 |
| | 8.84 | 11.59 | | 8.91 | 10.35 |
| | 10.00 | 9.52 | | 9.00 | 10.14 |
| | 10.04 | 9.33 | | 9.04 | 10.29 |
| | 10.16 | 12.11 | | 9.09 | 12.27 |
| | 15.07 | 9.61 | | 11.52 | 12.30 |
| | 15.26 | 12.60 | | 11.84 | 15.45 |
| | 19.72 | 12.97 | | 12.66 | 10.63 |
| | 20.00 | 9.75 | | 13.14 | 10.63 |
| | 29.80 | 12.78 | | 13.82 | 12.48 |
| | 29.81 | 13.23 | | 14.88 | 12.62 |
| | 36.12 | 13.95 | | 15.49 | 11.00 |
| | 37.19 | 11.53 | | 16.27 | 10.96 |
| | 40.93 | 13.99 | | 16.35 | 11.29 |
| | 46.58 | 13.62 | | 17.17 | 11.55 |
| | 54.00 | 15.09 | | 17.72 | 11.01 |
| | 62.27 | 16.62 | | 18.11 | 15.71 |
| | 64.00 | 14.23 | | 18.18 | 12.99 |
| | 70.61 | 15.17 | | 19.29 | 11.21 |
| | 75.86 | 12.41 | | 20.74 | 12.76 |
| | 76.23 | 14.27 | | 21.30 | 11.47 |
| | 80.20 | 10.04 | | 22.77 | 11.86 |
| | 80.62 | 15.29 | | 27.78 | 11.84 |
| | 83.84 | 17.63 | | 28.18 | 11.98 |
| | 83.90 | 15.98 | | 29.51 | 12.27 |
| | | | | 29.75 | 13.54 |
| | | | | 30.57 | 16.10 |

Table 9: Fatigue crack propagation data: as sintered, 6.70 Mgm.m$^{-3}$

Table 9: (cont.)

| Carbon content (%) | da/dNx10$^6$ [mm cycle$^{-1}$] | ΔK [MN.m$^{-3/2}$] | Carbon content (%) | da/dNx10$^6$ [mm cycle$^{-1}$] | ΔK [MN.m$^{-3/2}$] |
|---|---|---|---|---|---|
| 0.4% (cont.) | 31.97 | 12.73 | 0.65% (cont.) | 29.60 | 16.04 |
| | 35.19 | 12.90 | | 29.70 | 17.66 |
| | 36.36 | 12.49 | | 30.70 | 20.92 |
| | 37.20 | 15.02 | | 32.10 | 19.00 |
| | 39.17 | 13.23 | | 34.60 | 19.82 |
| | 41.50 | 13.29 | | 37.80 | 21.26 |
| | 48.25 | 15.44 | | 40.40 | 22.11 |
| | 48.89 | 13.25 | | 42.90 | 19.78 |
| | 55.00 | 13.84 | | 45.10 | 20.02 |
| | 55.04 | 14.30 | | 46.00 | 10.49 |
| | 55.00 | 14.80 | | 46.30 | 23.20 |
| | 57.60 | 14.08 | | 53.70 | 21.16 |
| | 65.27 | 13.04 | | 53.70 | 17.66 |
| | 66.82 | 15.39 | | 61.60 | 22.89 |
| | 74.42 | 14.55 | | 61.90 | 20.81 |
| | 80.44 | 13.93 | | 71.00 | 19.63 |
| | 88.36 | 16.12 | | 73.60 | 16.84 |
| | 92.73 | 17.19 | | 85.60 | 17.71 |
| | 97.07 | 15.62 | | 87.50 | 21.64 |
| | 105.9 | 15.04 | | 88.80 | 24.09 |
| | 106.4 | 17.10 | | 94.00 | 23.10 |
| | 130.2 | 18.46 | | 98.40 | 19.11 |
| | 140.4 | 14.41 | | 110.0 | 20.12 |
| | 144.4 | 13.78 | | 161.0 | 21.02 |
| | 166.7 | 16.75 | | 163.0 | 20.92 |
| | 180.5 | 14.96 | | 338.0 | 17.98 |
| | 213.4 | 19.89 | | 508.0 | 23.34 |
| | 217.4 | 16.01 | | C | $10^{-9.0}$ |
| | 336.8 | 19.33 | | m | 3.65 |
| | C | $10^{-9.8}$ | | | |
| | m | 4.71 | | | |
| 0.65% | 7.82 | 11.78 | | | |
| | 8.61 | 12.72 | | | |
| | 8.87 | 12.23 | | | |
| | 10.20 | 12.99 | | | |
| | 12.00 | 13.54 | | | |
| | 12.20 | 16.93 | | | |
| | 12.70 | 15.09 | | | |
| | 13.90 | 14.08 | | | |
| | 14.50 | 13.84 | | | |
| | 21.30 | 18.84 | | | |
| | 22.70 | 15.75 | | | |
| | 22.90 | 16.49 | | | |
| | 23.20 | 19.91 | | | |
| | 23.40 | 13.95 | | | |
| | 24.10 | 16.20 | | | |
| | 25.40 | 18.75 | | | |
| | 26.30 | 17.85 | | | |
| | 27.10 | 17.10 | | | |
| | 28.50 | 17.88 | | | |

| Density [Mgm.m$^{-3}$] | da/dNx10$^{6}$ [mm cycle$^{-1}$] | K [MN.m$^{-3/2}$] |
|---|---|---|
| 5.95 | 3.48 | 7.25 |
| | 4.08 | 8.34 |
| | 4.82 | 8.61 |
| | 5.43 | 10.69 |
| | 6.29 | 11.11 |
| | 6.46 | 7.63 |
| | 6.79 | 8.82 |
| | 8.42 | 8.85 |
| | 9.66 | 8.46 |
| | 10.28 | 9.15 |
| | 10.99 | 11.49 |
| | 13.24 | 11.80 |
| | 14.93 | 9.20 |
| | 15.50 | 9.00 |
| | 17.64 | 8.04 |
| | 17.64 | 8.05 |
| | 17.81 | 8.92 |
| | 19.18 | 12.09 |
| | 24.56 | 9.92 |
| | 28.31 | 9.47 |
| | 29.07 | 9.34 |
| | 33.43 | 9.41 |
| | 36.71 | 9.66 |
| | 41.05 | 12.41 |
| | 42.62 | 9.92 |
| | 45.59 | 9.71 |
| | 45.69 | 10.22 |
| | 47.57 | 10.36 |
| | 56.14 | 10.09 |
| | 68.15 | 10.59 |
| | 77.19 | 10.82 |
| | 79.86 | 12.86 |
| | 116.60 | 11.92 |
| | 123.50 | 11.13 |
| | 129.40 | 11.39 |
| | 185.70 | 11.81 |
| | 213.4 | 12.61 |
| | C | $10^{-9.7}$ |
| | m | 5.05 |
| 6.70 | 13.38 | 14.77 |
| | 16.00 | 13.74 |
| | 16.76 | 14.49 |
| | 17.27 | 13.54 |
| | 18.86 | 14.13 |
| | 19.00 | 13.91 |
| | 19.15 | 15.45 |
| | 24.58 | 14.41 |
| | 25.31 | 14.87 |
| | 26.36 | 14.53 |
| | 26.94 | 13.89 |
| | 27.38 | 15.32 |
| 6.70 (cont.) | 28.34 | 14.63 |
| | 31.00 | 14.87 |
| | 32.00 | 16.23 |
| | 37.42 | 15.35 |
| | 39.25 | 17.46 |
| | 40.75 | 16.16 |
| | 40.93 | 16.94 |
| | 43.38 | 18.03 |
| | 43.86 | 15.36 |
| | 44.00 | 15.24 |
| | 44.25 | 15.97 |
| | 48.75 | 18.58 |
| | 49.50 | 15.27 |
| | 58.63 | 16.67 |
| | 58.75 | 16.25 |
| | 58.75 | 17.29 |
| | 65.17 | 19.21 |
| | 69.25 | 16.16 |
| | 71.33 | 17.91 |
| | 71.87 | 17.15 |
| | 79.00 | 17.94 |
| | 79.53 | 17.22 |
| | 87.62 | 17.26 |
| | 81.90 | 21.15 |
| | 100.5 | 19.07 |
| | 148.8 | 21.62 |
| | 196.0 | 23.40 |
| | C | $10^{-9.7}$ |
| | m | 4.43 |
| 7.00 | 3.59 | 11.91 |
| | 4.69 | 12.00 |
| | 4.76 | 11.54 |
| | 6.20 | 12.50 |
| | 8.44 | 12.37 |
| | 11.00 | 14.16 |
| | 12.86 | 16.25 |
| | 14.06 | 15.76 |
| | 15.96 | 16.25 |
| | 17.00 | 16.50 |
| | 18.38 | 17.46 |
| | 19.37 | 17.37 |
| | 21.70 | 16.77 |
| | 24.38 | 18.35 |
| | 26.88 | 17.58 |
| | 27.56 | 16.86 |
| | 32.58 | 19.53 |
| | 34.19 | 17.77 |
| | 34.63 | 18.90 |

Table 10: Fatigue crack propagation data: heated treated, 0.4% carbon

Table 10 (cont.)

| Density [Mgm.m$^{-3}$] | da/dNx10$^{6}$ [mm cycle$^{-1}$] | ΔK [MN.m$^{-3/2}$] |
|---|---|---|
| 7.00 (cont.) | 35.00 | 18.55 |
| | 37.83 | 18.19 |
| | 39.56 | 19.52 |
| | 41.87 | 20.95 |
| | 42.00 | 20.19 |
| | 45.82 | 18.65 |
| | 48.67 | 19.52 |
| | 58.50 | 20.84 |
| | 60.50 | 20.49 |
| | 68.13 | 19.64 |
| | 68.14 | 22.45 |
| | 113.4 | 25.21 |
| | 114.8 | 26.10 |
| | 299.8 | 23.89 |
| | C | $10^{-9.9}$ |
| | m | 4.25 |

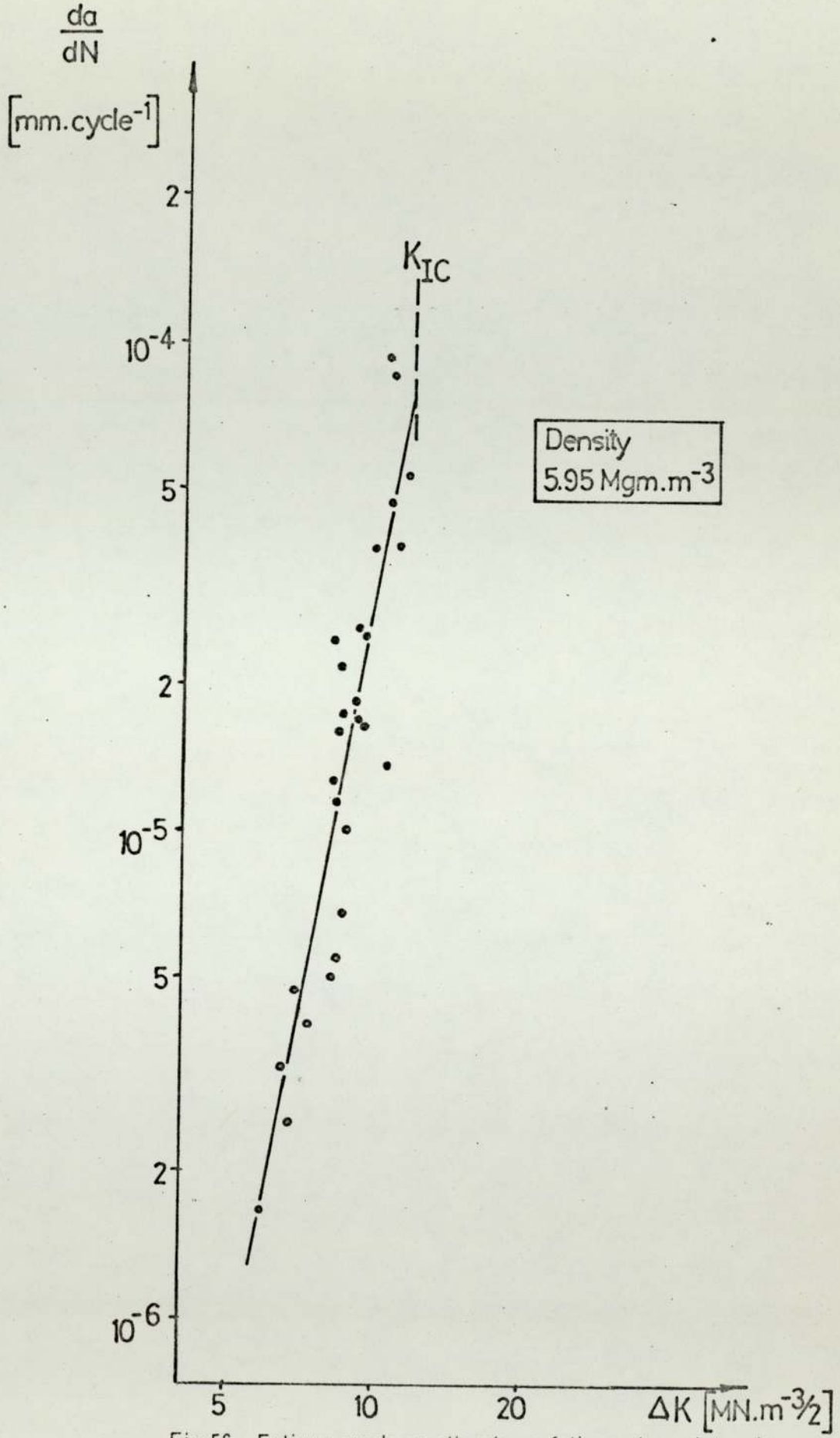


Fig.56 - Fatigue crack growth rate vs fatigue stress intensity for Ancoloy SA, as-sintered

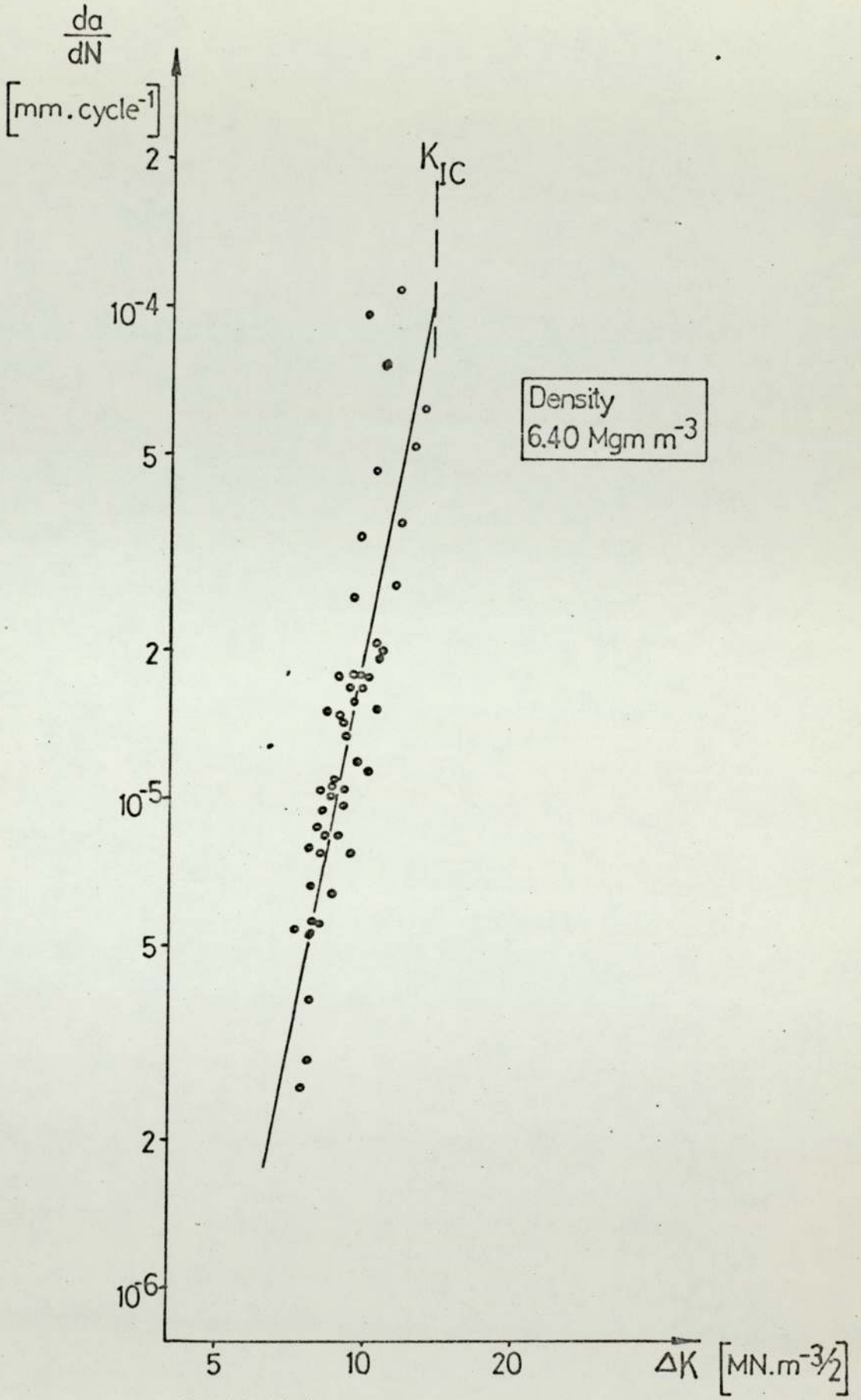


Fig.57 - Fatigue crack growth rate vs fatigue stress intensity for Ancoloy SA, as-sintered

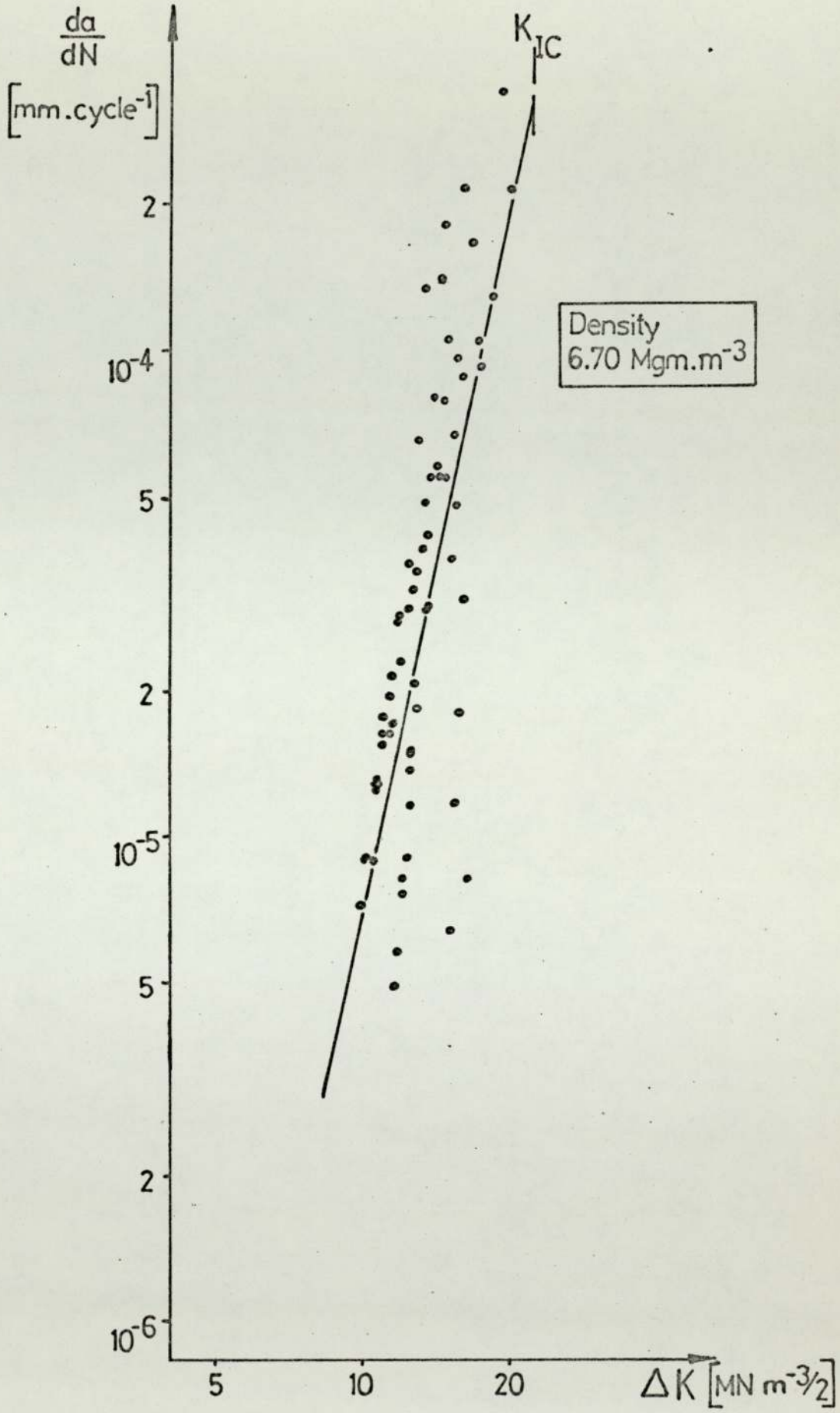


Fig.58 - Fatigue crack growth rate vs fatigue stress intensity for Ancoloy SA, as-sintered

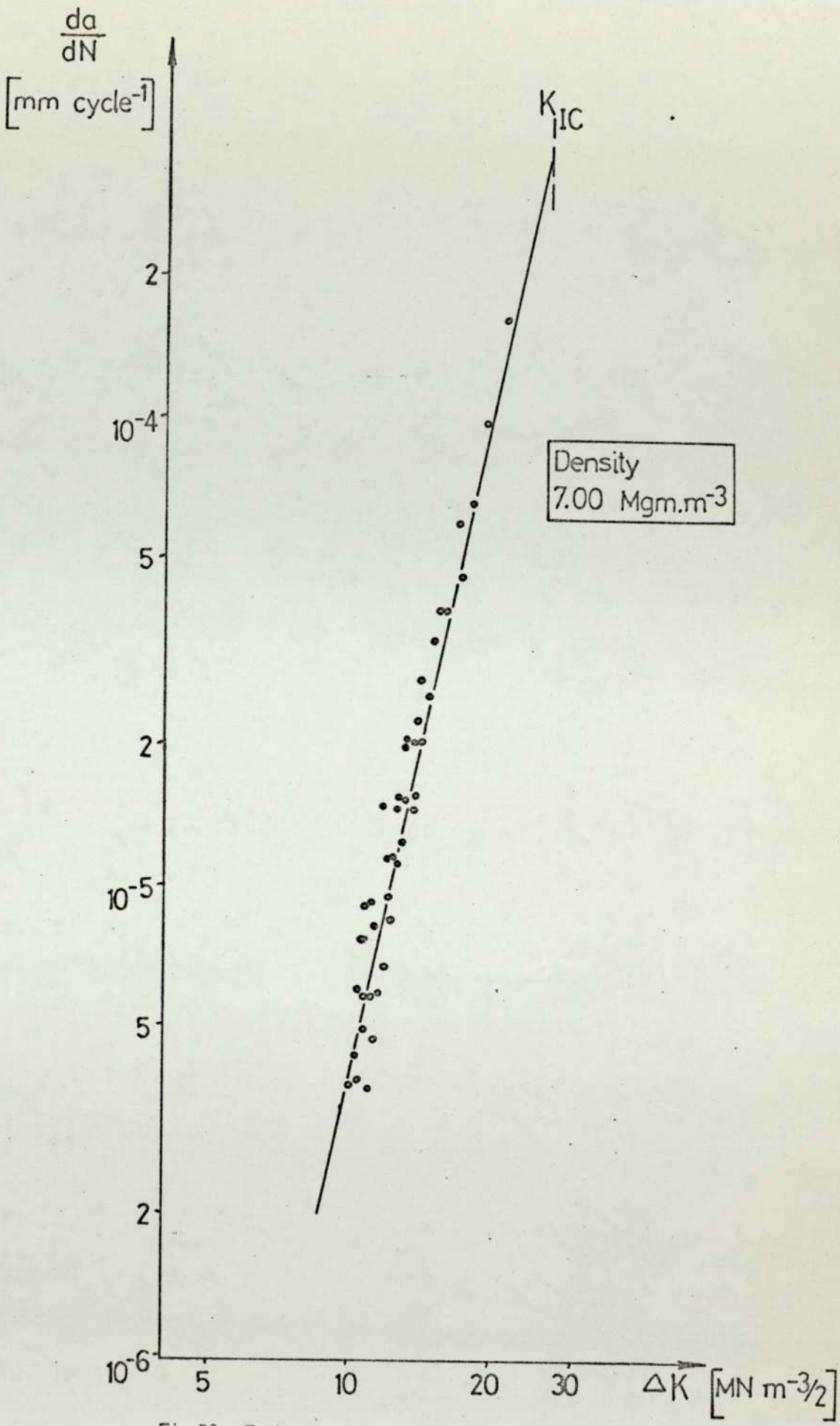


Fig.59 - Fatigue crack growth rate vs fatigue stress intensity for Ancoloy SA, as-sintered

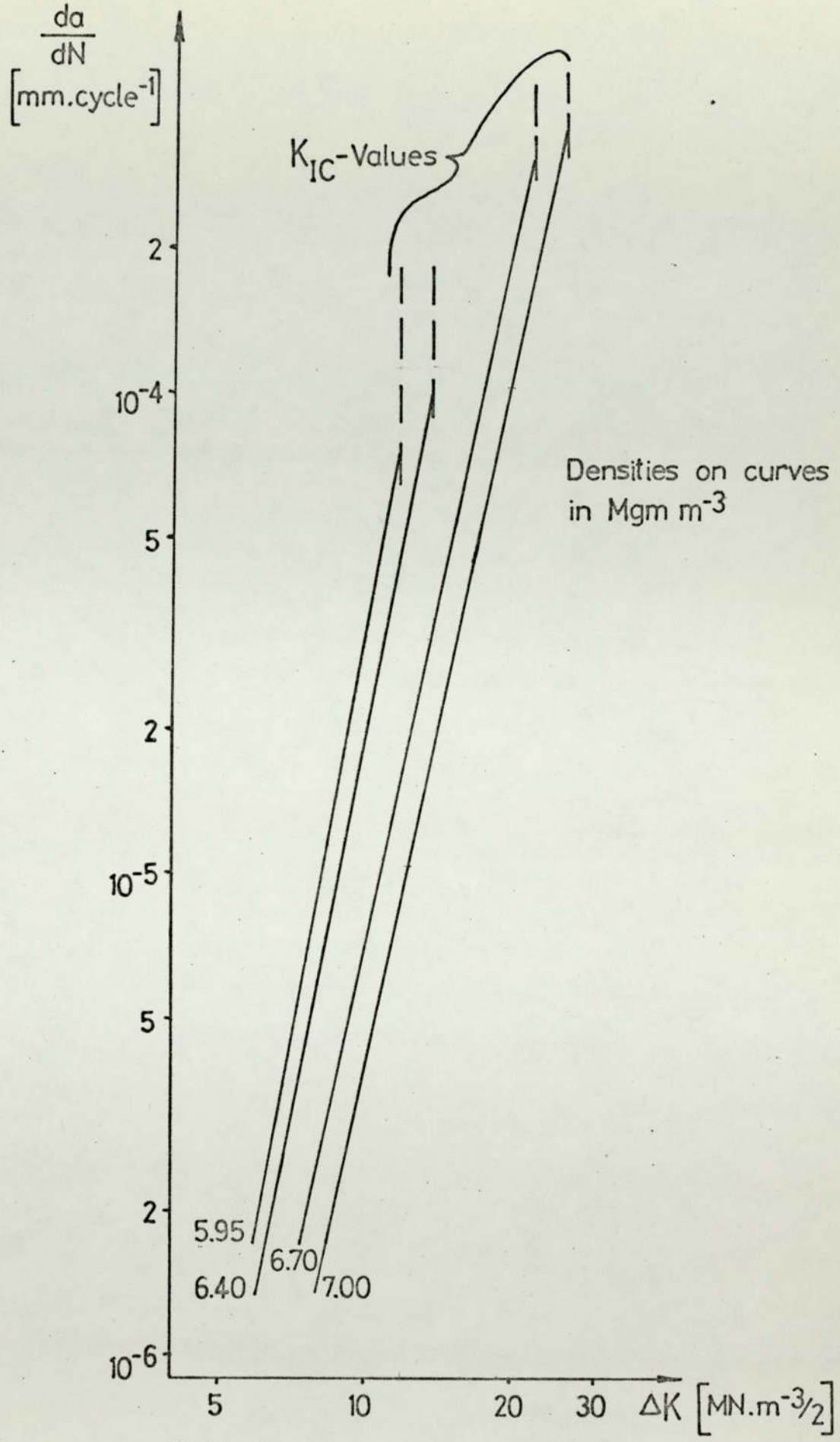


Fig.60 - Comparison of fatigue crack growth rates for Ancoloy SA, at various densities (as-sintered)

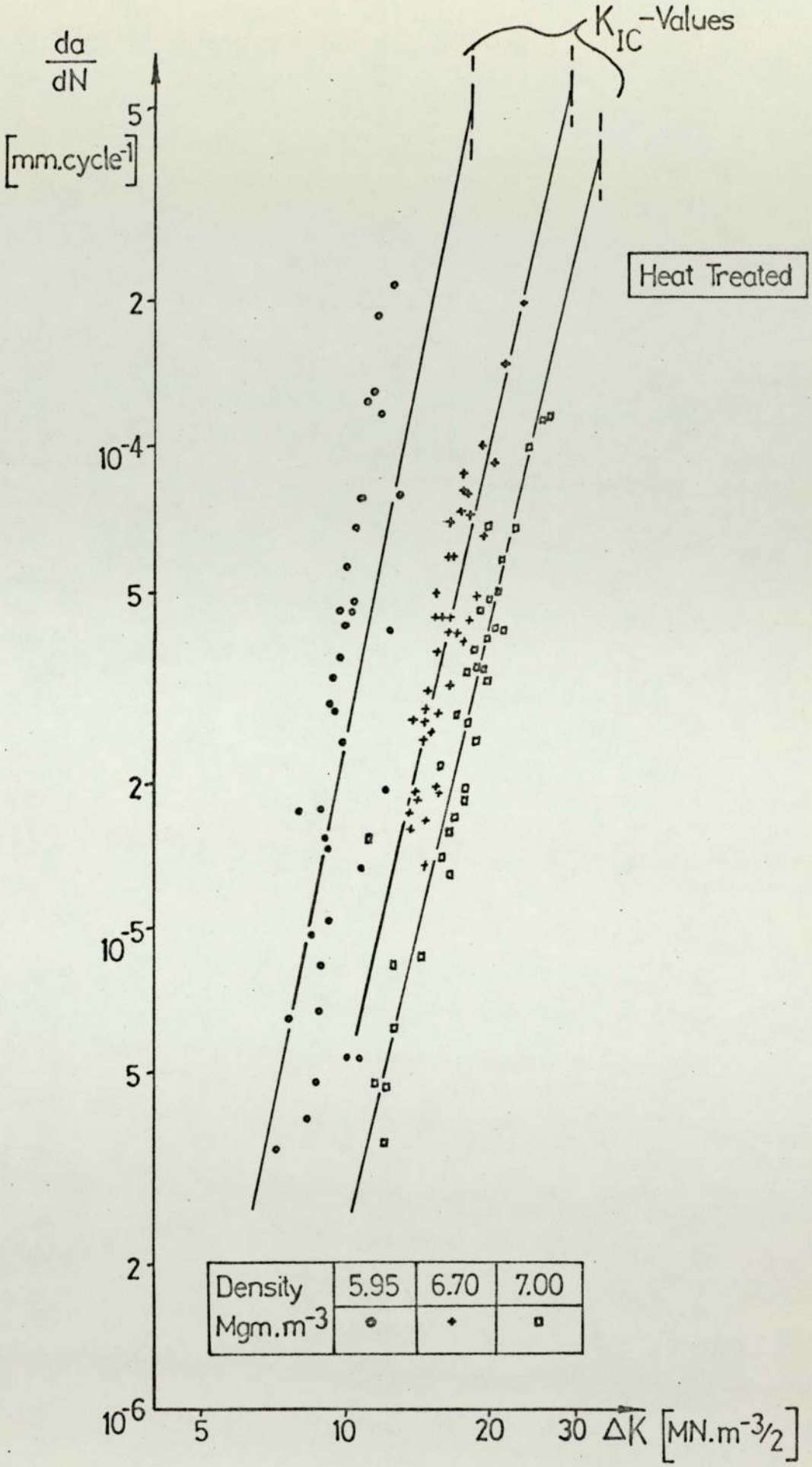


Fig.61 - Comparison of fatigue crack growth rates for Ancoloy SA in the heat treated condition

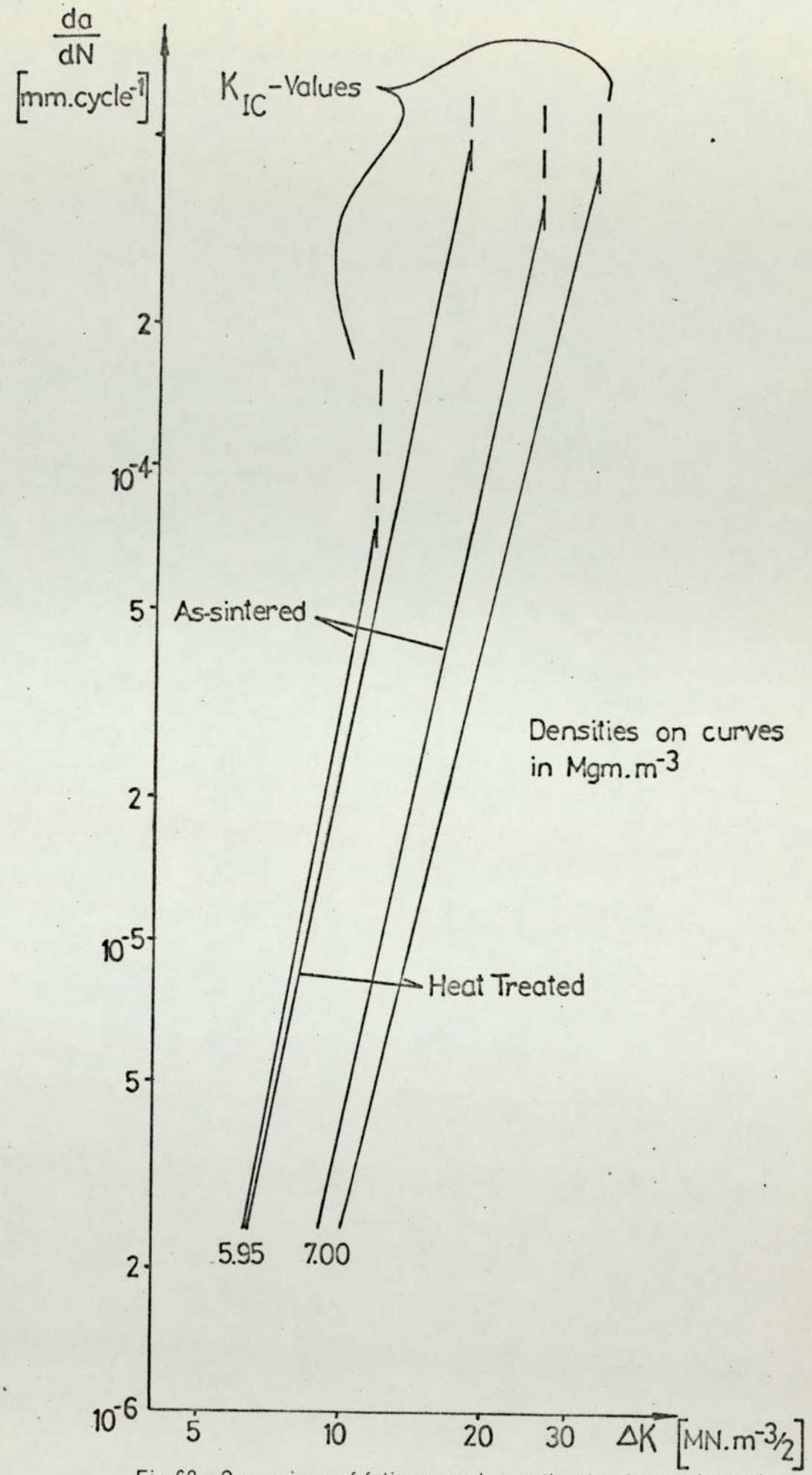


Fig.62 - Comparison of fatigue crack growth rates for as-sintered and heat-treated Ancoloy SA

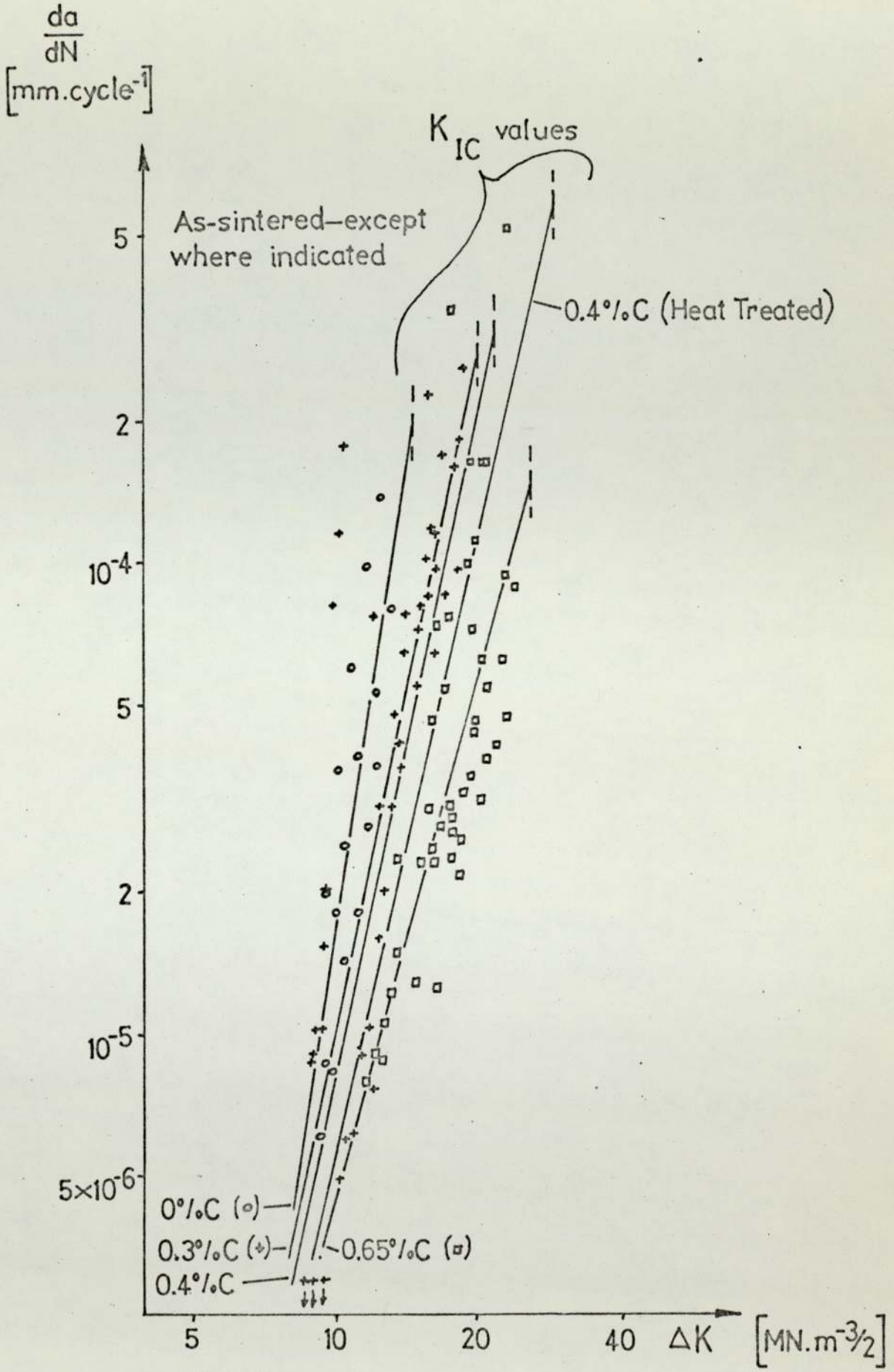


Fig.63 - Fatigue crack growth rates for Ancoloy SA at a density of 6.70 Mgm.m$^{-3}$ and various carbon contents

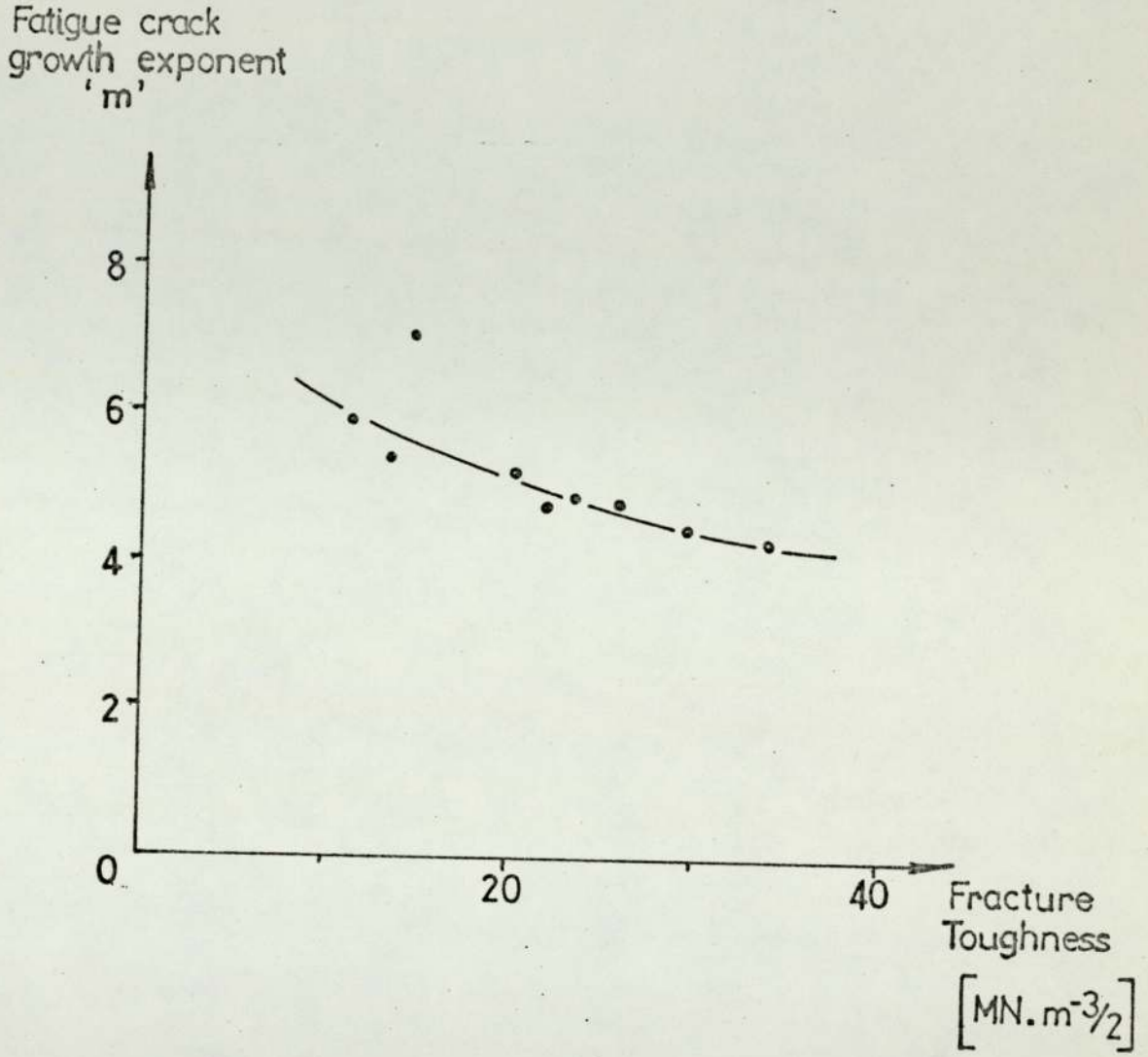


Fig.64 - Fatigue crack growth exponent vs fracture toughness of Ancoloy SA

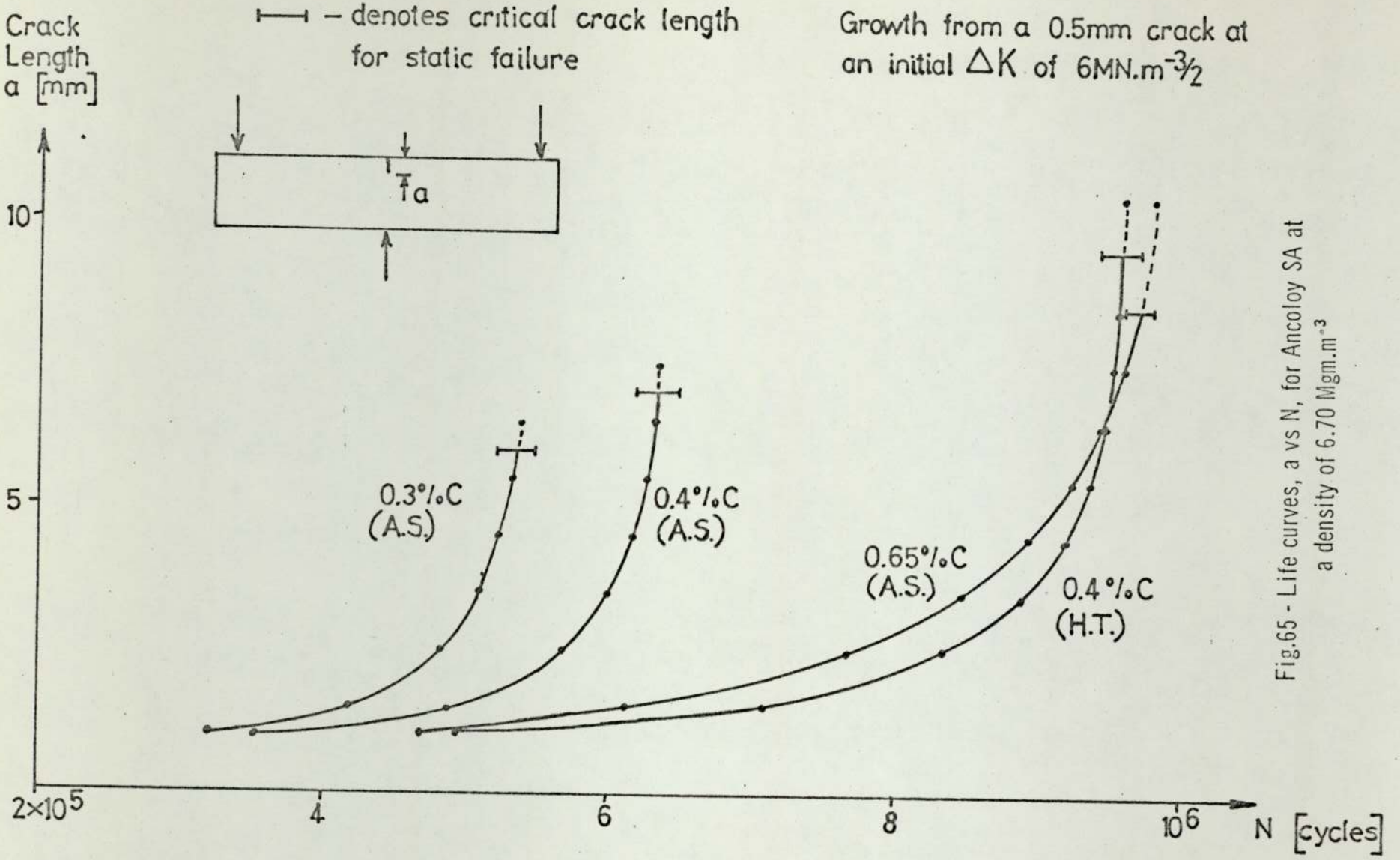


Fig.65 - Life curves, a vs N, for Ancoloy SA at a density of 6.70 Mgm.m$^{-3}$

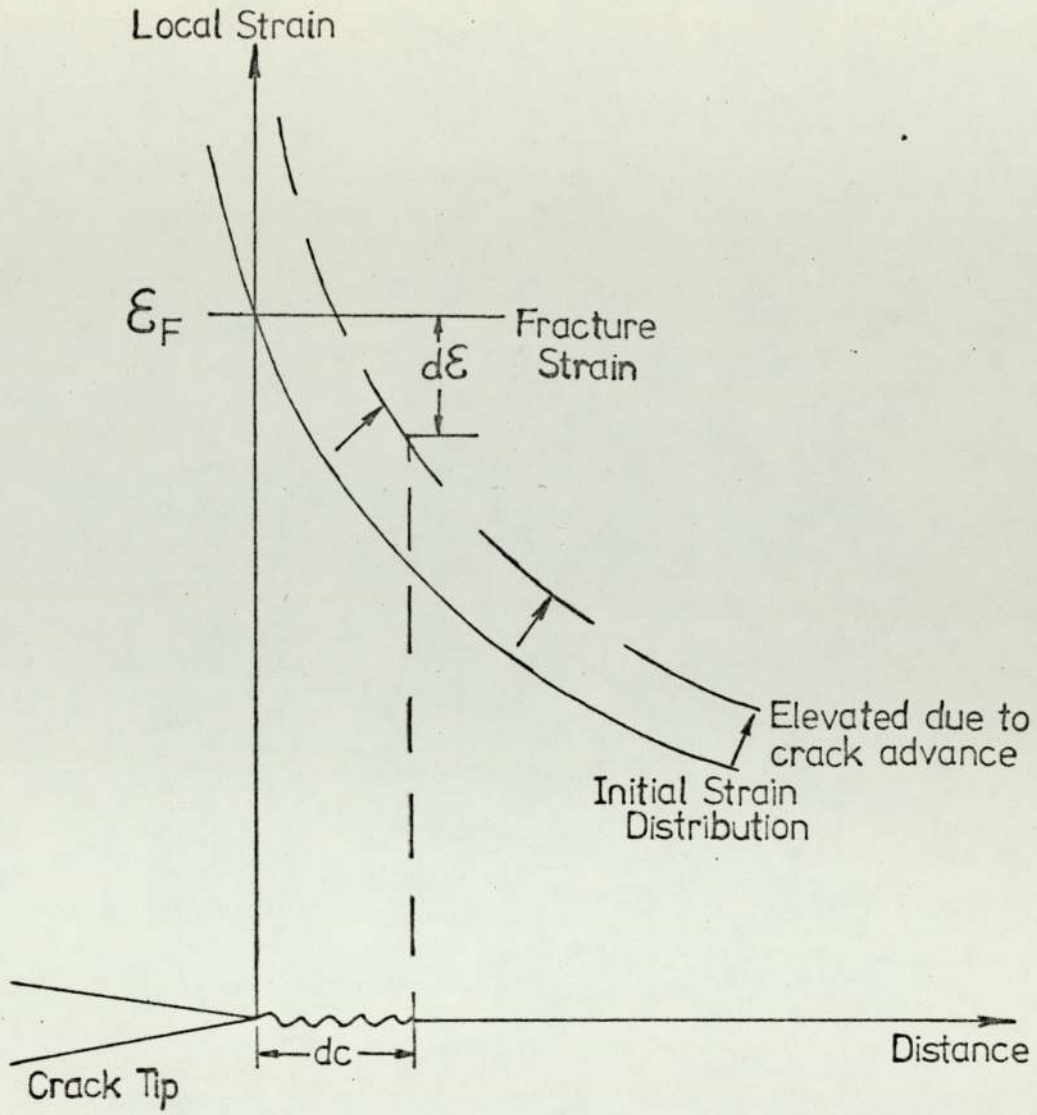


Fig.66 - Schematic representation of the mechanism of stable crack growth, (after McClintock)

Fig. 67: Various fracture surfaces of Ancoloy SA sintered low alloy steel powder, (S.E.M.)

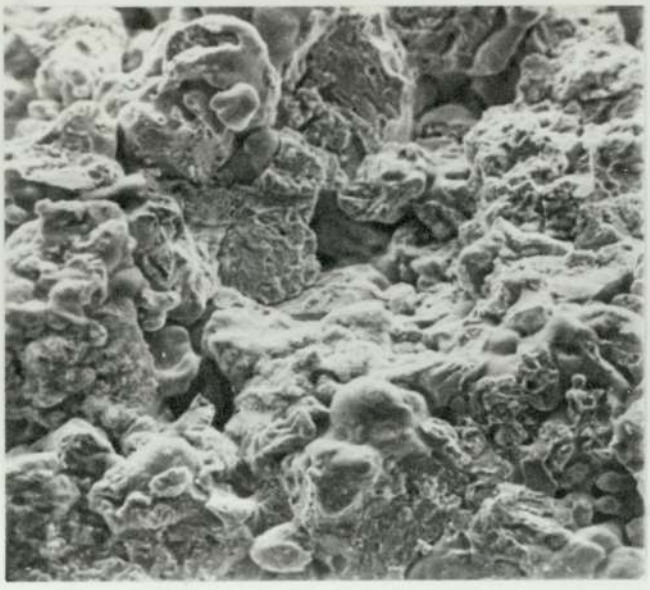

a) General fatigue fracture; density 5.95 Mgm. $m^{-3}$, as-sintered, (x 1000)

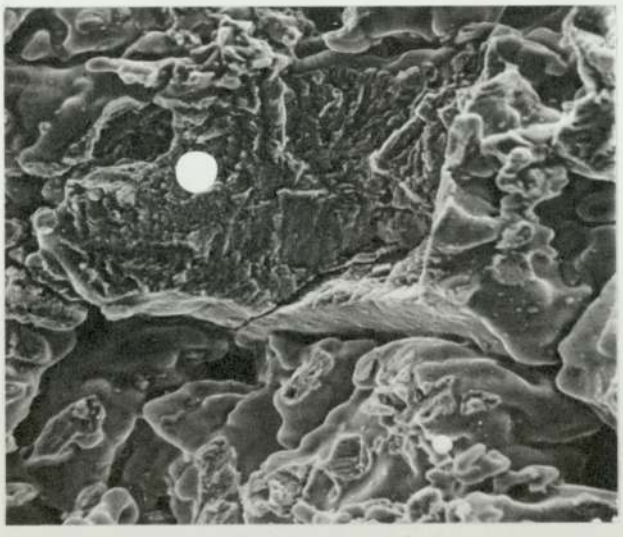

b) Ridged area of bond rupture (spotted) in fatigue; density 5.95 Mgm. $m^{-3}$, as-sintered, (x 2000)

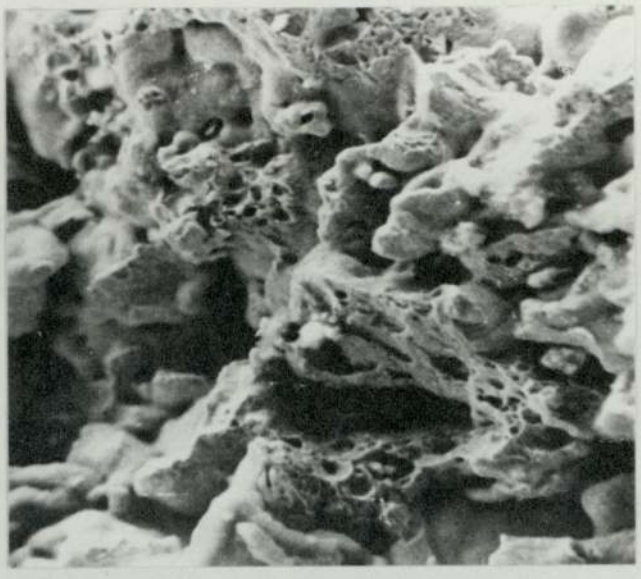

c) Fast fracture, (toughness test); density 5.95 Mgm. $m^{-3}$
heat treated, (x 1000)

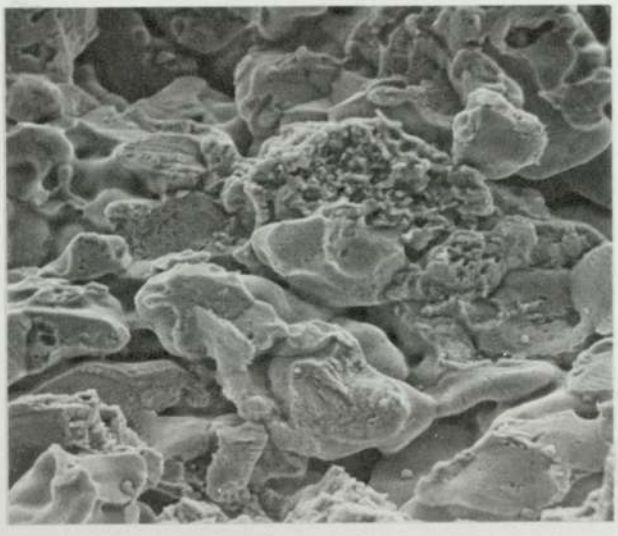

d) Fatigue fracture; density 6.70 Mgm. $m^{-3}$,
as-sintered, (x 1000)

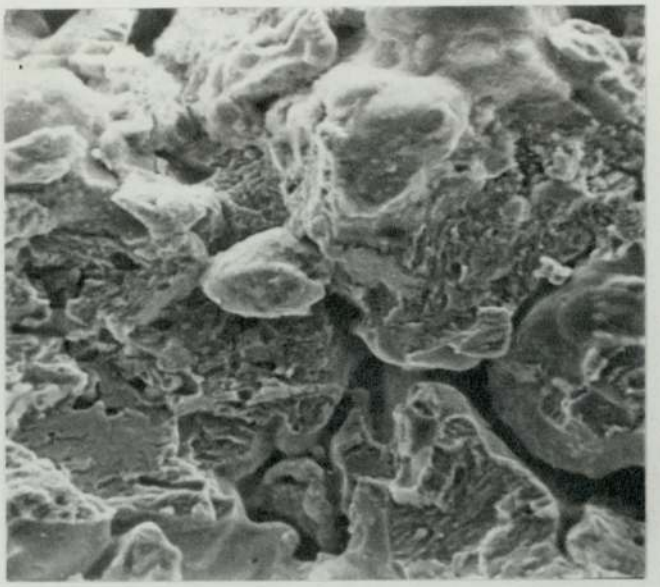

e) Fatigue fracture; density 6.70 Mgm. $m^{-3}$, heat treated, (x 1000)

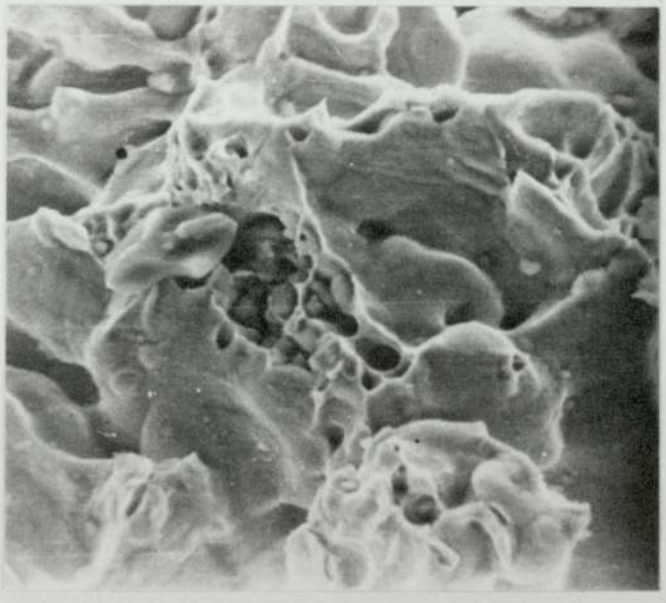

f) Fast fracture, (toughness test); density 6.70 Mgm. $m^{-3}$ as-sintered, (x 2000)

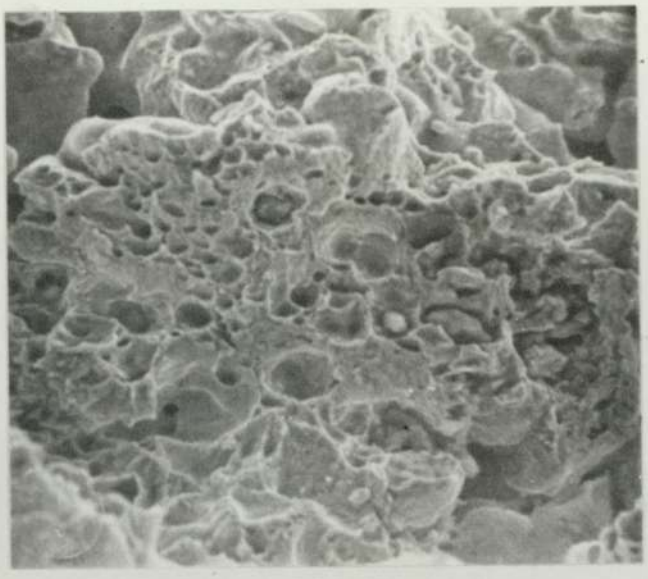

g) Fast fracture, (toughness test); density 6.70 Mgm. $m^{-3}$ as-sintered, (x 2000)

h) As g) but heat treated, (x 2000)

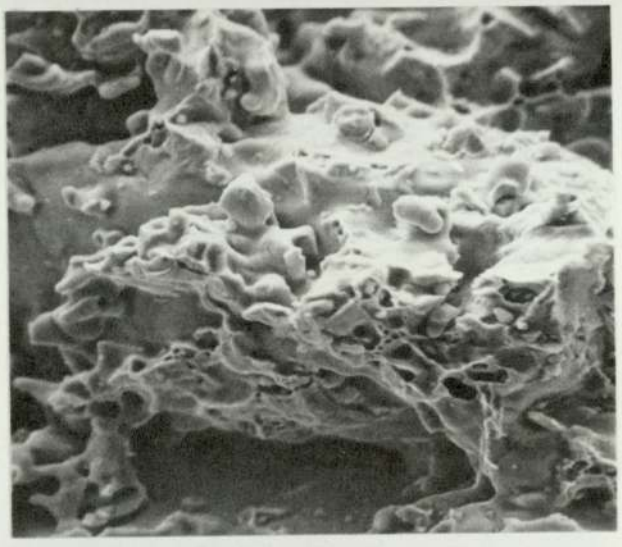

i) Tensile fracture; density 6.70 Mgm. $m^{-3}$, as-sintered, (x 2000)

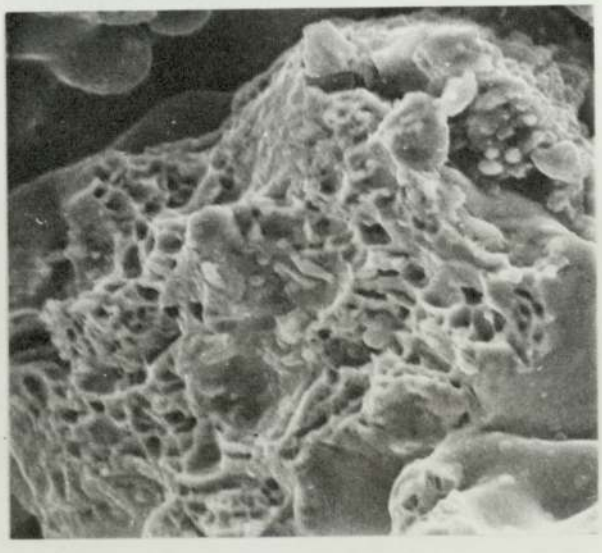

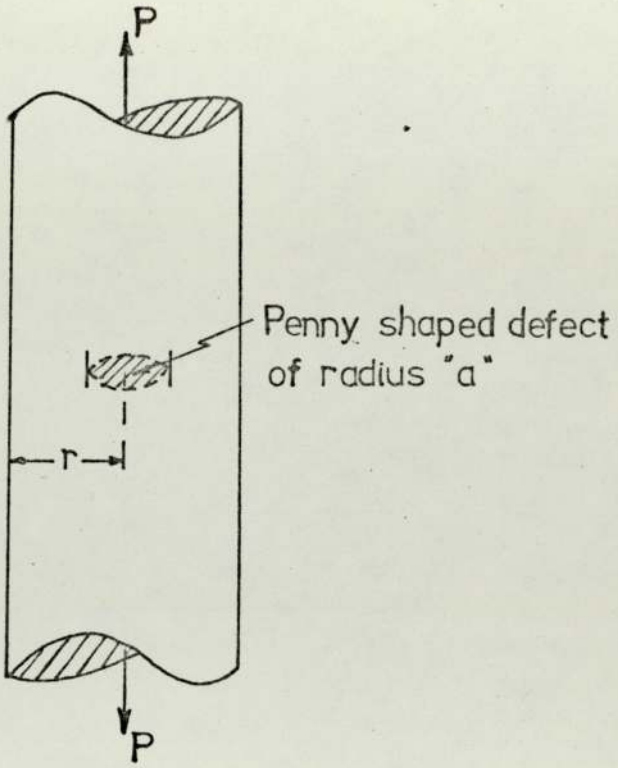


Fig.68 - Penny-shaped defect of radius a in a cylindrical bar of radius r loaded in uniaxial tension

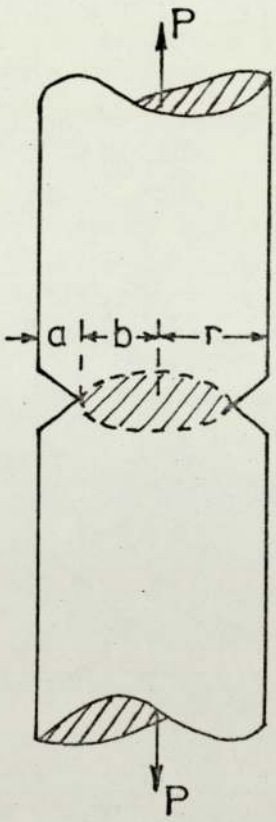


Fig.69 - Circumferential defect of depth a in a cylindrical bar of radius r loaded in uniaxial tension

## APPENDIX I

### NEUBER STRESS CONCENTRATION FACTOR, $K_t$

Neuber considers the two cases of a shallow and a deep notch in double notched bending.

i) Shallow notch

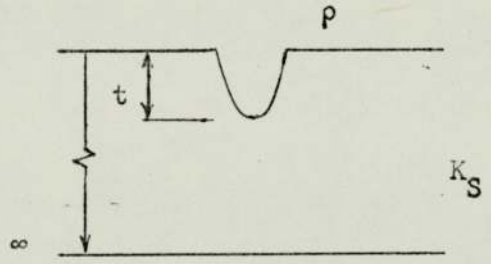


ii) Deep notch

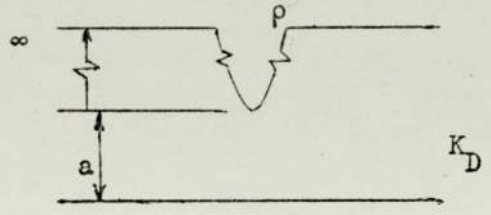


$$K_S = 1 + 2\left\{\frac{t}{\rho}\right\}^{\frac{1}{2}}$$

$$K_D = \frac{2\left(\frac{a}{\rho} + 1\right) - \alpha_1\left(\frac{a}{\rho} + 1\right)^{\frac{1}{2}}}{\left[4\left(\frac{a}{\rho} + 1\right)/\alpha_2\right] - 3\alpha_1}$$

Where $\alpha_1 = K_D$ for deep double notch tension

$$\alpha_1 = \frac{2\left(\frac{a}{\rho} + 1\right)\left(\frac{a}{\rho}\right)^{\frac{1}{2}}}{\left[\left(\frac{a}{\rho} + 1\right)\arctan\left(\frac{a}{\rho}\right)^{\frac{1}{2}}\right] + \left(\frac{a}{\rho}\right)^{\frac{1}{2}}}$$

and $\alpha_2 = K_D$ for deep double notch bending

$$\alpha_2 = \frac{4\left(\frac{a}{\rho}\right)\left(\frac{a}{\rho}\right)^{\frac{1}{2}}}{3\left[\left(\frac{a}{\rho}\right)^{\frac{1}{2}} + \left\{\left(\frac{a}{\rho} - 1\right)\operatorname{arc}\left[\tan^{-1}\left(\frac{a}{\rho}\right)^{\frac{1}{2}}\right]\right\}\right]}$$

From which : $K_t\ (\text{net}) = \dfrac{1 + (K_D - 1)(K_S - 1)}{\left[(K_D - 1)^2 + (K_S - 1)^2\right]^{\frac{1}{2}}}$

and $K_{t\ (\text{gross})} = K_{t\ (\text{net})} \cdot W^2/a^2$ (for SEN 3-pt bend specimens)

## APPENDIX II

### SIMPSON's ONE THIRD RULE

This method may be used to compute the area under a curve represented by discrete points

$$A = \int_{X_0}^{X_2} f(x).dx$$

$$= \frac{h}{3}(Y_0 + 4Y_1 + Y_2) - \frac{1}{90} h^5 f^{(4)}(\xi)$$

where $X_0 < \xi < X_2$

Graphically the integration is performed over two panels, (each of width h), as below

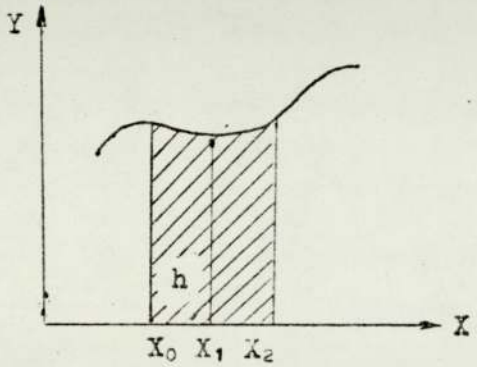


The application of Simpson's Rule over 2n panels between

$X_0 = a$ and $X_{2n} = b$ gives;

$$A = \int_a^b f(x).dx$$

$$= \frac{h}{3}(Y_0 + 4Y_1 + 2Y_2 + 4Y_3 + 2Y_4 + \ldots\ldots 4Y_{n-1} + Y_n)$$

$$- \frac{1}{180}(b - a)\, h^4\, f^{(4)}(\xi).$$

where $a < \xi < b$ and $f^{(4)}$ is the fourth derivative of $f(x)$ evaluated at $\xi$

The error term is neglected and it is necessary to choose h such that the error term is small. Usually $h << 1$ when $f^{(4)}(\xi)$ is unknown.

## REFERENCES


1. G. A. MOWBRAY: Powder Met., 8, (1965), 187

2. H. G. TAYLOR: Powder Met., 8 (1965), 285

3. W. D. JONES: "Fundamental Principles of Powder Metallurgy", Edward Arnold, London, (1960), 573

4. G. T. BROWN: Powder Met., 15, (1972), 95

5. S. I. HULTHEN: Powder Met., 13, (1970), 234

6. R. H. T. DIXON & W. A. CLAYTON: "Powder Metallurgy for Engineers" Machine Publishing Company, Brighton, (1971).

7. Iron and Steel Engineer, (January, 1972)

8. Metal Powders Handbook

9. A. B. BACKENSTO: "Perspectives in Powder Metallurgy", Volume 3, (1968), 8.

10. A. R. POSTER: "Perspectives in Powder Metallurgy", Volume 3, (1968), 20.

11. C. J. LEADBEATER, L. NORTHCOTT & F. HARGREAVES: "Perspectives in Powder Metallurgy", Volume 3, (1968), 72.

12. G. R. KRISHNAMOOTHY: Powder Met., 14, (1971), 164

13. J. W. KAPUTO & A. R. PELS: Int. J. Powder Met., 3, (1967), 17.

14. G. D. McADAM: J. I. S. I., 168, (1951), 346

15. M. EUDIER: Powder Met., 9, (1962), 278

16. V. T. MORGAN: Powder Met., 7, (1961), 44

17. V. T. MORGAN: Powder Met., 12, (1969), 72

18. V. GALLINA and G. MANNONE: Powder Met., 11, (1968), 73

19. G. H. GESSINGER, H. METZLER, F. ESPER & H. E. EXNER: Third European Powder Met. Symposium, (1971), Conf. Supp. Pt.1, 289

20. R. M. BROCKELMAN & K. A. FOWLER: Int. J. Powder Met., 2, (1966,) 45

21. L. ZAGORSKI & E. J. ECKEL: Int. J. Powder Met., 7, (1971), 41

22. S. M. KAUFMAN & S. MOCARSKI: Int. J. Powder Met., 7, (1971), 19

23. R. S. BANKOWSKI & W. H. FEILBACH: Int. J. Powder Met., 6, (1970), 23

24. H. A. SCHWARTZ & C. H. JUNGE: Proc. A. S. T. M., 41 (1941), 816

25. G. MEYERSBERG: Iron and Steel, 17, (1944), 243-247, 289-291, 323-328

26. A. THUM & H. UDE: Giesserei, 16, (1929), 502

27. A. THUM: Giesserei, 16, (1929), 1164

28. A. THUM & H. UDE: Giesserei, 17, (1930), 105

29. G. N. J. GILBERT: B.C.I.R.A. J. of R. & D., 6, (1957), 546

30. G. N. J. GILBERT: B.C.I.R.A. J. of R. & D., 7, (1959), 745

31. V. WEISS and S. YUKAWA: A.S.T.M. STP 381, (1964), 1

32. J. T. BARNBY: N.D.T., 4, (1971), 385

33. A. A. GRIFFITH: Phil. Trans. Roy. Soc. of London, 221, (1920), 163

34. G. R. IRWIN: J. App. Mech., 24, (1957), 361.

35. I. N. SNEDDON: Proc. Phys. Soc. of London, 187, (1946), 229

36. H. H. WESTERGAARD: Trans. A.S.M.E., 61, (1939), A39

37. J. I. BLUHM: Proc. A.S.T.M. 61, (1961), 1324

38. A. A. WELLS: Brit. Welding Res. Assn. Report, M13/63, (1963)

39. A. A. WELLS: "The Mechanics of the Fracture Transition in Yielding Materials", Internal Report, Dept. of Civ. Eng., Univ. of Belfast, (1969)

40. H. L. KUHN and C. L. DOWNEY: Int. J. Powder Met., 7, (1971), 15

41. J. T. BARNBY, D. C. GHOSH & K. DINSDALE: Powder Met., 16, (1973), 55

42. G. A. CLARKE & R. A. QUEENEY: Int. J. Powder Met., 8, (1972), 104

43. G. ARTUSIO, V. GALLINA, G. MANNONE & E. SGAMBETTERA: Powder Met., 9, (1966), 84

44. C. D. T. MINTON & G. C. SMITH: Powder Met., 12, (1963), 159

45. W. F. PAYNE: A.S.T.M. STP 381, (1964), 357

46. F. A. McCLINTOCK: Int. J. Fracture Mechs., 4, (1968), 101

47. P. R. THOMASON: J.I.M., 96, (1968), 360

48. J. R. RICE & D. M. TRACEY: J. of Mech. & Phys. of Solids, 17, (1969), 201

49. B. I. EDELSON & N. M. BALDWIN: Trans. A.S.M., 55, (1962), 230

50. S. W. McGEE & E. R. ANDREOTTI: "Modern Developments in Powder Met.," Vol.3, Edited by H. H. Hausner

51. M. CREAGER & P. C. PARIS: Int. J. Fracture Mechs., 3, (1967), 247

52. A. S. TETELMAN, T. R. WILSHAW & C. A. RAU: Int. J. Fracture Mechs., 4, (1968), 147

53. Private Communication

54. Private Communication

55. J. M. KRAFFT: App. Mats. Res., 3, (1964), 88

56. P. H. FRENCH & P. G. MARDON: Int. J. Powder Met., 3, (1967), 65

57. In "Alberts Versuchen and Erfindungen" by D. HOPPE; Stahl u. Eisen, 16, (1896), 437

58. N. J. M. RANKINE: Proc. Inst. Civ. Engineers, 2, (1843), 105

59. A. WOHLER in "Fatigue of Metals", R. CAZAUD, Chapman & Hall, (1953), 2

60. J. A. EWING & W. ROSENHAIN: Proc. Roy. Soc., 67, (1899), 85

61. J. A. EWING & J. C. W. HUMFREY: Phil. Trans. Roy. Soc., 200, (1903), 241

62. H. J. GOUGH & D. HANSON: Proc. Roy. Soc., 104A, (1923), 538

63. J. GILCHRIST: The Engineer, 90, (1900), 203

64. K. LAUTE & G. SACHSE: Zeitschrift Ver. Deutsche Ing., 72, (1928), 1188

65. W. P. MASON: "Symposium on Basic Mechanisms of Fatigue", A.S.T.M. STP 237, (1958), 36

66. D. H. FEGREDO & G. B. GREENOUGH: J.I.M., 87, (1958), 1

67. A. J. McEVILY & E. S. MACHLIN: "Fracture", ed. Averbach et al, Technology Press, Cambridge, Mass., (1959), 450.

68. E. ORDWAN: Proc. Roy. Soc., 171, (1939), 79

69. H. J. GOUGH & W. A. WOOD: Proc. Roy. Soc., 154A, (1936), 510

70. J. T. BARNBY: "Fatigue", Mills & Boon, (1970), 19

71. J. BAUSCHINGER: "Uber die Veränderungen der Elastizitätsgrenze und der Festigkeit des Eisens und Stahls durch Strecken, Quetschen, Erwarmen, Abkuhlen and durch oftmals wiederholte Belastung": Mitteilung, Mechanisches-Technisches Laboratorium, Munich (1886).

72. D. V. WILSON: Acta Met., 13, (1965), 807

73. J. T. BARNBY & F. M. PEACE: Acta Met., 19, (1971), 1351

74. D. V. WILSON: Phil. Mag., 22, (1970), 643

75. V. N. WHITTAKER: Phil. Mag., 13, (1966), 1301

76. P. J. E. FORSYTH: "AGARD", Rep. No. 610, (1973), 2.

77. O. H. BASQUIN: Proc. A.S.T.M., 10, (1910), 625

78. J. A. POPE: "Metal Fatigue", Chapman & Hall, London, (1959) 15.

79. H. J. GOUGH: "Fatigue of Metals", Scott & Greenwood, London, (1924), 63

80. P. G. FORREST: "Fatigue of Metals", Pergamon Press, (1962), 93

81. P. G. FORREST: "Fatigue of Metals", Pergamon Press, (1962), 93

82. J. A.POPE: "Metal Fatigue", Chapman & Hall, London, (1959), 24

83. M. A. MINER: J. App. Mech., 12, (1945), A159

84. R. H. W. BROOK & J. S. C. PARRY: J. Mech. Eng. Sci., 11, (1969) 243

85. S. W. MARCO & W. L. STARKEY: Trans. A.S.M.E., 76, (1954), 627

86. L. F. COFFIN: App. Mats. Res., 1, (1962), 129

87. S. S. MANSON: Proc. Soc. Exptl. Stress Analysis, 22 (1965) 193

88. P. J. E. FORSYTH: Nature, 171, (1953), 172

89. P. J. E. FORSYTH: Proc. Roy. Soc., A242, (1957), 198

90. P. J. E. FORSYTH & D. A. RYDER: Metallurgia, 63, (1961), 117

91. R. M. N. PELLOUX:: Trans. A.S.M., 57, (1964), 511

92. C. CRUSSARD, J. PLATEAU, R. TAMHANKAR, G. HENRY & D. LAJEUNESSE: "Fracture" ed. Averbach et al. Technology Press, Cambridge, Mass., (1959)

93. E. SMITH & J. T. BARNBY: Met. Sci. J., 1, (1967), 1.

94. C. Q. BOWLES & D. BROEK: NLR MP69014U, (1969)

95. B. TOMKINS & W. D. BIGGS: J. Mats. Sci., 4, (1969), 532

96. W. A. SPITZIG, P. M. TALDA & R. P. WEI: Eng. Fracture Mech., 1, (1968), 155

97. P. J. E. FORSYTH: "Cranfield Symposium on Crack Propagation", (September, 1961).

98. S. PEARSON: R.A.E. Tech. Rep. No. 71109, (1971)

99. H. NEUBER: J. App. Mech., (1961), 544

100. T. H. TOPPER, R. M. WETZEL & J. MORROW: J. of Mats., 4, (1969), 200

101. J. MORROW, R. M. WETZEL & T. H. TOPPER: A.S.T.M. STP462,(1970), 74

102. C. V. B. GOWDA, T. H. TOPPER & B. N. LEIS: "Proc. Int. Conf. on Mechanical Behaviour of Metals", Kyoto, Japan, (1971), Vol. 2, 187

103. J. R. RICE; A.S.T.M. STP415, (1967), 302

104. H. NEUBER: "Kerbspannungslehre", Springer, Berlin, (1958).

105. G. N. SAVIN: "Stress Concentrations Around Holes," Pergamon Press, New York, (1961)

106. G. R. IRWIN: "Fracture Mechanics", Proc. of 1st Naval Symposium on Structural Mechanics, Pergamon Press, New York, (1960).

107. P. C. PARIS & G. C. SIH: "Stress Analysis of Cracks", A.S.T.M. STP381, (1965).

108. B. H. BILBY, A. H. COTTRELL & K. H. SWINDEN: Proc. Roy. Soc., A272, (1963), 304

109. J. WEERTMAN: Int. J. Fracture Mechs., 2, (1966), 460

110. B. H. BILBY & P. T. HEALD: Proc. Roy. Soc., A305, (1968), 429

111. A. R. JACK & A. T. PRICE: Int. J. Fracture Mechs., 6, (1970), 401

112. A. N. MAY; Nature, 185, (1960), 303

113. A. N. MAY: Nature, 188, (1960), 573

114. J. H. GITTUS; Nature, 202, (1964), 788

115. E. SMITH; Proc. Roy. Soc., A299, (1967), 455

116. M. B. P. ALLERY & G. BIRKBECK: Eng. Fracture Mechs., 4, (1972) 325

117. R. G. FORMAN: Eng. Fracture Mechs., 4, (1972), 333

118. S. S. MANSON: Exptl. Mechs., 1, (1965), 193

119. S. S. MANSON & M. H. HIRSCHBERG: NASA TM X-52126, (1965).

120. H. GROVER: "Fatigue - An Interdisciplinary Approach", Syracuse University Press, New York, (1966), 361

121. R. A. SMITH & K. J. MILLER: "Fatigue at Notches", Cambridge Univ. Eng. Dept., C - MAT/TR.19 (1975)

122. W. J. PLUMBRIDGE: J. Mats. Sci., 7, (1972), 939

123. F. A. McCLINTOCK: "Fracture of Solids", A.I.M.M.E., Interscience, New York, (1963), 65

124. A. K. HEAD: Phil. Mag., 44, (1953), 925

125. N. E. FROST & D. S. DUGDALE: J. Mech. & Phys. of Solids, 6, (1958), 92

126. A. K. McEVILY & W. ILLG: NACA Tech. Note 4394, (1958)

127. J. WEERTMAN: Int. J. Fracture Mechs., 2, (1966), 460

128. A. K. McEVILY & T. L. JOHNSTON: Int. J. Fracture Mechs., 3, (1967), 45

129. P. C. PARIS, M. P. GOMEZ & W. E. ANDERSON: Trend in Engineering, 13, (1961), 9

130. P. C. PARIS, & F. ERDOGAN: J. Basic Engineering, 85, (1963) 528

131. P. C. PARIS: "Fatigue - An Interdisciplinary Approach", Syracuse University Press, New York, (1966), 107

132. F. A. McCLINTOCK & G. R. IRWIN: A.S.T.M. STP381 (1965), 84

133. S. R. SWANSON, F. CICCI & W. HOPPE: A.S.T.M. STP415, (1967) 312

134. D. R. DONALDSON & W. E. ANDERSON: Proc. Crack Propagation Symposium, Cranfield, (1962)

135. J. SCHIVJE & F. A. JACOBS: NLR-TR M2128, Amsterdam, (1964)

136. J. T. BARNBY, K. DINSDALE & R. HOLDER: Conf. on Practical Applications of Fracture Mechanics, Cambridge Univ. Paper 26, (January, 1975).

137. J. F. KNOTT: "Fundamentals of Fracture Mechanics", Butterworths, London, (1973), 246

138. E. TAYLOR: Private Communication

139. D. BROEK & J. SCHIVJE: NLR - TR M2111, (1963)

140 S.PEARSON: RAE - TR 68297, (1968)

141. N. E. FROST: J. Mech. Eng. Sci., 4, (1963), 22

142. N. J. F. GUNN: RAE - TR 64024, (1964)

143. R. G. FORMAN, V. E. KEARNEY & R. M. ENGLE: J. Basic Engineering, 89, (1967), 459

144. R. O. RITCHIE: "The Practical Implications of Fracture Mechanisms," Inst. of Met., Paper 1, (Spring 1973).

145. R. N. WRIGHT & A. S. ARGON: Metall. Trans., 1, (1970), 3065

146. C. E. RICHARDS: Acta Met., 19, (1971), 583

147. P. T. HEALD, T. C. LINDLEY & C. E. RICHARDS: Mats. Sci. Eng., 10, (1972), 235

148. R. O. RITCHIE & J. F. KNOTT: Mats. Sci. Eng., 14, (1974), 7

149. G. A. MILLER: Trans. A.S.M., 61, (1968), 442

150. C. J. BEEVERS, R. J. COOKE, J. F. KNOTT & R. O. RITCHIE: Met. Sci. J., 9, (1975), 119

151. J. M. KRAFFT: Trans. A.S.M., 58, (1965), 691

152. J. M. WHEATLEY & G. C. SMITH: Powder Met., 12, (1963), 141

153. R. HAYNES: Powder Met., 13, (1970), 465

154. S. H. WILLIAMS & R. HAYNES: Powder Met., 16, (1973), 387

155. A. F. KRAVIC & D. L. PASQUINE: Int. J. Powder Met., 5, (1969) 45

156. R. S. BANKOWSKI & W. H. FEILBACH: Int. J. Powder Met., 6, (1970) 23

157. C. G. GOETZEL & R. P. SEELIG: Trans. A.S.T.M. 40, (1940), 746

158. O. J. DUNMORE & G. C. SMITH: "Symposium on Powder Metallurgy", I.S.I. Special Report 58, (1956), 209

159. A. F. KRAVIC: Int. J. Powder Met., 2, (1966), 7.

160. V. GALLINA & G. MANNONE: Powder Met., 11, (1968), 73

161. I. D. RADOMYSEL'SKY, B. A. GRAYAZNOV & V. C. SEMASHKO: Soviet Powder Metallurgy & Metal Ceramics, 4(64), (1968), 213

162. S. R. ANTHONY & J. CONGLETON: "The Practical Implications of Fracture Mechanisms", Inst. of Met., Paper 1, (Spring, 1973).

163. S. W. McGEE: A.S.M.E., Preprint 66-MD-77, (1966)

164. Hoganas Corporation: "Ancoloy SA", Technical Bulletin PM70-1, (1973)

165: British Standards Inst: Draft for Development 3, (1971)

166. D. M. GILBEY & S. PEARSON: RAE-TR 66402, (1960)

167. G. R. IRWIN, J. A. KIES & H. L. SMITH: Proc. A.S.T.M., 58 (1958), 640

168. F. A. McCLINTOCK: J.Appl.Mech. 25, (1958), 582

169. R. H. INGLE, C. E. NICHOLSON & E. F. WALKER: B.I.S.RA. Research Report, PMC/6802/-/74/A, (May, 1974)

170. G. C. SIH: "Handbook of Stress Intensities for Research Workers and Engineers", Inst. of Fracture & Solid Mechanics, Lehigh Univ., Bethlehem, Penn., (1973).

171. J. P. BENTHAM & W. T. KOITER: "Assymptotic Approximations Applied to Crack Problems", Chapter 3 of "Methods of Analysis and Solutions to Crack Problems" edit. G. C. Sih, (Jan. 1972).

172. H. F. BUECKNER: "Field Singularities and Related Integral Representations" in "The Stress Analysis of Cracks Handbook", edit. H. Tada, P.C. Paris & G. R. Irwin, Del Res. Corp., Hellertown, Penn., (1973)

173. M. ISIDA: Bulletin of J.S.M.E., 13, No.59 (1970), 635

174. W. R. DELAMETER, G. HERRMAN & D. M. BARNETT: Trans. A.S.M.E., (J. App. Mechs.), (March 1975), 74

175. T. H. C.CHILDS & G. W. ROWE: Report on Progress in Physics, 36, (1973), 223

176. E. TAYLOR: "Study of Low Cycle Fatigue Behaviour of Titanium Alloys", Univ.of Aston, External Report for Procurement Executive of the Min. of Defence, AT/2097/022/MAT, (September, 1973).

177. R. O. RITCHIE: "The Practical Implications of Fracture Mechanisms" Inst. of Met., Paper 8, (Spring, 1973)

178 British Standards Institute: Draft for Development 19, (1972).